Universitat Politècnica de València

Doctoral Thesis

Doctoral Programme in Biotechnology

# ELECTROACTIVE ENVIRONMENTS FOR MESENCHYMAL STEM CELLS OSTEOGENIC DIFFERENTIATION

**Maria Teresa Guillot Ferriols**

**November 2022**

Supervised by:

Prof. Gloria Gallego Ferrer

Prof. José Luis Gómez Ribelles

Prof. Senentxu Lanceros Méndez

*A la meua família*

# Acknowledgements

Els que em coneixen probablement saben que porte pensant en com escriure aquestes línies des del moment en que vaig començar la tesi. Mai m'havia parat a reflexionar sobre el motiu d'aquest fet, però ara, mirant enrere, ho tinc clar. Sempre he sabut que hauria estat impossible, i impensable, embarcar-me en aquest projecte sense el suport de totes les persones a les quals van dedicades aquestes paraules. Espere que estiguen a la altura i serveixen com a gest, per xicotet que siga, per agrair-vos la vostra aportació a aquest treball. Ha sigut, sense dubte, el més exigent, dur, desesperant i al mateix temps gratificant que he emprès fins al moment.

En primer lugar, me gustaría dar las gracias a Gloria, José Luis y Senentxu, mis directores de tesis, por darme la oportunidad de participar en este proyecto y demostrarme a cada paso que confiaban en mí para ello.
A José Luis por su infinita paciencia y por no dejar que me desanimara en cada una de las reuniones que hemos tenido durante estos años. Tus ideas han sido un balón de oxígeno cuando no sabíamos cómo seguir. Tu pasión en cada uno de los proyectos que llevas a cabo, que no son pocos, se contagia y es un ejemplo para todos.
A Gloria por confiar siempre en mí, especialmente cuando yo menos lo he hecho. Tu constancia y esfuerzo son una guía para los que te conocemos. Gracias por tu racionalidad, a veces es necesaria para convertir las ideas en hechos, y poder tener el placer de ver hoy un trabajo acabado. A los dos, gracias por formar tan buen equipo y complementaros tan bien. Fomentáis un ambiente de trabajo envidiable, clave para los éxitos que, estoy segura, seguiréis cosechando muchos años más.
A Senentxu, por acogerme en su laboratorio al inicio de mi tesis, y ayudarme a sentar las bases de lo que ha sido este proyecto. Gracias por tu cercanía y tu saber hacer.

A Laia, que llegó en el momento indicado para aclarar nuestras dudas, por muchas que pudieran parecer, siempre con una sonrisa. Gracias por abrirnos las puertas de tu laboratorio. Ha sido genial contar contigo durante este tiempo.

A toda la gente que ha pasado por el CBIT durante estos años. Ha sido muy gratificante aprender de todos vosotros y compartir tanto tiempo juntos. Mención especial para Laura Teruel, por ser la guía de nuestro laboratorio y mantenerlo a flote. Creo que te lo decimos poco, pero aprovecho estas líneas para agradecerte tu trabajo, no sé qué haríamos sin ti. También a Guillermo, Ximo, Rafa, Darío, Rubén, Úrsula, Juan Carlos, Juan Jairo, Raquel, Inma, Luis y Pachi, que estuvieron en los inicios. A Julio, José, Ana, Estela e Irene por llegar al final para alegrar los días, ha sido un placer compartir tiempo juntos, fuera y dentro del laboratorio. A Annachiara, que llegó casi al final y por poco tiempo, demostrando que lo bueno, si breve, dos veces bueno.

En especial a Silvia, por animarme siempre, aunque no supiese de qué iba el problema. A Laura, por sus consejos, siempre en el momento adecuado. A Hayk, por contagiarme su entusiasmo por la investigación, el motivo por el que empezó todo esto. Gracias, no sé qué hubiese hecho sin vosotros.

A Sandra, por ser una de las partes más importantes de este trabajo, sin ti no hubiese sido posible. Gracias por dejarme aprender de ti, me has hecho crecer como investigadora, pero sobre todo como persona. Gracias por ofrecerme un espacio seguro en el que poder hablar, por aconsejarme y compartirlo todo conmigo. Te admiro mucho, sé que llegarás donde te propongas y espero que sea al sitio que te haga feliz. Ha sido un placer compartir este tiempo juntas.

Thanks to the CeMi group, especially to Mark and Eva, for being so kind and helpful during my research placement. Thanks to Matt, for giving me the opportunity to work in an amazing lab, guiding me and pushing me to work harder. Hard work always pays off.

Com diria Estellés, *"hi haurà un dia que no podrem més, i llavors ho podrem tot*". Eixe dia va arribar allà per 2020, i quan creia que ja no podia més, va haver-hi gent que em va ajudar a saber que ho podia tot.

Gracias a Érika y a Arantxa, os habéis convertido en imprescindibles. Gracias Érika, por estar, cerca o lejos, y por escucharme siempre, eres un gran apoyo. Gracias Arantxa, por compartir conmigo este camino, sin duda ha sido mucho más fácil hacerlo a tu lado. Admiro tu carácter y tu ímpetu, sé que vas a llegar muy lejos.

Gràcies Pedro, per aguantar-me i ajudar-me a no perdre la perspectiva, des de fa molt anys, però en especial aquests últims mesos. La teua alegria i les ganes de créixer em porten a superar-me i no rendir-me. Gràcies per estar i ser part de la meua família.

A mis amigos adoptivos, por acogerme cuando lo necesitaba y pasar tiempo conmigo. Gracias por vuestra compañía y cariño, ha sido muy importante durante esta etapa.

Gracias a todos mis amigos de la universidad, sois la familia que se elige. Después de 10 años me continuáis haciendo feliz y me alegráis la vida cuando estamos juntos.

A mis amigas, por confiar en mí siempre más de lo que yo lo hago y por verme con los mejores ojos, por permitirme ser siempre yo, sin miedo ni culpa. Por enseñarme el valor de la levedad, aún en momentos de mucho peso. Encontrar algo así es verdaderamente especial.

Per últim, gràcies a la meua família. Gràcies papà i mamà, per ensenyar-me el valor de l'esforç, de la feina ben feta i de la constància. Per inculcar-nos la passió per la biologia en els moments quotidians, i fer de la nostra família una família d'aquelles estranyes que parlen de microorganismes i expressió gènica quan estan sopant. Per saber demostrar sense grans gestos ni paraules que ens estimeu, que confieu i que esteu orgullosos de nosaltres. Ho diem poc, però crec que hui és el moment de deixar-ho per escrit, us estime. Gràcies Anna, per acompanyar-me, per alegrar-te dels meus triomfs de la mateixa manera que jo sempre m'alegre dels teus. Estic orgullosa de tu, del teu esforç i la teua constància, de la persona que eres. T'estime, gràcies per estar sempre.

Por último, la presente tesis doctoral no podría haberse realizado sin la financiación del Ministerio de Economía y Competitividad a través de la beca para formación de personal investigador BES-2017-080398 y a la Agencia Estatal de Investigación a través de los proyectos PID2019-106000RB-C21 / AEI / 10.13039/501100011033, PID2019-106099RB-C41 y –C43 / AEI / 10.13039/501100011033.

Gràcies a tots!

# Index

# List of figures

***Chapter 1***



***Chapter 2***

# List of tables

# Abstract

Life expectancy increase entails the presence of an increasingly aging population in which musculoskeletal disorders tend to appear, producing a strong impact in patients' quality of life. New bone regenerative therapies are focused on the use of mesenchymal stem cells (MSCs), main effectors of bone regeneration *in vivo*. MSCs are easy to obtain, present immunomodulatory properties and can differentiate into bone cells. These characteristics make them ideal candidates for their use in advanced regenerative approaches. Over the years, it has been demonstrated that the induction of a pre-differentiated phenotype *in vitro*, prior to MSCs implantation, results in a better capacity for bone tissue regeneration. For this purpose, biochemical approaches based on the use of osteogenic differentiation medium containing dexamethasone have traditionally been used. These methods are not efficient and can induce the appearance of adipogenic cells, which has favoured the use of physical methods as an alternative.

Bone is a piezoelectric tissue due to the collagen fibres that conform its extracellular matrix. This stimulus has been related to its ability to respond to mechanical stress and self-regenerate, process in which MSCs play a key role. MSCs find themselves subjected to an electroactive environment, and it is hypothesized that these physical signals may influence their osteogenic differentiation process and may be used to effectively pre-differentiate them *in vitro*. To test this hypothesis, along this Doctoral Thesis piezoelectric cell culture supports have been designed in 2 and 3 dimensions based on the use of the piezoelectric polymer poly(vinylidene) fluoride (PVDF) combined with magnetostrictive cobalt ferrite oxide (CFO) nanoparticles. This combination allows the stimulation of culture supports by applying a magnetic field with a bioreactor. This magnetic field induces the deformation of

the magnetostrictive component, which is transmitted to the polymeric matrix, generating a deformation and producing an electric field, which is transmitted to the MSCs to study its effect on their osteogenic differentiation.

In the first experimental chapter, electroactive PVDF membranes manufactured by the non-solvent induced phase separation (NIPS) technique were developed and characterized. Ethanol was used as a non-solvent, which gave rise to highly porous homogeneous membranes. These cell culture supports were crystallized mostly in the $\gamma$ phase, one of PVDF's electroactive phases. Their high porosity and hydrophobicity lead to optimize a coating protocol based on the layer-by-layer (LbL) technique, using elastin-like recombinamers (ELRs) containing RGD cell adhesion sequences. After optimization of the coating protocol, the MSCs initial cellular response was studied and compared with the same membranes coated with adsorbed fibronectin. The results revealed that the presence of the ELRs was necessary to promote MSCs initial adhesion in this type of supports.

In the second chapter, electroactive PVDF membranes combined with CFO were developed by NIPS method but using water as a non-solvent. The membranes presented a non-symmetrical structure, with a smooth surface, which was used for cell culture, and a porous one, as well as various crystalline phases, but with a majority of $\beta$ phase, the most electroactive one. The technique allowed the effective incorporation of the CFO nanoparticles. Membranes were coated by LbL with type I collagen and heparin, creating a biomimetic environment for MSCs culture. An initial grafting of amine groups on the surface was carried out by means of an alkaline treatment that allowed the first layer of LbL to be deposited. Once the coating was characterized, the MSCs behaviour was studied, revealing that the coating by LbL was essential for cell proliferation in the case of membranes containing magnetic nanoparticles.

Membrane's high porosity affects MSCs initial adhesion and hinders membrane polarization process, which is essential to maximize PVDF electroactive response. For this reason, in experimental chapter three, thinner and smoother materials were developed, which would facilitate both their polarization and initial cell adhesion. PVDF and PVDF-CFO films crystallized in the presence of the ionic liquid [Bmim][Cl] were produced. The presence of ionic liquid induced PVDF nucleation in the $\beta$ phase, despite being obtained from melt, which usually generates the non-electroactive $\alpha$-phase. [Bmim][Cl] was removed once films were crystallized and MSCs initial response was analysed, revealing the non-cytotoxicity of the films and the ability of the cells to adhere and proliferate. A balanced cell culture medium (1:1 osteogenic and adipogenic media) was selected for stimulation experiments, based on analysis of focal adhesions. Piezoelectric stimulation experiments were performed using a magnetic bioreactor and the selected medium. MSCs responded to stimulation by increasing the length of their focal adhesions, as well as reducing the presence of vimentin in the cytoplasm.

Finally, piezoelectric culture supports were designed in 3D. To this end, PVDF and PVDF-CFO microspheres were developed using the electrospray technique. This technique allowed to obtain $\beta$-phase microspheres, with diameters comprised between 1 and 5 $\mu$m

and with the correct incorporation of cobalt ferrite oxide. Microspheres were encapsulated in gelatin hydrogels together with MSCs to create a biomimetic three-dimensional environment. This approach was not cytotoxic for the cells at short or long term, in fact, after 14 days MSCs presented a completely extended cytoskeleton and fibroblastic morphology characteristic of this cell type. These cell culture supports were stimulated using a magnetic bioreactor, in combination with osteogenic culture medium. After 7 days, RUNX2 expression was enhanced in stimulated samples, master regulator of the osteogenic signalling pathway.

To summarize, 2D and 3D electroactive cell culture platforms have been developed and functionalized for piezoelectric stimulation of MSCs, demonstrating that these cells are indeed capable of responding to this physical stimulus.

# Resumen

El aumento de la esperanza de vida conlleva la presencia de una población cada vez más envejecida en la que a menudo aparecen problemas muscoloesqueléticos que suponen un fuerte impacto en la calidad de vida de los pacientes. La búsqueda de nuevas terapias regenerativas óseas pone el foco en el uso de las células madre mesenquimales, MSCs por sus siglas en inglés, encargadas de la regeneración del tejido *in vivo*. Las MSCs son fáciles de obtener, presentan propiedades inmunomoduladoras y además son capaces de diferenciarse hacia células óseas. Estas características las hacen idóneas para su uso en terapias regenerativas. A lo largo de los años se ha demostrado que la inducción de un fenotipo prediferenciado *in vitro*, previo a la implantación de las MSCs, resulta en una mejor capacidad de regeneración del tejido óseo. Por eso, habitualmente, se han empleado métodos bioquímicos basados en el uso de medios de diferenciación osteogénica que contienen dexametasona. Estos métodos son poco eficientes y pueden inducir a la aparición de células adipogénicas, por lo que el uso de métodos físicos como alternativa está adquiriendo relevancia.

El hueso es un tejido con propiedades piezoeléctricas debido a las fibras de colágeno que forman parte de su matriz extracelular. Este estímulo ha sido relacionado con su capacidad de responder al estrés mecánico y autoregenerarse, donde juegan un papel importante las MSCs. Éstas se encuentran en un entorno electroactivo, y son precisamente estas señales físicas las que pueden influir en su proceso de diferenciación osteogénica pudiendo ser empleadas para su prediferenciación *in vitro* de forma efectiva. Para comprobar esta hipótesis, en el desarrollo de la presente Tesis Doctoral se han diseñado soportes de cultivo piezoeléctricos en 2 y 3 dimensiones basados en el uso del polímero piezoeléctrico

polifluoruro de vinilideno (PVDF) combinados con partículas magnetostrictivas de ferrita de cobalto (CFO). Esta combinación permite la estimulación de los soportes de cultivo aplicando un campo magnético con un biorreactor. Este campo magnético genera la deformación del componente magnetostrictivo, que es transmitida a la matriz polimérica, deformándola y generando un campo eléctrico. Ésta última es transmitida a las células cultivadas en estos soportes para estudiar su efecto sobre la diferenciación osteogénica.

En el primer capítulo experimental se desarrollaron y caracterizaron membranas electroactivas de PVDF fabricadas por el método de separación de fases inducida por no-solventes (NIPS). Se empleó etanol como no-solvente, lo que dio lugar a membranas homogéneas altamente porosas. Estos soportes de cultivo cristalizan en fase $\gamma$, una de las fases electroactivas del PVDF. Su alta porosidad e hidrofobicidad hizo necesaria la optimización de un recubrimiento basado en la técnica capa a capa (LbL), empleando recombinámeros similares a la elastina (ELRs) que contenían secuencias de adhesión celular RGD. Tras la optimización del protocolo de recubrimiento, se estudió la respuesta celular inicial de las MSCs y se comparó con los mismos soportes recubiertos únicamente con fibronectina adsorbida. Los resultados revelaron que la presencia de los ELRs es necesaria para promover la adhesión inicial de las MSCs en este tipo de soportes.

En el segundo capítulo se desarrollaron membranas electroactivas de PVDF combinadas con CFO, empleado el mismo método de fabricación que en el capítulo anterior, pero usando agua como no-solvente. En este caso las membranas presentaban una estructura no simétrica, con una superficie lisa, que fue empleada para cultivo celular, y otra porosa, así como diversas fases cristalinas, pero con una mayoría en fase $\beta$, la más electroactiva. La técnica permitió la incorporación efectiva de las nanopartículas. Se recubrieron las membranas mediante LbL con colágeno tipo I y heparina, creando un entorno biomimético para las MSCs. Se realizó un injerto inicial de grupos amina en la superficie mediante un tratamiento alcalino que permitió unir la primera capa del LbL. Una vez caracterizado el recubrimiento se estudió el comportamiento de las MSCs, revelando que el recubrimiento mediante LbL resultaba esencial para la proliferación celular en el caso de las membranas que contenían nanopartículas magnéticas.

La elevada porosidad de las membranas producidas afecta a nivel biológico a la adhesión de las MSCs y a nivel físico al proceso de polarización de los soportes de cultivo, imprescindible para obtener la máxima respuesta piezoeléctrica. Por ello, en el capítulo experimental tres se desarrollaron nuevos materiales más finos y planos, que facilitasen tanto su polarización como la adhesión celular inicial. Para ello se produjeron films de PVDF y PVDF-CFO cristalizados en presencia del líquido iónico [Bmim][Cl]. La presencia de éste indujo la nucleación del PVDF en fase $\beta$ en los films, a pesar de ser obtenidos desde fundido, lo cual suele generar fase $\alpha$, no electroactiva. El líquido iónico fue eliminado una vez producida la cristalización y se estudió la respuesta inicial de las MSC, revelando la no citotoxicidad de los films y la capacidad de las células para adherirse y proliferar. Se seleccionó un medio de cultivo mixto (1:1 medio osteogénico y adipogénico) para los experimentos de estimulación, basado en el análisis de las adhesiones focales. Se realizaron ensayos de estimulación piezoeléctrica empleando un biorreactor magnético y el medio seleccionado. Las MSCs respondieron a la estimulación incrementado la longitud

de sus adhesiones focales, así como reduciendo la presencia de vimentina en el citoplasma.

Por último, se diseñaron soportes de cultivo piezoeléctricos en 3D. Para ello se desarrollaron microesferas de PVDF y PVDF-CFO mediante la técnica de electropulverizado Esta técnica permitió obtener microesferas de entre 1 y 2 μm de diámetro, en fase β y con la correcta incorporación de la ferrita de cobalto. Las microesferas se encapsularon en hidrogeles de gelatina junto con las MSCs para crear un entorno tridimensional biomimético. Esta aproximación no resultó citotóxica para las células, que, además, tras 14 días presentaban una morfología completamente extendida, característica de este tipo celular. Estos soportes de cultivo se estimularon empleando el biorreactor magnético, en combinación con medio de cultivo osteogénico. Tras 7 días, se observó un incremento en la expresión del factor de transcripción RUNX2 en las muestras estimuladas, eje central de la ruta de señalización osteogénica, demostrando que la estimulación piezoeléctrica es capaz de activar en mayor medida la diferenciación de las MSCs.

En resumen, se han desarrollado y funcionalizado plataformas de cultivo electroactivas en 2D y 3D para la estimulación piezoeléctrica de las MSCs, demostrando que, efectivamente, estas células son capaces de responder a este estímulo físico.

# Resum

L'augment de l'esperança de vida comporta la presència d'una població cada vegada més envellida en la que sovint aparèixen problemes muscoloesquelètics que suposen un fort impacte en la qualitat de vida dels pacients. La recerca de noves teràpies regeneratives òssies posa el focus en l'ús de les cèl·lules mare mesenquimals, MSCs per les sigles en anglès, encarregades de la regeneració del teixit *in vivo*. Les MSCs són fàcils d'obtenir, presenten propietats immunomoduladores i a més són capaces de diferenciar-se cap a cèl·lules òssies. Aquestes característiques les fan idònies per al seu ús en teràpies regeneratives. Al llarg dels anys s'ha demostrat que la inducció d'un fenotip prediferenciat *in vitro*, previ a la implantació de les MSCs, resulta en una millor capacitat de regeneració del teixit ossi. Per això, habitualment, s'han emprat mètodes bioquímics basats en l'ús de medis de diferenciació osteogènica que contenen dexametasona. Aquests mètodes són poc eficients i poden induir l'aparició de cèl·lules adipogèniques, per la qual cosa l'ús de mètodes físics com a alternativa està adquirint rellevància.

L'os és un teixit amb propietats piezoelèctriques a causa de les fibres de col·lagen que formen part de la seva matriu extracel·lular. Aquest estímul ha estat relacionat amb la seva capacitat de respondre a estímuls mecànics i autoregenerar-se, on juguen un paper important les MSCs. Aquests es troben en un entorn electroactiu, i són precisament aquests senyals físics els que poden influir en el seu procés de diferenciació osteogènica podent ser emprats per a la seva prediferenciació *in vitro* de manera efectiva. Per comprovar aquesta hipòtesi, en el desenvolupament de la present Tesi Doctoral s'han dissenyat suports de cultiu piezoelèctrics en 2 i 3 dimensions basats en l'ús del polímer piezoelèctric polifluorur de vinilidè (PVDF) combinats amb partícules magnetostrictives de ferrita de

cobalt (CFO). Aquesta combinació permet l'estimulació dels suports de cultiu aplicant un camp magnètic amb un bioreactor. Aquest camp genera la deformació del component magnetostrictiu, que és transmesa a la matriu polimèrica, deformant-la i generant un camp elèctric. Aquesta última és transmesa a les cèl·lules cultivades en aquests suports per estudiar-ne l'efecte sobre la diferenciació osteogènica.

Al primer capítol experimental es van desenvolupar i caracteritzar membranes electroactives de PVDF fabricades pel mètode de separació de fases induïda per no-solvents (NIPS). Es va emprar etanol com a no-solvent, cosa que va donar lloc a membranes homogènies altament poroses. Aquests suports de cultiu cristal·litzen en fase $\gamma$, una de les fases electroactives del PVDF. La seva alta porositat i hidrofobicitat va fer necessària l'optimització d'un recobriment basat en la tècnica de capa per capa (LbL), emprant recombinàmers similars a l'elastina (ELRs) que contenien seqüències d'adhesió cel·lular RGD. Després de l'optimització del protocol de recobriment, es va estudiar la resposta cel·lular inicial de les MSCs i es va comparar amb els mateixos suports recoberts únicament amb fibronectina adsorbida. Els resultats van revelar que la presència dels ELR és necessària per promoure l'adhesió inicial de les MSCs en aquest tipus de suports.

Al segon capítol es van desenvolupar membranes electroactives de PVDF combinades amb CFO, emprant el mateix mètode de fabricació que al capítol anterior, però usant aigua com a no-solvent. En aquest cas les membranes presentaven una estructura no simètrica, amb una superfície llisa, que va ser emprada per a cultiu cel·lular, i una altra porosa, així com diverses fases cristal·lines, però amb una majoria en fase $\beta$, la més electroactiva. Aquesta tècnica va permetre la incorporació efectiva de les nanopartícules. Es van recobrir les membranes mitjançant LbL amb col·lagen tipus I i heparina, creant un entorn biomimètic per a les MSCs. Es va realitzar un empelt inicial de grups amina a la superfície mitjançant un tractament alcalí que va permetre unir la primera capa del LbL. Un cop caracteritzat el recobriment es va estudiar el comportament de les MSCs, revelant que el recobriment mitjançant LbL resultava essencial per a la proliferació cel·lular en el cas de les membranes que contenien nanopartícules magnètiques.

L'elevada porositat de les membranes produïdes afecta a nivell biològic a l'adhesió de les MSCs i físic al procés de polarització dels suports de cultiu, imprescindible per obtenir la màxima resposta piezoelèctrica. Per això, en el capítol experimental tres es van desenvolupar nous materials més fins i plans, que en facilitessin tant la polarització com l'adhesió cel·lular inicial. Per això es van produir films de PVDF i PVDF-CFO cristal·litzats en presència del líquid iònic [Bmim][Cl]. La presència d'aquest va induir la nucleació del PVDF en fase $\beta$ als films, tot i ser obtinguts des de fos, la qual cosa sol generar fase $\alpha$, no electroactiva. El líquid iònic va ser eliminat una vegada produïda la cristal·lització i es va estudiar la resposta inicial de les MSCs, revelant la no citotoxicitat dels films i la capacitat de les cèl·lules per adherir-se i proliferar. Es va seleccionar un medi de cultiu mixt (1:1 medi osteogènic i adipogènic) per als experiments d'estimulació, basat en l'anàlisi de les adhesions focals. Es van realitzar assajos d'estimulació piezoelèctrica emprant un bioreactor magnètic i el medi seleccionat. Les MSCs van respondre a l'estimulació incrementant la longitud de les seves adhesions focals, així com reduint la presència de vimentina al citoplasma.

Finalment, es van dissenyar suports de cultiu piezoelèctrics en 3D. Per això es van desenvolupar microesferes de PVDF i PVDF-CFO mitjançant la tècnica d'electropulveritzat. Aquesta tècnica va permetre obtenir microesferes d'entre 1 i 2 μm de diàmetre, en fase β i amb la correcta incorporació de la ferrita de cobalt. Les microesferes es van encapsular en hidrogels de gelatina juntament amb les MSCs per crear un entorn tridimensional biomimètic. Aquesta aproximació no va resultar citotòxica per a les cèl·lules que, a més, després de 14 dies presentaven una morfologia completament estesa, característica d'aquest tipus cel·lular. Aquests suports de cultiu es van estimular emprant el bioreactor magnètic, en combinació amb medi de cultiu osteogènic. Després de 7 dies, es va observar un increment en l'expressió del factor de transcripció RUNX2 a les mostres estimulades, eix central de la ruta de senyalització osteogènica, demostrant que l'estimulació piezoelèctrica és capaç d'activar la diferenciació de les MSCs.

En resum, s'han desenvolupat i funcionalitzat plataformes de cultiu electroactives en 2D i 3D per a l'estimulació piezoelèctrica de les MSCs, demostrant que, efectivament, aquestes cèl·lules són capaces de respondre a aquest estímul físic.

# Glossary

| | |
|---|---|
| **[Bmim][Cl]** | 1-Butyl-3-methyl-imidazolium-chloride |
| **[Ch][DHP]** | 2-hydroxyethyl-trimethylammonium dihydrogen phosphate |
| **[Emim][Cl]** | 1-ethyl-3-methylimidazolium chloride |
| **2D** | Two-dimension |
| **3D** | Three-dimension |
| **AFM** | Atomic force microscopy |
| **ALP** | Alkaline phosphatase |
| **β-TCP** | β-tricalcium phosphate |
| **BMP** | Bone morphogenetic proteins |
| **BMPR** | Bone morphogenetic protein receptors |
| **BSA** | Bovine serum albumin |
| **BSP** | Bone sialoprotein |
| **CaM** | Calmodulin |
| **CaMK** | Calmodulin-dependent protein kinases |
| **cAMP** | Cyclic adenosine monophosphate |
| **CCFE** | Capacitively coupled electrical fields |
| **CCFE** | Inductive coupling |
| **CFO** | Cobalt ferrite oxide |
| **CNT** | Carbon nanotubes |

| | |
|---|---|
| **COL I** | Collagen type I |
| **DAB** | 1,4-diaminobutane dihydrochloride |
| **DAPI** | 2-(4-amidinophenyl)-1H-indole-6-carboxamidine |
| **DC** | Direct coupling |
| **DMA** | Dimethylacetamide |
| **DMEM** | Dulbecco's modified Eagle medium |
| **DMF** | Dimethylformamide |
| **DMSO** | Dimethyl sulfoxide |
| **DPBS** | Dulbecco's phosphate saline buffer |
| **DSC** | Differential scanning calorimetry |
| **ECM** | Extracellular matrix |
| **EDC** | 1-ethyl-3-(3 dimethylaminopropyl) carbodiimide hydrochloride |
| **ELRs** | Elastin-like recombinamers |
| **ERK 1/2** | Extracellular signal-regulated kinases 1/2 |
| **ES** | Electrical stimulation |
| **FA** | Focal adhesions |
| **FAK** | Focal adhesion kinase |
| **FBS** | Fetal bovine serum |
| **FDA** | Food and Drug Administration |
| **FESEM** | Field emission scanning electron microscopy |
| **FGF** | Fibroblast growth factor |
| **FIB** | Focused ion beam |
| **FTIR** | Fourier transform infrared spectroscopy |
| **GAPDH** | Glyceraldehyde-3-phosphate dehydrogenase |
| **GES** | General electrical stimulation |
| **GMP** | Good manufacturing practices |
| **GO** | Graphene oxide |
| **GPCR** | G-protein coupled receptors |
| **Grb2** | Growth factor receptor bound 2 |
| **HRP** | Horseradish peroxidase |
| **Hsp27** | Heat shock protein 27 |
| **IC** | Capacitive coupling |
| **IFN-γ** | Interferon-gamma |
| **IL** | Ionic liquid |
| **IL-17** | Interleukin-17 |
| **IL-β1** | Interleukin-beta 1 |
| **ITC** | Inverse transition cycling |
| **LbL** | Layer-by-layer |
| **M-CSF** | Macrophage colony stimulating factor |

| | |
|---|---|
| **MALDI-ToF** | Matrix-assisted laser desorption/ionization time-of-flight |
| **MAPK** | Mitogen-activated protein kinases |
| **ME** | Magnetoelectric |
| **MNP** | Magnetostrictive nanoparticles |
| **MP** | Membrane potential |
| **MSCs** | Mesenchymal stem cells |
| **MTS** | 3-(4,5-dimethylthiazol-2-yl)-5-(3-carboxymethoxyphenyl)-2-(4-sulfophenyl)-2H-tetrazolium |
| **NEAA** | Non-essential aminoacids |
| **NHS** | N-hydroxysuccinimide |
| **NICD** | Notch intracellular domain |
| **NIPS** | Non-solvent induced phase separation |
| **NMR** | Nuclear magnetic resonance |
| **NS** | Non-stimulated |
| **OCN** | Osteocalcin |
| **OM** | Osteogenic medium |
| **OPN** | Osteopontin |
| **OSX** | Osterix |
| **P/S** | Penicillin/Streptomycin |
| **PANI** | Polyaniline |
| **PCL** | Polycaprolactone |
| **PDMS** | Polydimethylsiloxane |
| **PEDOT** | Poly(3,4-ethylenedioxythiophene) |
| **PEFM** | Pulsed electromagnetic fields |
| **PFM** | Piezoresponse force microscopy |
| **PHB** | Polyhydroxybutyrate |
| **PKC** | Protein kinase C |
| **PLA** | Poly-lactic acid |
| **PLC** | Phospholipase C |
| **Ppy** | Polypyrrole |
| **PVDF** | Poly(vinylidine) fluoride |
| **PVDF-TrFE** | Poly(vinylidene fluoride-trifluoroethylene) |
| **RANKL** | Receptor activator of nuclear factor kappa-b ligand |
| **ROS** | Reactive oxygen species |
| **RUNX2** | Runt-related transcription factor 2 |
| **S** | Stimulated |
| **SDS-PAGE** | Sodium dodecyl sulphate polyacrylamide gel electrophoresis |
| **Sos** | Sons of sevenless |

| | |
|---|---|
| **TC** | Transformer-like coupling |
| **TCF/LEF** | T cell factor/ lymphoid enhancer factor |
| **TE** | Tissue engineering |
| **TGF-β1** | Transforming growth factor-β1 |
| **THF** | Tetrahydrofuran |
| **Tm** | Melting temperature |
| **TNF-a** | Tumour necrosis factor-alfa |
| **VEGF** | Vascular endothelial growth factor |
| **VGCC** | Voltage Gate Calcium Channels |
| **VSM** | Vibrating sample magnetometer |
| **Xc** | Crystallinity |
| **XPS** | X-ray photoelectron spectroscopy |

# Introduction

This chapter was adapted from the review article published in *Biomaterials Advances.*

Guillot-Ferriols, M.; Lanceros-Méndez, S.; Gómez Ribelles, J. L.; Gallego-Ferrer, G. Electrical Stimulation: Effective Cue to Direct Osteogenic Differentiation of Mesenchymal Stem Cells? *Biomater. Adv.* 2022, 138 (May).

DOI: 1016/j.bioadv.2022.212918.

**Personal contribution**

The ideas presented in this review article were conceptualized by M. Guillot Ferriols. First version of the manuscript and figure design was carried out by M. Guillot Ferriols. S. Lanceros Méndez, J.L Gómez Ribelles and G. Gallego Ferrer helped with conceptualization, reviewed the manuscript and provided financial support.

## 1. Bone Tissue

Bone is a strong connective tissue, which performs several functions within the human body. It is responsible for movement and structural support. It also protects diverse organs including the bone marrow and regulates mineral homeostasis, constituting calcium reservoirs that can be mobilized to the bloodstream under demand. The human skeleton is composed by 206 bones, that can be classified, attending to their shape, into long (extremity bones such as femur and humerus, in charge of providing support), short (tarsal, carpal and vertebrae, providing movement and stability) and flat (skull, ribs, coxal or scapulae, focused on organ protection) (Strandring 2008).

Adult bone tissue is constituted by spongy or trabecular and compact or cortical bone, which differ in their macroscopic aspect and the way mineralized sheets, or lamellae, are organized in their structure. Cortical bone presents a dense aspect and is usually found in the peripheral region of mature bones. On the other hand, trabecular bone shows a honeycombed structure with interconnected pores and it is located within metaphysis, epiphysis, and medullary cavity at the end of long bones, and in short bones as well (Tzelepi et al. 2014).

From a structural point of view, in cortical bone, lamellae are organized around the blood vessels, conforming closely coupled columns called osteons or Haversian systems, the functional unit of bone, as can be seen in Figure 1. Each one of these osteons presents a central canal, or Haversian canal, in which the capillaries, post-capillary venules and nerves can be found surrounded by a wall formed by several overlapping lamellae. These canals are created by bone resorption. Osteoclasts, remodelling cells, are in charge of destroying bone tissue, creating cavities that are filled by osteoblasts, bone matrix forming cells. Osteoblasts are located in the central canal, close to the blood vessels and are in charge of producing new lamellae around it. When they reach a certain stage of maturation, osteoblasts become osteocytes and remain trapped in small cavities called lacuna (Figure 1). Spongy bone can also present Haversian systems in the large trabeculae, whereas smaller ones are made of bone lamellae oriented in the same direction as trabeculae. Bone marrow is found in the spaces between trabeculae (Tzelepi et al. 2014).

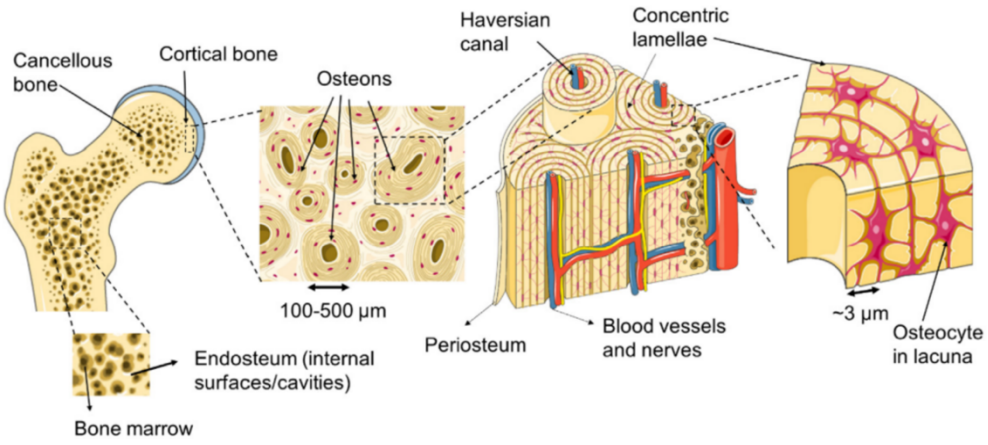


**Figure 1. Schematic representation of bone structure. Macroscopic to microscopic view of trabecular and compact bone. Adapted from (D. Lopes et al. 2018).**

## 1.1. Microstructure of bone

### 1.1.1. Bone cell types

Bone is a highly cellular tissue and despite of its macroscopic structure and the organization of its lamellae, cell types are usually conserved.

*Osteoblasts* are extracellular matrix (ECM) producing cells, responsible for its synthesis and calcification. They are derived from the differentiation of osteoprogenitor or mesenchymal stem cells (MSCs), spindle-shape cells that can be found in the periosteum (the thin connective tissue layer that covers the external surface of bones) and the osteons (Shapiro 2008).

*Mesenchymal stem cells* are multipotent stem cells that can be found, apart from bone, in many organs and tissues in the human body. These cells were first described by Friedenstein in 1974 (Friedenstein 1976). MSCs are characterized by their plastic adherence when cultured in standard conditions, the expression of the surface antigens CD105, CD73 and CD90, the lack of expression of CD45, CD34, CD14, CD19 and HLA class II and their differentiation capacity into osteoblasts, adipocytes and chondroblasts (Dominici et al. 2006).

Under physiological conditions, MSCs osteogenic differentiation is a complex and orchestrated process which involves the activation of selected signalling pathways and leads to the progressive expression of osteogenic-related genes, starting with the key integrator transcriptional factor RUNX2 (Runt-related transcription factor 2) (Rahman et al. 2015). On a first stage of differentiation, MSCs become *preosteoblasts*, an intermediary state from progenitor cells to mature osteoblasts. They are characterized by the expression of RUNX2, which in turn activates the expression of the zinc finger transcription factor Osterix (OSX). Subsequently, alkaline phosphatase (ALP) and collagen type I (COL I) are expressed and can be considered as mid-stage indicators of the differentiation process (Figure 2) (Franz-Odendaal, Hall, and Witten 2006). Preosteoblasts show a spindle-shape similar to MSCs and are able to proliferate but not to secrete bone matrix, only precursor molecules of collagen type I (Cohen 2006). When the differentiation process progresses, preosteoblasts acquire a cuboidal shape, and give rise to mature *osteoblasts*. Although they also express ALP and COL I, the expression of bone sialoprotein (BSP), osteocalcin (OCN), osteopontin (OPN) and several bone morphogenetic proteins (BMP) may be used to differentiate these two cell types, as depicted in Figure 2 (Franz-Odendaal, Hall, and Witten 2006)

During embryonic development, MSCs osteoblastogenesis can take place by two different mechanisms, endochondral and intramembranous ossification, which produce microscopically indistinguishable bone structures. While intramembranous ossification is basically observed in the formation of flat bones of the skull, endochondral ossification gives rise to osteoblasts in the rest of the bones. The difference between these two processes is based on the presence of an intermediary cartilaginous tissue that serves as a template to produce the bone lamellae (D. Lopes et al. 2018).

During endochondral ossification MSCs give rise to chondrocytes and perichondral cells. The chondrocytes proliferate and deposit extracellular matrix, rich in proteoglycans and collagen type II. In the meantime, the perichondral cells differentiate into osteoblasts which deposit mineralized bone generating a centre of ossification in the cartilaginous tissue. The chondrocytes undergo hypertrophy and swelling, followed by a secretion of collagen type X, matrix mineralization and chondrocyte apoptosis. The cartilage is then slowly resorbed and the structure is invaded by blood vessels accompanied by MSCs while the osteoblast deposit layers of osteoid along the surface of the cartilage (D. Lopes et al. 2018).

On the other hand, intramembranous ossification is based on the differentiation of MSCs into osteoblasts, with no cartilaginous anlage. The osteoblasts begin to synthesize bone matrix that will mineralize, entrapping the cells that will become osteocytes (D. Lopes et al. 2018).

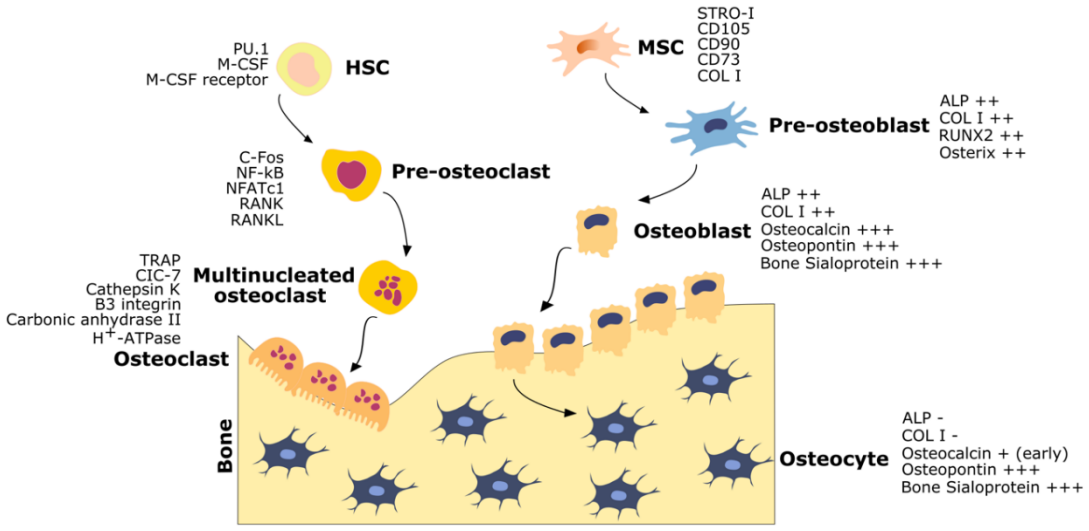


**Figure 2. Schematic representation of cell types that conform bone tissue, including mesenchymal and hematopoietic progenitors. Mesenchymal stem cells (MSCs) differentiate into pre-osteoblasts that later become osteoblasts. Some of them proliferate and remain in the bone surface while others become osteocytes and get trapped in the bone matrix. Hematopoietic stem cells (HSC) differentiate into pre-osteoclasts that after fusion give rise to multinucleated osteoclasts and finally mature osteoclasts. Figure adapted from (D. Lopes et al. 2018).**

Once an osteoblast is entrapped in the mineralized bone matrix it is considered an *osteocyte*. Osteocytes are the most numerous cell type in the bone, with a presence of almost 95 % among all cell types. Their phenotype is characterized by the presence of numerous dendrites extended along the bone matrix that allow their communication and their ability to sense mechanical stimuli. Upon mechanical stimulation osteocytes influence the activity of MSCs, osteoblasts and osteoclasts that can respond by remodelling bone mass. They can also sense changes in ion concentration and trigger the ion exchange between bone matrix and extracellular fluid (Tzelepi et al. 2014).

*Osteoclasts* are multinucleated giant cells with the ability to remodel the bone matrix by resorbing bone. Unlike osteoblasts and osteocytes, osteoclasts are derived from the hematopoietic lineage. The fusion of preosteclasts, originated from the differentiation of mononuclear hematopoietic progenitor cells, gives rise to osteoclasts, as can be seen in Figure 2. Osteoclasts can be found in Howship's lacunae or resorption pits, spaces they create due to their catalytic activity. The secretion of hydrogen ions leads to the acidification of the bone microenvironment dissolving the mineral extracellular matrix. Cathepsin K is also secreted to enzymatically digest the collagen type I that conforms the insoluble fraction of the matrix. Osteoclast maturation is regulated by osteoblasts and MSCs that produce receptor activator of nuclear factor kappa-β ligand (RANKL) and macrophage colony stimulating factor (M-CSF) (Boyle, Simonet, and Lacey 2003).

Osteoblast, osteocyte and osteoclast activities are tightly regulated and influenced by each other through the secretion of diverse factors. This regulation should be balanced to maintain the equilibrium between bone formation and bone resorption, which disruption can produce bone pathologies such as osteoporosis.

### 1.1.2. Bone extracellular matrix

All these cell types are immersed in an extracellular matrix (ECM) composed by organic and inorganic components.

Bone organic ECM represents 30 % of bone's dry weight and it basically contains collagenous proteins (90 %). Most of this collagen is organized in type I fibres formed by two a1 chains and one a2 chain which are assembled into a triple helix. Collagen is produced by osteoblasts and organized in layers where collagen fibres are highly oriented and patterned. Other non-collagenous proteins are present although in a small proportion (Nair et al. 2013). Osteocalcin, osteopontin, osteonectin, fibronectin and bone sialoprotein II are either produced by osteoblast or concentrated from the serum and are involved in bone's mineralization (Shapiro 2008).

A major part of bone ECM is composed by inorganic components. They represent approximately 60-70 % of its composition. Hydroxyapatite [$Ca_{10}(PO_4)_6(OH)_2$] is the most common bone mineral and mineralizes in the gaps left by the organization of collagen fibrils. This association generates a scaffold responsible for bone's stiffness and strength (Shapiro 2008).

Bone's extracellular matrix not only provides structural support but it plays a major role in bone homeostasis. It is able to retain growth factors, such as BMP, that will regulate cellular functions and intervene in bone growth and regeneration. Also, the presence of adhesion sequences in some of the proteins that conform its organic matrix mediate the interaction between bone cells and bone matrix through adhesion molecules. Moreover, some of its constituents provide physical cues to bone residing cells.

## 1.2. Bone's adaptative and regenerative potential

Bone is a dynamic tissue with the ability to repair and self-regenerate. Many fractures heal without further complications in a process that resembles many events that take place

during embryonic development. Fracture-healing may be considered as a truly regenerative process, since the outcome results in a new bone tissue with the same structure, cellular composition and biological function as the pre-injured one (Einhorn and Gerstenfeld 2015).

Bone regeneration after injury follows a four-step process. Immediately after the damage is produced, a hematoma is formed to contain the bleeding. This hematoma is infiltrated by platelets, macrophages and other inflammatory cells that generate an inflammatory state by secreting cytokines and growth factors. These factors promote the recruitment of mesenchymal stem cells, specially from the periosteum and bone marrow, in a process called homing. Mesenchymal stem cells are key players in *in vivo* bone regeneration, their presence is essential for the process. The following steps are similar to endochondral ossification, in most cases. First, a fibrocartilage template is formed by chondrocytes derived from mesenchymal progenitors. This structure is called soft callus and serves to provide mechanical support to the fracture. After, MSCs differentiate into osteoblasts in the presence of osteogenic factors, especially members of the BMP family. Osteoblasts deposit a mineralized bone matrix in a process known as primary bone formation and soft callus is gradually removed and replaced by a hard callus. Finally, the woven bone is remodelled into cortical or trabecular bone configuration. Osteoclasts take part in the final step of the process (Schindeler et al. 2008; Einhorn and Gerstenfeld 2015).

This regeneration process takes place when the fracture does not exceed a critical size. Critical-sized bone defects require further clinical intervention and will be discussed in subsequent sections.

Bone dynamics also include the ability to adapt to mechanical stress. In the 19$^{th}$ century Julius Wolff proposed what later would be called Wolff's Law; bone is remodelled to meet its mechanical demands. In other words, bone is deposited and reinforced in the regions where a mechanical stress is applied. A great example that confirms it is the loss of bone mass by astronauts that have been on a mission for long time or the increased bone density of diverse athletes such as tennis players or weightlifters (J. H. Chen et al. 2010).

As main effectors of bone regeneration and growth, osteoblasts, osteocytes and their mesenchymal progenitors should be involved in this response to mechanical stress. How these cell types are able to perceive forces has been a matter of debate. Since the discovery of bone piezoelectric properties, this property was proposed as a mechanism by which osteoblast, osteocytes and MSCs could detect mechanically stressed areas within the bone.

## 1.3. Bone's piezoelectricity

Piezoelectricity is defined as the generation of electricity due to the asymmetric displacement of ions or charges and the subsequent change in the electric polarization produced by a mechanical deformation. In other words, it is the conversion of the mechanical strain into electrical output. Piezoelectric materials can also display a converse piezoelectric effect, a mechanical deformation is produced when a voltage is applied (Z. L. Wang 2007).

Bone's piezoelectricity was first described by Yasuda in 1954. After the discovery, studies on boiled bone revealed that the observed piezoelectric properties were not ascribable to living cells. Therefore, the response should had been produced by some other component of bone's structure (Fukada and Yasuda 1957). Piezoelectric properties were attributed to the presence of the collagen fibres that form the organic component of its extracellular matrix. Collagen fibres are organized in α-helices within bone's ECM forming a right-handed coil, as can be seen in Figure 3I. The -CO- and -NH- units present in the amide bonds of the backbone amino acids of the protein can act as permanent dipoles (Figure 3I). The positively and negatively charged centres are aligned in the helical structure of the α-helix and cause significant permanent polarization. When the collagen fibres slip past each other under tension or compression, the distortion of the dipoles generates a surface charge (T. Zheng et al. 2020; Rajabi, Jaffe, and Arinzeh 2015).

This hypothesis was confirmed by measuring the piezoelectricity of single collagen fibres using a piezoresponse force microscopy (PFM), a modification of atomic force microscopy (AFM) where an electric field is applied through the sample and the deformation due to the piezoelectric effect is detected by the AFM tip. The measurements revealed that collagen fibrils showed lateral piezoresponse along the fibril axis, revealing the unidirectional polarization (Minary-Jolandan and Yu 2009). AFM and PFM images are shown in Figure 3II.

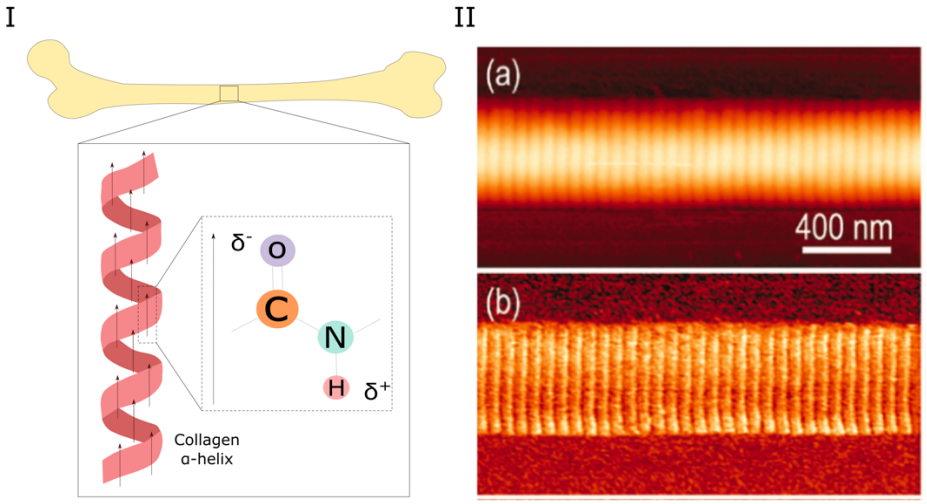


**Figure 3. I. Illustration of a collagen α-helix molecule present in bone's organic extracellular matrix, responsible for the piezoelectricity due to the permanent dipoles associated to the -CO- and -NH- units present in the amide bonds. Adapted from (Guillot-Ferriols et al. 2022) II. High resolution piezoresponse force microscopy images showing piezoelectric heterogeneity in single collagen fibrils. (a) Topography image showing a collagen fibril on Au-coated Si surface; (b) PFM piezoresponse amplitude image showing the variation in piezoresponse in the gap and overlap regions (Minary-Jolandan and Yu 2009).**

As soon as piezoelectric properties of bone were described they were suggested as a potential mechanism to explain bone's capacity to adapt to mechanical stress. The applied stress generates local potential gradients along the collagen fibres providing a stimulus sensed by bone-forming cells.

This hypothesis has been a matter of debate since there are some dissimilarities between the way strain potential is generated in dry and wet bone. While in dry bone piezoelectricity is considered as the main mechanism, in wet bone its role is less clear and streaming potential was more accepted. Ahn an Grodzinsky proposed an hypothesis combining both mechanisms where surface charge density of collagen fibers is increased by piezoelectricity, which leads to an increase in zeta potential, intensifying the streaming potential (Ahn and Grodzinsky 2009).

## 2. MSCs as main candidates for bone regeneration therapies

Bone self-regeneration allows fracture healing without additional difficulties. Nevertheless, when the defect exceeds a critical size due to trauma, tumour resection or infection, challenging medical interventions are required (Roddy et al. 2018). Injuries longer than 2 cm are not usually resolved spontaneously in humans (Nauth et al. 2011).

An autogenous bone graft from the iliac crest is the gold standard treatment nowadays since it possesses osteogenic, ostoinductive and osteoconductive properties, is histocompatible and has no disease transmission risk. However, it involves some associated drawbacks such as increased patient morbidity, lack of vascularization or the limited quantity and availability of healthy tissue (Tang et al. 2016; Oryan et al. 2014). Donor site morbidity was reviewed by Younger and Chapman in 243 autogenous bone graft procedures and reported major complications in 8.6 % of the studied cases and minor complications in 20.6 % (Younger and Chapman 1989). Other options, including allografts or xenografts, can be related to disease transmission, immune rejection and may fail to be osteoinductive in humans (Jamjoom and Cohen 2015).

MSCs-based therapies have been proposed as a potential alternative for bone regeneration. Mesenchymal stem cells are the obvious choice due to their self-renewal and differentiation capacity to osteoblasts, among other cell types such as chondrocytes, adipocytes and hematopoiesis supporting-stroma cells (Bianco et al. 2001). Their immunomodulatory properties and the fact that they are easy to obtain make them perfect candidates to attain suitable clinical outcomes (Uccelli, Moretta, and Pistoia 2008).

For bone reconstruction purposes, different therapeutic approaches including the use of MSCs have been developed. These approaches cover the use of undifferentiated or pre-differentiated MSCs combined or not with a biomaterial that serves as a matrix.

The easiest approach consists of the obtainment of the bone's marrow mononuclear fraction that contains the MSCs in a small proportion, by means of an aspirate. The aspirate is injected percutaneously in the injured site and MSCs are expected to differentiate into osteoblasts to contribute to the bone regeneration process. The outcome is determined by the MSCs concentration in the aspirate, which can be concentrated prior to injection, but

also by their differentiation capacity (Hernigou et al. 2006). Decreased bone formation can be observed in old bone marrow cells due to their age reduced osteogenic differentiation potential.

MSCs, previously selected from the mononuclear bone marrow fraction, can also be combined with synthetic or natural osteo-conducting matrices before implantation. Calcium-phosphate ceramics are the most common osteoconductive materials used for bone replacement although they lack to be osteogenic nor osteoinductive. They are usually combined with hydroxyapatite and tricalcium phosphate granules (Laurencin, Khan, and El-Amin 2006).

These techniques rely on MSCs potential to differentiate at the injured site. Although the number of pre-clinical studies using MSCs and biomaterials to treat bone defects has increased in the recent years, the approaches that made their way into clinical studies, with low number of patients, show non consistent results (Perez et al. 2018; Gómez-Barrena et al. 2015). These inconsistent results may be related with MSCs limitations regarding cell selection, association of cells and biomaterials, MSCs susceptibility to compromised microenvironments and the lack of osteogenic differentiation of the implanted cells. MSCs are highly sensitive to harsh environments, which can be one of the reasons for their inefficient osteogenic differentiation once implanted. The altered homeostasis of the stem cell niche at the injured site may not provide the right cues to initiate the osteogenic differentiation cascade in MSCs.

These drawbacks can be solved by means of priming or pre-differentiation approaches.

## 2.1. Mesenchymal stem cells priming

The priming concept can be considered as a pre-condition or preparation of the cells for some specific function or lineage-specific differentiation to enhance their therapeutic potential. It may involve cell activation, molecular signalling, genetic or epigenetic modifications and phenotypic changes (Noronha et al. 2019). Originally, this term was used in the immunology field to refer to cells that had been licensed or pre-conditioned with pro-inflammatory molecules (Y. Zhou, Tsai, and Li 2017), nevertheless, it has been adapted for the stem cell pre-conditioning scope. Priming approaches exploit the best properties of MSCs and prepare them for an inhospitable microenvironment *in vivo*.

Some examples of priming techniques for MSCs are hypoxia treatment, 3D culture (spheroids), growth factors, cytokines, genetic modification, pharmacological or chemical agents and physical cues. Although the final aim of these pre-conditioning methods is to enhance MSCs therapeutic potential, different methods improve different MSCs characteristics. Regarding the scope, three categories can be described:

- Pre-condition treatments that aim to enhance MSCs therapeutic potential by improving their immunomodulatory properties.
- Priming approaches that alter survival characteristics such as migratory, anti-apoptotic and angiogenic properties.
- Pre-differentiation approaches that enhance MSCs fate determination.

Since MSCs-based therapies have emerged as an option for bone regeneration, priming should be focused on improving MSCs engraftment and osteogenic differentiation potential when pursuing the treatment of bone disorders.

As a general picture, priming approaches related with the enhancement of immunomodulatory MSCs properties are usually based on the use of pro-inflammatory cytokines. MSCs priming with cytokines improves the immunosuppressive function by increasing their secretion of anti-inflammatory and immunomodulatory factors. Usually, once obtained, MSCs are cultured in the presence of interferon-gamma (IFN-$\gamma$), tumour necrosis factor-alpha (TNF-$\alpha$), interleukin-beta1 (IL-$\beta$1) or combinatory strategies of the aforementioned cytokines to increase their immunomodulatory potential (Noronha et al. 2019). Although cytokines are not usually used to determine MSCs fate, the results about this topic are conflicting. Some authors have reported the use of interleukin-17 (IL-17) to promote human MSCs osteogenic differentiation and inhibition of adipogenic differentiation (Shin, Shin, and Noh 2009). Nevertheless, Chang et al. (Chang et al. 2013), have shown a suppression in osteoblastogenesis in murine MSCs while Mojsilović et al. (Mojsilović et al. 2011) claim to observe no effect in the differentiation potential of murine MSCs. This type of priming, then, is usually applied for MSCs used in inflammatory disease therapies.
MCSs have also been primed with hypoxia, *in vitro* low oxygen concentrations (1-7 %), that resemble the ones found in the bone marrow (Fehrer et al. 2007). Hypoxia pre-condition increases resistance to oxidative stress which improves the engraftment, survival in ischemic microenvironments and angiogenic potential (Noronha et al. 2019). Nevertheless, the use of hypoxia on determining MSCs fate has a controversial role in literature. Some authors have reported a significant impairment of osteogenic differentiation when cells were cultured under hypoxia (P. Zhang et al. 2017; Malladi et al. 2006; Potier et al. 2007; Volkmer et al. 2010), others have reported enhanced osteogenic differentiation (Grayson et al. 2006; Lennon, Edmison, and Caplan 2001; Boyette et al. 2014) or even equal differentiation potential of MSCs cultured under both normoxia and hypoxia (Y. Hu et al. 2018; Holzwarth et al. 2010; J. Liu et al. 2015). These diverse data are associated to a variation in the experimental design among studies. The moment when hypoxia is introduced can vary, the studies generally involving expansion in normoxia and cells differentiation under hypoxia or expansion in hypoxia and differentiation in normoxia.

## 2.2. Priming approaches for MSCs osteogenic fate determination

The most common approach for determination of MSCs osteogenic fate *in vitro* is based on biochemical induction. MSCs are usually cultured with osteogenic medium (OM) containing dexamethasone, ascorbic acid and glycerophosphate.

The experimental results support the use of pre-differentiated MSCs for bone regeneration therapies against pristine MSCs. Peters et al. (Peters et al. 2009) demonstrated that MSCs cultured in osteogenic medium prior to transplantation showed a better healing in delayed bone healing than non-pre-differentiated MSCs. Non-pre-differentiated MSCs, in fact, showed the same outcome than the Sham group, contrary to what was expected at first.

The stage of commitment in which MSCs are delivered also plays an important role. Castano-Izquierdo et al. (Castano-Izquierdo et al. 2006) showed that MSCs cultured in

osteogenic medium for 4 days retained the highest regenerative potential compared to 10 and 16 days of culture and MSCs cultured in basal medium. 4-day pre-differentiated MSCs were not osteoblasts and kept a strong proliferation potential that allow them to increase their number after implantation. At the same time, the short exposure may have already initiated their osteoblastic differentiation promoting their healing capacity.

Yoshikawa et al. (Yoshikawa, Ohgushi, and Tamai 1996) compared the efficiency of MSCs primed in basal or osteogenic medium containing dexamethasone seeded on a ceramic scaffold by implanting them at syngeneic rat subcutaneous sites. One week after the implantation, primed scaffolds showed histologically new bone formation while non-primed did not show it. These results are supported by Ye et al. (X. Ye et al. 2012). Whose work demonstrated that pre-differentiated MSCs seeded on β-tricalcium phosphate (β-TCP) were more efficient in the formation of ectopic bone in athymic mice than non-pre-differentiated MSCs delivered on the same scaffold or non-pre-differentiated MSCs without matrix. This work corroborates that ectopic osteogenesis is more dependent on the pre-differentiation treatment prior to implantation than on the matrix cells are delivered together with. Also, osteo-differentiated MSCs hold the highest potential concerning *in vivo* bone regeneration.

Although most of the approaches for MSCs osteogenic priming are based on the use of dexamethasone, it can produce the undesired guidance of MSCs towards the adipogenic lineage besides inducing osteogenic differentiation (Ghali et al. 2015). Moreover, MSCs osteogenic phenotype induced by biochemical pre-treatment is reversible after stimuli deprivation unless cells are deployed with an extracellular matrix resembling environment (Hoch et al. 2016).

Due to the reduced specificity of this type of biochemical approach, biophysical cues have been investigated as possible candidates to direct MSCs differentiation in bone tissue engineering strategies, since their precise action has been demonstrated by metabolomic techniques (Hodgkinson et al. 2021). Recent evidence for biophysical control of MSCs differentiation has been described using cyclic mechanical strain, shear fluid stress, matrix stiffness and topography, microgravity or electrical stimulation (Halim et al. 2020).

Electrical stimulation (ES) has gained attention since bone piezoelectric properties were described and was correlated with the bone's capacity to adapt to mechanical stress and self-regenerate (Fukada and Yasuda 1957; Ahn and Grodzinsky 2009; Yasuda 1953). From then on, hundreds of articles appeared in the scientific literature describing the effects of electrical stimulation on bone healing. Basset, Pawluk & Pilla (Basset, Pawluk, and Pilla 1974) were among the first to prove the therapeutic effect of inductively coupled electromagnetic fields in canine osteotomies in 1974. Later, many clinical studies reported successful outcomes in the treatment of non-union fractures (Simonis et al. 2003; Traina et al. 1991; Gupta, Srivastava, and Avasthi 2009), osteoporosis (Tabrah et al. 1990; H. F. Liu et al. 2013) or osteonecrosis (Massari et al. 2006; Cebrián et al. 2014) in humans, delivering ES by means of capacitively coupled electrical fields (CCFE) or pulsed electromagnetic fields (PEMF). This led to the production of medical devices able to provide electrical cues for clinically treating indicated bone defects, the first of which was approved by the US Food and Drug Administration (FDA) in 1979.

The satisfactory clinical outcomes of ES at tissue-level encouraged the scientific community to try to explain the underlying cellular mechanism. Mesenchymal stem cells are key players in *in vivo* bone regeneration being the main effectors in different stages of bone repair. These different stages of bone repair take place in the bone niche, where MSCs find themselves subjected to an electrically active environment due to the presence of the collagen fibres that conform the organic component of bone's ECM. This physical stimulus together with other biochemical cues may play a role in MSCs differentiation towards the osteogenic lineage, supporting the regeneration of bone tissue and enhancing the results of regenerative therapies. It can be useful for inducing MSCs commitment or priming in bone tissue engineering strategies when combined with the appropriate scaffolds, recapitulating aspects of the *in vivo* niche.

## 3. *In vitro* MSCs electrical stimulation

Different approaches have been used to try to induce osteogeblastogenesis in MSCs using electrical stimulation. The different methods can be classified in general electrical stimulation (GES) and substrate mediated electrical stimulation, where conductive and piezoelectric materials can be found.

### 3.1. General electrical stimulation

General electrical stimulation is based on the application of an electric field to cells cultured either on tissue culture plates or on non-conductive scaffolds, with the electrical stimulus transmitted through the culture medium. Three main methods of delivering this cue have been described: Direct Coupling (DC), Capacitive Coupling (CC) and Inductive Coupling (IC) (Thrivikraman, Boda, and Basu 2018; C. Chen et al. 2019; Balint, Cassidy, and Cartmell 2013).

#### 3.1.1. Direct coupling

In the direct coupling method conductive electrodes are placed inside the cell culture wells or stimulation chamber in direct contact with the cell culture medium and the MSCs. Few authors have described this approach to exploring MSCs differentiation towards the osteogenic lineage. Electrical fields ranging from 2 to 3300 V/m have been used (Balint et al. 2013; Leppik et al. 2018; Mobini, Leppik, and Barker 2016; Mobini et al. 2017; Srirussamee et al. 2021; Hronik-Tupaj et al. 2011; Tandon et al. 2009; Hammerick et al. 2010; Z. Zhao et al. 2011). A schematic representation of direct coupling method can be found in Figure 4.

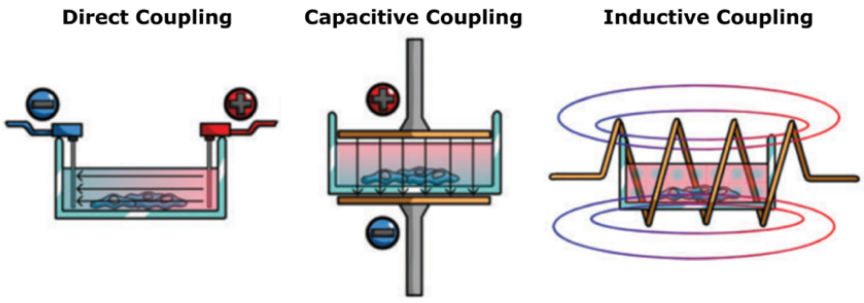


**Figure 4. The three main techniques to deliver general electrical stimulation, direct, capacitive and inductive coupling. Adapted from (Balint, Cassidy, and Cartmell 2013).**

Barker's group made an in-depth study of the effect of DC on MSCs differentiation by means of a stimulation chamber composed of platinum electrodes coupled to a 6-well plate lid. Their studies showed that DC ES of 100 V/m for 1 hour/day, combined with osteogenic medium upregulated genes related to the osteogenic differentiation process (RUNX2, OPN and COL I). However, it also activated different cellular mechanisms in MSCs from different sources (bone marrow and adipose tissue) (Mobini et al. 2017).

This stimulation combined with β-TCP scaffolds, enhanced ALP activity, as well as Transforming growth factor-β1 (TGF-β1), BMP-2 and OPN expression to a greater extent than cells cultured on tissue culture plates. Interestingly enough, calmodulin (CaM) was also up-regulated compared to the control, suggesting the involvement of the calcium/calmodulin pathway in the ES mediated differentiation process (Leppik et al. 2018).

The combination of ostoinductive factors with direct coupling stimulation has also been explored by Hronik-Tupaj et al. (Hronik-Tupaj et al. 2011). Cells electrostimulated in OM supplemented with BMP-2 showed upregulated ALP and COL I expression compared to non-stimulated cells cultured in OM plus BMP-2. Stress markers such as heat shock protein 27 (Hsp27) were also upregulated, although the relationship between stress markers, osteogenic markers and ES is not yet fully understood.

This approach has certain disadvantages, including the production of reactive Faradic by-products from the electrochemical reactions (hydrogen peroxide, hydroxyl ions and other free radicals), changes in the pH or the oxidation of bare metallic electrodes, which can liberate traces into the cell culture medium. Also, the cells closest to the electrodes can suffer morphological changes (Mobini, Leppik, and Barker 2016). Concerned about these facts, Srirussamee et al. (Srirussamee et al. 2021) studied the effect of the $H_2O_2$ produced by platinum electrodes used for DC electrical stimulation in MSCs differentiation. Surprisingly, $H_2O_2$ produced by ES enhanced MSCs proliferation, without causing oxidative damage, but did not have any influence on their differentiation. However, by-products other than $H_2O_2$ enhanced OPN expression in electrically stimulated cells.

To overcome these issues some researchers have used different setups consisting of isolated chambers connected via agar salt bridges to external Ag/AgCl electrodes immersed in Steinberg's solution. In this approach short stimulation times (only 2 hours at the beginning of the culture) have demonstrated that MSCs can migrate towards the anode, but the short stimulation time neither increases or reduces their osteogenic potential based on calcium deposition analysis using OM (Z. Zhao et al. 2011). Reduced expression of osteogenic related gene OPN was found in the presence of growth medium (Tandon et al. 2009). Longer times and continued stimulation may be needed to induce osteogenic differentiation, as described by Hammerick et al. (Hammerick et al. 2010), in which 6 h/day stimulation enhanced ALP, COL I and OPN expression, probably due to the increased cytosolic free-calcium and reduced cyclic adenosine monophosphate (cAMP).

### 3.1.2. Capacitive coupling

Capacitive coupling is a non-invasive electrical stimulation method in which an electric field is created between two parallel conductive layers, capacitor plates, connected to a generator. These are on the edges of the cell culture chamber or cell culture well, usually above and below the cell culture medium, but not in contact with it. A small gap of air is left between the upper conductive layer and the cell culture medium in the well, an illustration of this stimulation method is depicted in Figure 4. If this space between the medium and the top capacitor plate is missing, the approach is known as *semi-capacitive coupling*. The electric field created is homogeneously transmitted through the cell culture medium and the cells are evenly stimulated, whatever their position in the cell culture well is (Hartig, Joos, and Wiesmann 2000; Griffin et al. 2011).

This approach has not been reported for MSCs stimulation to induce osteogenic differentiation. Capacitive coupling by capacitor plates not in contact with the cell culture medium to stimulate other osteogenic cell types such as osteoblasts has been described though (Hartig, Joos, and Wiesmann 2000; Stephan et al. 2020; Clark, Wang, and Brighton 2014).

### 3.1.3. Inductive coupling

Inductive coupling stimulation is based on inducing an electric field by means of a conductive coil or a solenoid around the cell culture system. An alternating current flows through the coil generating a magnetic and an alternating electric field perpendicular to the magnetic (Pickering and Scammell 2002) (Figure 4). This stimulation method avoids direct cell contact with the electrodes and eliminates the presence of undesirable by-products.

Inductive coupling is the most commonly used approach in terms of ES for stimulating MSCs. There is no consensus on the optimal stimulation conditions to guide MSCs differentiation towards the osteogenic lineage, making comparison between the published research studies difficult. Different magnetic field densities, frequencies, pulse durations and stimulation times have been applied (Bagheri et al. 2017; Ferroni et al. 2018; Petecchia et al. 2015; Fu et al. 2014; L. Y. Sun et al. 2010; Tsai et al. 2009; Jansen et al. 2010; Lim et al. 2013; Schwartz et al. 2008; Yong et al. 2014; Martini et al. 2020; Hess, Neubert, et al. 2012). However, it seems clear that osteogenic medium is required in combination with electromagnetic fields (EMF) to induce an osteogenic phenotype, although some authors have reported the effect of EMF on osteogenic differentiation using growth medium

Petecchia et al. (Petecchia et al. 2015) found that pulsed EMF by its own was not enough to enhance ALP and COL I expression, while the combination with OM increased these early osteogenic markers through the expression of L-type Voltage Gate Calcium Channels (VGCC) and the modulation of the concentration of cytosolic free $Ca^{2+}$. These results agree with Bagheri et al. (Bagheri et al. 2017), who combined pulsed EMF with OM, describing a synergistic effect which enhanced calcium deposition, ALP production and expression of osteogenic markers (RUNX2, Dlx5, OSX) compared to OM alone.

Martini et al. (Martini et al. 2020) went further by also adding BMP-2, proving additive effects due to the simultaneous activation of Smad 1/5/8 and p38 MAPK pathways. These results

disagree with those obtained by Schwartz et al. (Schwartz et al. 2008), when calcium phosphate disks combined with PEMF and BMP-2 were needed to produce a synergistic effect, and not only tissue culture plates as cell substrate. Changes in the cell culture surface make MSCs more sensitive to BMP-2 and BMP-2 treated cells are more responsive to PEMF. This supports the hypothesis that PEMF can influence MSCs osteogenic differentiation, although an osteoblast-inductive stimulus combined with an osteogenic environment is required.

PEMF stimulation strategy inevitably links the presence of an electric and a magnetic field, which can also contribute to MSCs stimulation. To get over this disadvantage Hess et al. (Hess, Jaeschke, et al. 2012; Hess, Neubert, et al. 2012) developed a device based on Transformer-like Coupling (TC) to apply electrical stimulation without the interference of a magnetic field. Their results confirm firstly that PEMF alone cannot induce osteogenic differentiation unless combined with OM, and secondly supports Schwart's hypothesis. MSCs cultured in high-sulfated hyaluronan derivatives, which are able to present growth factors efficiently, may be acting as the BMP-2 in the supplemented medium.

## 3.2. Substrate-mediated electrical stimulation

Substrate-mediated electrical stimulation uses conductive and/or electroactive supports to apply an electrical stimulus directly to cultured cells.

### 3.2.1. Conductive cell culture supports

Electrically conductive polymers are one of the most popular choices when developing cell culture supports for substrate-mediated stimulation due to their chemical, electrical, and physical tailoring possibilities. Among the generally investigated polymers for tissue engineering applications, such as polypyrrole (PPy), poly(3,4-ethylenedioxythiophene) (PEDOT) or polyaniline (PANI) PPy is one of the most intensively studied. In the context of tissue engineering, polypyrrole is mainly used in the field of neural regeneration (Forciniti et al. 2014; Y. Zhao et al. 2020; Tomaskovic-Crook et al. 2020; Gopalakrishnan-Prema et al. 2020), although it has also been applied to bone tissue engineering, specifically for inducing MSCs osteogenic differentiation via substrate-mediated ES (Pelto et al. 2013; W. W. Hu et al. 2014; Hardy et al. 2015; J. Zhang et al. 2016; J. Zhang, Neoh, and Kang 2018; W. W. Hu et al. 2019; Jing et al. 2019).

PPy has poor mechanical properties and its processing once synthesized is by no means simple (Mao and Zhang 2018), which makes it difficult to use by itself so that it tends to appear in combination with other biodegradable polymers as a coating or filler, e.g. with poly-lactic acid (PLA) (Zou et al. 2016; Xu et al. 2019), polycaprolactone (PCL) (Vijayavenkataraman et al. 2019; Maharjan et al. 2020) or chitosan (J. Huang et al. 2010; Qi et al. 2013; J. Zhang, Neoh, and Kang 2018).

In addition to electroactive polymers, the family of carbon nanomaterials such as graphene, graphene oxide (GO) or carbon nanotubes (CNT) has gained importance in the biomedical field. In tissue engineering, their large surface area and easy functionalization with bioactive molecules have driven their use, but above all their outstanding electrical characteristics make them an effective component for designing electroactive cell culture supports (Z.

Zhang et al. 2018). As in the case of conductive polymers, carbon nanomaterials have been especially used to deliver electrical signals to well-known excitable cell types, such as neural and muscle cells. Despite this, the rise of substrate-mediated MSCs stimulation has promoted carbon nanomaterials for electroactive bone tissue engineering (Zhu et al. 2017; Jamal and De Guzman 2017; J. Li et al. 2020; Balikov et al. 2016; Sayyar et al. 2016).

Conductive cell culture platforms transmit the stimulus *in situ* to the cells when connected to an external supply source. A common setup for substrate-mediated ES is based on the presence of a conductive 2D biomaterial, usually in the form of a film. This cell culture support is in direct contact with the electrodes at its ends and wired to an external current source. A sealed chamber, usually made of polystyrene, polypropylene or polymethylmethacrylate is placed on the film containing the cell culture medium and limiting the space for cell seeding, as shown in Figure 5 (W. W. Hu et al. 2019, 2014; J. Li et al. 2020; J. Zhang et al. 2013). This assembly avoids direct contact between the electrodes and the culture medium. This eliminates some of the drawbacks of GES based on direct coupling, such as Faradic by-products or changes in pH due to medium electrolysis.

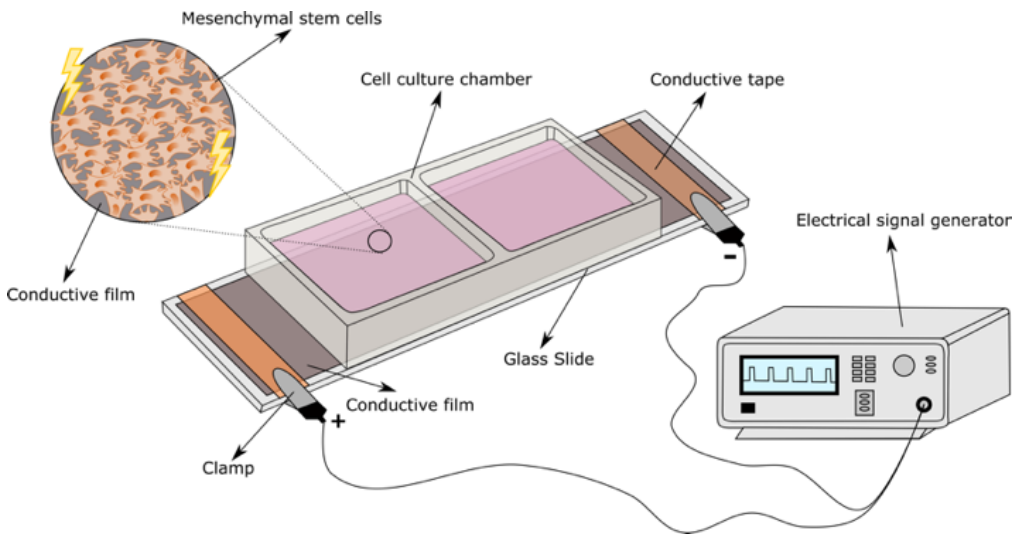


**Figure 5. Schematic representation of a common set-up for substrate-mediated electrical stimulation using 2D conductive cell culture supports (Guillot-Ferriols et al. 2022)**

It is not always possible to avoid electrode immersion in the cell culture well. In these cases, the electrodes are placed in direct contact with the cell culture support to maximize the total current transmitted. In fact, some authors have shown that the current present in these setups in the cell culture medium is negligible (J. Zhang et al. 2016). 3D culture systems such as scaffolds or hydrogels are two examples of electrodes immersed in the medium (J. Zhang et al. 2016; J. Zhang, Neoh, and Kang 2018; Creecy et al. 2013; Pelto et al. 2013; Y. Huang et al. 2019). However, they provide homogeneous stimulation regardless of the distance to the electrode while they provide a more biomimetic environment than 2D conductive supports.

The scaffolds used to deliver substrate-mediated ES to MSCs are usually composites manufactured from biocompatible polymers and conductive materials such as PPy coatings or graphene fillers. The commonly used architectures include highly porous interconnected scaffolds with a diameter range of hundreds of microns (J. Zhang et al. 2016; J. Zhang, Neoh, and Kang 2018; Ravikumar, Boda, and Basu 2017). Nonwoven mats of extruded fibers (Pelto et al. 2013) or electrospinning technique (Jing et al. 2019; Zhu et al. 2017; Hardy et al. 2015) have also been used for MSCs stimulation. 3D printing is making its way in the field and 3D-printed conductive scaffolds are emerging as possible candidates for substrate-mediated ES (Sayyar et al. 2016).

The conductivity of the scaffolds produced after incorporating the electroactive coatings and fillers are between $10^{-11}$ and $10^{-1}$ S/cm (J. Zhang et al. 2016; J. Zhang, Neoh, and Kang 2018; Jing et al. 2019; Zhu et al. 2017; Sayyar et al. 2016; Ravikumar, Boda, and Basu 2017), according to the type of conductive component incorporated and its concentration.

Most of the studies performed in the field support the hypothesis that an initial osteogenic stimulus from an inductive cell culture medium containing supplements such as dexamethasone, ascorbic acid and β-glycerophosphate is necessary to trigger the effects of ES. Li et al. (J. Li et al. 2020) studied the effect of electrical stimulation on MSCs osteogenic differentiation using conductive graphene oxide-cellulose films in growth and osteoinductive media. A combination of ES and osteogenic medium improved mineral deposition more than growth medium and ES together. It should be noted that osteogenic medium alone had the same effect as expansion medium combined with ES in terms of ALP expression.

Interestingly, Sayyar and collaborators (Sayyar et al. 2016) cultivated MSCs in OM 5 days before applying electrical stimulation on graphene/poly(trimethylene carbonate). This induction was indeed necessary to observe the effects of electrical stimulation on osteogenic differentiation. ALP and Col I were upregulated in treated cells compared to non-treated subjected to the same stimulation parameters. Other authors have performed their studies in the presence of growth medium and failed to obtain any improvement in osteogenic differentiation combined with electrical stimulation (Creecy et al. 2013; Pelto et al. 2013).

The lack of an initial osteogenic stimulus provided by osteoinductive supplements can be overcome by combining ES with other physical cues such as nanopatterned surfaces. It has been proved that these have a similar efficiency to that of osteogenic medium in stimulating MSCs to produce bone mineral *in vitro* (Dalby et al. 2007). Balikov et al. (Balikov et al. 2016) studied the effect of graphene patterned surfaces and ES in the absence of supplemented medium. When used alone the patterned surfaces enhance the expression of the early marker RUNX2, although they fail to enhance late osteogenic marker OPN, unless combined with ES. The authors also investigated MSCs differentiation toward a neurogenic lineage due to the potential of stem cells for multi-lineage commitment enhancing both neurogenic and osteogenic markers. This shows the need to study markers from diverse lineages in differentiation experiments and has scarcely been addressed to avoid the presence of mixed populations.

Other research groups used coatings or osteoinductive biomaterials such as hydroxyapatite in combination with conductive cell culture supports and ES to make up for the absence of supplemented medium (Jing et al. 2019; Ravikumar, Boda, and Basu 2017).

### 3.2.2. Piezoelectric cell culture supports

Since the discovery of bone's piezoelectric properties, piezoelectric materials have emerged as a possible approach to mimic the electrophysiological environment of bone tissue. These biomaterials can convert mechanical strain into electrical output and *vice versa*, a mechanical deformation is produced when a voltage is applied, known as the converse piezoelectric effect (Z. L. Wang 2007). This property generates electrical charges on the surface without the need for any external electric supply, as in the case of other stimulation approaches, such as substrate-mediated ES by conductive cell culture supports.

Piezoelectric biomaterials can be divided in two main categories, organic materials such as synthetic or natural polymers, and ceramics, which are inorganic in nature.

Ceramics with piezoelectric properties are crystalline materials with a non-centrosymmetric structure. Their piezoelectricity is typically based on the relative displacement of the ionic species (Chorsi et al. 2019). Some of the different piezoelectric crystals also show ferroelectric properties, meaning that they exhibit an in-built spontaneous electrical polarization reversible under an applied electric field. Zinc oxide (ZnO) and barium titanate ($BaTiO_3$) are normally used as examples of nonferroelectric and ferroelectric materials, respectively, which coincides with their crystallization form in the wurtzite or perovskite structure (Cafarelli et al. 2021). ZnO and $BaTiO_3$ structures are represented in Figure 6 Ia. Barium titanate ($BaTiO_3$), lithium niobate ($LiNbO_3$) or sodium potassium niobate (K0.5Na0.5NbO3 ; KNN) have been used to influence MSCs fate toward the osteogenic lineage (Yu et al. 2017; J. Li et al. 2015; Yang et al. 2020; Y. Li et al. 2017; Fan et al. 2020; W. Liu et al. 2020).

Regarding organic materials, synthetic polymers have emerged as an alternative to ceramics. Even though bone is a hard tissue, some applications require mechanical flexibility, while polymers are easier and less expensive to process. Their piezoelectricity is mostly based on the repositioning of molecular dipoles (Chorsi et al. 2019).

Poly(vinylidene) fluoride (PVDF), poly(L-lactic) acid (PLLA) or polyhydroxybutyrate (PHB) are some of the most frequently used piezopolymers for tissue engineering applications.

Most of the piezopolymers used for bone tissue engineering approaches are semi-crystalline, so that their structure can be described as randomly oriented microscopic crystals which contain the aforementioned dipoles dispersed around the amorphous regions (Figure 6 IIb). These dipoles can be reoriented to maximize the material's piezoelectric response in a process called poling, during which a high electric field is applied at a high temperature to align the dipoles. When the dipoles are aligned, as represented in Figure 6 IIb, the sample is cooled down in the presence of the electric field to maintain the dipoles' orientation (Ramadan, Sameoto, and Evoy 2014). Poling is directly related to a higher

piezoelectric response characterized by the piezoelectric coefficient $d_{ij}$, which is defined as the electric polarization variation along direction *i* in the material per unit mechanical stress of index *j* applied to it or *vice versa*. $d_{31}$ and $d_{33}$ are the coefficients describing the electric polarization generated either in the same direction or perpendicular to the direction of the applied stress (Harrison and Ounaies 2001).

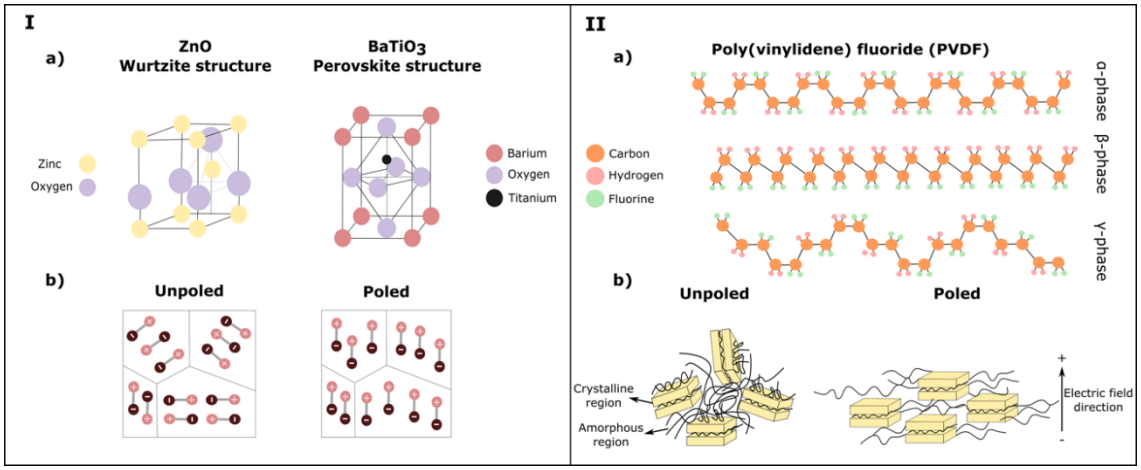


**Figure 6. Schematic representation of piezoelectric biomaterials. I. a) Schematic illustration of piezoelectric ceramics with wurtzite and perovskite structures. b) Crystalline structure of unpoled and poled ceramics. Dipoles are oriented after poling process. II. a) Chain conformation of α, β and γ phases of poly(vinylidene) fluoride. The electronegativity of fluorine atoms compared to hydrogen ones generates an electrical dipole moment in the monomer unit. The all trans conformation (TTT) and $GT_3GT_3G'$ of β and γ phases lead to an overall dipolar contribution of the polymer chain, while the trans-gauche–trans-gauche (TGTG') conformation of α-phase is non-polar, conferring non-electroactive properties to this polymorph. b) Crystalline and amorphous regions of PVDF with randomly oriented dipoles before the poling process, that are oriented after it. Adapted from (Guillot-Ferriols et al. 2022)**

#### 3.2.2.1. Poly(vinylidene) fluoride

Poly(vinylidene) fluoride is a semi-crystalline electroactive polymer which shows a complex structure. It can be considered as a smart material since its piezoelectricity allows it to respond to an external stimulus (applied stress) by modifying its surface charge. This property has favoured its use in different applications, such as sensors, actuators, energy harvesting and as cell culture support in the biomedical field (Bar-Cohen and Zhang 2008).

PVDF can present five polymorphs, α, β, γ, δ and ε depending on the chain conformation. α and δ phases show a TGTG' (trans-gauche-trans-gauche) structure, γ and ε present a $T_3GT_3G'$ chain conformation while β-phase is designed as all trans (TTT) planar zigzag (Martins, Lopes, and Lanceros-Mendez 2014). Although five polymorphs exist, α, β and γ are the most commonly obtained and studied ones. Their structure is schematized in Figure 6 IIa.

These conformations determine the electroactive properties of the described polymorphs. PVDF monomer unit shows a strong electrical dipole moment (5-8 x $10^{-30}$ C $m^{-1}$) due to the

difference in electronegativity between fluorine and hydrogen atoms (Giannetti 2001). These monomers are distributed in the chain generating an overall dipolar contribution per unit cell as is the case for β and γ phases. Due to its structure, β-phase is the one with the highest dipolar moment per unit cell ($8 \times 10^{-30}$ C $m^{-1}$) (H. M. G. Correia and Ramos 2005). In the case of α-phase, the anti-parallel packing of the dipoles within the unit cell hinders its electroactive properties. Therefore, applications requiring an electrically active response need the presence of β or γ-phase. Usually, β is preferred due to its highest piezoelectric, pyroelectric and ferroelectric properties (Sencadas, Gregorio, and Lanceros-Méndez 2009). Its $d_{33}$ coefficient can reach values up to -34 pC/N depending on the structure and the processing conditions (Gomes et al. 2010), which can determine the nucleation in this electroactive phase.

On the other hand, PVDF copolymer poly(vinylidene fluoride-trifluoroethylene) (PVDF-TrFE) always presents the β crystalline phase for specific VDF/TrFE ratios. The addition of the third fluoride in the TrFE monomer unit with large steric hindrance favours the all-trans conformation and thus induces the ferroelectric β-phase regardless of the processing method. PVDF-TrFE is substantially more expensive than the homopolymer, PVDF, reducing its use in bone tissue engineering approaches (Martins, Lopes, and Lanceros-Mendez 2014).

#### 3.2.2.1.1. PVDF β-phase nucleation

*I. α-phase mechanical stretching*

Different processing methods allow β-phase formation. When cooling from the melt, PVDF usually crystallizes in the non-electroactive α-phase. The most common way to obtain its electrically active analog is by mechanical stretching, a process in which α-phase films are stretched at 80 ºC and a stretch ratio of 5. During the procedure, polymer chains are aligned within the polymer crystals switching from a TGTG' conformation to TTT one. Microscopically, the typical spherulitic conformation from α-phase is transformed into a microfibrillar structure (Sencadas, Gregorio, and Lanceros-Méndez 2009).

Focusing on PVDF application in the biomedical field, mechanical stretching is a valid technique for achieving PVDF β-phase, although it is only applicable for 2D cell culture supports (flat films). Also, it is a two-step process, since α-films need to be produced and then stretched. Other techniques allow PVDF crystallization in β-phase and are compatible with the manufacture of 3D cell culture supports. Some examples are the application of an external electric field (electrospray/electrospinning) (D. M. Correia et al. 2014; Zhong et al. 2011; Lund and Hagström 2010; J. Zheng et al. 2007), from solution crystallization under 70 ºC using dimethylformamide (DMF) or dimethylacetamide (DMA) as solvents (Gregorio and Cestari 1994; Morales-Román et al. 2019; Guillot-Ferriols et al. 2020; Sencadas, Gregorio Filho, and Lanceros-Mendez 2006) or by the addition of nucleating fillers (clays, $BaTiO_3$, ferrite, palladium or gold) (Supriya, Kumar, and Kar 2019; Martins, Costa, and Lanceros-Mendez 2011; Mandal, Kim, and Lee 2012; W. Wang et al. 2011).

### II. Application of an external electric field

Electrospinning technique is based on the application of an electric field to a polymer solution resulting in the formation of an electrostatically driven jet that is collected on a grounded plate (Damaraju et al. 2013). The polymer solution is pumped through a syringe coupled to a needle, connected to a high voltage power source. The formed jet is collected in form a non-woven mat in the grounded plate or collector. Depending on the concentration of the polymer solution fibres or microspheres can be obtained. The obtaining of microspheres using this approach is a variation of the electrospinning technique and is called electrospray (Bock, Dargaville, and Woodruff 2012). A schematic representation of the process can be found in Figure 7a.

In the case of PVDF, concentrations ranging from 5 to 10 % (w/v) give rise to microspheres. More concentrated solutions, from 10 to 20 % (w/v) produce a mixture of fibres and beads, while 20 to 30 % (w/v) solutions generate fibres, as can be seen in Figure 7b (D. M. Correia et al. 2014).

When the jet is formed due to the application of a high voltage it is subjected to a high stretching ratio, similar to the one applied during mechanical stretching to transform $\alpha$ to $\beta$-phase films (Davis et al. 1978), giving rise to PVDF crystallization in $\beta$-phase. Evaporation of the solvent leading to crystallization during the process is the main contributor to $\beta$-phase presence since it usually takes place under 70 ºC.

During electrospray or electrospinning process, parameters such as applied voltage, flow rate of the dispensed polymeric solution, needle diameter and distance to the grounded collector can influence the $\beta$-phase percentage in the sample (C. Ribeiro et al. 2010).

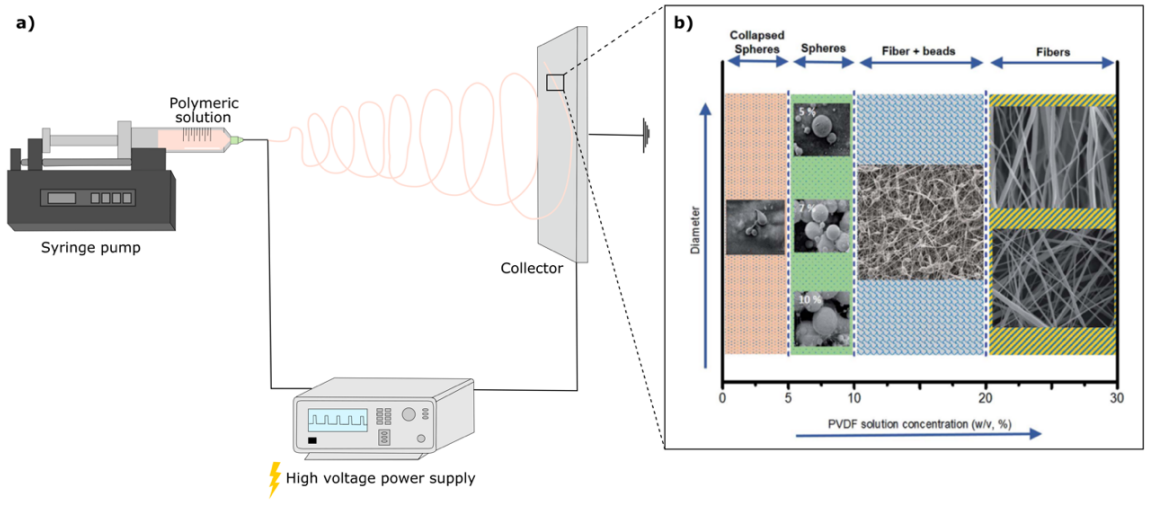


**Figure 7. a) Schematic representation of electrospinning process. b) Schematic diagram of the influence of PVDF solution concentration in the production of microparticles and fibers by electrospray and electrospinning. Adapted from (D. M. Correia et al. 2014).**

*III. Inclusion of fillers*

Inclusion of fillers in the polymeric PVDF solution has been demonstrated to help crystallization in the β-phase. Several nucleation agents have been used, including $BaTiO_3$, clays, hydrated ionic salts, $TiO_2$ and nanoparticles such as ferrite, palladium, gold and carbon nanotubes.

The nucleation mechanism varies depending on the filler used. When using salts with different charges as fillers, positive and negative nucleation agents, Wu et al. (Y. Wu et al. 2012) described a more effective role in β-phase crystallization by using positively charged surfaces. The crystallization rate of β-PVDF was increased when using this type of fillers due to the specific ion-partial dipole ($CF_2$) interaction. Nevertheless, Martins et al. (Martins, Costa, Benelmekki, et al. 2012) described a different behaviour when using two types of ferrite, $CoFe_2O_4$ and $NiFe_2O_4$. Negatively charged surfaces of ferrites promote the interaction with the positive $CH_2$ charge density of the PVDF chains. This allows the alignment of the chains on the surface of the nanoparticle in the extended all trans conformation producing the crystallization of the electroactive β-phase. These results are also supported by other authors using PVDF and $CoF_2O_4$ as fillers (Martins, Costa, Ferreira, et al. 2012; Supriya, Kumar, and Kar 2019).

Besides of the surface charge, nanoparticle concentration affects the percentage of β-phase present in the sample. $CoFe_2O_4$ needs a lower concentration (5 w/v %) than $NiFe_2O_4$ (50 w/v %) to achieve a 90 % composition of β-phase (Martins, Costa, Benelmekki, et al. 2012). Nevertheless, when β-phase PVDF is nucleated by the presence of $BaTiO_3$ ceramic filler, achieving an 80 % of this polymorph, the concentration of the filler is independent from the percentage of β-phase and depends on the filler size (H.-J. Ye, Shao, and Zhen 2013).

Regardless of the nucleation mechanism, it seems clear that the presence of a filler is able to nucleate the most electrically active PVDF polymorph. Concentration, geometrical factors due to the nanosize of the fillers and the interactions at the interface between the nanoparticles and the PVDF chains play a significant role in the amount of β-phase present in the samples.

The inclusion of fillers is compatible with diverse manufacturing techniques to obtain cell culture supports in 3D such as electrospray (Gonçalves, Martins, Correia, et al. 2015), electrospinning (Gonçalves, Martins, Moya, et al. 2015), solvent casting using nylon templates (Fernandes et al. 2019) or non-induced phase separation for the production of porous membranes (Guillot-Ferriols et al. 2020).

#### 3.2.2.2. The magnetoelectric effect

Filler inclusion, besides of favouring the nucleation of the electroactive β-phase, can also produce additional effects. When the nucleating agents show magnetostrictive properties their combination with the piezoelectric matrix generates a magnetoelectric (ME) composite. ME materials show a change in the electrical polarization when a magnetic field is applied, or *vice versa,* magnetization can be modified by an applied electric field. When a magnetic field is applied to the composite a deformation is induced in the magnetostrictive

component. This is transmitted to the piezoelectric matrix, which undergoes a change in electrical polarization. This effect, thus, is called the magnetoelectric effect (Martins and Lanceros-Méndez 2013). The ME response in this type of composites depends on the composite microstructure and the coupling interaction in the interface regions.

Most ME composites are based on piezoelectric ceramics (barium titanate or lead zirconate titanate) due to their large piezoelectric coefficients compared to electroactive polymers. Nevertheless, as stated before, ceramics are fragile, difficult to tailor and expensive, which limits their application in the bone tissue engineering field. Regarding the magnetostrictive component, Terfenol-D is widely used due to its magnetostriction, but it has several disadvantages such as its fragility and its high cost.

The use of ME materials based on the combination of PVDF and ferrite can help to overcome these issues. PVDF has been combined with cobalt ferrite oxide ($CoFe_2O_4$ or CFO) to produce magnetoelectric composites for their application in bone tissue engineering. These composites have been tailored in different morphologies for different applications (Gonçalves, Martins, Moya, et al. 2015; Gonçalves, Martins, Correia, et al. 2015; Fernandes et al. 2019; Guillot-Ferriols et al. 2020). The effective coupling of both interfaces has been demonstrated in these type of ME composites by Gonçalves et al. (Gonçalves, Martins, Correia, et al. 2015) where an application of a magnetic field of 220 mT to PVDF-CFO microspheres exhibited a piezoelectric response, measured as a variation in the piezoelectric coefficient $d_{33}$. An increase in the CFO content led to an increase in the $d_{33}$, reaching a maximum value of approximately 30 pC/N when the CFO content was 27 % (w/v).

#### 3.2.2.3. Piezoelectric stimulation at cell culture level

From a biomedical point of view the ME effect can be exploited to transmit the piezoelectric stimulation at cell culture level. The transmission of the piezoelectric stimulus relies on the application of a mechanical strain to obtain the maximum electric response. This could be achieved by applying a magnetic field that will deform the magnetostrictive component, deforming the polymer matrix and generating a variation on the surface charge of the PVDF. The magnetic field can be applied by means of a bioreactor compatible with cell culture conditions. Lanceros-Mendez group has developed a magnetic bioreactor based on the movement of neodymium magnets below the cell culture plate (Figure 8 Ia and Ib), generating an alternating magnetic field whose intensity depends on the position of the well, as can be seen in the simulation in Figure 8 Ic. Displacement of the magnets (5-25 mm) and frequency (0.1-2 Hz) can be adjusted as well as the stimulation programs. Tested stimulation programs when using this bioreactor are based on the simulation of daily human activity meaning 16 h of stimulation, divided in cycles of 5 minutes of activity and 25 minutes of rest, and 8 h of rest (Castro et al. 2020).

Other types of bioreactors, not based on the ME effect, have been developed to stimulate cells using piezoelectric cell culture supports. Again, the Lanceros-Mendez research group has developed different bioreactors based on mechanical deformation using a vertical vibration module to deform the polymer matrix (Figure 8 IIa) (C. Ribeiro, Pärssinen, et al. 2015; S. Ribeiro et al. 2020; C. Ribeiro, Moreira, et al. 2012) in which the same stimulation

program as the one in the magnetic bioreactor has been applied, as can be seen in Figure 8 IIb. Bioreactors based on dynamic compression (Z. Zhou et al. 2019; Damaraju et al. 2017; C. C.-Y. Huang et al. 2004) (Figure 8 III) or ultrasound activation (Yang et al. 2020; Fan et al. 2020; Cafarelli et al. 2021) have also been described. Commercial fracture healing systems approved by the FDA have already been used to stimulate cells with ultrasound *in vitro* by connecting them to a tissue culture plate (Figure 8 IV) (Nolte et al. 2001). In the same setup, piezoelectric biomaterials can be placed in the wells of the tissue culture plate to electrically stimulate the MSCs activating the cell culture supports by US.

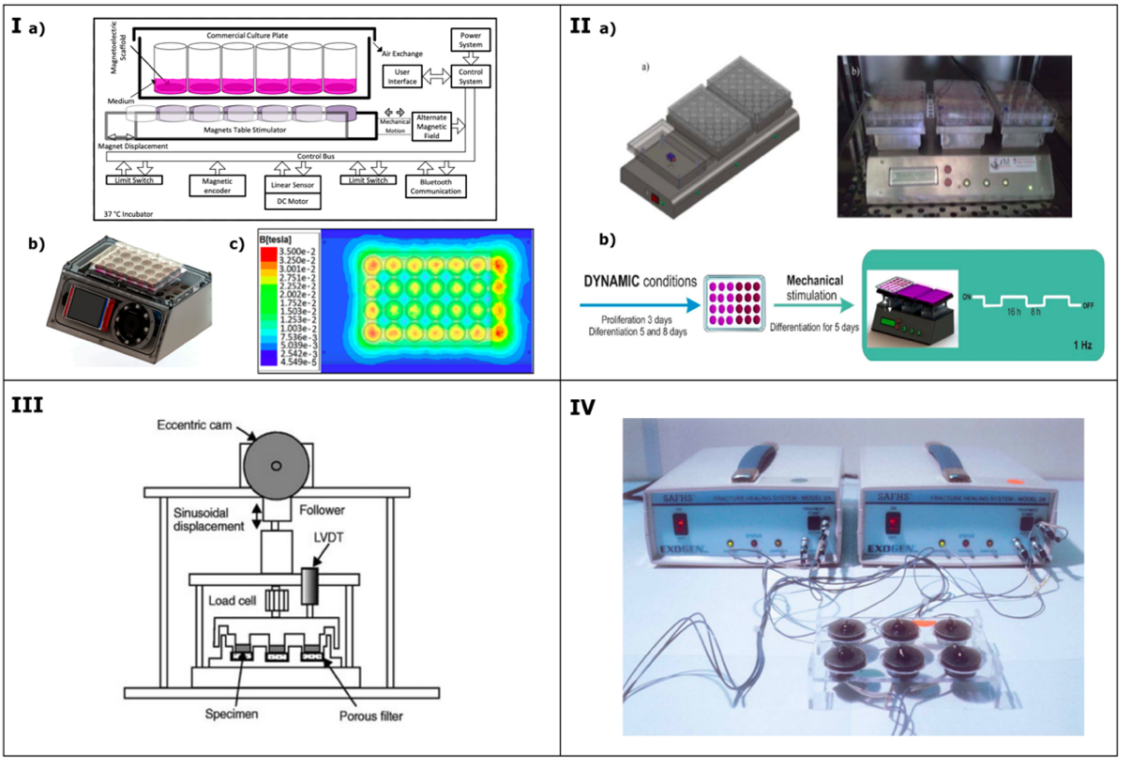


**Figure 8. Examples of bioreactors used for generating an electric response on piezoelectric cell culture supports. I. a) Magnetoelectric bioreactor operating principle using electrical and mechanical controls to produce an alternated magnetic field for the stimulation of biomaterials based on the combination of piezoelectric polymers and magnetostrictive nanoparticles. I. b) Schematic representation of the bioreactor assembled with a cell culture plate. I. c) Magnetic field intensity distribution at the bottom of 24-well cell culture plates. Adapted from (Castro et al. 2020). II. a) Schematic representation (left) and actual image (right) of a mechanical bioreactor based on a vertical vibration module. Several cell culture plates can be placed on top of the bioreactor. Adapted from (C. Ribeiro, Moreira, et al. 2012) II. b) Diagram of a proposed stimulation program using a vertical vibration module bioreactor to reproduce daily human activity by applying 16 h of stimulation and 8 h of rest. Adapted from (S. Ribeiro et al. 2020). III. Schematic representation of a cyclical compression bioreactor in which the specimens are subjected to dynamic compressive loading. A load cell and a linear variable differential transformer (LVDT) measure the load response of specimens and the imposed displacement. Adapted from (C. C.-Y. Huang et al. 2004). IV. Ultrasound therapy unit for the application of low-intensity ultrasound in vitro. The therapy unit consists of two sonic accelerated fracture healing system SAFHS® devices and transducers (with coupling gel) to**

**which the tissue culture plate can be connected. Adapted from (Nolte et al. 2001). Figure adapted from (Guillot-Ferriols et al. 2022)**

Poled piezoelectric cell culture supports do not always rely on electromechanical stimulation due to the piezoelectric effect. The polarization process and consequently the dipole alignment, implies the presence of charged positive and negative surfaces with an associated surface potential, which can also affect MSCs differentiation by maintaining an electric microenvironment. Two options arise at this point, culturing the cells either on the positively or negatively charged surface.

Pärssinen et al. (Pärssinen et al. 2015) studied the effect of poled-positive and negative surfaces of β-phase PVDF films coated with fibronectin (FN) on MSCs behaviour. Polarization enhances PVDF hydrophilicity best on negatively charged surfaces favouring the adhesion of fibronectin in a more active formation, exposing RGD sequences. This enhances cell adhesion and cytoskeleton tension and is reflected in a higher number and area of focal adhesions (FA). Cell cytoskeleton tension is related to the activation of RhoA and MAPK pathways and subsequent cell signalling cascades, which can determine MSCs fate via integrin mediated signalling. An increase in the number and size of FAs has been reported during osteogenic differentiation (Engler et al. 2006), although the authors simply demonstrated increased osteogenic differentiation based on ALP activity. These results agree with those obtained by Zhou et al. (Z. Zhou et al. 2016) in which negatively charged surfaces were seen to accumulate the cations present in the cell culture medium, which in turn attracted proteins such as fibronectin and the negatively charged cytomembrane of cells, favouring their adhesion and subsequent osteogenic differentiation, in agreement with the results of Pärssinen et al.

Li et al. (J. Li et al. 2015) used lithium niobate wafer, a ferroelectric crystal, with positive, negative or neutral surface charges to investigate their effects on MSCs fate. Positive surfaces showed greater cell areas than negative and non-charged surfaces, resulting in enhanced OPN, OCN and RUNX2 expression and ALP activity. This phenomenon is associated with the capacity of positive surfaces to accumulate negative charges due to the ionic component of the medium, and the ability of different proteins and molecules such as dexamethasone to attract positive charges, generating electrostatic interactions between the charged molecules and the charged surface. This can influence the distribution of bioactive molecules regulating MSCs fate.

It is not easy to decide whether MSCs should be cultured on positively or negatively charged surfaces given the contradictory information published in recent years. What can be extracted from the presented information is that either a positive or negative surface charge enhances protein adsorption, helping adhesion and spreading of mesenchymal stem cells. The activation of integrin mediated signalling will eventually lead to the activation of mechanosensitive genes, ultimately promoting changes in cell growth, morphology and differentiation potential.

Interestingly enough, this concept was investigated in depth by Jia et al. (Jia et al. 2019) by using PVDF-TrFE films containing Terfenol-D alloy, also coated with FN. These films were responsive under a magnetic field, allowing to control the surface potential by applying

different intensities (0 to 2800 Oe). Positive and negative surfaces with different surface potentials were investigated. The spatial distribution of two functional sites of FN, RGD and PHSRN, which act in synergy, is affected by the surface potential. While positive charged surfaces show a tight formation of the functional sites at 55 mV, the same is true for negative surfaces at -20 mV. This tight FN formation with distances below 3.5 nm fully binds the integrin and produces the strongest integrin-mediated osteogenic differentiation.

The results obtained by Jia et al. disagree with those of Zhang et al. (X. Zhang et al. 2016), who developed PVDF-TrFE membranes containing different concentrations of $BaTiO_3$ nanoparticles and therefore different surface potentials. Membranes with a surface potential of -76.8 mV were selected for cell culture because of their similarity to endogenous biopotential (C. Ribeiro, Correia, et al. 2015), comparing their performance with non-poled ones. The best osteogenic behaviour was found when the cells were cultured on the negative surface with this surface potential. However, Zhang et al. (C. Zhang et al. 2018) also studied different surface potentials of PVDF-TrFE films, varying the β-phase content and showed that lower surface potentials (-53 mV) (a range not taken into account in (X. Zhang et al. 2016) enhanced MSCs osteogenic differentiation more than higher surface potentials (-76 mV).

These differences can be attributed to the fact that Jia et al. used a magnetic bioreactor to modulate surface potential in the polymer matrix due to the presence of magnetostrictive nanoparticles, while Zhang et al. used different β-phase contents to do so, thus with different material surface stiffness and dynamic stimulation.

## 4. Expression profile of stimulated MSCs and activated signalling pathways

Bone morphogenetic proteins are osteogenic inductive cytokines that belong to the TGF-β family and are the ligands of the BMP signalling pathway, which plays a fundamental role in the regulation of bone organogenesis. They are able to bind and bring together the serine/threonine kinase bone morphogenetic protein receptors I and II (BMPRI; BMPRII) forming the heteromeric complex required for signal propagation (Allendorph, Vale, and Choe 2006). BMP ligand initiates a signalling cascade based on Smad proteins, the downstream effectors taking charge of transducing the signals from the cell surface to the nucleus. Once imported to the nucleus, these proteins can regulate transcription of targeted genes by directly binding to specific DNA sequences.

MSCs osteogenic differentiation is based on the physical interaction of RUNX2, master regulator of the osteogenic differentiation pathway, and Smad (Rahman et al. 2015). BMP ligands can also activate mitogen-activated protein kinases (MAPK) signalling pathways, especially extracellular signal-regulated kinases 1/2 (ERK1/2) and p38, which are smad-independent, as described in Figure 9c. MAPK pathways (ERK1/2, p38 and c-Jun N-terminal kinases (JNK)) have been reported to be activated in a time-dependent manner during MSCs differentiation in osteoinductive cultures (Jaiswal et al. 2000).

Due to the important character of the BMP pathway on MSCs osteogenic fate determination, several authors have evaluated different molecular players of this cascade as potential targets activated by electrical stimulation.

Pulsed electromagnetic fields, either used alone or in combination with BMP-2, have been demonstrated to simultaneously activate by phosphorylation Smad 1/5/8 and the non-smad MAPK pathway p38 in MSCs. PEMFs can also enhance BMPRI (ALK2) expression in the middle-late phase of MSCs osteogenic differentiation. Inhibition of these signalling pathways resulted in a reduced expression of RUNX2, ALP activity and OCN production (Martini et al. 2020). Similarly, Zhang et al. (J. Zhang, Neoh, and Kang 2018) confirmed the upregulation of BMP-2 and its receptor BMPRIA (ALK3) when MSCs were cultured and electrically stimulated on chitosan/polypyrrol scaffolds. Huang et al. (Y. Huang et al. 2019) also used conductive silicon surfaces to stimulate osteogenic progenitors and related their differentiation to BMP-2 and 4 upregulation and phosphorylation of Smad 1/5/9. All these results show the ability of ES to promote osteogenesis via BMP/Smad signalling pathway, among other signalling cascades.

Yong et al. (Yong et al. 2014) corroborated the role of MAPK signalling cascades in osteogenic fate determination of MSCs when stimulated by electromagnetic fields. p38 and ERK1/2 were phosphorylated whereas JNK was found not to be activated. The authors also confirmed the involvement of the cAMP-PKA pathway, but no relation was described between both signalling cascades, bringing out the fact that electromagnetic fields could independently activate at least two signalling pathways. On the other hand, Jansen et al. (Jansen et al. 2010) did not find increased ERK phosphorylation after MSCs stimulation and osteogenic differentiation using PEMFs. The use of different magnetic fields (frequencies, strengths and waveforms) leads to contradictory results, indicating that different stimulation parameters could induce different signalling pathway activities and result in different effects.

General ES by direct coupling has also proved that the signal is transduced to the cells through MAPK pathways (Srirussamee et al. 2021). ES induced ERK1/2 phosphorylation within the first 30 minutes of treatment leading to an increase in c-FOS and c-JUN mRNA expression in the early stage of ES. Once again, JNK could not be related to osteogenic differentiation mediated by ES, narrowing the circle to p38 and ERK1/2 as main effectors of the MAPK pathway in response to electrical stimulation. Hronik-Tupaj et al. (Hronik-Tupaj et al. 2011) went further and demonstrated the upregulation of hsp27 and hsp70 and hypothesized that hsp70 can activate the ERK1/2 pathway through Raf-1 and Bag1, enhancing the expression of RUNX2.

Intracellular calcium oscillations have also been described as potential effectors of MSCs differentiation caused by ES, since $Ca^{2+}$ is a well-known second messenger involved in several cellular responses (Berridge, Lipp, and Bootman 2000). Osteoinductive factors, including physical stimuli, have been shown to reduce intracellular calcium spikes to a similar level to those found in terminally differentiated human osteoblasts. Electrical stimulus seems to be involved in mediating differentiation through G-protein coupled receptors (GPCR), coupling to phospholipase C (PLC) near the cell surface, which in turn liberates $Ca^{2+}$ from the endoplasmic reticulum. It is hypothesized that PLC-mediated

signaling can activate Protein kinase C (PKC) and potentially couple to the MAPK cascades, as described in Figure 9a (S. Sun et al. 2007).

Calcium ion channels, such as VGCC, can also mediate $Ca^{2+}$ influx into the cell in response to membrane depolarization and might activate ERK1/2 cascade acting downstream of Ras (Wortzel and Seger 2011). They have been considered as the main targets of PEMF action (Pall 2013). Petecchia et al. (Petecchia et al. 2015) detected an augmented expression of L-type VGCC when MSCs were stimulated with osteogenic media and PEMF for 27 days, while PEMF seemed to influence $[Ca^{2+}]_i$ after 9 days of exposure, leading to an increase of 30 % compared to cells cultured in OM. Zhang et al. (J. Zhang et al. 2016) also described the role of VGGC in MSCs osteoblastogenesis in response to substrate-mediated ES, demonstrating that matrix mineralization was mediated by an influx of $Ca^{2+}$ and not via $Ca^{2+}$ release from internal stores. They also detected the role of other ion channels ($Na^+$, $K^+$ and $Cl^-$) in the ES-induced enhancement of MSCs functions, but not as important as that of VGCC. Jing et al. (Jing et al. 2019) corroborated this hypothesis reporting an increase in $[Ca^{2+}]_i$ in MSCs stimulated on conductive coated PPy fibres attributed to the activation of voltage-gated $Ca^{2+}$ channels.

This increase in intracellular calcium concentration is mainly mediated by the $Ca^{2+}$ binding protein calmodulin, which undergoes pronounced conformational changes to activate downstream effectors (Berridge, Lipp, and Bootman 2000). CaM expression has reported to be increased in MSCs after 21 days of ES suggesting the involvement of calcium/calmodulin pathway in the differentiation process mediated by this stimulus (Leppik et al. 2018). Osteogenic differentiation activated by $Ca^{2+}$/CaM might be related with the activation of the osteoblast specific transcription factor Osterix. CaM is able to interact with calmodulin-dependent protein kinases (CaMK), specially CaMKII, which in turn regulate OSX during osteoblast differentiation. Osterix proteins regulate the expression of many osteogenic factors including osteonectin, osteopontin, osteocalcin and alkaline phosphatase (Choi et al. 2013). Piezoelectric stimulation has proven to activate the same signalling pathway. Liu et al. (W. Liu et al. 2020) demonstrated an increase in intracellular calcium concentration which lead to p38 phosphorylation and promotion of osterix expression, thereby achieving the osteogenic differentiation of MSCs when cultured in dynamic conditions in piezoelectric cell culture supports (Figure 9b).

Other signaling pathways have been proposed as activated in response to ES, such as the Notch pathway. Notch receptors are activated by a ligand (Jagged-1,-2 and Delta-like (DII)-1,-3 and -4) on adjacent cells, resulting in the cleavage of the Notch intracellular domain (NICD) and its translocation to the nucleus, activating the transcription of nuclear gens of the Hes/Hey family, described in Figure 9e (Luo et al. 2019). Contradictory effects of Notch cascade on osteoblastogenesis have been described due to its role in the inhibition of the Wnt/β-catenin pathway, but the overexpression of NICD or ligand jagged1 enhanced mineralization in MSCs cultures (Deregowski et al. 2006). Bagheri et al. (Bagheri et al. 2017) described the upregulation of the Notch target genes Hes5, Hes1 and Hey1 during the middle-late times of differentiation (14-21 days) in response to PEMFs. Nevertheless, the inhibition of the Notch pathway did not reduce the expression of Hey1, indicating that it is not directly modulated by Notch but might be regulated by the BMP pathway. This again

highlights the idea of a synergistic activation of different signalling cascades acting together in response to electrical stimulation.

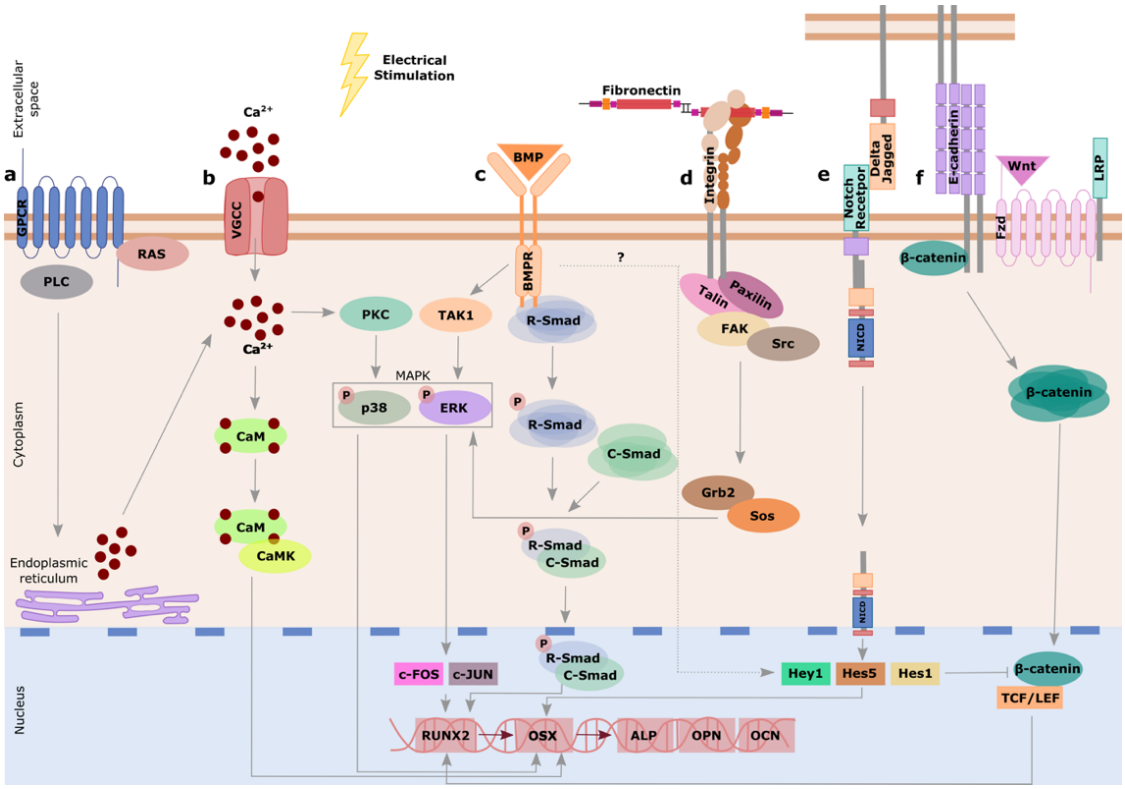


**Figure 9. Activated signaling pathways in MSCs by electrical stimulation. a) G-protein coupled receptors bind phospholipase C (PLC) liberating $Ca^{2+}$ from the endoplasmic reticulum. The increase in intracellular calcium concentration activates protein kinase C (PKC) activating MAPK pathway. b) Voltage gate calcium channels allow the entrance of calcium in the cytoplasm, which binds to calmodulin (CaM) that interacts calmodulin-dependent protein kinases (CaMKs) promoting osterix (OSX) expression. c) Bone morphogenetic protein receptors can be activated by a combination of BMP ligands and electrical stimulation, activating either the smad-dependent pathway, which leads to Runt-related transcription factor (RUNX2) expression or the independent one by activation of Mitogen activated protein kinases (MAPK) ERK and p38, which in turn can induce RUNX2 and OSX expression. d) Piezoelectric substrates with associated surface potential enhance protein adsorption and can modify their conformation, exposing adhesion domains recognized by integrins. Integrins mediate the response by activating focal adhesion kinase (FAK). e) Notch signaling pathway may be activated by electrical stimulation, promoting Hey1, Hes5 and Hes1 expression when the Notch receptor intracellular domain (NICD) is cleaved and travels to the nucleus. f) Cell-cell connections together with piezoelectric stimulation can produce the activation of the Wnt/β-catenin signaling pathway. β-catenin liberates from E-cadherin, due to a reduction in intracellular calcium concentration, leading to its accumulation in the cytoplasm and its translocation to the nucleus, promoting T cell factor/ lymphoid enhancer factor (TCF/LEF) expression (Guillot-Ferriols et al. 2022).**

Activated signalling pathways take a different turn when culturing MSCs on piezoelectric cell culture supports. The presence of an associated surface potential can influence protein

conformation, either from cell culture media or coatings, and exposure of adhesion motifs, modifying cell response. Fibronectin is a typically used protein to coat hydrophobic biomaterials lacking cell adhesion properties, specially the piezoelectric polymer PVDF (C. Ribeiro, Panadero, et al. 2012; Guillot-Ferriols et al. 2020; Sobreiro-Almeida et al. 2017). It has been demonstrated that RGD adhesion domain presentation can vary depending on the presence of a surface charge (C. Ribeiro, Panadero, et al. 2012). It is therefore obvious to think of integrins, the principal receptors for binding extracellular matrix proteins and integrating the signals between the ECM and the cytoskeleton (Alberts et al. 2002), activating mechanotransduction signalling pathways. Jia et al. (Jia et al. 2019) described the expression of α5-β1 integrin pair, a fibronectin receptor, in MSCs cultured on PVDF-TrFE films with different surface potentials coated with fibronectin. This expression was consistent with the one of focal adhesion kinase (FAK), the main protein of the integrin-mediated osteogenic differentiation signalling pathway. When FAK is recruited to focal adhesions by cytoskeletal anchor proteins such as talin and paxillin, clustered FAK molecules phosphorylate, create a phosphotyrosine docking site for members of the Src family These Src protein bind Growth factor receptor bound 2 / son of sevenless (Grb2/Sos), which in turn are able to activate ERK (Figure 9d) (Guan 1997; Alberts et al. 2002). As explained earlier, ERK activation leads to MSCs osteogenic differentiation. Other authors have described an increase in cell adhesion and consequently an enhanced osteogenic differentiation when MSCs were cultured on charged substrates, which may lead to hypothesizing about the involvement of the FAK/ERK signalling pathway (Z. Zhou et al. 2016; Pärssinen et al. 2015).

Mitochondrial function, and therefore changes in oxygen metabolism, have also been related to the regulation of MSCs osteodifferentiation induced by electroactive materials (C. Zhang et al. 2018). Mitochondrial membrane potential (MP) and reactive oxygen species (ROS) can vary regarding the surface charge of the piezoelectric material and their $d_{33}$ coefficient, indicating that the electrical environment has a dose-response relationship with bone regeneration. Nevertheless, no related signalling pathway has been proposed to be activated in response to these variations in Mitochondrial MP and ROS. Further research may be needed to elucidate the underlying mechanism.

Besides interactions with ECM proteins, cell-cell connections through connexins such as E-cadherin and their cytoplasmatic effectors, catenins, have been described as potential mechanisms of piezoelectric signalling transduction. Zhang et al. described an increase in β-catenin expression in the middle-late stage (14 days) closely related to the presence of more connected cells. This connection help to generate a stable hyperpolarization in the cell membrane potential in response to piezoelectric stimulation. In earlier stages, cells are not well connected, leading to the impossibility of reaching a stable hyperpolarized state. In response to cell membrane hyperpolarization calcium channels close, resulting in the separation of β-catenin from E-cadherin and its accumulation in the cytoplasm. Wnt/β-catenin signalling pathway is hypothesized as responsible activated signalling cascade, depicted in Figure 9f (Jiamin Zhang et al. 2020). In fact, Wnt/β-catenin can activate osteogenic differentiation program in MSCs through β-catenin binding to T cell factor/ lymphoid enhancer factor (TCF/LEF) transcription factor (Day et al. 2005). The involvement of the Wnt signalling pathway was also described by Li et al. (J. Li et al. 2015). Wnt4 was

found to be urpregulated during MSCs osteogenic differentiation cultured on piezoelectric crystal substrates. BMP2 was also overexpressed, although there is insufficient evidence to explain the relationship between TFG-β/Wnt signalling pathways and osteogenic differentiation. This work reinforces the idea of the influence of a charged surface in enhancing serum protein adsorption and therefore enhancing MSCs spreading ability

# Hypothesis and Objectives

## 1. Hypothesis

Mesenchymal stem cells play an essential role in bone's growth and regeneration *in vivo*. Their self-renewal and differentiation capacity to osteoblasts and the fact that they are easy to obtain make them suitable candidates for bone therapeutic approaches after injury. Nevertheless, as has been discussed in the previous chapter, MSCs are highly sensitive to harsh microenvironments. The altered homeostasis of the stem cell niche at the injured site may not provide the right cues to initiate the osteogenic differentiation of injected MSCs. Although the number of pre-clinical studies using MSCs and biomaterials to treat bone defects has increased in the recent years, the approaches that made their way into clinical studies, with low number of patients, show non consistent results. The inconsistency may be related with the lack of osteogenic differentiation of the implanted cells. In fact, several authors have demonstrated that a stable pre-differentiated phenotype induced *in vitro*, prior to transplantation, is an essential requirement for the success of MSCs-based therapies.

Biochemical induction based on dexamethasone is the most common approach for determination of MSCs osteogenic fate *in vitro*. However, this corticosteroid can produce the undesired guidance of MSCs towards the adipogenic lineage besides inducing osteogenic differentiation. Alternatives based on physical cues have demonstrated to act more precisely and have emerged as an alternative to direct MSCs differentiation towards the osteogenic lineage. MSCs find themselves subjected to an electrically active environment due to the piezoelectric properties of the collagen fibres that conform bone's organic extracellular matrix. Bone piezoelectricity has been correlated with its capacity to adapt to mechanical stress and self-regenerate. For that reason, in this Doctoral Thesis it

is hypothesized that electromechanical stimulation of MSCs provided by biomimetic piezoelectric cell culture supports can be used to pre-differentiate them, specifically guiding their differentiation towards the osteogenic lineage and enhancing the results of bone regenerative therapies.

## 2. Objectives

In order to address the proposed hypothesis, the main objective is to produce and optimize 2D and 3D biomimetic piezoelectric cell culture supports to electromechanically stimulate MSCs and test their differentiation *in vitro*. These supports will be made of poly(vinylidene) fluoride combined with cobalt ferrite oxide magnetostrictive nanoparticles. The combination of a piezoelectric and a magnetostrictive phase will produce magnetoelectric composites that can be stimulated at cell culture level using a magnetic bioreactor. The deformation of the magnetostrictive phase under the effect of the magnetic field produced by the bioreactor will, in turn, deform the polymer matrix, generating a change in the surface charge of the piezoelectric polymer and transmitting the stimulus to the cultured MSCs.

To achieve the proposed objectives, the following methodology has been implemented:

I. Manufacturing of stimulable piezoelectric cell culture supports with different morphologies (flat films, membranes and microspheres) based on the combination of PVDF and CFO.
II. Electric, magnetic and physical characterization of the cell culture platforms.
III. Obtainment of biomimetic microenvironments for MSCs culture by functionalization of the proposed supports with biomolecules present in bone's extracellular matrix.
IV. Evaluation of electromechanical stimulation on MSCs viability, proliferation, and differentiation towards the osteogenic lineage.

# Chapter 1. Effective elastin-like recombinamers coating on poly(vinylidene) fluoride membranes for mesenchymal stem cells culture

This chapter was published in *European Polymer Journal*

Guillot-Ferriols, M.; del Barrio, A.; Costa, C. M.; Lanceros Méndez, S.; Rodríguez-Cabello, J. C.; Gómez Ribelles, J. L.; Santos, M.; Gallego Ferrer, G. Effective Elastin-like Recombinamers Coating on Poly(vinylidene) Fluoride Membranes for Mesenchymal Stem Cells Culture. *Eur. Polym. J.* 2021, *146* (January).

DOI: 10.1016/j.eurpolymj.2021.110269

**Personal contribution**

Membrane production, physical characterization and cell culture tests were performed by M. Guillot-Ferriols. ELRs synthesis and membrane coating was carried out at University of Valladolid by A. del Barrio and M. Santos. Membrane polarization was performed by C.M. Costa.

M. Guillot-Ferriols designed the experiments, analyzed the data, prepared the figures and wrote the first version of the manuscript. J.C Rodríguez-Cabello, M. Santos, S. Lanceros-Méndez, J.L. Gómez Ribelles and G. Gallego Ferrer helped with experimental design, reviewed the manuscript and provided financial support.

# 1. Effective elastin-like recombinamers coating on poly(vinylidene) fluoride membranes for mesenchymal stem cells culture

Guillot-Ferriols, M. [1,2], del Barrio, A. [3], Costa, C. M. [4,5], Lanceros Méndez, S. [4,6,7], Rodríguez-Cabello, J.C [2,3], Gómez Ribelles, J.L. [1,2], Santos, M. [2,3], Gallego Ferrer, G. [1,2]

*[1] Centre for Biomaterials and Tissue Engineering (CBIT), Universitat Politècnica de València, 46022 Valencia, Spain*
*[2] Biomedical Research Networking Center on Bioengineering, Biomaterials and Nanomedicine (CIBER-BBN), Valencia, Spain*
*[3] BIOFORGE Group, Centro de Investigación Científica y Desarrollo Tecnológico, Universidad de Valladolid, 47011, Valladolid, Spain*
*[4] Centre of Physics, Universidade Do Minho, 4710-058 Braga, Portugal*
*[5] Centre of Chemistry, Universidade Do Minho, 4710-058 Braga, Portugal*
*[6]BCMaterials, Basque Center for Materials, Applications and Nanostructures, UPV/EHU Science Park, 48940 Leioa, Spain*
*[7]IKERBASQUE, Basque Foundation for Science, 48013 Bilbao, Spain.*

## Abstract

Bone's inherent piezoelectricity is a key factor in regulating bone growth and mesenchymal stem cells (MSCs) fate towards the osteogenic lineage. The piezoelectric polymer poly(vinylidene) fluoride (PVDF) was thus used to manufacture electroactive membranes by means of non-solvent induced phase separation (NIPS), producing porous membranes with approximately 90 % of γ-phase for MSCs culture. The combination of the porous surface and PVDF hydrophobicity hinders cell adhesion and requires a coating to improve cell culture conditions. A layer-by-layer (LbL) method was used to deposit elastin-like recombinamers (ELRs) containing RGD sequences applying click cross-linking chemistry. ELRs potential was confirmed by comparing traditional fibronectin adsorption with ELRs LbL on PVDF electroactive membranes. Porcine bone marrow MSCs preferred ELRs-coated surfaces, which enhanced initial cell adhesion and improved proliferation after 7 days. These findings lead to new possibilities for regenerative therapies in the area of bone tissue engineering, offering the advantages of MSCs commitment towards the osteogenic lineage by applying electro-mechanical stimulation on electroactive substrates.

## Keywords

Poly(vinylidene) fluoride; piezoelectricity; elastin-like recombinamers; RGD; layer-by-layer; mesenchymal stem cells

## 1.1. Introduction

Poly(vinylidene) fluoride (PVDF) is a piezoelectric semi-crystalline polymer which can crystallize into five polymorphs, α, β, γ, δ and ε. Chain conformations, all trans (TTT) planar zigzag and $T_3GT_3G$ for β and γ phases respectively (Lovinger 1982), and the electronegativity difference between fluorine and hydrogen atoms create a net dipole moment in these polymorphs and confer them electroactive properties (Martins, Lopes, and Lanceros-Mendez 2014).

PVDF has been proposed as a candidate for bone tissue engineering (TE) applications due to its capacity to produce a surface charge variation when a mechanical input is applied (Jacob et al. 2018), reproducing bone's inherent piezoelectricity, as discovered by Fukada and Yasuda (Fukada and Yasuda 1957). This mechanism is hypothesized to be involved in bone's capacity to adapt to mechanical stress and tissue regeneration (Ahn and Grodzinsky 2009). Electro-mechanical stimulation has been shown to enhance cell viability, proliferation and differentiation on osteogenic progenitors (C. Ribeiro, Moreira, et al. 2012; C. Ribeiro, Correia, et al. 2015; Sobreiro-Almeida et al. 2017).

Specific bioreactors, compatible with cell culture conditions, have been designed to fulfil the need of transmitting stimulus or cues to different cell types cultured on a wide variety of supports (Castro, Ribeiro, et al. 2020; Castro, Fernandes, et al. 2020). As a matter of fact, bioreactor systems based on a vertical vibration module have been used to electro-mechanically stimulate human adipose stem cells, mechanically deforming the PVDF matrix and transmitting the electrical stimulus to the cells (C. Ribeiro, Pärssinen, et al. 2015; S. Ribeiro et al. 2020).

The interest in using PVDF in bone TE lies in the presence of the electroactive phases, which can be obtained during the manufacturing process. The PVDF $\alpha$-phase is usually obtained as crystallization from the melt results in this polymorph (Gregorio 2006). The $\beta$-phase can be produced by uniaxial stretching of the $\alpha$ polymorph (Sencadas, Gregorio, and Lanceros-Méndez 2009), which is a two-step process. Crystallization below 70 ºC using polar solvents such as dimethylformamide can obtain both $\beta$ and $\gamma$ electroactive phases (Pagliero et al. 2020; Boccaccio et al. 2002), reducing the manufacturing process to a single step (C. Ribeiro et al. 2018) and allowing the support to be manufactured in complex shapes.

Non-solvent induced phase separation (NIPS), which consists of the precipitation of the polymer cast on a surface by immersing it in a coagulation bath containing a non-solvent, is compatible with the above-mentioned parameters (Wang et al. 2009; Cheng 1999). Different topographies and diverse electroactive contents can be obtained from different applied manufacturing conditions (Liu et al. 2011) in a reliable, cost-effective and simple method of producing electroactive PVDF supports for cell culture (Guillot-Ferriols et al. 2020).

When considering PVDF for biological applications the surface properties must be modified to control cell behaviour due to its high hydrophobicity (Webb, Hlady, and Tresco 1998). When culturing cells with osteogenic characteristics fibronectin adsorption is usually applied to enhance their initial adhesion and proliferation (Sobreiro-Almeida et al. 2017; C. Ribeiro, Panadero, et al. 2012; C. Ribeiro, Pärssinen, et al. 2015), however fibronectin has proven to be ineffective in highly porous PVDF supports regarding mesenchymal stem cell (MSCs) adhesion (Morales-Román et al. 2019). Elastin-like recombinamers (ELRs) have arisen as suitable biomolecules for biomimetic polymer coatings that include specific biofunctional sequences. ELRs are synthetic elastin-inspired polypeptides, produced by DNA recombinant technologies, formed by repetitive sequences comprising the most widely used

pentapeptide domain Val-Pro-Gly-X-Gly (VPGXG), X being any natural or modified amino acid, with the exception of L-proline (Rodríguez-Cabello et al. 2009). ELRs can be engineered to incorporate bioactive sequences with specific properties for cell attachment, proliferation and differentiation (Girotti et al. 2004). In this regard, the Arg-Gly-Asp (RGD) sequence, found in a number of extracellular matrix proteins, is known to mediate cell attachment and spreading (Berg et al. 2004; Ruoslahti 1996). This domain was one of the first bioactive motifs introduced to the ELR main chain (Nicol, Channe Gowda, and Urry 1992) and was applied as a substrate coating, showing improved cell affinity (Costa et al. 2009). Besides mediating cell adhesion, the RGD sequence has been shown to be involved in MSCs differentiation towards the osteogenic lineage (Qu et al. 2010; Yang et al. 2005; Shin et al. 2005; Anderson et al. 2012).

Biocompatible ELRs click hydrogels can be obtained by interchain crosslinking via catalyst-free Hüisgen 1,3-dipolar cycloaddition under physiological conditions in a mild and cell-friendly process with atom economy (I. González De Torre et al. 2014). These click hydrogels are outstanding candidates for tissue engineering (Nettles, Chilkoti, and Setton 2010) in general and as layer-by-layer (LbL) stable and biomimetic coatings, with increased adhesion and proliferation when RGD is incorporated, establishing the basis of future biomedical applications (Sousa et al. 2017).

In this study we combined electroactive PVDF membranes produced by NIPS with ELRs containing RGD sequences deposited on their surface by the LbL technique, applying the click crosslinking approach, as cell culture supports for *in vitro* mesenchymal stem cell culture. The effectiveness of ELRs LbL coating on PVDF electroactive supports was compared with traditional fibronectin adsorption using porcine bone marrow MSCs. The results on cell proliferation on the ELRs-coated materials obtained show that they are promising candidates for electro-mechanical stimulation approaches.

## 1.2. Materials and methods

### 1.2.1. Electroactive membrane preparation

Poly(vinylidene) fluoride membranes were produced by the non-solvent induced phase separation technique, for which a 20 % (w/v) PVDF solution (Solef® 6010 PVDF Homopolymer, Solvay) was prepared in dimethylformamide (DMF) (Scharlab, synthesis grade). The solution was magnetically stirred at 60 ºC until complete dissolution of the polymer. Prior to membrane preparation, the solution was kept non-stirred for 30 min to remove air bubbles and then spread on a glass plate with a 750 μm casting knife. The plate was immersed in a coagulation bath containing absolute ethanol (Scharlab) at 25 ºC for 1 h. After complete precipitation, the membranes were washed under agitation for 24 h in deionized water to remove excess ethanol and remaining traces of DMF, with a water change every two hours. Once washed, the membranes were frozen at -80 ºC and lyophilized for 24 h.

### 1.2.2. Membrane characterization

#### 1.2.2.1. Morphological analysis

Membrane surface and cross-section morphology were analysed by means of Field Emission Scanning Electron Microscopy (FESEM). Samples were coated with platinum following a standard sputtering protocol for 90 s (JFC 1100, JEOL, Japan) and visualized in an Ultra 55 microscope (Zeiss). Accelerating voltage was 2 kV. Surface spherulite diameter was measured using ImageJ software (National Institutes of Health, Bethesda, Maryland, USA). Three different membranes from three different batches were analysed with 100 spherulites per sample.

ELRs deposition by the layer-by-layer technique was also confirmed by acquiring images of the coated surface and the cross-section by FESEM applying an accelerating voltage of 1 kV.

Porosity of the developed membranes was measured filling the pores with ethanol and applying Equations 1 and 2:

$$V_{pores} = \frac{m_{wet} - m_{dry}}{\rho_{ethanol}} \qquad \text{Eq. 1}$$

$$\emptyset = \frac{V_{pores}}{V_{pores} + V_{PVDF}} \qquad \text{Eq. 2}$$

where $m_{wet}$ and $m_{dry}$ are the weight of the membranes before and after immersion in ethanol, respectively. $\rho_{ethanol}$ is ethanol density (0.789 g/cm$^3$). PVDF volume ($V_{PVDF}$) was calculated from the dry weight of the membrane and assuming a density of 1.775 g/cm$^3$.

Three replicates per sample were measured from three different samples produced in different preparations.

#### 1.2.2.2. Analysis of the electroactive phases

The electroactive phase content present in the membranes was assessed by Fourier-transform Infrared Spectroscopy (FTIR). Benz and Euler (Benz and Euler 2003) defined a simple method to quantify PVDF crystalline phases present in a sample, especially in the remarkable presence of γ-phase. Different phases were identified by their representative absorption bands (762 cm$^{-1}$ for α, 1279 cm$^{-1}$ for β and 835 cm$^{-1}$ for γ). Since the absorption band at 835 cm$^{-1}$ has contributions from β, γ and the amorphous phase, the γ -phase fraction (F(γ)) present in the sample can be calculated applying the following equations (Benz and Euler 2003; Chang et al. 2016):

$$F(\gamma) = \frac{X_\gamma}{X_\gamma + X_\alpha} \qquad \text{Eq. 3}$$

$$A_{835} = (K_\gamma^{835} X_\gamma + K_\beta^{835} X_\beta + K_{am}^{835}(1 - X_{total}))t \qquad \text{Eq. 4}$$

$$A_{762} = K_\alpha^{762} X_\alpha \, t \qquad \text{Eq. 5}$$

$$A_{1279} = K_\beta^{1279} X_\beta \, t \qquad \text{Eq. 6}$$

Where $X_\alpha$ and $X_\gamma$ are the fraction of $\alpha$ and $\gamma$ phases and $A_\alpha$ and $A_\gamma$ are their absorptions at 762 and 835 $cm^{-1}$, respectively. K is the characteristic absorption coefficient at the characteristic wavenumber of each of the phases ($K_\alpha^{762}$ = 0.365 $\mu m^{-1}$, $K_\gamma^{835}$ = 0.15 $\mu m^{-1}$, $K_{am}^{835}$ = 0.0259 $\mu m^{-1}$ (Benz and Euler 2003)), $X_{total}$ is total sample crystallinity and *t* is its thickness. The $\beta$-phase contribution to Equation 4 is negligible since there is no peak presence at 1279 $cm^{-1}$. Also, the high crystallinity of the membranes makes $K_{am}^{835}$ much larger than $K_{am}^{835}(1 - X_{total})$ and $K_\gamma^{835}$ is five times larger than $K_{am}^{835}$. In this case, equation 3 can be reduced to:

$$F(\gamma) = \frac{A_{835}}{\left(\frac{K_\gamma^{835}}{K_\alpha^{762}}\right) A_{762} + A_{835}} \qquad \text{Eq. 7}$$

Measurements were taken on an ALPHA FTIR spectrometer (Bruker) in ATR mode from 4000 to 400 $cm^{-1}$ at a wavelength resolution of 4 $cm^{-1}$. Three different membranes from three different batches were analysed.

#### 1.2.2.3. Membrane's crystalline content

Differential Scanning Calorimetry (DSC) was used to determine the degree of crystallinity ($X_c$) of the PVDF membranes produced and their melting temperature. The samples were scanned in a DSC Pyris 1 (PerkinElmer) calorimeter, previously encapsulated in aluminium pans, from 0 °C to 200 °C at a heating range of 20 °C/min in a dry nitrogen atmosphere.
$X_c$ was determined by means of the following equation (Benz and Euler 2003; Lopes et al. 2011; Chang et al. 2016):

$$X_c = \frac{\Delta H_m}{\Delta H_{100}} \times 100 \qquad \text{Eq. 8}$$

Where $\Delta H_m$ is the melting enthalpy of the PVDF membranes measured in DSC and $\Delta H_{100}$ is the melting enthalpy for a 100 % crystalline sample of pure PVDF, whose value is 104.7 J/g (Nakagawa and Ishida 1973). Three different membranes from three different batches were analysed.

#### 1.2.2.4. Poling method and piezoelectric coefficient evaluation

The porous membranes were poled by the contact method, with the polymer membranes placed inside a silicone oil bath to prevent electrical breakdown. Adhesive aluminium tape was used as electrode materials on both membrane surfaces. Polarization conditions were optimized to a final electric field of ~10 kV at a constant current of 10 $\mu$A for 1 h at a temperature of 120 ºC. After the poling time, the membranes were cooled down to room temperature under the application of the electric field.
The piezoelectric $d_{33}$ response was analysed on a Wide Range d33-meter Model 8000, APC Int Ltd).

### 1.2.3. Elastin-like recombinamers deposition on poly(vinylidene) fluoride membranes

#### 1.2.3.1. Biosynthesis and purification of elastin-like recombinamers

ELRs were bioproduced by genetic engineering technology and purified by Inverse Transition Cycling (ITC) (Pinedo-Martín et al. 2014; Meyer and Chilkoti 1999), exploiting their thermosensitive behaviour. The ELR thus obtained was named as HRGD and its amino acid sequence was:

HRGD: MGSSHHHHHHSSGLVPRGSH-MESLLP-{[(VPGIG)2(VPGKG)(VPGIG)2]2-AVTGRGDSPASS- [(VPGIG)2(VPGKG)(VPGIG)2]2]}6-V

The polymer contained VPGKG pentapeptide located uniformly along the main chain to enable further chemical modification through the ε-amine group of lysines. The HRGD biopolymer also contained the peptide loop found in human fibronectin, the carrier of the specific RGD sequence for cell adhesion. ELR purity and chemical characterization were verified by sodium dodecyl sulphate polyacrylamide gel electrophoresis (SDS–PAGE), matrix-assisted laser desorption/ionization time-of-flight (MALDI-ToF) mass spectrometry, amino acid composition analysis, differential scanning calorimetry and nuclear magnetic resonance (NMR) (Girotti et al. 2015). $^{1}$H-NMR spectroscopy and MALDI-ToF-mass spectrometry were carried out in the Instrumental Techniques Laboratory (LTI) of the Research Facilities of the University of Valladolid.

#### 1.2.3.2. Elastin-like recombinamers chemical modification

ELRs were chemically modified to carry cyclooctyne or azide groups in the lateral chain, obtaining the corresponding modified biopolymers (the one bearing cyclooctyne derivatization was labelled RGD-CO and the one with azide groups RGD-N3). The biopolymer chemical functionalization was carried out by modifying the ε-amine groups, as previously described (I. González De Torre et al. 2014).

To modify HRGD with a cyclooctyne group, the ELR was dissolved in DMF (Sigma) at a final concentration of 0.05 g/mL at room temperature in an inert atmosphere. Bicyclo [6.1.0] non-4-yn-9-yl-methyl N-succinimidyl carbonate (0.6 eq, Mw 291.30 mg/mmol, GalChimia, A Coruña, Spain) dissolved in DMF was then added to the ELR solution at a final concentration of 3.3 mg/mL. The resulting mixture was stirred for 48 h at room temperature in an argon atmosphere. The modified RGD-CO was purified by precipitation with diethyl ether. The resulting white solid was washed 3 times with acetone and dried under reduced pressure. The solid was re-dissolved in cold ultrapure MQ water at 4 °C, dialyzed against MQ water, filtered through 0.22 μm filters (Nalgene) and the sterile solution was freeze-dried prior to storage.

Following the same procedure, HRGD was modified to bear an azide group. This time 2-Azido ethyl (2,5-dioxopyrrolidin-1-yl) carbonate (0.6 eq, Mw 228.17 mg/mmol, GalChimia, A Coruña, Spain) was dissolved in DMF and then added to the ELR solution at a final concentration of 1.3 mg/mL. RGD-N3 was purified as previously described.

The modified RGD-CO and RGD-N3 biopolymers were characterized by NMR, MALDI-ToF and Fourier-transform infrared spectroscopy (FTIR-ATR) (supplementary material). MALDI-ToF and $^{1}$H-NMR (in DMSO-d6) enabled us to quantify the degree of lysine modification.

#### 1.2.3.3. Layer-by-Layer procedure for elastin-like recombinamers-covered poly(vinylidene) fluoride membranes

PVDF membranes cut into 1 cm$^2$ squares were used as the substrate for the ELRs coating. The square surfaces were indicated by a sign on the opposite face to the cell culture. These substrates were first cleaned and activated by argon plasma treatment. This treatment is a cleaning and activation step aimed at promoting a better coating improving adsorption of the first layer onto the surface. The membranes were placed in the chamber and vacuum was generated (P=600 mTorr), a high-frequency (29.6 W) 20 mL/min argon plasma flow passed through the samples for the appropriate time (1, 5, 20 and 30 minutes) to optimize the plasma treatment activation time.

Secondly, different ELRs solution concentrations and immersion orders were studied to achieve the best coating for cellular assays. The ELRs modified with either cyclooctyne or azide groups were dissolved at 10 or 25 mg/mL, according to the assay, in water at 4 ºC overnight and stored at this temperature in separate containers. pH value of the different solutions was 7.5. pH control is less critical than in other conventional layer-by-layer protocols since the link between layers is produced by click reaction between azide and cyclooctine groups, non-acid species. Selecting the optimized plasma treatment protocol, the activated PVDF membranes were sequentially immersed in the ELRs solutions with either RGD-N3 or RGD-CO as the first layer for two seconds and left to dry for five minutes between dippings to generate the first bilayer. A drying step, instead of washing, was chosen in order to assure that the click reaction between the layers was produced. Washings would probably remove the coating without letting the covalent crosslink to end. The process was then repeated and after being left to dry for 45 minutes the membranes were freeze-dried. Two bilayers were selected as the optimal number of layers as it was enough to completely cover the surface obtaining the thinnest membrane coating. The optimized protocol is described in Scheme 1.1.

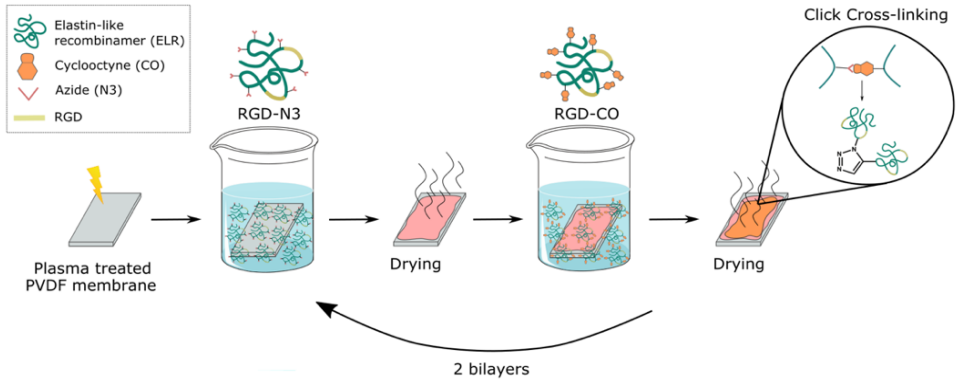


**Scheme 1.1. Illustration of the optimized layer-by-layer process with RGD-N3 (as first layer) and RGD-CO ELRs onto plasma treated PVDF membranes.**

#### 1.2.3.4. Characterization of elastin-like recombinamers-covered poly(vinylidene) fluoride membranes

As process control, the non-activated, activated and the final biofunctionalized membranes were evaluated by contact angle measurements determined by a sessile drop method using a Data Physics OCA20 instrument equipped with an adapted CCD video camera. The coating performance was analysed by Fourier-transform infrared spectroscopy (FTIR-ATR) on a Bruker TENSOR 27 acquiring 64 scans between 500-4000 $cm^{-1}$ to compare the spectra of the biofunctionalized, plasma treated and non-coated membranes. The membrane surfaces and cross-section morphology were analysed by FESEM as described in Section 2.2.1.

### 1.2.4. Cell culture assays

Porcine bone marrow mesenchymal stem cells (pMSCs) were used to study the cell proliferation response. pMSCs were expanded in basal medium containing Dulbecco's modified Eagle medium (DMEM) high glucose (4.5 g/L) with GlutaMAX™ (Gibco), 10 % (v/v) Foetal Bovine Serum, FBS (Gibco), 100 U/mL penicillin-100 μg/mL streptomycin, P/S (Life technologies), and 5 ng/mL of Fibroblast Growth Factor 2, FGF-2 (Eurobio), at 37 ºC in a humidified atmosphere with 5 % $CO_2$. All the experiments were performed in passage 5.

After choosing the best layer-by-layer protocol for ELRs deposition, coated (PVDF + ELRs) and non-coated membranes (PVDF) were cut into 8 mm disks to fit on the bottom of a 48 well plate. Samples were sterilized by UV for 20 minutes on each side, after which the membranes were washed in ethanol 70 % (v/v) for 15 minutes under shacking and washed 6 times in Dulbecco's Phosphate Buffered Saline, DPBS (Sigma-Aldrich) to eliminate possible traces of ethanol. Glass slides, used as controls, were sterilized by sonication in ethanol for 10 minutes and then were exposed to UV for 20 minutes each side.

After sterilization, the non-coated membranes and glass slides were incubated in a solution of human plasma fibronectin (Sigma-Aldrich; 20 μg/mL) for 1 hour at room temperature. Fibronectin coating was used to compare the effectiveness of ELRs layer-by-layer deposition and the traditional protein adsorption. After fibronectin coating, the samples were washed twice with DPBS to remove non-adsorbed fibronectin. The samples were placed in a 48 well plate, 3 replicates per group, and silicon rings were used to prevent the membranes from floating inside the wells, glass slides included. Basal medium without FBS or FGF-2 was added to the wells to condition the membranes before cell seeding.

12 h before cell seeding, the cells were starved in basal medium containing 1 % (v/v) FBS to synchronize the cell cycle. To study cell proliferation the cells were seeded at a density of 8 x $10^3$ cells/$cm^2$ in basal medium without FBS to promote cell adhesion either to fibronectin or ELRs containing RGD sequences. 100 μL containing the required number of cells was deposited on top of each sample inside the silicon rings. 3 h later, after cell attachment, the required volume of basal medium and FBS for a final concentration of 10 % (v/v) was added to each well. The medium was changed every 2 or 3 days. After 24 h, 3

and 7 days the samples were fixed in a 4 % (v/v) paraformaldehyde solution (Panreac) for 20 minutes.

Initial adhesion and proliferation studies were carried out by means of staining cell cytoskeleton and nucleus. After fixation, the samples were permeabilized and blocked in 1 % (w/v) bovine serum albumin (BSA; Sigma-Aldrich) solution in DPBS/0.1 % (v/v) Tween-20 (Sigma-Aldrich) for 1 h at room temperature and then incubated with Alexa Fluor Phalloidin 488 (1:100 Fisher Scientific) for 2 hours in a humidified chamber. After washing the samples 3 times with DPBS/0.1 % (v/v) Tween-20 (Sigma-Aldrich), the PVDF membranes were treated with Sudan Black B solution following the protocol described in Morales-Román et al. (Morales-Román et al. 2019). As PVDF autofluorescence hinders image acquisition and cell counting, Sudan Black B treatment is necessary to obtain quality images of the cells. The samples were then washed 3 times with DPBS and incubated for 20 minutes with DAPI (1:200; Sigma-Aldrich) in mounting medium.

Four representative areas of each sample were studied, acquiring images with a fluorescence microscope (Nikon Eclipse 80i). The images were analysed on ImageJ software (National Institutes of Health, Bethesda, Maryland, USA). Two independent assays were carried out with three replicates per group. Results were normalized by initial cell seeding density (8 x $10^3$ cells/$cm^2$) and calculated as relative cell proliferation, expressed as $Log_2$ of the ratio obtained. Each unit represents a doubling in the cell population. This representation method highlights MSCs initial adhesion and proliferation rate on the different conditions tested. Negative values indicate that the number of retained cells is lower than the initial number of seeded cells onto the biomaterial.

#### 1.2.5. Statistical analysis

All results were expressed as mean ± standard deviation. Statistical analysis was performed on SPSS Software. Two-way ANOVA analysis was applied to the homogeneous groups after checking homoscedasticity by the Levene test. A 95 % confidence interval was set to accept significant inter-group differences (*p-value* < 0.05).

### 1.3. Results and discussion

#### 1.3.1. Membrane characterization

PVDF membranes were produced by non-solvent induced phase separation (NIPS) in an ethanol bath at 25 ºC. Of the wide variety of parameters, the selection of the proper non-solvent in the coagulation bath is instrumental in membrane morphology formation. As PVDF is a semi-crystalline polymer, its precipitation during this process is determined by two events associated with crystallization: liquid-liquid demixing and solid-liquid demixing (Liu et al. 2011). The presence of ethanol in the coagulation bath, a soft non-solvent, reduces the solvent-nonsolvent exchange, allowing crystallization, a slower process, before liquid-liquid demixing takes place. Membrane structure and morphology were characterized by FESEM, as shown in Figure 1.1. Figure 1.1 (b) shows the symmetrical PVDF membranes with both porous surfaces on the top (Figure 1.1 (a)) and bottom (images of the bottom surface are not displayed). The use of soft solvents in the coagulation bath gives rise to symmetric membranes without the characteristic presence of finger-like structures or macrovoids present in water-bath produced membranes (Jung et al. 2016). Crystallization

occurs before crossing the binodal line, allowing crystalline globules to grow and coalesce (Pagliero et al. 2020).

Surface topography is formed by a particulate-like morphology composed of PVDF globules or microbeads. These structures measure 1.1 ± 0.2 μm, in agreement with previous results reported by Lin et al (Lin et al. 2006). Pagliero et al. (Pagliero et al. 2020) manufactured PVDF membranes in ethanol baths varying the PVDF concentration in the initial solution. Highly concentrated PVDF solutions (above 14 % w/v) gave rise to smaller spherulites than the ones obtained from diluted solutions. A polymer concentration rise in the initial solution increases solution viscosity, favouring PVDF entanglements, restraining chain mobility and reducing spherulite growth, generating a more compact interconnected network, as in the case of the present membranes using 20 % w/v PVDF solution as shown in Figure 1.1 (a). These globules are connected to each other by fibrils, probably with the thickness of one or more folded lamellae, as previously reported by Lin et al. (Lin et al. 2003).

Porosity was determined by filling the membrane pores with ethanol and applying Eqs. (1) and (2). Ethanol was chosen since PVDF is hydrophobic and its pores cannot be filled with water and this would underestimate the pore volume (Morales-Román et al. 2019). The PVDF membranes produced by NIPS in an ethanol coagulation bath had a porosity of 81.7 ± 0.5 %.

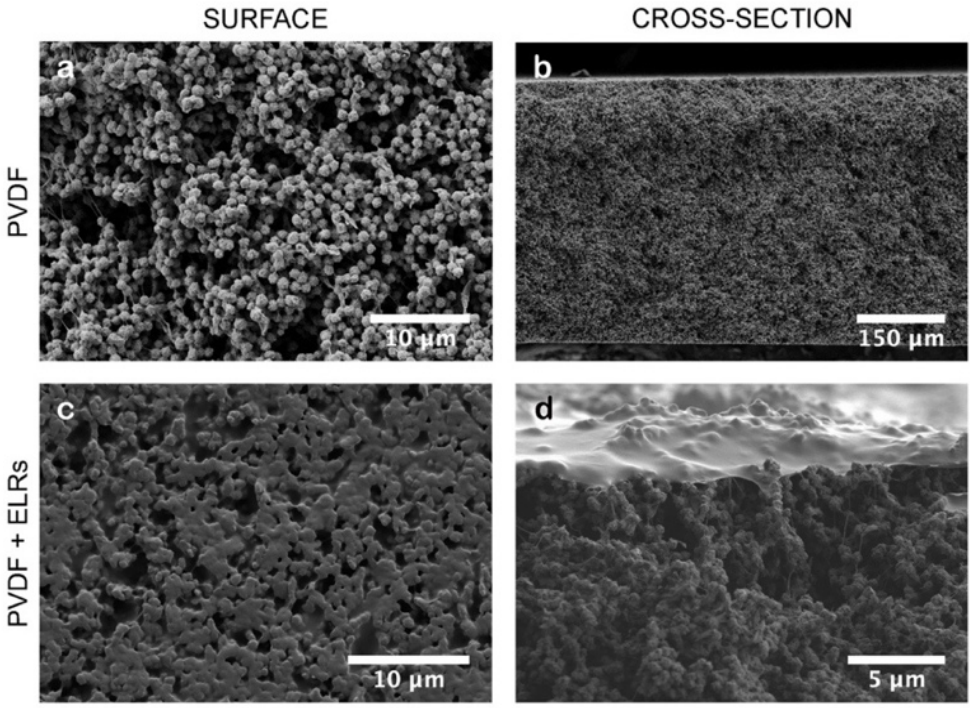


**Figure 1.1. Surface and cross-section FESEM images of PVDF membranes produced by non-solvent induced phase separation before ELRs deposition by layer-by-layer (a and b) and after (c and d).**

Fourier-transform infrared spectroscopy (FTIR) has proven to be a valid method of identifying and quantifying the PVDF polymorphs present in different samples, applying the

equations cited in Section 2.2.3. Martins et al. (Martins, Lopes, and Lanceros-Mendez 2014) reviewed the characteristic absorption bands of the most common crystalline phases α, β and γ. The non-electroactive α-phase is defined by the wavenumbers at 532, 614, 762, 795, 855, 976 $cm^{-1}$, the most representative and thus used to calculate its fraction being at 762 $cm^{-1}$. The bands at 445, 510, 840 and 1279 $cm^{-1}$ are used to identify the β-phase, while 431, 512, 812, 835 and 1234 $cm^{-1}$ are used for the γ-phase.

The representative FTIR-ATR spectrum of PVDF membranes is displayed in Figure 1.2 (a). α-phase characteristic bands at 614, 762 and 976 $cm^{-1}$ can be seen, as highlighted in the graph. Surprisingly, no β-phase peaks are present, especially the absence of one at 1279 $cm^{-1}$. However, most of the γ-phase characteristic bands can be found in the sample, including 431, 835 and 1234 $cm^{-1}$. Since 1234 $cm^{-1}$ tends to appear as a shoulder, 835 $cm^{-1}$ is used to quantify the percentage of γ-phase present in the membranes (Benz and Euler 2003; Lopes et al. 2011; Chang et al. 2016, 2017). The absence of β-phase peaks makes its contribution to this 835 $cm^{-1}$ negligible, allowing Equation 7 to be applied to obtain the γ-phase fraction. The γ-phase is 93.3 ± 1.4 %, with just a small contribution from the α-phase (6.7 ± 1.4 %).

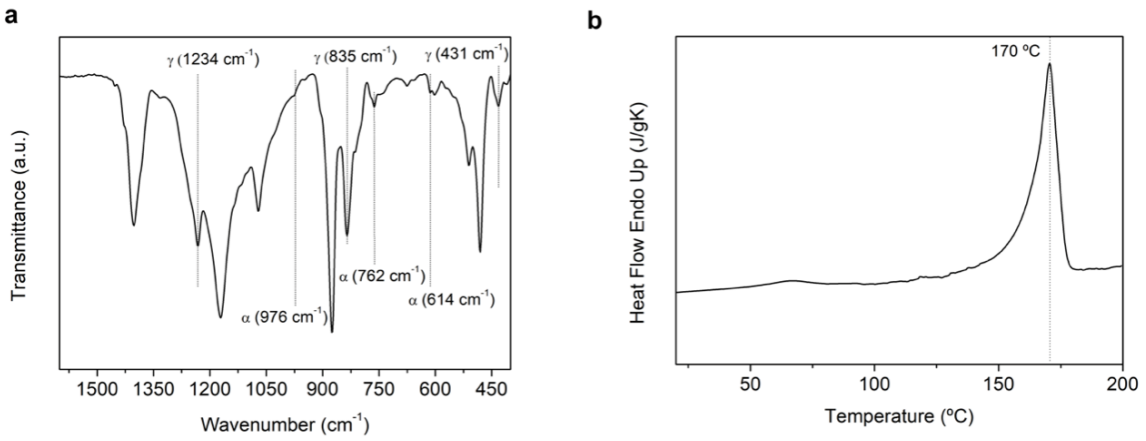


**Figure 1.2. Representative (a) FTIR-ATR spectrum and (b) DSC curve of PVDF membranes produced by non-solvent induced phase separation.**

Using FTIR to identify electroactive β and γ phases is still a subject of debate, since their similar structure provides characteristic absorption bands which are a superposition of both phases. Traditionally, the band at 840 $cm^{-1}$ has been used to identify the β-phase. Nonetheless, the presence of this band is sometimes shown as a shoulder at 833 $cm^{-1}$ in the 840 $cm^{-1}$ band, or as it is the case in the spectrum presented, the peak appears displaced towards 835 $cm^{-1}$ indicating the presence of the γ-phase. This subtle displacement alone is not enough to assure the presence of this polymorph, however bands at 1279 and 1234 $cm^{-1}$ can be used to clearly identify them, since the β and γ contributions, respectively, are unique at these wavenumbers.

Obtaining the γ-phase is more difficult than β and traditionally has only been achieved by isothermal crystallization at extremely high temperatures and slow cooling rates (Kim et al. 2003). Adding fillers (Lopes et al. 2011) and crystallization under vacuum (Lizundia et al. 2020) have also produced PVDF supports in this electroactive phase. Some authors have reported obtaining it by means of NIPS (Boccaccio et al. 2002; Chang et al. 2016). Highly polar solvents, such as dimethylformamide or dimethylacetamide, favour crystallization in trans phases due to their interaction with the polymer, rotating the C-F bond around the C-C bonds of the chain backbone (Salimi and Yousefi 2004). In other words, the membranes' γ-phase is produced by the dipole rotation (α to γ) induced by solvent polarity. The presence of alcohols in the coagulation bath has been found to favour the interaction between its -OH groups and the DMF solvent (Chang et al. 2016). This phenomenon partially allows the rotation back to α conformation, leading to the low contribution to the sample content.
Membrane electroactive potential was confirmed by measuring the piezoelectric $d_{33}$ response after poling the samples. Corona discharge poling could not be used due to the high membrane porosity (up to 80 %), which produced an electrical breakdown, so the direct contact poling method filling the pores with silicone oil was used. Immediately after polarization, the $|d_{33}|$ response (typical negative values for PVDF were obtained) varied between 3 and 6 pC/N, depending on the position of the measurement site.

The obtained $d_{33}$ coefficient is in agreement with the values expected for γ-phase PVDF, -7 pC/N as reported by Lopes et al. (Lopes et al. 2011) for PVDF samples containing 91 % of γ-phase, confirming the majority presence of this polymorph in the produced membranes.

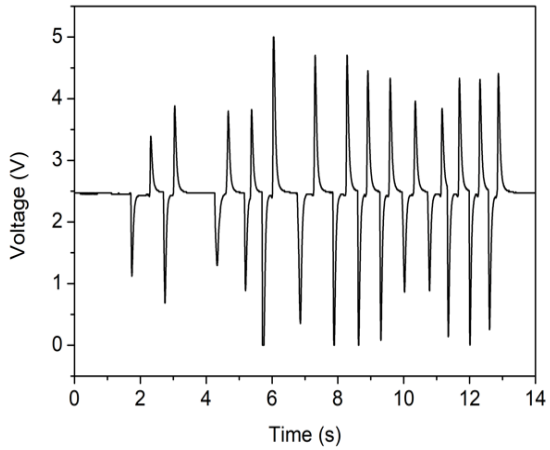


**Figure 1.3. Voltage generation throughout the piezoelectric PVDF membrane under pressure cycles.**

These piezoelectric membranes were coupled to a readout electronic circuit (Gonçalves et al. 2019) to determine the voltage generated under cycling pressure solicitation by gentle finger pressing and releasing. The output of the amplifying circuit in unloaded conditions, as shown by Gonçalves et al. in (Gonçalves et al. 2019), averaged to 2.5 V, leading to non-zero voltage values when the membrane was not pressed. When loading was applied by finger pressing, a negative voltage peak was generated while a positive peak appeared

when released. Figure 1.3 shows the voltage generated when the membrane was under cycling pressure solicitation, the height of the peaks was not constant since the compression load was not controlled. Under mechanical deformation due to gentle finger pressure a stable voltage was generated, compatible with the measured piezoelectric response.

Despite the many efforts to elucidate the bone piezoelectric coefficients, the published data varies widely. Those attributed either to bone or tendons containing oriented collagen fibers usually differ by more than one order of magnitude (Liboff and Furst 1974; Fukada 1968; Fukada and Yasuda 1964; Lang 2000; Jacob et al. 2018). Halperin et al. (Halperin et al. 2004) studied the piezoelectric coefficients in dry and wet human bone and concluded that they vary in the range of 7 to 8 pC/N, in agreement with the results published by other authors (Fukada and Yasuda 1964; Liboff and Furst 1974). Even though γ-PVDF electroactive response is lower than that of β-PVDF, the piezoelectric coefficient obtained is in the same order of magnitude as those reported by the aforementioned authors, indicating that γ-PVDF membranes are suitable candidates for future mesenchymal stem cell differentiation approaches.

PVDF thermal properties and degree of crystallinity were assessed by differential scanning calorimetry. The melting endotherm obtained at a heating range of 20 ºC/min is shown in Figure 1.2b. The melting peak indicating the melting temperature ($T_m$) of the PVDF membranes appears at 169.4 ± 1.2 ºC. Even though the γ polymorph shows a $T_m$ around 8 ºC higher than α and β, as described by Gregorio (Gregorio 2006), this polymorph is obtained from the isothermal crystallization at 166 ºC. Higher crystallization temperatures lead to higher crystallite sizes and raise the melting temperature. The PVDF membranes described here were obtained at 25 ºC, which resulted in a lower melting temperature, in agreement with the findings of Chang et al. (Chang et al. 2016, 2017), who manufactured PVDF membranes by the NIPS technique using different solvents and alcohols in the coagulation bath and obtained mostly γ-phase membranes with melting temperatures around 165-170 ºC.

The membrane's degree of crystallinity was obtained by applying Equation 8. $X_c$ is 65 ± 1 % for PVDF membranes, which confirms that liquid-liquid demixing is delayed by the non-solvents due to the reduced solvent-nonsolvent exchange rate. This delay allows crystallization to take place including nucleation and spherulite growth, producing membranes with a high percentage of crystalline phase within their structures.

### 1.3.2. Elastin-like recombinamers deposition by the layer-by-layer technique

Surface fibronectin adsorption is a common technique when using PVDF as the cell culture support since its hydrophobicity hinders initial cell adhesion. However, the surface can be coated completely with other approaches, such as layer-by-layer ELRs deposition. Strong covalent bonds are formed between the layers ensuring a permanent coating suitable for the tissue engineering field. This coating is considered cell-friendly because of ELRs' biocompatibility, as has been shown in previous works (Gónzalez De Torre et al. 2015) and

the copper-free click cross-linking between the layers. The click method involves the 1,3-dipolar cycloaddition of an azide and an especially active alkyne group, such as cyclooctyne (based on annular tension), allowing the reaction to take place without a catalyst (Israel González De Torre et al. 2014) and applying atom economy.

An initial study was performed comprising the optimization and characterization of diverse coating conditions. The membrane activation time using the plasma treatment was first optimized and the RGD-N3 and RGD-CO solution concentration and the deposition order of the first layer was then studied. Once the optimal conditions were obtained the PVDF membranes were coated for cell culture tests by depositing two ELRs bilayers.

The PVDF membranes were activated by a simple, clean and effective plasma treatment method. The argon plasma flow (20 mL/min) was passed through a vacuum chamber (600 mTorr) and several time periods (1, 5, 20 and 30 minutes) were applied to the samples deposited inside. This step was controlled by measuring the contact angle of a drop of water on the PVDF membrane surface, as well as by FTIR-ATR. The activation step provides some oxidation of covalent bonds introducing a small number of hydroxyl groups at the surface that promote a small variation in the contact angle value observed before and after performing the activation. The small difference in the contact angle between non-activated (133 ± 1°) and activated membranes at different times (non-significant differences in contact angle values around 120°) slightly reduced hydrophobicity despite the plasma treatment.

FTIR-ATR of both pristine PVDF membrane and plasma activated one were performed after plasma treatment (see supplementary material, Figure S1.1). The amount of hydroxyl groups introduced by argon plasma is not high enough to show substantial changes in the FTIR spectrum. However, in all the time periods tested, the activation was enough to immerse the samples in aqueous solutions for ELRs coating. The minimum activation time of 1 minute was chosen for the LbL process to avoid damaging the membranes.

Before membrane coating, the ELRs were chemically modified to carry azide and cyclooctyne functional groups, giving rise to RGD-N3 and RGD-CO, respectively. Both biopolymers were functionalized by modifying the ε-amine groups present in the lysines side chain, as described in Section 2.3.2. RGD-N3 and RGD-CO were characterized by $^{1}$H-NMR spectroscopy, MALDI-ToF mass spectrometry and FTIR-ATR (see supplementary material).

The presence of twenty-four lysine residues distributed along the aminoacidic chain of the HRGD biopolymer allowed the amidation reaction of their amine groups with an N-succinimidyl carbonate derivative as a cyclooctyne carrier, giving rise to the RGD-CO biopolymer bearing cyclooctyne groups distributed along the ELR chain. A total of thirteen lysines were modified by 0.6 reagent equivalents, which yielded 90 % conversion. This conversion was determined by the MALDI-ToF and $^{1}$H-NMR (in DMSO-d6) analysis, which enabled the quantification of the degree of lysine modification (supplementary material). The RGD-CO structure (Figure S1.2) was identified from the NMR signals and, above all, the integral value of H-N hydrogen from the newly formed carbamate allowed to quantify the number of amine groups modified. This lysine conversion value was consistent with the

molecular weight increase recorded by the RGD-CO MALDI-ToF spectrometry (Figure S1.3).

Using 0.6 equivalents of an N-succinimidyl carbonate carrying azide group, HRGD was chemically modified in a similar amidation reaction to achieve RGD-N3. In this process, fourteen lysines were modified, giving a 97 % conversion rate. The number of lysines modified was calculated as explained above for RGD-CO (Figure S1.4 and S1.5 for $^{1}$H-NMR and MALDI-ToF, respectively) but, in this case, the appearance of a new band at 2100 $cm^{-1}$ in the FTIR-ATR spectrum confirmed the presence of azide groups in the RGD-N3 biopolymer chain (Figure S1.6).

After optimizing the time of PVDF membrane activation with plasma treatment and adequately modifying the biopolymers to achieve RGD-N3 and RGD-CO, the PVDF membrane coating process was optimized following the coating method described in Section 2.3.4. Layer-by-layer assays were performed at different RGD-CO and RGD-N3 solution concentrations (10 and 25 mg/mL) to study the influence of the ELRs solution concentration on the coating (Table 1.1). As the membranes were sequentially immersed in the ELRs solutions, the influence of the order of deposition of the first layer was also evaluated, obtaining four different types of coated membranes (a-d) (Table 1.1). The best coating was verified by the weight difference between uncoated and coated membranes per square cm as well as by water contact angle measurement (Table 1.1). As can be seen in Table 1.1, the largest weight increases were produced in membrane types a and b, which were first coated with RGD-N3, finishing the second bilayer with RGD-CO. The best of both coatings was obtained by the highest solution concentration of 25 mg/mL in membrane b. Coating verification by contact angle values showed lower hydrophobicity for membranes a and b than c and d, which is also consistent with the better coating of membranes a and b, and was optimal for membrane b, with the lowest contact angle value. These results are in agreement with the FTIR-ATR recorded for membranes a-d (Figure S1.7).

**Table 1.1. Parameters measured for different coatings on PVDF membranes to optimize coating protocol.**

| *Sample* | *First layer* | *Concentration (mg/mL)* | *$\Delta W/S$ ($mg/cm^2$)* | *Contact Angle (°)* |
|---|---|---|---|---|
| a | RGD-N3 | 10 | 0.51 | 77 ± 3 |
| b | RGD-N3 | 25 | 1.10 | 71 ± 1 |
| c | RGD-CO | 10 | 0.06 | 92 ± 6 |
| d | RGD-CO | 25 | 0.28 | 90 ± 6 |

Figure S1.7 gives the coated membrane spectrum showing the signals of the ELRs primarily characterized by absorption bands at 3300 and 1700 $cm^{-1}$ of the N-H and C=O amidic bonds present in the main chain of ELRs, together with the characteristic absorption bands of the PVDF membranes in Figure 1.2, with bands ranging from 1300 to 500 $cm^{-1}$. Of the four

types of FTIR-ATR membrane spectra, the largest absorption bands at 1700 $cm^{-1}$ were those of membrane types a and b.

The PVDF membrane coating combination structure and morphology were also characterized by FESEM (Figure S1.8) and confirmed the results previously obtained by FTIR-ATR on the difference in weight and water contact angle. Sample b, coated with 25 mg/mL solutions of ELRs and RGD-N3 as the first layer deposited, was chosen to perform cell culture assays. Scheme 1.1 contains a description of the optimized chosen layer-by-layer protocol.

The characterization of the optimized layer-by-layer protocol is shown in Figure 1.4. Figure 1.4a shows the FTIR-ATR spectra of the coated and non-coated membranes, where the ELRs peaks can be seen at about 1700 $cm^{-1}$ and 3300 $cm^{-1}$, reconfirming the best LbL coating method. Images of water contact angles before and after coating are shown in Figure 4b, confirming the reduced hydrophobicity accompanied by a smoother surface, as shown in Figure 1.1. Both the surface and cross-section FESEM images show the porous structure of the type b membranes. The cross-section image verifies correct membrane coating with a thin film evenly covering the surface.

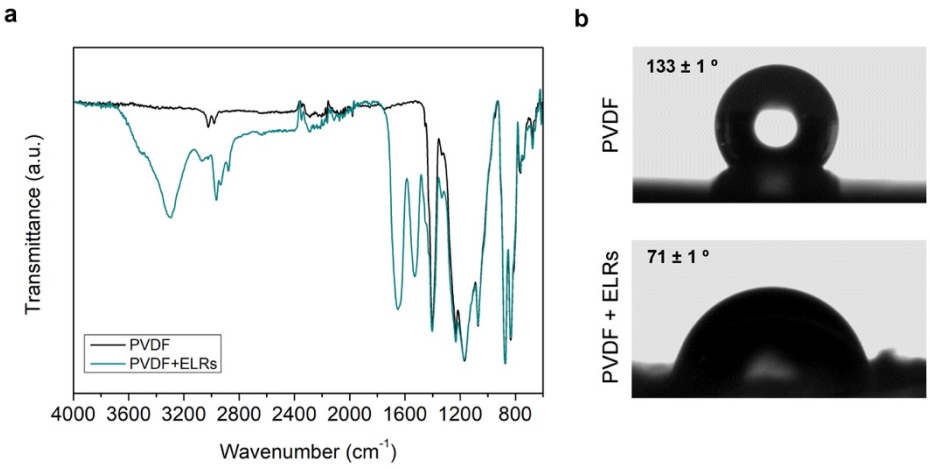


**Figure 1.4. a) Comparison of FTIR-ATR spectra from type b coated membrane (blue line), and non-coated membrane (black line). b) Images of the contact angles before (PVDF) and after (PVDF + ELRs) deposition of ELRs by the optimized protocol.**

### 1.3.3. Porcine mesenchymal stem cells response to elastin-like recombinamers layer-by-layer coating

Porcine mesenchymal stem cells were used to test the initial cell adhesion and proliferation in PVDF membranes coated by LbL with ELRs or traditionally coated with adsorbed fibronectin. A glass slide coated with fibronectin was also used as the standard control. Nucleus-cytoskeleton staining at 24 h, 3 and 7 days was evaluated, as reported in Figure 1.5.

Figure 1.5a shows that after 24 h cells had adhered in all the surfaces, showing an extended cytoskeleton in every condition. Despite this well-developed cytoskeleton, the differences in cell number between conditions are significant. The PVDF membranes coated with fibronectin showed a negative fold change in cell proliferation, meaning that a lower number of cells than the initial cell seeding density attached on the surface. In the PVDF + ELRs condition, the cells had adhered and some had even proliferated after 24 h, as can be seen in Figure 1.5b, showing no significant differences with the glass slide control. However, the initial adhesion to PVDF was really poor and was not even able to retain the initial number of seeded cells. The different proliferation rate can be seen after 7 days, when PVDF + ELRs and the glass slide have reached confluence, the fibronectin-coated PVDF has few cells and the proliferation rate is lower than in the other conditions.

Hydrophobicity is a key feature of PVDF, as demonstrated by the PVDF membrane contact angle before coating (133 ± 1 º). This effect is greatly increased by the membrane surface roughness due to spherulitic conformation.

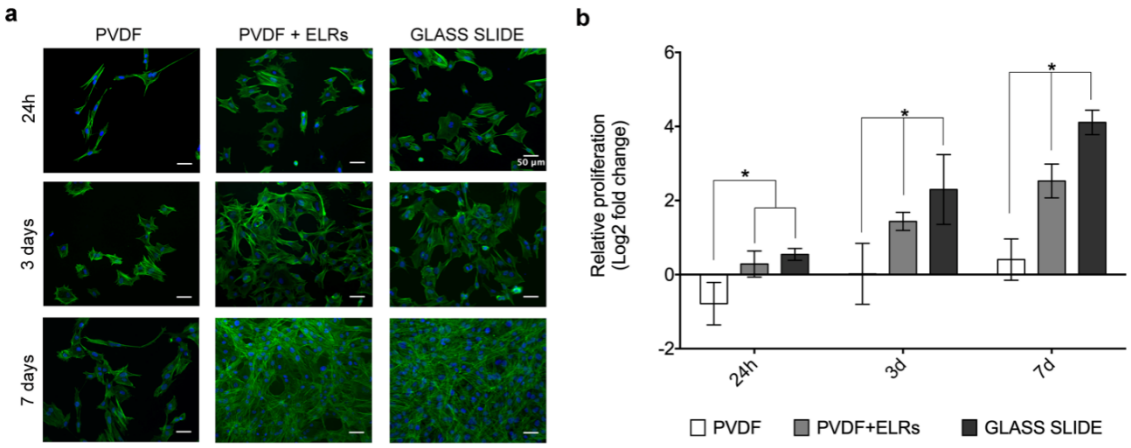


**Figure 1.5. a) Representative images of actin (cytoskeleton-green) and DAPI (nucleus-blue) staining after 24 h, 3 and 7 days of culture for coated and uncoated PVDF membranes and glass slide control. Scale bar is 50 µm. (b) Cell count based on the analysis of 4 images taken from 3 replicates per condition at 24 h, 3 and 7 days from two independent assays. * p-value < 0.05**

This characteristic makes surface treatments an unavoidable approach for cell culture on PVDF. Since this polymer was first used in the tissue engineering field it has been traditionally coated with fibronectin (C. Ribeiro, Panadero, et al. 2012; Sobreiro-Almeida et al. 2017; C. Ribeiro, Pärssinen, et al. 2015). In this study we found that fibronectin adsorption was not enough to promote initial cell adhesion to PVDF microporous membranes. This type of coating has been proven to be inefficient in spherulite-like PVDF membranes (Morales-Román et al. 2019). In a previous study we found that small changes in the degree of porosity in fibronectin-coated PVDF membranes can influence initial cell adhesion and proliferation in porcine bone marrow mesenchymal stem cells.

Contact angle is closely related to polymer wettability and also to surface roughness. Layer-by-layer deposition of elastin-like recombinamers reduced the water contact angle in PVDF membranes (71 ± 1 º), partially due to surface smoothing. The presence of RGD sequences in the ELRs and their deposition by LbL, which flattened the membrane surface, increased initial pMSCs adhesion in PVDF + ELRs membranes. The combination of both features makes this coating a suitable option for mesenchymal stem cell culture on porous PVDF membranes.

These findings lead the way to the use of PVDF membranes coated with elastin-like recombinamers containing RGD sequences in future MSCs differentiation approaches to the osteogenic lineage.

## 1.4. Conclusions

Non-solvent induced phase separation has proven to be a cost-effective and reliable technique for manufacturing PVDF membranes. The use of ethanol as non-solvent produced homogeneously porous membranes with more than 90 % $\gamma$-phase and up to 65 % overall crystalline content. Its electroactive potential was confirmed after poling by the contact method by measuring the $d_{33}$ piezeoelectric coefficient, obtaining values within the bone piezoelectricity range. The membranes were coated with elastin-like recombinamers containing RGD sequences to improve their initial cell adhesion properties. ELRs were deposited by the layer-by-layer technique applying click cross-linking chemistry. After coating optimization, modified ELRs containing azide groups were selected for deposition as the first layer, followed by ELRs modified to contain cyclooctyne groups. Both layers reacted by interchain crosslinking via catalyst-free Hüisgen 1,3-dipolar cycloaddition, generating a stable bilayer. Two bilayers were deposited, reducing surface roughness and contact angle value. Cell adhesion and proliferation were tested on porcine bone marrow MSCs in a short-term culture (1 to 7 days). ELRs deposition by LbL was compared to traditional fibronectin adsorption and showed that cells preferred ELRs-coated surfaces for initial adhesion and proliferation. Fibronectin adsorption showed poor cell attachment and was not able to retain the initial number of seeded cells, while ELRs favoured adhesion and enhanced proliferation after 7 days. These findings open the door for the combination of electroactive PVDF membranes and synthetic peptides containing biofunctional sequences for mesenchymal stem cell culture and differentiation towards the osteogenic lineage.

## 1.5. Acknowledgements

This work was supported by the Spanish State Research Agency (AEI) through Projects PID2019-106000RB-C21 / AEI / 10.13039/501100011033 and PID2019-106099RB-C43 / AEI / 10.13039/501100011033 (including FEDER funds). Maria Guillot-Ferriols received government funding for her Doctoral Thesis [grant number BES-2017-080398FPI]. The CIBER-BBN initiative is funded by the VI National R&D&I Plan 2008-2011, Iniciativa Ingenio 2010, Consolider Program. CIBER actions are financed by the Instituto de Salud Carlos III with assistance from the European Regional Development Fund. The authors are grateful for the funding from the Spanish Government (MAT2016-78903-R, RTI2018-096320-B-C22), Junta de Castilla y León (VA317P18), Interreg V España Portugal POCTEP (0624_2IQBIONEURO_6_E) and Centro en Red de Medicina Regenerativa y Terapia Celular de Castilla y León. This work was also supported by the Portuguese Foundation for

Science and Technology (FCT) in the framework of the Strategic Funding UID/FIS/04650/2020. The authors thank FCT and FEDER funds (COMPETE 2020) under projects PTDC/BTM-MAT/28237/2017, PTDC/EMD-EMD/28159/2017 and PTDC/FIS-MAC/28157/2017. Carlos M. Costa is grateful to the FCT [grant number FRH/BPD/112547/2015]. Financial support was also received from the Basque Government under the ELKARTEK, HAZITEK and PIBA (PIBA-2018-06) programs.

## 1.6. References

Ahn, A.C., and A. J. Grodzinsky. 2009. “Relevance of Collagen Piezoelectricity to ‘Wolff’s Law’: A Critical Review.” *Medical Engineering and Physics* 31 (7): 733–41. https://doi.org/10.1016/j.medengphy.2009.02.006.

Anderson, J. M., J. B. Vines, J. L. Patterson, H. Chen, A. Javed, and H-W. Jun. 2012. “Osteogenic Differentiation of Human Mesenchymal Stem Cells Synergistically Enhanced by Biomimetic Peptide Amphiphiles Combined with Conditioned Medium.” *Acta Biomaterialia* 7 (2): 675–82. https://doi.org/10.1016/j.actbio.2010.08.016.

Benz, M., and W. B. Euler. 2003. “Determination of the Crystalline Phases of Poly(Vinylidene Fluoride) under Different Preparation Conditions Using Differential Scanning Calorimetry and Infrared Spectroscopy.” *Journal of Applied Polymer Science* 89 (4): 1093–1100. https://doi.org/10.1002/app.12267.

Berg, M. C., S. Y. Yang, P. T. Hammond, and M. F. Rubner. 2004. “Controlling Mammalian Cell Interactions on Patterned Polyelectrolyte Multilayer Surfaces.” *Langmuir* 20 (4): 1362–68. https://doi.org/10.1021/la0355489.

Boccaccio, T., A. Bottino, G. Capannelli, and P. Piaggio. 2002. “Characterization of PVDF Membranes by Vibrational Spectroscopy.” *Journal of Membrane Science* 210 (2): 315–29. https://doi.org/10.1016/S0376-7388(02)00407-6.

Castro, N., M. M. Fernandes, C. Ribeiro, V. Correia, R. Minguez, and S. Lanceros-Mendez. 2020. “Magnetic Bioreactor for Magneto-, Mechano- and Electroactive Tissue Engineering Strategies.” *Sensors* 20 (12): 3340. https://doi.org/10.3390/s20123340.

Castro, N., S. Ribeiro, M. M. Fernandes, C. Ribeiro, V. Cardoso, V. Correia, R. Minguez, and S. Lanceros-Mendez. 2020. “Physically Active Bioreactors for Tissue Engineering Applications.” *Advanced Biosystems* 4 (10): 1–29. https://doi.org/10.1002/adbi.202000125.

Chang, H. H., L. K. Chang, C. D. Yang, D. J. Lin, and L. P. Cheng. 2016. “Effect of Polar Rotation on the Formation of Porous Poly(Vinylidene Fluoride) Membranes by Immersion Precipitation in an Alcohol Bath.” *Journal of Membrane Science* 513: 186–96. https://doi.org/10.1016/j.memsci.2016.04.052.

Chang, H. H., L. K. Chang, C. D. Yang and D. J. Lin 2017. “Effect of Solvent on the Dipole Rotation of Poly(Vinylidene Fluoride) during Porous Membrane Formation by Precipitation in Alcohol Baths.” *Polymer* 115: 164–75. https://doi.org/10.1016/j.polymer.2017.03.044.

Cheng, L. P. 1999. “Effect of Temperature on the Formation of Microporous PVDF Membranes by Precipitation from 1-Octanol/DMF/PVDF and Water/ DMF/PVDF Systems.” *Macromolecules* 32 (20): 6668–74. https://doi.org/10.1021/ma990418l.

Costa, R. R., C. A. Custódio, A. M. Testera, F.J. Arias, J. C. Rodríguez-Cabello, N. M. Alves, and J. F. Mano. 2009. “Stimuli-Responsive Thin Coatings Using Elastin-like Polymers for Biomedical Applications.” *Advanced Functional Materials* 19 (20): 3210–18. https://doi.org/10.1002/adfm.200900568.

Fukada, E. 1968. “Mechnical Deformation and Electrical Polarization in Biological Substances.” *Biorheology* 5 (3): 199–208. https://doi.org/10.3233/BIR-1968-5302.

Fukada, E., and I. Yasuda. 1957. “On the Piezoelectric Effect of Bone.” *Journal of the Physical Society of Japan* 12 (10): 1158–62. https://doi.org/10.1143/JPSJ.12.1158.

Fukada, E, and I Yasuda. 1964. “Piezoelectric Effects in Collagen.” *Japanese Journal of Applied Physics, Part 1: Regular Papers and Short Notes and Review Papers* 3 (8): 502B. https://doi.org/10.1143/jjap.3.502b.

Girotti, A., D. Orbanic, A. Ibáñez-Fonseca, C. Gonzalez-Obeso, and J. C. Rodríguez-Cabello. 2015. “Recombinant Technology in the Development of Materials and Systems for Soft-Tissue Repair.” *Advanced Healthcare Materials* 4 (16): 2423–55. https://doi.org/10.1002/adhm.201500152.

Girotti, A., J. Reguera, J. C. Rodríguez-Cabello, F. J. Arias, M. Alonso, and A. M. Testera. 2004. “Design and Bioproduction of a Recombinant Multi(Bio)Functional Elastin-like Protein Polymer Containing Cell Adhesion Sequences for Tissue Engineering Purposes.” *Journal of Materials Science: Materials in Medicine* 15 (4): 479–84. https://doi.org/10.1023/B:JMSM.0000021124.58688.7a.

Gonçalves, S., J. Serrado-Nunes, J. Oliveira, N. Pereira, L. Hilliou, C. M. Costa, and S. Lanceros-Méndez. 2019. “Environmentally Friendly Printable Piezoelectric Inks and Their Application in the Development of All-Printed Touch Screens.” *ACS Applied Electronic Materials* 1 (8): 1678–87. https://doi.org/10.1021/acsaelm.9b00363.

González De Torre, I., M. Santos, L. Quintanilla, A. Testera, M. Alonso, and J. C. Rodríguez Cabello. 2014. “Elastin-like Recombinamer Catalyst-Free Click Gels: Characterization of Poroelastic and Intrinsic Viscoelastic Properties.” *Acta Biomaterialia* 10 (6): 2495–2505. https://doi.org/10.1016/j.actbio.2014.02.006.

Gónzalez De Torre, I., F. Wolf, M. Santos, L. Rongen, M. Alonso, Stefan Jockenhoevel, J. C. Rodríguez-Cabello, and P. Mela. 2015. “Elastin-like Recombinamer-Covered Stents: Towards a Fully Biocompatible and Non-Thrombogenic Device for Cardiovascular Diseases.” *Acta Biomaterialia* 12 (1): 146–55. https://doi.org/10.1016/j.actbio.2014.10.029.

Gregorio, R. 2006. “Determination of the α, β, and γ Crystalline Phases of Poly(Vinylidene Fluoride) Films Prepared at Different Conditions.” *Journal of Applied Polymer Science* 100 (4): 3272–79. https://doi.org/10.1002/app.23137.

Guillot-Ferriols, M., J. C. Rodríguez-Hernández, D. M. Correia, S. A. C. Carabineiro, S. Lanceros-Méndez, J. L. Gómez Ribelles, and G. Gallego Ferrer. 2020. “Poly(Vinylidene) Fluoride Membranes Coated by Heparin / Collagen Layer-by-Layer, Smart Biomimetic Approaches for Mesenchymal Stem Cell Culture.” *Materials Science & Engineering C* 117: 111281. https://doi.org/10.1016/j.msec.2020.111281.

Halperin, C., S. Mutchnik, A. Agronin, M. Molotskii, P. Urenski, M. Salai, and G. Rosenman. 2004. “Piezoelectric Effect in Human Bones Studied in Nanometer Scale.” *Nano Letters* 4 (7): 1253–56. https://doi.org/10.1021/nl049453i.

Jacob, J., N. More, K. Kalia, and G. Kapusetti. 2018. “Piezoelectric Smart Biomaterials for Bone and Cartilage Tissue Engineering.” *Inflammation and Regeneration* 38 (1): 1–11. https://doi.org/10.1186/s41232-018-0059-8.

Jung, J. T., J. F. Kim, H. H. Wang, E. di Nicolo, E. Drioli, and Y. M. Lee. 2016. “Understanding the Non-Solvent Induced Phase Separation (NIPS) Effect during the Fabrication of Microporous PVDF Membranes via Thermally Induced Phase Separation (TIPS).” *Journal of Membrane Science* 514: 250–63. https://doi.org/10.1016/j.memsci.2016.04.069.

Kim, K. M., W. S. Jeon, N. G. Park, K. S. Ryu, and S. H. Chang. 2003. “Effect of Evaporation Temperature on the Crystalline Properties of Solution-Cast Films of Poly(Vinylidene Fluoride)S.” *Korean Journal of Chemical Engineering* 20 (5): 934–41. https://doi.org/10.1007/BF02697302.

Lang, S. B. 2000. “Piezoelectricity, Pyroelectricity and Ferroelectricity in Biomaterials: Speculation on Their Biological Significance.” *IEEE Transactions on Dielectrics and Electrical Insulation* 7 (4): 466–73. https://doi.org/10.1109/94.868063.

Liboff, A. R., and M. Furst. 1974. “Pyroelectric Effect in Collagenous Structures.” *Annals of the New York Academy of Sciences* 238 (1): 26–35. https://doi.org/10.1111/j.1749-6632.1974.tb26777.x.

Lin, D. J., K. Beltsios, C. L. Chang, and L. P. Cheng. 2003. “Fine Structure and Formation Mechanism of Particulate Phase-Inversion Poly(Vinylidene Fluoride) Membranes.” *Journal of Polymer Science, Part B: Polymer Physics* 41 (13): 1578–88. https://doi.org/10.1002/polb.10513.

Lin, D. J., K. Beltsios, T. H. Young, Y. S. Jeng, and L. P. Cheng. 2006. “Strong Effect of Precursor Preparation on the Morphology of Semicrystalline Phase Inversion Poly(Vinylidene Fluoride) Membranes.” *Journal of Membrane Science* 274 (1–2): 64–72. https://doi.org/10.1016/j.memsci.2005.07.043.

Liu, F., N. A. Hashim, Y. Liu, M. R. M. Abed, and K. Li. 2011. “Progress in the Production and Modification of PVDF Membranes.” *Journal of Membrane Science* 375 (1–2): 1–27. https://doi.org/10.1016/j.memsci.2011.03.014.

Lizundia, E., A. Reizabal, C. M. Costa, A. Maceiras, and S. Lanceros-Méndez. 2020. “Electroactive γ-Phase, Enhanced Thermal and Mechanical Properties and High Ionic Conductivity Response of Poly (Vinylidene Fluoride)/Cellulose Nanocrystal.” *Materials* 13 (3): 743. https://doi.org/doi:10.3390/ma13030743.

Lopes, A. C., C. M. Costa, C. J. Tavares, I. C. Neves, and S. Lanceros-Mendez. 2011. “Nucleation of the Electroactive γ Phase and Enhancement of the Optical Transparency in Low Filler Content Poly(Vinylidene)/Clay Nanocomposites.” *Journal of Physical Chemistry C* 115 (37): 18076–82. https://doi.org/10.1021/jp204513w.

Lovinger, A. J. 1982. “Annealing of Poly(Vinylidene Fluoride) and Formation of a Fifth Phase.” *Macromolecules* 15 (1): 40–44. https://doi.org/10.1021/ma00229a008.

Martins, P., A. C. Lopes, and S. Lanceros-Mendez. 2014. “Electroactive Phases of Poly(Vinylidene Fluoride): Determination, Processing and Applications.” *Progress in Polymer Science* 39 (4): 683–706. https://doi.org/10.1016/j.progpolymsci.2013.07.006.

Meyer, D. E., and A. Chilkoti. 1999. “Purification of Recombinant Proteins by Fusion with Thermally-Responsive Polypeptides.” *Nature Biotechnology* 17 (11): 1112–15. https://doi.org/10.1038/15100.

Morales-Román, R. M., M. Guillot-Ferriols, L. Roig-Pérez, S. Lanceros-Mendez, G. Gallego-Ferrer, and J. L. Gómez Ribelles. 2019. “Freeze-Extraction Microporous Electroactive Supports for Cell Culture.” *European Polymer Journal* 119 (June): 531–40. https://doi.org/10.1016/j.eurpolymj.2019.07.011.

Nakagawa, K., and Y. Ishida. 1973. “Annealing Effects in Poly(Vinylidene Fluoride) as Revealed by Specific Volume Measurements, Differential Scanning Calorimetry, and Electron Microscopy.” *Journal of Polymer Science Part A-2: Polymer Physics* 11 (11): 2153–71. https://doi.org/10.1002/pol.1973.180111107.

Nettles, D. L., A. Chilkoti, and L. A. Setton. 2010. “Applications of Elastin-like Polypeptides in Tissue Engineering.” *Advanced Drug Delivery Reviews* 62 (15): 1479–85. https://doi.org/10.1016/j.addr.2010.04.002.

Nicol, A., D. Channe Gowda, and D. W. Urry. 1992. “Cell Adhesion and Growth on Synthetic Elastomeric Matrices Containing ARG-GLY–ASP–SER–3.” *Journal of Biomedical Materials Research* 26 (3): 393–413. https://doi.org/10.1002/jbm.820260309.

Pagliero, M., A. Bottino, A. Comite, and C. Costa. 2020. “Novel Hydrophobic PVDF Membranes Prepared by Nonsolvent Induced Phase Separation for Membrane Distillation.”

*Journal of Membrane Science* 596 (September 2019). https://doi.org/10.1016/j.memsci.2019.117575.

Pinedo-Martín, G., M. Santos, A. M. Testera, M. Alonso, and J. C. Rodríguez-Cabello. 2014. "The Effect of NaCl on the Self-Assembly of Elastin-like Block Co-Recombinamers: Tuning the Size of Micelles and Vesicles." *Polymer* 55 (21): 5314–21. https://doi.org/10.1016/j.polymer.2014.08.053.

Qu, Z., J. Yan, B. Li, J. Zhuang, and Y. Huang. 2010. "Improving Bone Marrow Stromal Cell Attachment on Chitosan/Hydroxyapatite Scaffolds by an Immobilized RGD Peptide." *Biomedical Materials* 5 (6). https://doi.org/10.1088/1748-6041/5/6/065001.

Ribeiro, C., D. M. Correia, S. Ribeiro, V. Sencadas, G. Botelho, and S. Lanceros-Méndez. 2015. "Piezoelectric Poly(Vinylidene Fluoride) Microstructure and Poling State in Active Tissue Engineering." *Engineering in Life Sciences* 15 (4): 351–56. https://doi.org/10.1002/elsc.201400144.

Ribeiro, C., C. M. Costa, D. M. Correia, J. Nunes-Pereira, J. Oliveira, P. Martins, R. Gonçalves, V. F. Cardoso, and S. Lanceros-Méndez. 2018. "Electroactive Poly(Vinylidene Fluoride)-Based Structures for Advanced Applications." *Nature Protocols* 13 (4): 681–704. https://doi.org/10.1038/nprot.2017.157.

Ribeiro, C., S. Moreira, V. Correia, V. Sencadas, J.G. Rocha, F. M. Gama, J. L. Gómez Ribelles, and S. Lanceros-Méndez. 2012. "Enhanced Proliferation of Pre-Osteoblastic Cells by Dynamic Piezoelectric Stimulation." *RSC Advances* 2 (30): 11504. https://doi.org/10.1039/c2ra21841k.

Ribeiro, C., J. A. Panadero, V. Sencadas, S. Lanceros-Mendez, M. N. Tamaño, D. Moratal, M. Salmeron-Sanchez, and J. L. Gomez Ribelles. 2012. "Fibronectin Adsorption and Cell Response on Electroactive Poly(Vinylidene Fluoride) Films." *Biomedical Materials* 7 (3). https://doi.org/10.1088/1748-6041/7/3/035004.

Ribeiro, C., J. Pärssinen, V. Sencadas, V. Correia, S. Miettinen, V. P. Hytönen, and S. Lanceros-Méndez. 2015. "Dynamic Piezoelectric Stimulation Enhances Osteogenic Differentiation of Human Adipose Stem Cells." *Journal of Biomedical Materials Research - Part A* 103 (6): 2172–75. https://doi.org/10.1002/jbm.a.35368.

Ribeiro, S., C. Ribeiro, E. O. Carvalho, C. R. Tubio, N. Castro, N. Pereira, V. Correia, A. C. Gomes, and S. Lanceros-Méndez. 2020. "Magnetically Activated Electroactive Microenvironments for Skeletal Muscle Tissue Regeneration." *ACS Applied Bio Materials* 3 (7): 4239–52. https://doi.org/10.1021/acsabm.0c00315.

Rodríguez-Cabello, J. C., L. Martín, M. Alonso, F. J. Arias, and A. M. Testera. 2009. "'Recombinamers' as Advanced Materials for the Post-Oil Age." *Polymer* 50 (22): 5159–69. https://doi.org/10.1016/j.polymer.2009.08.032.

Ruoslahti, E. 1996. “RGD and Other Recognition Sequences for Integrins.” *Annual Review of Cell and Developmental Biology* 12 (1): 697–715. https://doi.org/10.1146/annurev.cellbio.12.1.697.

Salimi, A., and A. A. Yousefi. 2004. “Conformational Changes and Phase Transformation Mechanisms in PVDF Solution-Cast Films.” *Journal of Polymer Science, Part B: Polymer Physics* 42 (18): 3487–95. https://doi.org/10.1002/polb.20223.

Sencadas, V., R. Gregorio, and S. Lanceros-Méndez. 2009. “α to β Phase Transformation and Microestructural Changes of PVDF Films Induced by Uniaxial Stretch.” *Journal of Macromolecular Science, Part B: Physics* 48 (3): 514–25. https://doi.org/10.1080/00222340902837527.

Shin, H., J. S. Temenoff, G. C. Bowden, K. Zygourakis, M.C. Farach-Carson, M. J. Yaszemski, and A. G. Mikos. 2005. “Osteogenic Differentiation of Rat Bone Marrow Stromal Cells Cultured on Arg-Gly-Asp Modified Hydrogels without Dexamethasone and β-Glycerol Phosphate.” *Biomaterials* 26 (17): 3645–54. https://doi.org/10.1016/j.biomaterials.2004.09.050.

Sobreiro-Almeida, R., M. Tamaño-Machiavello, E. Carvalho, L. Cordón, S. Doria, L. Senent, D. Correia, et al. 2017. “Human Mesenchymal Stem Cells Growth and Osteogenic Differentiation on Piezoelectric Poly(Vinylidene Fluoride) Microsphere Substrates.” *International Journal of Molecular Sciences* 18 (11): 2391. https://doi.org/10.3390/ijms18112391.

Sousa, M. P., I. Gonzalez de Torre, M. B. Oliveira, J. C. Rodríguez-Cabello, and J. F. Mano. 2017. “Biomimetic Click Assembled Multilayer Coatings Exhibiting Responsive Properties.” *Materials Today Chemistry* 4: 150–63. https://doi.org/10.1016/j.mtchem.2017.04.001.

Wang, X., L. Zhang, D. Sun, Q. An, and H. Chen. 2009. “Formation Mechanism and Crystallization of Poly(Vinylidene Fluoride) Membrane via Immersion Precipitation Method.” *Desalination* 236 (1–3): 170–78. https://doi.org/10.1016/j.desal.2007.10.064.

Webb, K., V. Hlady, and P. A. Tresco. 1998. “Relative Importance of Surface Wettability and Charged Functional Groups on NIH 3T3 Fibroblast Attachment, Spreading, and Cytoskeletal Organization.” *Journal of Biomedical Materials Research* 41 (3): 422–30. https://doi.org/10.1002/(SICI)1097-4636(19980905)41:3<422::AID JBM12>3.0.CO;2-K.

Yang, F., C. G. Williams, D. A. Wang, H. Lee, P.N. Manson, and J. Elisseeff. 2005. “The Effect of Incorporating RGD Adhesive Peptide in Polyethylene Glycol Diacrylate Hydrogel on Osteogenesis of Bone Marrow Stromal Cells.” *Biomaterials* 26 (30): 5991–98. https://doi.org/10.1016/j.biomaterials.2005.03.018.

## 1.7. Supplementary material

Supplementary data associated with this article can be found in supplementary material: $^{1}$H-NMR, MALDI-ToF and FTIR-ATR of RGD-CO and RGD-N3 for structure characterization of modified biopolymers together with FTIR-ATR of plasma-treated and PVDF-coated membranes and FESEM images of PVDF-coated and non-coated membranes for establishing optimal conditions.

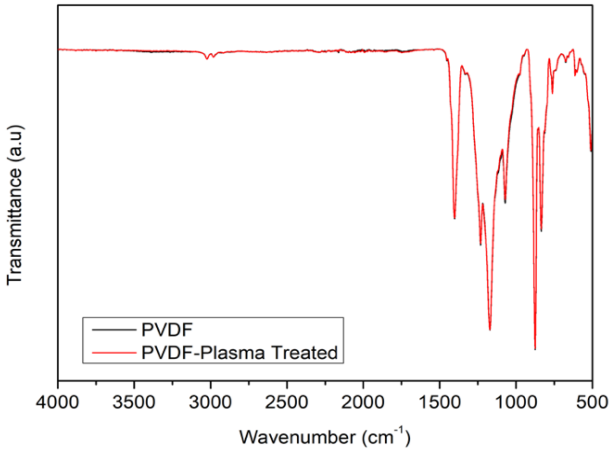


**Figure S1.1. FTIR spectra of the PVDF membranes before and after argon plasma treatment. The amount of hydroxyl groups introduced by argon plasma is not appreciated in the FTIR spectrum since no substantial changes are observed. Nevertheless, the activation was enough to immerse the samples in aqueous solutions for ELRs coating, reducing their initial hydrophobicity. The spectra were recorded using a Bruker TENSOR 27 acquiring 64 scans between 500-4000 cm$^{-1}$.**

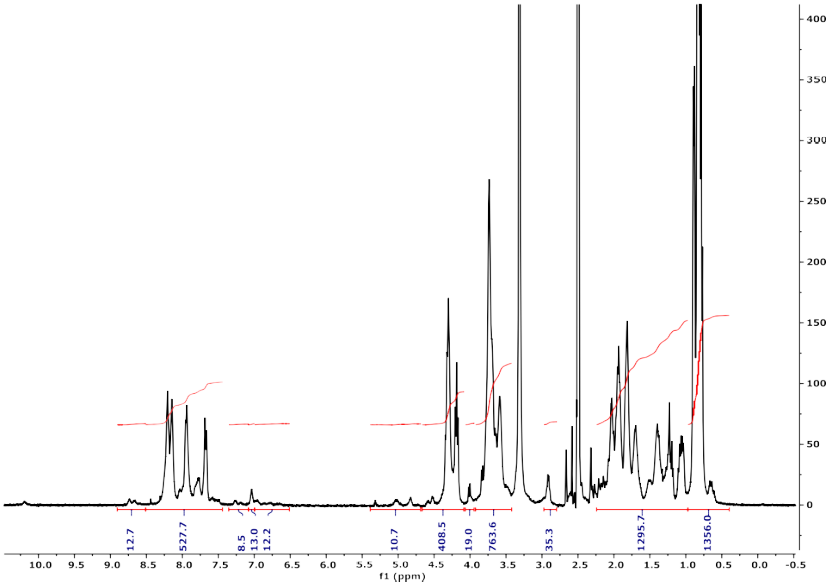


**Figure S1.2. Nuclear magnetic resonance spectrum $^{1}$H-RMN of RGD-CO. The spectrum shows the presence of a signal at 7 ppm, which corresponds to the hydrogen belonging to the**

**carbamate formed from the amine groups of the lysine, with an integral of 13 hydrogens corresponding to a total of 13 modified lysines. Another new signal at 3 ppm corresponding to the hydrogens of the methylene group adjacent to the amine group of the modified lysine is observed. Nuclear magnetic resonance (NMR) of samples prepared in DMSO-$d_6$ at 10 mg/mL were recorded using a 400 MHz Agilent spectrometer (Laboratory of Instrumental Techniques, University of Valladolid) with a 1 s relaxation delay between transients, 45° pulse width, 512 transients per sample and a spectral width of 6410 Hz.**

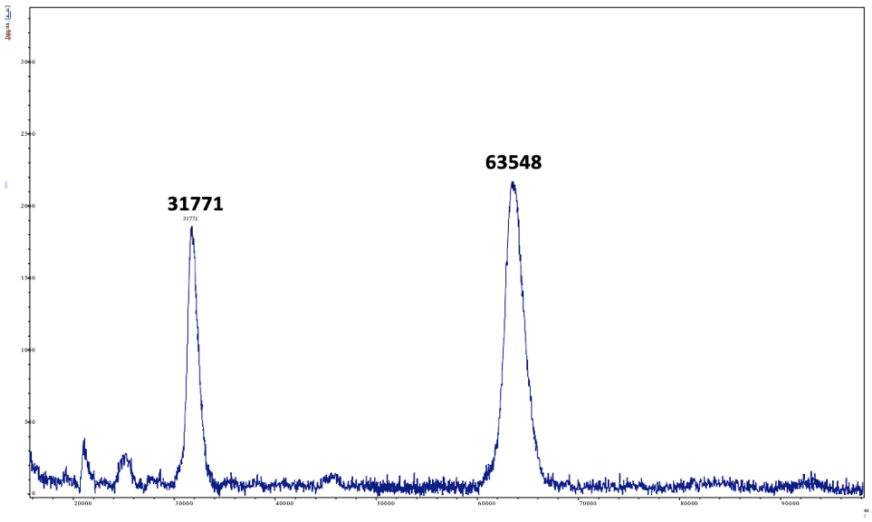


**Figure S1.3. MALDI-ToF spectrum of RGD-CO. The peaks correspond to the singly and doubly charged ions, respectively. Samples were dissolved at 1 mg/mL in mQ water and measured into a MALDI-ToF Bruker Autoflex. MALDI-ToF spectrum represents non-quantitative intensity (a.u.) against m/z (mass/net charge).**

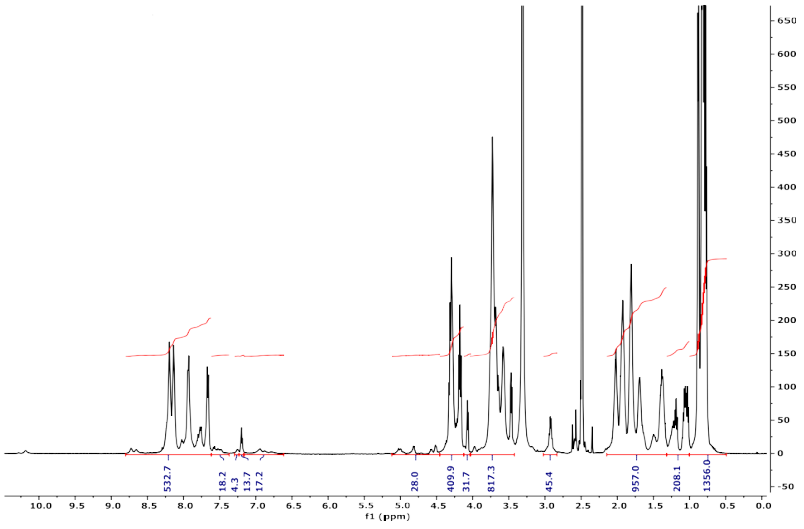


**Figure S1.4. Nuclear magnetic resonance spectrum $^1$H-RMN of RGD-N3. The spectrum shows the presence of a signal at 7 ppm, which corresponds to the hydrogen belonging to the carbamate formed from the amine groups of the lysine, with an integral of 14 hydrogens corresponding to a total of 14 modified lysines. Two other new signals at 3 and 4 ppm are observed, corresponding to the hydrogens of the methylene group adjacent to the amine**

**group of the modified lysines and to the methylene hydrogens located between the cyclooctine group and the new formed, respectively. Nuclear magnetic resonance (NMR) of samples prepared in DMSO-$d_6$ at 10 mg/mL were recorded using a 400 MHz Agilent spectrometer (Laboratory of Instrumental Techniques, University of Valladolid) with a 1 s relaxation delay between transients, 45° pulse width, 512 transients per sample and a spectral width of 6410 Hz.**

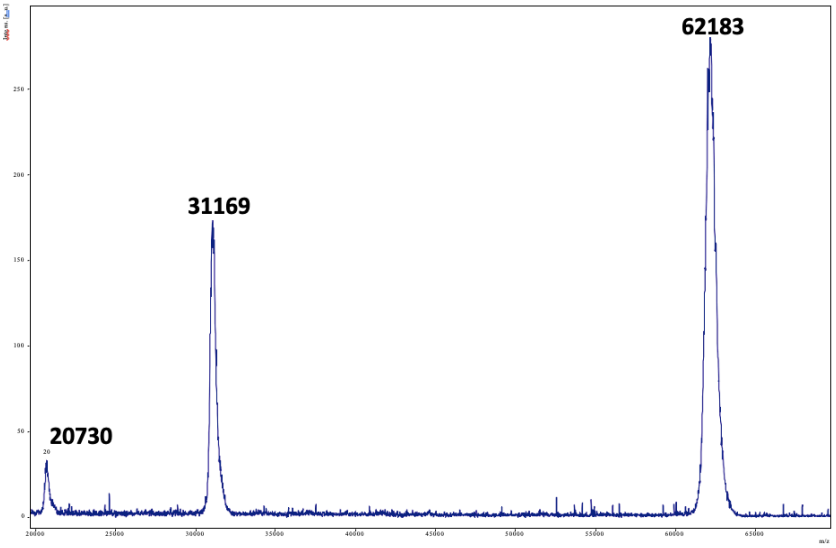


**Figure S1.5. MALDI-ToF spectrum of RGD-N3. The peaks correspond to the singly, doubly and triply charged ions, respectively. Samples were dissolved at 1 mg/mL in mQ water and measured into a MALDI-ToF Bruker Autoflex.**

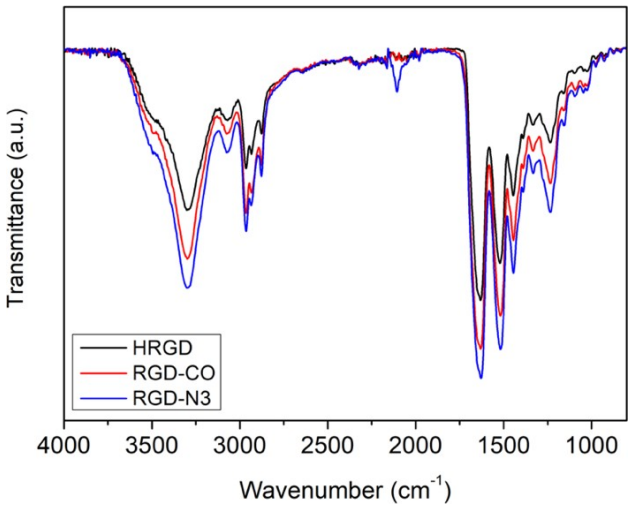


**Figure S1.6. FTIR-ATR stacked spectra of unmodified HRGD, RGD-CO and RGD-N3. The presence of azide groups in RGD-N3 was corroborated by FTIR spectroscopy since the azide group has a characteristic band at a frequency of 2100 $cm^{-1}$, not observed in the unmodified polymer HRGD spectrum. Spectra were recorded using a Bruker TENSOR 27 acquiring 64 scans between 800-4000 $cm^{-1}$**

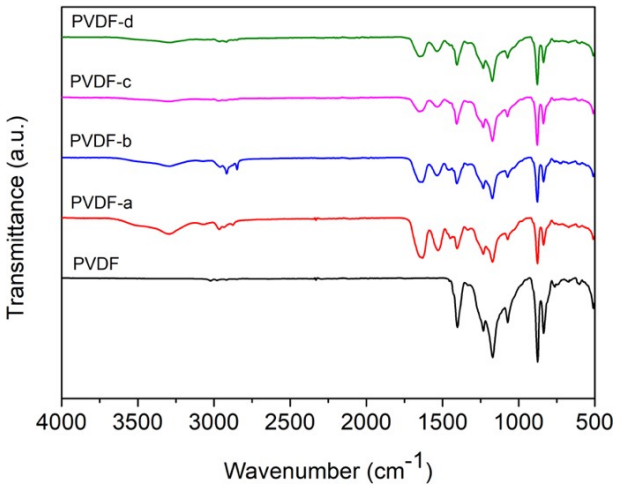


**Figure S1.7. FTIR-ATR spectra of PVDF non-coated and coated membranes types a-d (corresponding to the different coating conditions explained in table 1.1) after ELRs deposition by layer-by-layer. The spectra were recorded using a Bruker TENSOR 27 acquiring 64 scans between 500-4000 $cm^{-1}$.**

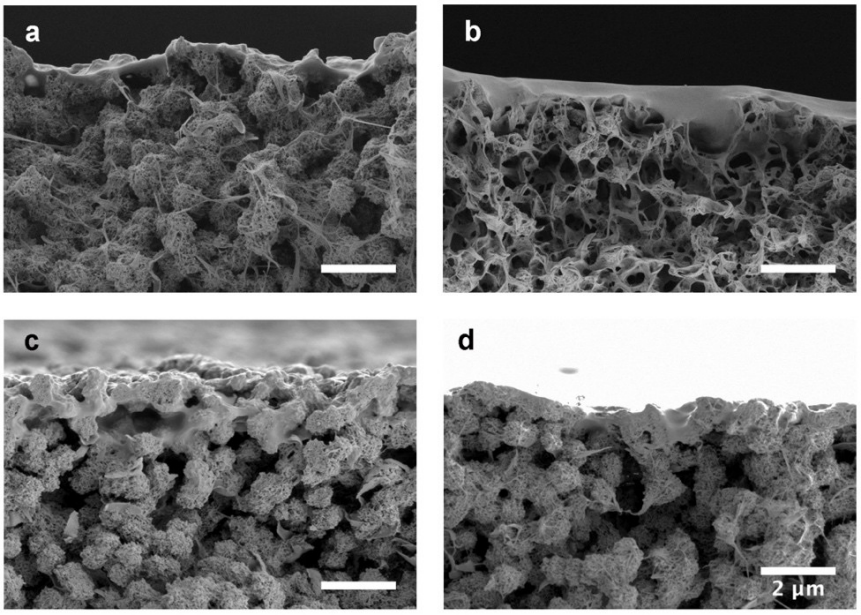


**Figure S1.8. Cross-section FESEM images of PVDF coated membranes types a-d (corresponding to the different coating conditions explained in table 1.1) after ELRs deposition by layer-by-layer. Samples were visualized in an Ultra 55 microscope (Zeiss) applying an accelerating voltage of 1 kV**

# Chapter 2. Poly(vinylidene) fluoride membranes coated by heparin/collagen layer-by-layer, smart biomimetic approaches for mesenchymal stem cells culture

This chapter was published in *Materials Science and Engineering C*

Guillot-Ferriols, M.; Rodríguez-Hernández, J. C.; Correia, D. M.; Carabineiro, S. A. C.; Lanceros-Méndez, S.; Gómez Ribelles, J. L.; Gallego Ferrer, G. Poly(Vinylidene) Fluoride Membranes Coated by Heparin / Collagen Layer-by-Layer, Smart Biomimetic Approaches for Mesenchymal Stem Cells Culture. *Mater. Sci. Eng. C* 2020, *117*.

DOI: 10.1016/j.msec.2020.111281

**Personal contribution**

Membrane production, layer by layer coating, characterization of coated and uncoated membranes and cell culture tests were performed by M. Guillot-Ferriols. XPS was carried out by S.A.C Carabineiro and its analysis was performed by D.M. Correia. J.C. Hernández-Rodríguez obtained AFM data and analyzed it.

M. Guillot-Ferriols designed the experiments, analyzed the data, prepared the figures and wrote the first version of the manuscript. S. Lanceros-Méndez, J.L. Gómez Ribelles and G. Gallego Ferrer helped with experimental design, reviewed the manuscript and provided financial support.

## 2. Poly(vinylidene) fluoride membranes coated by heparin/collagen layer-by-layer, smart biomimetic approaches for mesenchymal stem cell culture

Guillot-Ferriols M.[1,2], Rodríguez-Hernández J.C.[1], Correia D.M.[3,4], Carabineiro S.A.C.[5], Lanceros-Méndez S.[3,6,7], Gómez Ribelles J.L.[1,2], Gallego Ferrer G.[1,2]

*[1] Centre for Biomaterials and Tissue Engineering (CBIT), Universitat Politècnica de València, 46022 Valencia, Spain*
*[2] Biomedical Research Networking Center on Bioengineering, Biomaterials and Nanomedicine (CIBER-BBN), Valencia, Spain*
*[3] Centre/Department of Physics, Universidade do Minho, 4710-057 Braga, Portugal*
*[4]Centre of Chemistry, Universidade do Trás-os-Montes e Alto Douro, Vila Real 5000-801, Portugal*
*[5]LAQV-REQUIMTE, Department of Chemistry, NOVA School of Science and Technology, Universidade NOVA de Lisboa, 2829-516 Caparica, Portugal*
*[6] BCMaterials, Basque Center for Materials, Applications and Nanostructures, UPV/EHU Science Park, 48940 Leioa, Spain*
*[7]IKERBASQUE, Basque Foundation for Science, 48013 Bilbao, Spain*

### Abstract
The use of piezoelectric materials in tissue engineering has grown considerably since inherent bone piezoelectricity was discovered. Combinations of piezoelectric polymers with magnetostrictive nanoparticles (MNP) can be used to magnetoelectrically stimulate cells by applying an external magnetic field which deforms the magnetostrictive nanoparticles in the polymer matrix, deforming the polymer itself, which varies the surface charge due to the piezoelectric effect. Poly(vinylidene) fluoride (PVDF) is the piezoelectric polymer with the largest piezoelectric coefficients, being a perfect candidate for osteogenic differentiation. As a first approach, in this paper, we propose PVDF membranes containing magnetostrictive nanoparticles and a biomimetic heparin/collagen layer-by-layer (LbL) coating for mesenchymal stem cell culture. PVDF membranes 20 % (w/v) with and without cobalt ferrite oxide (PVDF-CFO) 10 % (w/w) were produced by non-solvent induced phase separation (NIPS). These membranes were found to be asymmetric, with a smooth surface, crystallinity ranging from 65 % to 61 %, and an electroactive β-phase content of 51.8 % and 55.6 % for PVDF and PVDF-CFO, respectively. Amine groups were grafted onto the membrane surface by an alkali treatment, providing positive charges for the assembly of heparin/collagen layers by the LbL technique. Five layers of each polyelectrolyte were deposited, ending with collagen. Ninhydrin test and X-ray photoelectron spectroscopy (XPS) revealed the presence of free amines on the surface, indicating a homogeneous LbL coating. Human mesenchymal stem cells (hMSC) were used to test cell response in a short-term culture (1, 3 and 7 days). Nucleus cell counting showed that LbL favored cell proliferation in PVDF-CFO over non-coated membranes.

### Keywords
Poly(vinylidene) fluoride; non-solvent induced phase separation; layer-by-layer; collagen; mesenchymal stem cells; piezoelectricity.

## 2.1. Introduction

Bone is a dynamic tissue which is constantly remodelling itself and has the ability to self-regenerate. It is a complex organ that plays many roles in the human body, including structural support, hematopoietic and immunological function or calcium homeostasis (McGovern, Griffin, and Hutmacher 2018). As human life expectancy has increased in the last decades, this has favoured the appearance of musculoskeletal diseases, including critical size defects due to trauma or cancer, or bone resorption and formation imbalances, leading to osteoporosis (Marie 1992). These bone loss related disorders have a great impact on the patients' quality of life and are costly for national health systems, since hundreds of millions of people are affected around the world (Woolf and Pfleger 2003).

Bone autografts, which are currently the gold standard treatment, involve great challenges, such as the lack of healthy tissue, invasive surgeries and the transplant failures after short periods of time (H. D. Kim et al. 2017). Tissue engineering (TE) approaches have arisen over the years as valid candidates for bone healing and regeneration and bone TE has shown the need for specific polymers able to reproduce the physiological characteristics of the tissue itself. The importance of smart materials has recently increased in this field. When exposed to an external stimulus, these polymers are able to reverse one or more structural or functional properties (Jacob et al. 2018). Apart from their physical properties, these materials can be tailored to mimic specific characteristics of extracellular matrix (ECM) components or growth factors (B. W. Kim 2017).

Smart materials can be a suitable approach to reproducing bone's inherent piezoelectricity. This phenomenon was hypothesized by Fukada and Yasuda in the 60's and was described as a change in the electric polarization under an applied mechanical stress, due to the collagen fibres that form its ECM (Fukada and Yasuda 1957). Since then, it has been proposed as one of the mechanisms involved in bone's capacity to adapt to mechanical stress and tissue regeneration (Jacob et al. 2018; Ahn and Grodzinsky 2009).

Poly(vinylidene) fluoride (PVDF), a piezoelectric material, has gained growing interest in bone TE approaches. PVDF is a semi-crystalline polymer with one of the highest known piezoelectric coefficients. PVDF has five crystalline phases, the β-phase being the most electroactive due to its net permanent dipole generated by the all-trans conformation (TTT). The strong dipole moment is produced by the difference between the electronegativity of the fluorine atoms and hydrogen atoms in its structure (Martins, Lopes, and Lanceros-Mendez 2014).

Processing conditions and solvents are determinant in PVDF's crystallization in the β-phase. The α-phase, the most frequently obtained, always results in melt crystallization at any temperature (Gregorio 2006). Uniaxial stretching of α-phase PVDF films is the most common way of inducing the β-phase (Sencadas, Gregorio, and Lanceros-Méndez 2009), although crystallization below 70 ºC by polar solvents such as dimethylformamide (DMF) or dimethylacetamide (DMA) also produces highly porous β-phase membranes (Gregorio and Borges 2008; Sencadas, Gregorio Filho, and Lanceros-Mendez 2006).

Non-solvent induced phase separation (NIPS) has been described as a method of β-phase crystallization below 70 ºC (Buonomenna et al. 2007; Ribeiro et al. 2018). This technique consists of precipitating the polymer cast on a surface by immersing it in a coagulation bath containing a non-solvent. The polymer solvent, non-solvent coagulation bath, bath temperature, additives and evaporation times can all influence the membrane morphology, which can range from highly homogeneous porous membranes to finger-like asymmetric structures with a flat surface (F. Liu et al. 2011). NIPS membranes, mostly used in water remediation applications, have been poorly explored in the TE field (Abzan, Kharaziha, and Labbaf 2019; Young et al. 2010), despite their easy processing. We consider them to be excellent candidates for mesenchymal stem cell culture.

Piezoelectric polymers can be combined with magnetostrictive phases to induce an electric charge through the magnetoelectric effect. When an external magnetic field is applied, the deformation of the magnetostrictive phase transfers this deformation to the polymer matrix resulting in a dielectric polarization variation due to the piezoelectric effect (Gonçalves, Martins, Correia, et al. 2015). This approach has been used in PVDF scaffolds, microspheres and electrosprayed fibres for electromechanical stimulation of osteogenic precursors (Fernandes et al. 2019; Hermenegildo et al. 2019; Gonçalves, Martins, Moya, et al. 2015).

PVDF's piezoelectric properties are of great interest for bone regeneration, although mimicking the cell's environment requires other factors and molecules, which can be added to the equation by coating them onto the polymer surface, for which layer-by-layer (LbL) has been postulated as an easy, cost-effective and reliable technique. LbL allows the controlled deposition of multilayers that imitate the organization of native tissues using natural polyelectrolytes, such as polysaccharides and proteins. These biomolecules are suitable candidates due their lack of cytotoxicity and their obvious mimicking of cell ECM, which triggers migration, growth and cell organization (Silva, Costa, and Mano 2016; Costa and Mano 2014; Castilla-Casadiego et al. 2018).

Collagen type I is the main protein in bone's ECM. As mentioned above, its structure confers bone's inherent piezoelectricity. It is positively charged at pH below its isoelectric point (5.5) (Mhanna, Vörös, and Zenobi-Wong 2011). Heparin, a highly sulphated polysaccharide, is involved in cell migration, proliferation and differentiation due to its ability to bind members of the major growth factor and signalling protein families, including Wnt, hedgehog, bone morphogenetic protein (BMP), fibroblast growth factor (FGF) and vascular endothelial growth factor (VEGF) families (Billings and Pacifici 2015).

Combination of heparin/collagen as polyelectrolytes has been studied previously on different substrates and cell types, from simple approaches, improving adhesion properties of polydimethylsiloxane (PDMS) (Mhanna, Vörös, and Zenobi-Wong 2011) to using heparin property as anticoagulant to coat titanium surfaces, providing thromboresistance and rapid re-endothelialization (K. Zhang et al. 2016; Cherng et al. 2019; Chen et al. 2016) or PLLA electrosprayed fiber coatings for releasing neurotrophic factors (K. Zhang et al. 2017). Regarding mesenchymal stem cells (MSCs), heparin/collagen LbL has proven to be a versatile approach for multiple scopes. It has been used to induce human MSCs osteogenic

differentiation and mineralization (Ferreira et al. 2016), to increase vascularization *in vivo* promoting MSCs differentiation to endothelial cells (Jin et al. 2016) or to enhance human MSCs immunomodulatory properties in combination with interferon-γ, reducing its antiproliferative effect (Castilla-Casadiego et al. 2019).

As a first approach, the objective in this study was to develop and characterize novel PVDF membranes, using the NIPS technique, with magnetostrictive nanoparticles coated by collagen/heparin layer-by-layer. To the best of our knowledge, this is the first time that PVDF membranes have been produced containing cobalt ferrite oxides (CFO) by the NIPS method. Membranes with and without CFO nanoparticles were successfully aminolyzed to provide positive surface charges for layer-by-layer deposition. Heparin and collagen layer-by-layer assembly was confirmed by means of field emission scanning microscopy (FESEM), atomic force microscopy (AFM) and Fourier-transformed infrared spectroscopy (FTIR). Heparin/collagen multilayers were initially tested *in vitro* using hMSC. A short-term cell culture (1, 3 and 7 days) was performed to assess cell adhesion and proliferation by nucleus and cytoplasm staining to confirm PVDF-CFO membranes suitability for future bone TE approaches.

## 2.2. Materials and methods

### 2.2.1. Membrane preparation by non-solvent induced phase separation

PVDF membranes with and without cobalt ferrite oxide (CFO) were prepared by non-solvent induced precipitation (NIPS) using deionized water as non-solvent. A 20 % (w/v) PVDF (*Solef® 6010 PVDF Homopolymer, Solvay)* solution was prepared by dissolving the PVDF in dimethylformamide (DMF) (synthesis grade; Scharlab) at 60 °C under stirring. For the preparation of the composite solution (PVDF-CFO), cobalt ferrite oxide mangnetostrictive nanoparticles (CFO MNP; $CoFe_2O_4$) were used with diameters ranging from 35 to 55 nm (Nanoamor) at a concentration of 10 % (w/w). This concentration proved to be the most appropriate to induce a magnetoelectric response in PVDF (Martins et al. 2014). CFO MNP were dispersed in DMF solvent and citric acid (Sigma-Aldrich) (0.2 mg/g PVDF) in an ultrasound bath to help its dispersion and prevent agglomeration (Martins et al. 2014). After 4 h, PVDF was added and stirred with a Teflon mechanical stirrer, keeping the solution in the ultrasonic bath at 60 °C until complete dissolution of the polymer. PVDF solution was spread on a glass plate using a 750 µm casting knife and placed in a water bath at 25 °C for 30 minutes. After complete coagulation, the membranes were detached from the glass and were transferred to a new water bath to remove possible traces of DMF. The membranes were washed under shacking for 24h and then frozen at -80 ºC and lyophilized for 24 h, assuring the elimination of possible remaining DMF traces.

### 2.2.2. Heparin and collagen type I Layer-by-Layer

Membranes were aminolyzed in two steps. In the first, the membranes were treated with a 3.75 M NaOH (Scharlab) solution for 1 hour at room temperature to eliminate some fluorine and hydrogen atoms, creating an unsaturation in the PVDF backbone. They were then introduced in a solution of 1,4-diaminobutane dihydrochloride (DAB; Sigma-Aldrich) 1M in sodium carbonate (Sigma-Aldrich), with a final pH of 12, for 24 h at 55 °C to graft amine groups onto the membrane's surface. Membranes were washed with deionized water. The

amount of the amino groups present on the surface was determined by the ninhydrin test, following the protocol described in (Gamboa-Martínez et al. 2015). Treated membrane disks of 4 mm diameter were then immersed in 2 mL of ninhydrin solution and incubated at 80 °C for 20 minutes. The solution was then diluted with 3 mL of 2-propanol (Scharlab) 50% (v/v) in deionized water. Absorbance was read at 570 nm in a Victor3 microplate reader (Perkin Elmer). Non-treated membranes were used as blanks and amine concentration was determined by a glycine standard curve. All measurements were performed in triplicate.
Positively charged PVDF surfaces were washed with ultrapure water pH 5 to protonate amine groups. LbL was performed alternating one layer of heparin (Sigma-Aldrich) and one layer of collagen type I (Advanced Biomatrix). Solutions were prepared at a concentration of 1 mg/mL using ultrapure water pH 5, adjusting final pH to 5 (Ferreira et al. 2016). A volume of 70 µL of each solution was deposited on 8 mm diameter PVDF samples for 10 minutes. After washing with pH 5 ultrapure water, the complementary layer was deposited until 5 layers of each solution coated the surface.

### 2.2.3. Membrane characterization

#### 2.2.3.1. Field emission scanning electron microscopy

Membrane structure (both surfaces and cross-section) and deposition of the heparin/collagen layers were evaluated by field emission scanning electron microscopy (FESEM) (Ultra 55, Zeiss) with an accelerating voltage of 1 kV. The membranes were coated with platinum following a standard sputtering protocol for 90 s (JFC 1100, JEOL, Japan). Membrane spherulite diameter was assessed from FESEM images. 100 spherulites from each of three different membranes, produced in three different syntheses, were measured using ImageJ software (National Institutes of Health, Bethesda, Maryland, USA).

#### 2.2.3.2. Fourier transformed infrared spectroscopy

Fourier transformed infrared spectroscopy (FTIR) was carried out to determine the presence of PVDF's most electroactive form, the β-phase. Measurements were performed by an ALPHA FTIR spectrometer (Bruker) in ATR mode from 4000 to 400 $cm^{-1}$ at a wavenumber resolution of 4 $cm^{-1}$. Representative absorption bands at 840 $cm^{-1}$ and 760 $cm^{-1}$, which correspond to the β and α phase respectively, were identified and their content was determined using the procedure proposed by Gregorio and Cestari, yielding Eq. (1) (Gregorio and Cestari 1994).

The β-phase fraction, $F(\beta)$ is:

$$F(\beta) = \frac{A_\beta}{\left(K_\beta / K_\alpha\right) A_\alpha + A_\beta} \qquad \text{Eq. 1}$$

The method assumes that FTIR absorption follows the Lambert-Beer law, $K_\alpha$ and $K_\beta$, are the characteristic absorption coefficients at the characteristic wavenumbers of the α and β-phases (760 and 840 $cm^{-1}$, respectively). These were determined in reference (Gregorio and Cestari 1994) from samples containing only α or β-phase, obtaining values of $6.1\times10^4$ and $7.7\times10^4$ $cm^2/mol$, respectively. $A_\alpha$ and $A_\beta$ are the measured absorbances at 760 and 840 $cm^{-1}$ respectively.

Presence of collagen and heparin after layer-by-layer coating was also assessed by FTIR.

#### 2.2.3.3. Differential scanning calorimetry

Thermal properties of the membranes were evaluated by differential scanning calorimetry (DSC) using a DSC Pyris 1 (PerkinElmer) in a dry nitrogen atmosphere. Samples between 2 and 6 mg encapsulated in aluminium pans were used in the experiments. Scans were performed from 0 °C to 200 °C at a heating range of 20 °C/min. Degree of sample crystallinity ($X_c$) was determined using Eq. (2) (Martins, Costa, and Lanceros-Mendez 2011):

$$\Delta X_c = \frac{\Delta H_m}{w_{PVDF}(x\Delta H_\alpha + y\Delta H_\beta)} \qquad \text{Eq. 2}$$

where $\Delta H_m$ is the melting enthalpy of PVDF membranes measured in DSC and $\Delta H_\alpha$ and $\Delta H_\beta$ are the melting enthalpies of a 100% crystalline sample in the α and β phases, whose values are 93.07 J/g and 103.4 J/g, respectively. $w_{PVDF}$ is the mass fraction of PVDF within the membranes (provided by their magnetic properties), and *x* and *y* are the percentage of α and β phases present in the sample, obtained by FTIR measurements.

#### 2.2.3.4. Vibrating sample magnetometer

Magnetic properties of the composite membranes (PVDF-CFO) were evaluated using a Microsense 2 Tesla vibrating sample magnetometer (VSM). Magnetization loops M(H) were evaluated up to 18.5 kOe. To determine the real percentage of CFO in the composite samples, the saturation magnetization value of the pure CFO nanoparticles was compared with those obtained using Eq. (3) (Gonçalves, Martins, Correia, et al. 2015):

$$CFO\ wt\ \%\ membranes = \frac{Saturation\ magnetization\ membranes}{Saturation\ magnetization\ pure\ CFO} x100 \qquad \text{Eq. 3}$$

The value of saturation magnetization of pure CFO being 60 emu/g.
Three different zones of the same PVDF-CFO membrane were evaluated to ensure homogeneous CFO distribution within the membrane matrix.

#### 2.2.3.5. X-ray photoelectron spectroscopy

Two-step amynolization was assessed by X-ray photoelectron spectroscopy by means of a XPS Kratos Axis Ultra HSA apparatus, which uses a micro-focused monochromatic Al Kα X-ray source (1486.6 eV) covering an analysing area of 300 x 700 μm (90 W power). Survey spectra were collected at a pass energy of 160 eV, step size of 1 eV, and dwell time of 200 ms with the spectrometer operated in hybrid lens mode. High-resolution C1s regional spectra were collected using a pass energy of 40 eV, step size of 0.1 eV, and dwell time of 200 ms. High-resolution regional spectra of N1s and O1s were collected using the same parameters, except for the dwell time, which was 1500 ms. High-resolution spectra envelopes were processed using CasaXPS software.

#### 2.2.3.6. Determination of heparin concentration

Heparin deposition on PVDF and PVDF-CFO membrane's surface after layer-by-layer was confirmed measuring its concentration by Taylor's blue colorimetric method using Glycosaminoglycan Assay Blyscan (Biocolor). LbL was performed in membranes with a surface of 1 $cm^2$ applying 1, 3 or 5 layers of heparin. Samples were labelled as H and the corresponding number of layers of the biomolecule. Shortly, membranes were soaked in 1 mL of Blyscan dye reagent containing 1,9-dimethylmethylene blue and incubated for 30 minutes under shacking at room temperature. After incubation, samples were washed with distilled water and transferred to a new eppendorf. 0.5 mL of dissociation reagent were added to favour heparin dissociation from 1,9-dimethylmethylene. Absorbance was read at 652 nm (Victor3 microplate reader; Perkin Elmer) transferring 100 μl of each sample to a 96-well plate. Heparin concentration was determined using a heparin calibration curve (0-5 μg). All measurements were performed in triplicate.

#### 2.2.3.7. Atomic force microscopy

Collagen layer deposition on PVDF membranes was confirmed by means of atomic force microscopy (AFM). Non coated PVDF samples and samples containing 1 (C1) and 5 bilayers (C5) were analysed. Atomic force microscopy was performed on a Multimode 8 (Bruker) operating in tapping mode in air. RFESPA silicon probes from Bruker were used with a force constant of 3 N/m and resonance frequency of 75 kHz. The tapping frequency was slightly lower than the resonance (around 10%), in which the phase signal was set to zero. The linear speed of the tip was set at 2 μm/s and the drive amplitude was modified to obtain an oscillation-free length of 700 mV. The ratio between setpoint and drive amplitude was maximized to obtain images with the least surface deformation (i.e. soft tapping).

### 2.2.4. Cell response

Human bone marrow mesenchymal stem cells (hMSCs) (Promocell, Germany) were used to evaluate cell response. A short-term culture (1, 3 and 7 days) was carried out to check cell proliferation on PVDF and PVDF-CFO membranes coated by collagen/heparin layer-by-layer.

hMSCs were expanded in a basal medium containing Dulbecco's Modified Eagle Medium (DMEM) high glucose (4.5 g/L) (Gibco) supplemented with 10% (v/v) foetal bovine serum (FBS; Gibco), 4 mM L-glutamine (Lonza), 1X non-essential aminoacids (Gibco), 1 mM sodium pyruvate (Gibco), 70 U/mL penicillin, 70 μg/mL streptomycin (P/S; Life technologies) and 0.25 μg/mL fungizone (Life technologies), at 37 ºC in a humidified atmosphere with 5 % $CO_2$. All experiments were performed at passage 4.

After aminolyzing the membranes, 8 mm diameter disks were obtained and sterilized by UV exposition for 1 hour. PVDF membranes were then immersed in ethanol 70 % (v/v) for 20 minutes and washed 5 times with ultrapure water, last wash with pH 5 ultrapure water to protonate amine groups. Layer-by-layer was performed in sterile conditions, nonetheless, as pH adjustment of collagen solution required non-sterile conditions PVDF and PVDF-CFO membranes already coated were sterilized again using the same protocol.

PVDF and PVDF-CFO membranes, non aminolyzed, and glass slides coated with fibronectin from human plasma (Sigma-Aldrich) were used as controls to compare the effect of layer-by-layer coating with a conventional protein adsorption. Since the scope of our work was to compare the established fibronectin coating protocol with more complex approaches involving other biomolecules, non-coated surfaces were not used. All controls were coated after sterilization by incubation in a 20 μg/mL fibronectin solution for 1 hour at room temperature.

12 h before cell seeding, cells were starved in basal media containing 1 % (v/v) FBS to synchronize cell cycle. To study cell proliferation cells were seeded at a density of 8 x $10^3$ cells/$cm^2$ in basal medium without FBS (3 replicates per group) to promote cell adhesion either to fibronectin or collagen. A 100 μL drop containing the right number of cells was deposited on the surface of the samples. After 3 h the required volume of basal medium and FBS for a final concentration of 10 % (v/v) were added to each well. Silicon rings were used to keep the membranes fixed on the bottom of the well. These rings were also used in glass slides controls. After 1, 3 and 7 days cells were fixed in a 4 % (v/v) paraformaldehyde solution (Panreac) for 20 minutes.

Cell proliferation was assessed by nuclei counting using nucleus and cytoplasm staining. Before staining, PVDF and PVDF-CFO membranes were treated with a 0.2 % (w/v) Sudan Black B solution for 40 minutes to avoid PVDF autofluorescence, which hinders image acquisition and quantification (Qi et al. 2017). Membranes were washed 3 times with Dulbecco's Phosphate Saline Buffer (DPBS; Sigma-Aldrich). Subsequently, samples were permeabilized and blocked in 1 % (w/v) bovine serum albumin (BSA; Sigma-Aldrich) solution in DPBS/0.1 % (v/v) Tween-20 (Sigma-Aldrich) for 1h at room temperature and incubated with Actin Red 555 Ready Probes reagent (Fisher Scientific) following manufacturer's instructions, then washed 3 times with DPBS/0.1 % (v/v) Tween-20 and incubated for 20 minutes with Hoechst (1:400; Thermo Fisher) in mounting medium.

Images of four representative fields of every sample were taken with a fluorescence microscope (Nikon Eclipse 80i) and analysed using ImageJ software (National Institutes of Health, Bethesda, Maryland, USA). Cell number was expressed as the number of cells per square centimetre. ImageJ software was also used to quantify cell spreading after 24h of cell culture. Briefly, masks of images were obtained by previous segmentation and cell area was measured for the scaled images. Approximately 60 cells per condition, from different replicates, were measured.

### 2.2.5. Statistical analysis

Statistical analysis was assessed by Graphpad Prism 6 software (Graphpad Software, United States). For cell counting data analysis, homoscedasticity was checked by Snedecor's F-distribution. T-test was used to find significant differences between each studied group. For cell spreading analysis, after checking homoscedasticity, a non-parametric Kruskal-Wallis test was performed to detect significant differences. Significance was accepted as $p\text{-value} < 0.05$

## 2.3. Results and discussion

### 2.3.1. Membrane characterization

The non-solvent induced precipitation technique can obtain a wide variety of membrane morphologies according to the different parameters involved in polymer precipitation. PVDF and PVDF-CFO membranes were produced using distilled water at 25 ºC as non-solvent and immersing them immediately in the coagulation bath to reduce air exposure to the minimum. The non-solvent selection plays a crucial role in the final membrane morphology. Water is known to be a strong non-solvent for PVDF and leads to asymmetric structures like those shown in Figure 2.1. Membranes produced using harsh baths, e.g. water, exhibited a smooth surface, non-porous at the micrometre level, followed by macrovoids or finger-like structures which continued with a porous structure composed of spherulites, as can be seen in Figure 2.1c. Top surface of image 1c is that of the smooth surface shown in image 1b, while image 1a is of the bottom surface in contact with the casting glass.

PVDF precipitation into a membrane is governed by two events: liquid-liquid demixing and crystallization due to the semi-crystalline nature of PVDF. The importance of these phenomena lies in the order in which they take place. Water-induced precipitation leads to rapid liquid-liquid demixing before crystallization, giving rise to asymmetric membranes such as those obtained (Young et al. 1999).

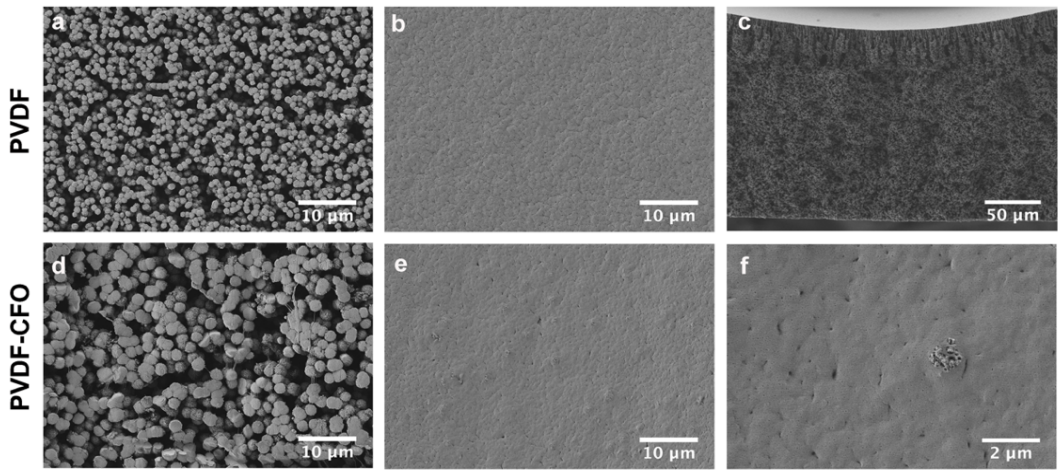


**Figure 2.1. FESEM images of PVDF and PVDF-CFO NIPS membranes. a), d) Porous, bottom surface. b), e) Smooth, top surface of PVDF and PVDF-CFO membranes, respectively. c) PVDF membrane cross-section showing the top finger-like structure and the underlying microporous structure formed by PVDF spherulites. f) CFO trapped on PVDF-CFO top surface (magnification of image e)).**

Coagulation bath temperature also contributes to the membrane structure (Cheng 1999). Higher temperatures up to 65 ºC provide a favourable condition for liquid-liquid demixing and tend to form larger finger-like structures, while low temperatures such as those used here reduce their formation, giving place to small macrovoids and sponge-like membranes similar to those obtained from soft non-solvents. Adding CFO did not modify the overall membrane structure, as shown in FESEM images 1d and e. The difference in spherulite size can be seen in images 1a and d. Measurements revealed that PVDF spherulite

diameter was 0.99 ± 0.17 μm, while PVDF-CFO spherulites doubled theirs to 2.15 ± 0.42 μm. This difference could be explained by the addition of CFO nanoparticles to the initial solution. Supriya et al. (Supriya, Kumar, and Kar 2019) studied the effect of CFO MNP diameter on the performance of dielectric PVDF nanocomposites. They postulated that CFO nanoparticles are negatively charged, making them interact with the positively charged $CH_2$ bond, acting as a core and giving place to a core-shell structure formed by CFO and PVDF. They observed that the larger the CFO nanoparticle diameter, the larger the granular structures present in the PVDF nanocomposites and also that they were prone to agglomerate at larger diameters. It is plausible that CFO MNP aggregates could be acting as nucleation centers for the formation of PVDF spherulites, obtaining larger diameters than the PVDF membranes.

Lin et al (Lin et al. 2006) described the change of the spherulite diameter in PVDF membranes produced in 1-octanol baths, according to the precursor-solution preparation temperature. Lower temperatures favoured a higher density of nuclei available for the initiation of crystallization. Although the solutions looked macroscopically similar, those at higher temperatures contained less undissolved and invisible pre-nucleation aggregates. Even if the applied temperature is the same, the presence of CFO in the solution requires different preparation methods, including mechanical stirring and ultrasounds for longer periods. This protocol may lead to fewer nuclei, reducing the crystallization points and increasing spherulite diameter. Further experiments will be needed to confirm which of these hypotheses can explain the variation in spherulite diameter.

The main objective when producing PVDF cell culture supports able to subject cells to electrical stimulation during culture is to obtain electroactive phases. As mentioned in the Introduction, PVDF has 5 polymorphs, $\alpha$, β and $\gamma$ being the most important. $\alpha$ is a non-electroactive phase, due to antiparallel dipole packing within the unit cell (TGTG) (Cai et al. 2017). All-trans (TTT) or $T_3GT_3G$ structures present in β and $\gamma$ phases, respectively, make them the most piezoelectric and give them very similar conformations, which makes it difficult to distinguish between both phases using Fourier transformed infrared spectroscopy or X-ray diffraction peaks, due to their proximity. The β and $\gamma$ phases usually show a typical peak at 840 $cm^{-1}$, which tends to form a shoulder at 833 $cm^{-1}$ at a high $\gamma$ phase contribution, while no such shoulder is shown for pure β phase (Martins, Lopes, and Lanceros-Mendez 2014). Many authors agree in using 1234 $cm^{-1}$ and 1279 $cm^{-1}$ to differentiate between $\gamma$ and β, respectively, since they are exclusive to each polymorph (Cai et al. 2017).

Synthesized membranes showed different FTIR spectra in the smooth and porous sides, as can be noted in Figure 2.2a and b. The smooth surface was a mixture of $\alpha$ and β, in which characteristic non-polar phase peaks can be appreciated, 532, 614, 795, 975 $cm^{-1}$ among others. 760 $cm^{-1}$ is the most characteristic and was used to calculate the percentage of $\alpha$ polymorph present in the sample. A strong band at 840 $cm^{-1}$ was present with no signs of 1234 $cm^{-1}$ $\gamma$ characteristic band, being only visible 1279 $cm^{-1}$ in this region of the spectrum, corresponding to β-phase.

Eq. (1) was used to calculate the percentage of each phase, since this side will be used as a cell culture support for human mesenchymal stem cells. The percentages of β-phase were 51.8 % for PVDF and 55.6 % for PVDF-CFO membranes. It has previously been shown that including fillers in the PVDF matrix enhances β-phase crystallization and increases its percentage in the nanocomposites, compared to the PVDF structures (Martins, Costa, and Lanceros-Mendez 2011). Regarding the porous surface, the FTIR spectra showed a mixture of $\gamma$ and β-phase, with no $\alpha$-phase content. Characteristic peaks at 431, 776 and 1234 $cm^{-1}$ revealed the presence of $\gamma$ and peaks at 445, 840 and 1279 $cm^{-1}$ reinforced β-phase. The strong band at 840 $cm^{-1}$ with no shoulder at 833 $cm^{-1}$ led to the conclusion that β is the main phase in the porous surface. Nonetheless, the $\gamma$-phase could be noted, giving rise to a mostly electroactive membrane, since the porous structure's contribution to the membrane was much greater than that of the smooth surface. As previously mentioned, the difficulty in distinguishing between both phases makes it difficult to quantify β-phase percentage by FTIR spectra only.

These findings agree with those obtained by Boccaccio et al. (Boccaccio et al. 2002), who made an exhaustive analysis of PVDF membranes using DMF as solvent by the NIPS manufacturing method, assessing the PVDF phases by different FTIR techniques. They found that membranes were mostly β-phase in the finger-like structure, with a contribution of $\gamma$-phase to the porous part. The smooth surface, some microns thick, was composed of $\alpha$ and β, though no percentage of each phase was given. Other studies confirmed the presence of a mixture $\alpha$ and β phase on the membrane surface, although different solvents and coagulation bath temperatures were used (J. Liu, Lu, and Wu 2013; M. Zhang et al. 2008).

Differential scanning calorimetry was used to determine the crystalline fraction present in the studied sample. Differences in the melting temperatures ($T_m$) of PVDF crystalline phases can be used as an indicator of their presence in the sample, although they should be used as a complementary method to FTIR only, since $T_m$ is also affected by crystalline defects and are especially present when the sample contains a filler (Martins, Lopes, and Lanceros-Mendez 2014). Figure 2.2c shows the presence of the endothermic peaks around 170 ºC. PVDF membranes had their $T_m$ at 170.2 ºC, while PVDF-CFO presented two endothermic peaks, the $T_m$ being 168.4 ºC. The presence of more than one endothermic peak can be attributed to two phenomena: either the coexistence of two different crystalline phases in the same sample, or crystallite perfection. The presence of two endothermic peaks can only be seen in composite PVDF-CFO membranes. Since the coexistence of more than one polymorph has been described in both types of membranes by means of FTIR, the double endotherm peak present in PVDF-CFO must be due to different crystal sizes because of the presence of CFO.

Crystallinity ($X_c$) can be calculated applying Eq. (2) using the melting enthalpies extracted from the DSC analysis. No contribution from the $\alpha$-phase was assumed, since this phase, measuring only a few micrometres, is only present in the smooth surface. The results show that PVDF membranes had higher crystallinity (66 %) than PVDF-CFO membranes (61 %).

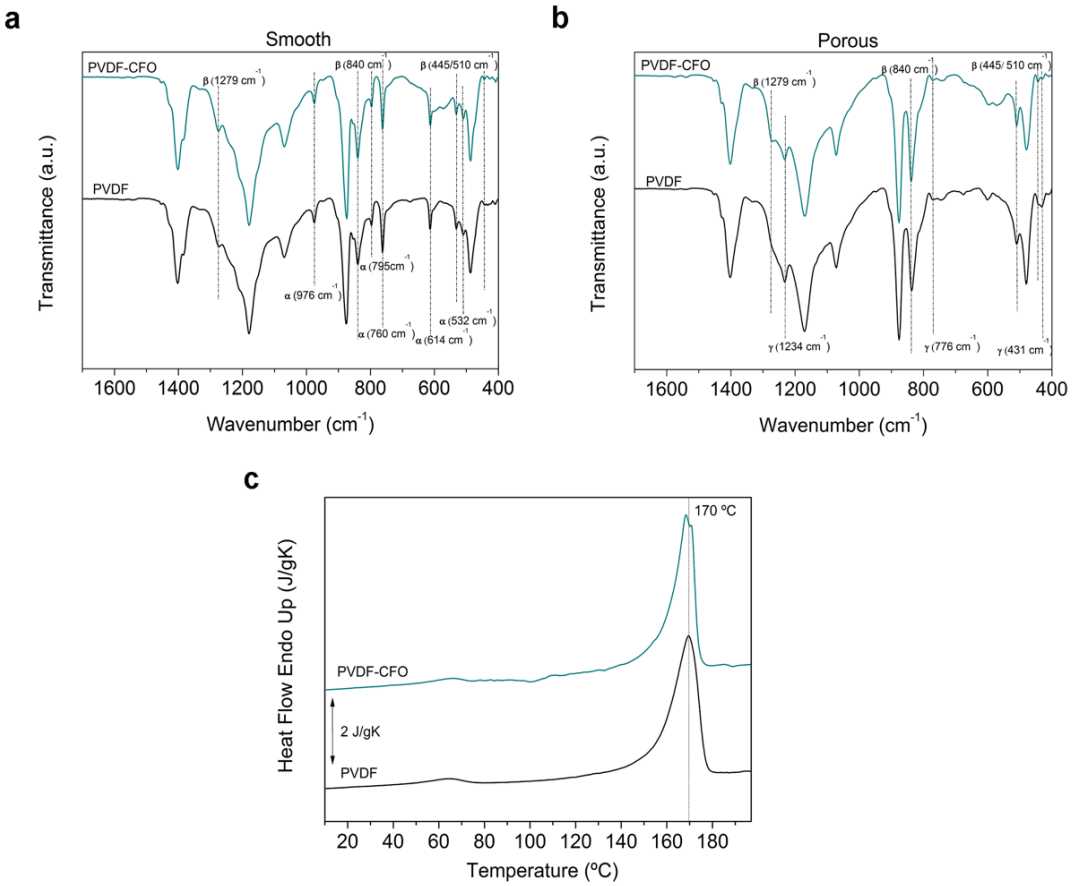


**Figure 2.2. a) Infrared spectra of smooth surface of PVDF and PVDF-CFO membranes where characteristic peaks of α and β phases are highlighted. b) Infrared spectra of porous surface of PVDF and PVDF-CFO membranes where characteristic peaks of β and γ phases are highlighted. c) DSC heating thermograms of PVDF and PVDF-CFO membranes.**

These high contents indicate that crystallization also occurs during polymer precipitation, even though liquid-liquid demixing takes place first. Low temperature coagulation baths favour a lower mass exchange between solvent and non-solvent, delaying liquid-liquid demixing and giving more time to the crystallization process (M. Zhang et al. 2008). The difference in $X_c$ between PVDF structures with and without CFO MNP was explained by Martins et al. (Martins, Costa, and Lanceros-Mendez 2011). PVDF composites tended to have a lower degree of crystallinity than pristine PVDF. As shown by the two endothermic peaks in the DSC, composite membranes possessed more crystal defects, which can contribute to lower $X_c$.

Incorporating CFO nanoparticles into the membranes was assessed by the Vibrating Sample Magnetometer (VSM), measuring the magnetic response. VSM can be used to determine the real content of CFO nanoparticles present in a sample and therefore nanoparticle loss during the composite manufacturing process (Gonçalves, Martins, Correia, et al. 2015; Gonçalves, Martins, Moya, et al. 2015).

Figure 2.3a shows the typical hysteresis loop for PVDF-CFO nanocomposites. Magnetization increased when the intensity of the applied field was raised until it saturated. The CFO content was calculated by Eq. (3), being 9.04 % ± 0.01 % in the sample, starting from a 10 % (w/w) concentration in the polymer solution. These data were obtained by measuring the magnetic response in three different zones of the same membrane, ensuring the correct distribution of the MNP within the composite sample. The cross-section of PVDF-CFO membrane in Figure 2.3(b) and (c) shows good CFO MNP distribution within the polymer matrix, as confirmed by VSM. Nevertheless, cobalt ferrite oxide tends to form aggregates up to 1 µm, as can be seen in the FESEM image in Figure 2.3(c).

In addition to being a simple process, these data show that NIPS is a valid technique for incorporating CFO into the polymer matrix. Unlike other techniques for producing PVDF nanocomposites, e.g. electrospinning (Gonçalves, Martins, Moya, et al. 2015), electrospray (Gonçalves, Martins, Correia, et al. 2015) or solvent casting (Fernandes et al. 2019), in which nanoparticle loss is more than 30 %, NIPS can incorporate up to 90 % of the MNP.

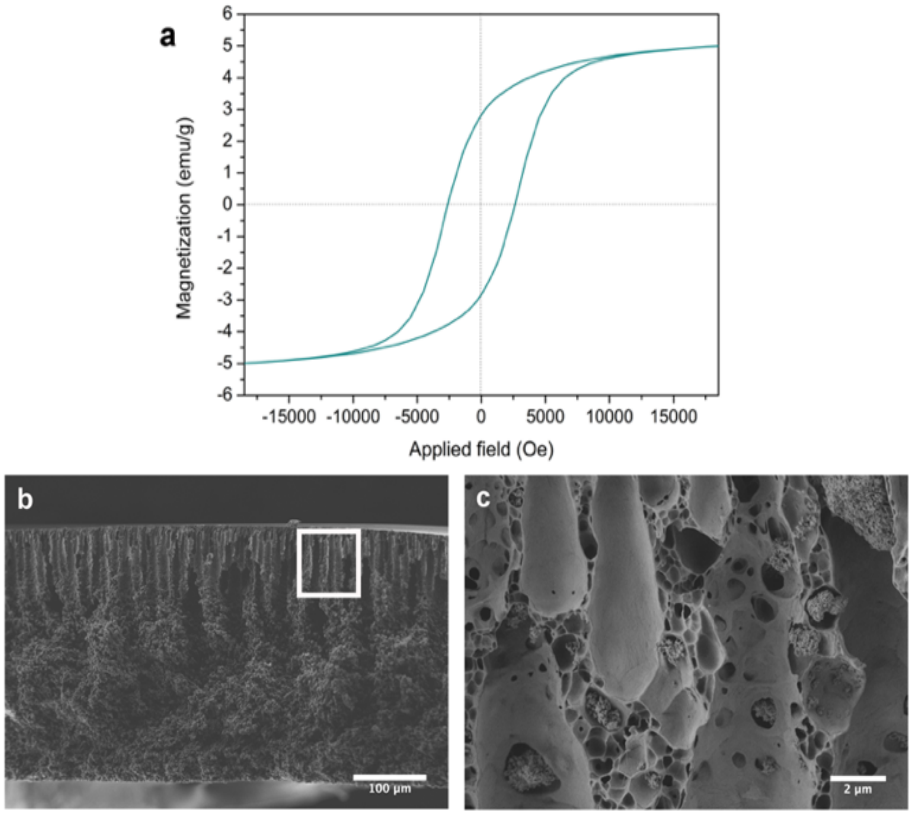


**Figure 2.3. a) Room-temperature hysteresis loop of PVDF-CFO membranes. b) Cross-section FESEM image of a PVDF-CFO membrane. c) Magnification of the square zone in b) where aggregation of CFO nanoparticles can be seen within the polymer matrix.**

### 2.3.2. Amine graft characterization

PVDF is a widely used fluoropolymer due to its strong chemical resistance, which means it is difficult to modify its chemical structure, claiming the need of aggressive treatments. A

two-step treatment was used to graft free amine groups onto the PVDF surface. PVDF and PVDF-CFO membranes were first immersed in a 3.75 M NaOH solution for 1 hour at room temperature to dehydrofluorinize the polymer, followed by the formation of a conjugate double bond or polyene structure (C=C). After NaOH treatment the membranes became brownish, a macroscopic indicator of PVDF fluorine and hydrogen elimination (Xiao et al. 2015).This bond can be attacked by specific molecules, such as 1,4-diaminobutane, which contains two primary amine groups. One group is able to bond to the polyene structure while the other will remain free to act in an acidic pH medium as a positive charge on the surface to promote the union of the first heparin layer. Incubation with 1,4-diaminobutane was performed for 24 h at 55 ºC, following Algieri et al. (Algieri, Donato, and Giorno 2017) optimized protocol.
An XPS analysis was carried out to study the efficiency of the chemical modification on both the PVDF and PVDF-CFO surfaces. The scan spectra of C1s, F1s, O1s and N1s are shown in Figure 2.4. The elemental composition of all samples is given in Table 2.1.

The C1s spectra of PVDF and PVDF-CFO before and after NaOH chemical treatment are shown in Figure 2.4a. Whatever the surface, both untreated PVDF and PVDF-CFO display the main C1s PVDF characteristic peaks at 286.4 eV and 291.4 eV attributed to the $CH_2$ and $CF_2$ groups, respectively, and the peak at 285.0 eV assigned to the C-C group (Duca, Plosceanu, and Pop 1998; Correia et al. 2015). Some differences were found in the intensity of the XPS scans in the NaOH treated samples. The intensity of the characteristic $CF_2$ and $CH_2$ peaks was seen to fall, while the C-C group's characteristic peak rose, indicating the loss of hydrogen and fluorine atoms after the post-chemical treatment with NaOH. No significant changes were seen after the DAB chemical treatment, showing the main C1s peaks PVDF characteristics. The C-C group was attenuated in PVDF-CFO composites on both treated and untreated surfaces (Figure 2.4a and 2.4b).

Two peaks at 688 eV and 684 eV associated to the C-F groups (Correia et al. 2015; Lim et al. 2004) can be seen in the F1s scan spectra in Figure 2.4c. The peak at 533 eV at O1s is attributed to oxygen groups from the water formed during the dehydrofluorination process (Figure 2.4e), as reported in (Algieri, Donato, and Giorno 2017). The DAB reaction with the polymer chain is proven by the assigned peak at 400 eV (Figure 2.4f), attributed to $NH_2$ groups (Kehrer et al. 2019).

The quantitative elemental composition of PVDF and PVDF-CFO composites before and after the chemical treatments are summarized in Table 2.1, in which surface chemical modifications can be checked. No significant changes were found in the elemental composition of the surfaces of untreated PVDF and PVDF-CFO composites, nor were there significant changes in the amount of carbon atoms, but the number of fluorine atoms dropped, accompanied by small numbers of oxygen atoms from the dehydrofluorination process, as reported in (Algieri, Donato, and Giorno 2017). The NaOH treatment reduced the F/C ratio from 0.92 to 0.84 in PVDF and 0.97 to 0.86 in PVDF-CFO, indicating that NaOH treatment leads to the cleavage of the C-F and C-H bonds and promotes the formation of radicals that can be recombined, leading to the formation of C=C bonds. DAB chemical treatment also reduces the F/C ratio samples and increases the amount of carbon. As shown in Table 2.1, the F/C ratio drops from 0.92 to 0.52 and 0.97 to 0.72 for both PVDF

and PVDF-CFO, respectively. No significant changes can be seen in the number of oxygen atoms. According to (Algieri, Donato, and Giorno 2017), the presence of nitrogen indicates that DAB is able to react with the -$CH_2$-CH=CF-$CH_2$- chain, inducing the formation of an amino group.

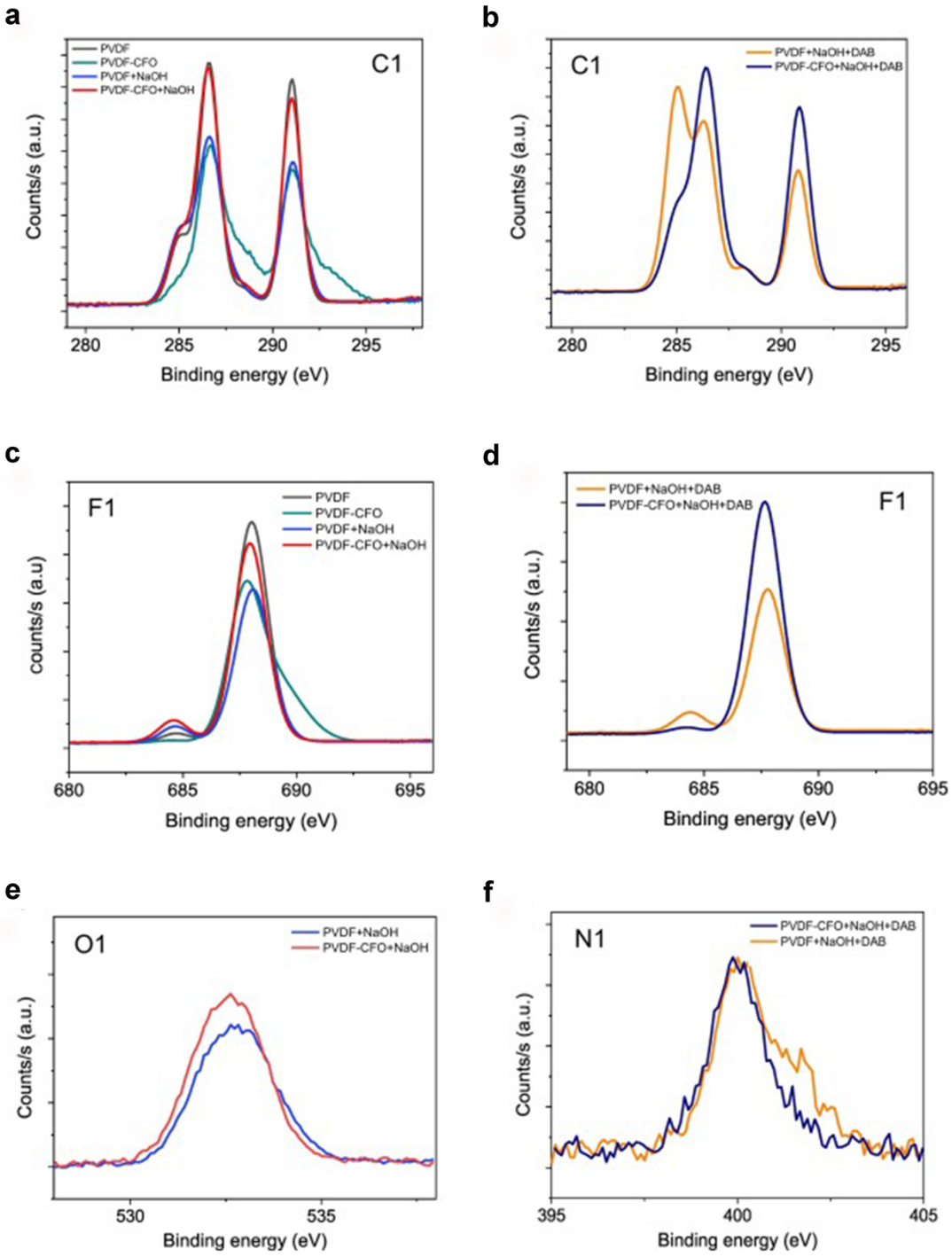


**Figure 2.4. XPS spectra of untreated and chemically treated PVDF and PVDF-CFO samples C1 and F1 scan spectra for PVDF and PVDF-CFO after NaOH a), c), and DAB treatments b),**

**d), respectively. O1 and N1 spectra for PVDF and PVDF-CFO after the NaOH treatment e) and DAB f).**

**Table 2.1. Surface chemical composition of PVDF and PVDF-CFO surface composites before and after chemical treatment.**

| | ELEMENTAL COMPOSITION (%) | | | | |
|---|---|---|---|---|---|
| **SURFACE** | *C1s* | *F* | *O* | *N* | *F/C* |
| *PVDF* | 51.9 | 48.1 | - | - | 0.92 |
| *PVDF-CFO* | 50.7 | 49.3 | - | - | 0.97 |
| *PVDF+NAOH* | 51.5 | 43.7 | 4.8 | - | 0.84 |
| *PVDF-CFO+NAOH* | 51.3 | 44.2 | 4.6 | - | 0.86 |
| *PVDF+NAOH+DAB* | 64.3 | 33.3 | | 2.4 | 0.52 |
| *PVDF-CFO+NAOH+DAB* | 54.4 | 39.4 | 4.7 | 1.6 | 0.72 |

To verify the results obtained from the XPS surface analysis, the ninhydrin test, a colorimetric assay, was conducted to quantify the amino groups. These groups present on the membrane surface reacted with ninhydrin to form a purple compound. Quantification by the glycine calibration curve revealed that the concentration of amine groups was 30.1 ± 5.5 μmol/g for PVDF membranes and 27.7 ± 4.8 μmol/g for PVDF-CFO.

### 2.3.3. Layer-by-layer assembly

Five layers of each polyelectrolyte were deposited on the membrane smooth surface, starting with a layer of heparin and ending with collagen. This surface was chosen as cell culture support due to the high porosity of the bottom surface. In a previous study we found that PVDF membranes with porosities ranging from 80 to 85 % had very different outcomes regarding initial cell adhesion and proliferation, that is to say, small porosity differences can significatively influence cell behaviour. Focusing on studying LbL effect and to exclude this parameter cells were seeded on the smooth surface (Morales-Román et al. 2019).

Representative FESEM images after layer-by-layer assembly show good deposition and a homogenous coating on the surface of both membranes. Figure 2.5(1) shows PVDF and PVDF-CFO membranes before and after layer-by-layer assembly, with no difference in layer-by-layer coating due to the incorporation of CFO MNP in the polymer matrix, or even the presence of CFO aggregates on the membrane smooth surface. FTIR spectra confirmed the FESEM images. Figure 2.5(2) shows representative FTIR spectra of a PVDF membrane with and without LbL. New peaks, highlighted with arrows, can be seen in the spectra of the last heparin (H5) and collagen layers (C5). FTIR graphs of PVDF-CFO membranes are not shown since the new peaks of both conditions were similar. The most representative absorptions in the collagen α-helix are those of the amide A N-H stretching, with a peak appearing around 3330 $cm^{-1}$, the amide I C=O stretching at 1655 $cm^{-1}$ and the

amide II C-N stretching and N-H bending combination, typically appearing at 1550 $cm^{-1}$ (Camacho et al. 2001). The absence of PVDF characteristic peaks in these regions made it easy to identify the previously mentioned collagen absorptions in the LbL coated membrane, starting with an intense amide A peak at 3330 $cm^{-1}$.

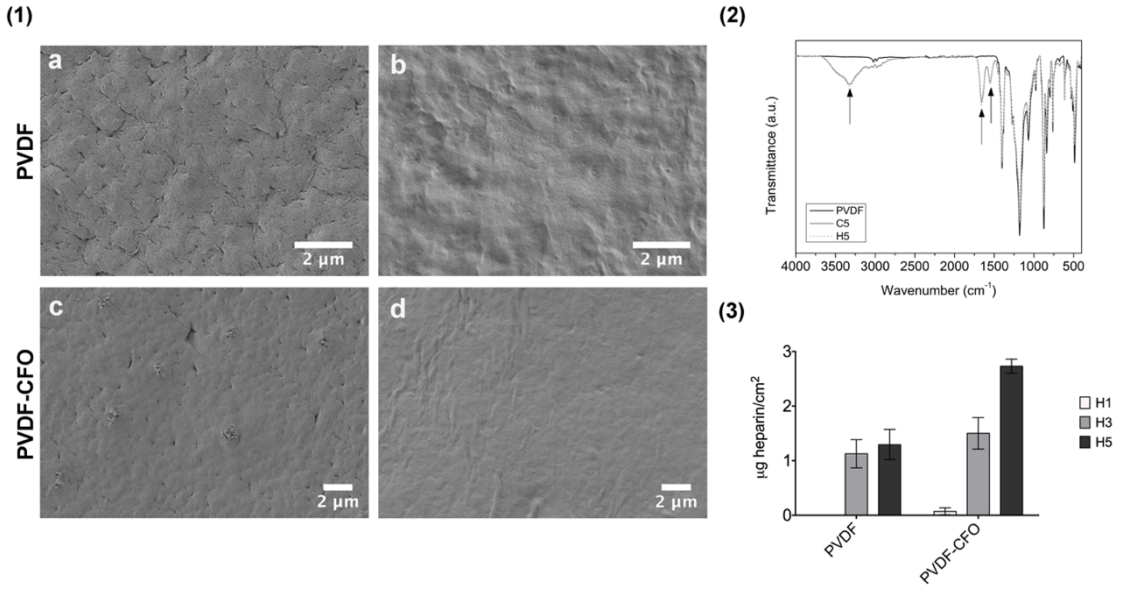


**Figure 2.5. (1) FESEM images of layer-by-layer coating on the top surface of PVDF and PVDF-CFO membranes. a) PVDF and c) PVDF-CFO smooth surface without coating. b) PVDF and d) PVDF-CFO LbL coated surface. (2) FTIR spectra of PVDF membrane without LbL and PVDF membrane showing last layer of heparin (H5) and last layer of collagen (C5). Arrows highlight the characteristic peaks of the polyelectrolytes used. (3) Bar diagram of heparin concentration in PVDF and PVDF-CFO membranes after 1 (H1), 3 (H3) and 5 (H5) heparin layers.**

The last heparin layer spectra (dashed line) have exactly the same peaks as the last collagen layer, since proteoglycans share characteristic absorption bands with the proteins of primary and secondary amides. The C-O-S stretching band at 850 $cm^{-1}$ cannot be distinguished due to the abundance of pronounced typical PVDF peaks in that region, especially the β-phase band at 840 $cm^{-1}$. To prove heparin presence in the coated membranes, since it could not be detected by means of FTIR, heparin concentration was determined using Taylor's blue colorimetric method. As can be seen in figure 2.5(3), heparin presence was only detected in the first layer of PVDF-CFO membranes, concentration of H1 in PVDF membranes was too low to be detected by this colorimetric method. After 3 layers, both types of membranes showed similar biomolecule concentrations, 1.13 ± 0.26 μg of heparin/$cm^2$ for PVDF membranes and 1.5 ± 0.29 μg of heparin/$cm^2$ in the membranes containing CFO. The increase in heparin concentration between H1 and H3 did not follow a linear rise. This could probably be due to the presence of the subsequent layers of collagen, which provided a higher number of amine groups and positive charges than the ones obtained after amynolization, increasing the concentration of heparin deposited in the following layers. Interestingly enough, after depositing 5 layers of heparin, PVDF-CFO membranes showed a linear increase in the concentration, reaching 2.73 ± 0.13 μg of

heparin/cm$^2$. Nonetheless, concentration of heparin was saturated after 3 layers in PVDF membranes, not showing a significant increase after the deposition of 5 layers. Differences in heparin deposition could be related with the presence of CFO, but further studies will be needed to reach a conclusion.

Deposition of collagen layers was also confirmed by atomic force microscopy. Figure 2.6 shows PVDF sample AFM images before and after coating with alternate layers of heparin and collagen, PVDF-C1 and PVDF-C5, for 1 and 5 bilayers respectively (from a to f). At first glance, there is not a huge difference between them when examining a large area: the height profiles at the bottom of Figure 2.6 are all very similar. However, there is a more subtle change which was eventually revealed by the surface roughness parameters: the more layers in the LbL process, the lower the surface roughness ($R_a$ ranging from 28 nm for neat PVDF to 22 nm for PVDF-C5). The coating process deposits a thin layer on the PVDF surface which preferentially fills the lower parts of the topography, giving more rounded profiles with smaller differences between peaks and valleys.

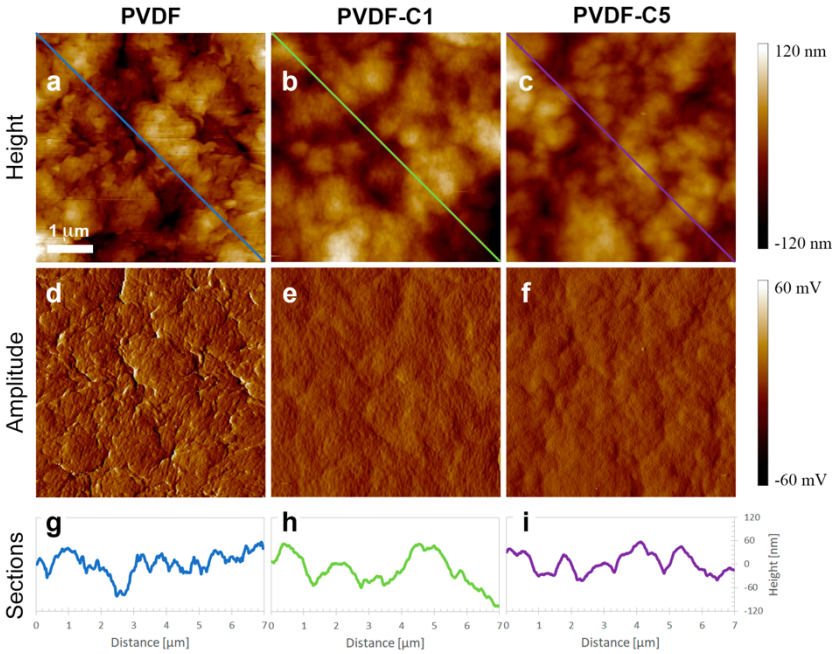


**Figure 2.6. Height and amplitude AFM images of neat PVDF and PVDF coated by different numbers of alternating heparin/collagen layers (1 and 5 bilayers for C1 and C5, respectively). Height profiles of straight lines are also displayed at the bottom of the figure.**

### 2.3.4. Cell response to layer-by-layer coated membranes

Human mesenchymal stem cells were used to test initial cell response in PVDF and PVDF-CFO membranes, assuring their future use in bone tissue engineering applications. To compare the effectiveness of layer-by-layer coating, PVDF and PVDF-CFO membranes with adsorbed fibronectin were used as controls. Fibronectin is usually applied as a simple coating to favour initial cell adhesion in non-adherent biomaterials. A glass slide coated with fibronectin was also used, generally considered a standard control. A short-term culture

was carried out, after 24h cell spreading was evaluated and cell number was assessed at 1, 3 and 7 days by cytoplasm-nucleus cell counting.

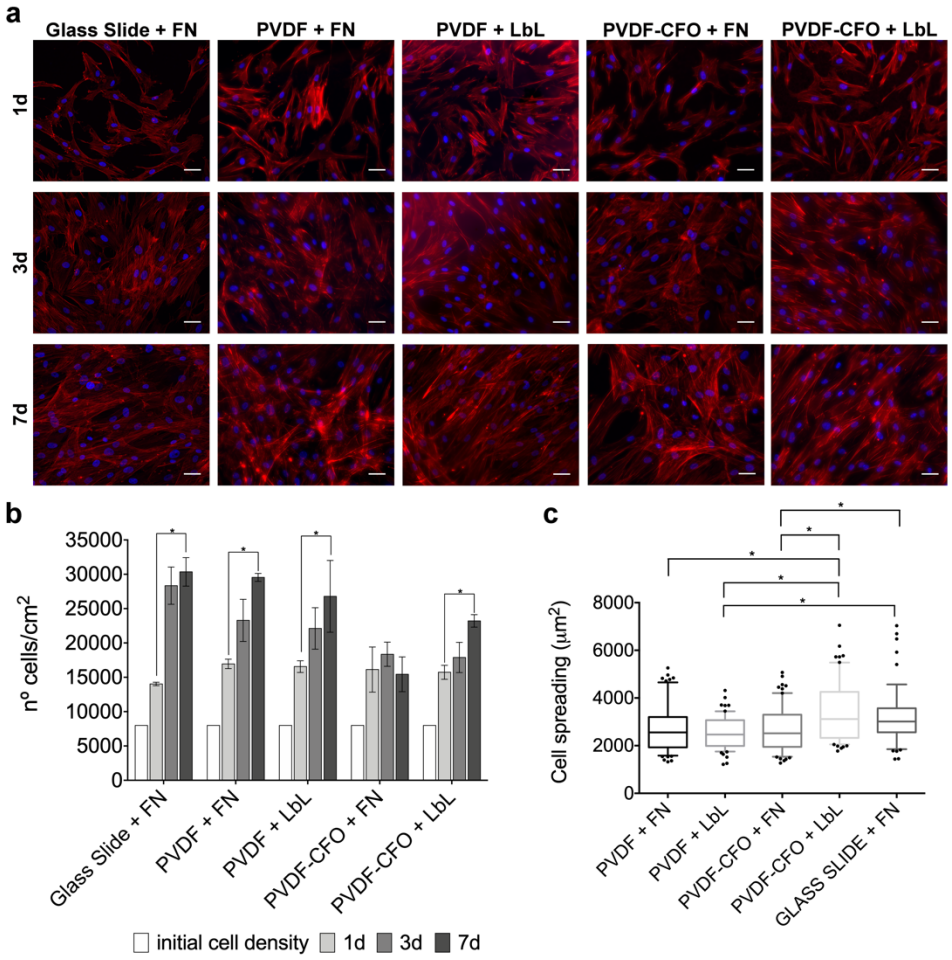


**Figure 2.7. (a) Representative images of actin (cytoplasm-red) and Hoechst (nucleus-blue) staining after 1, 3 and 7 days of culture. High cell seeding density (8000 cells/cm$^2$) allows cells to reach confluence after 3 days. Scale bar is 50 µm. (b) Box and whiskers (10-90 percentile) of cell areas measured after 24h in each condition (c) Cell count based on the analysis of 4 images taken from 3 replicates per condition at 1, 3 and 7 days. * p-value < 0.05**

A high cell seeding density (8 x 10$^3$ cells/cm$^2$) was chosen. As can be seen in Figure 2.7a the cells adhered in every condition after 24h, showing well-developed cytoskeletons and fusiform morphologies typical of hMSCs. Cell spreading was assessed in every condition analysing the images taken at the first time point studied. Figure 2.7b shows the obtained plots. Although significant differences can be found between different conditions, they are minimal and probably associated with the heterogeneity displayed by hMSCs morphologies once they adhered to the surfaces.

As indicated by the cell count, the cells duplicated within the first 24h. Cell number after 24h shows no significant differences between conditions, demonstrating the non-cytotoxic effect of CFO in the PVDF-CFO membranes at short term. The cells continued to proliferate over

time, reaching confluence after 3 days of culture, which will be the proper time to introduce external differentiation stimuli, chemical if media supplements are added or physical if differentiation is induced by electromechanical cues. In PVDF substrate not containing CFO, cells multiplied continuously up to day 7. Cell adhesion and proliferation on PVDF substrates has traditionally been ensured by a fibronectin coating on the surface, since MSCs adhesion to PVDF substrates based only on the proteins adsorbed from serum is not effective. Since Ribeiro et al. (Ribeiro et al. 2012) studied fibronectin adsorption on PVDF substrates in different crystalline phases, fibronectin has been used as a routine coating for cell culture in PVDF samples (Ribeiro et al. 2015; Sobreiro-Almeida et al. 2017). Coating our supports with FN attained cell numbers of the same order as glass control. Layer-by-layer coating had similar cell number after 24 h, showing that the collagen type I layer is a suitable adhesion protein for these cells.

Introducing CFO into the membrane raises the question of whether it could compromise the viability of the cells cultured on it, since cobalt ferrite oxide has been shown to be cytotoxic to human mesenchymal stem cells (Moise et al. 2017). As can be seen in Figure 2.1e, the smooth surface of PVDF-CFO membranes had some isolated CFO aggregates encapsulated in the polymer matrix. Some of them were exposed to the surface (Figure 2.1f) and could have been in contact with hMSCs during the culture. Combinations of non-biodegradable polymers, as PVDF, and cobalt ferrite oxides have been previously used in cell culture approaches and its leaching has been tested (Fernandes et al. 2019). The publications have shown that PVDF matrices retain CFO during cell culture, with no release of nanoparticles into the cell culture medium. Interestingly enough, cells adhered to and were viable on PVDF-CFO supports with a fibronectin coating, since the cell number did not decrease with time. It is worth noting that no significant difference in cell spreading is shown in PVDF-CFO+FN sample with respect to glass slide + FN, and nevertheless cell number did not grow with culture time. They duplicated their numbers between seeding and day 1 but then the interaction with ferrite particles seemed to hinder further proliferation. As shown in Figure 2.7(c), there were no significant differences in cell numbers between days 1 and 7, although PVDF-CFO + LbL showed significant cell proliferation, indicating that the LbL coating here presented was able to cover the exposed ferrite particles (Figure 2.5(1)-d) hindering the direct contact of hMSCs with the CFO. LbL is effective for hMSCs culture in our magnetic responsive PVDF composites produced by the NIPS technique.

These findings open the door for future cell culture approaches in bone tissue engineering using the magnetoelectric effect to induce the differentiation of human mesenchymal stem cells towards the osteogenic lineage.

## 2.4. Conclusions

NIPS has been shown to be an easy and reliable technique for producing PVDF membranes containing magnetostrictive nanoparticles for bone tissue engineering approaches. NIPS obtained electroactive membranes with a smooth surface, a thin layer with a mixture of $\alpha$ and β-phases, and a porous core which was completely electroactive, combining the β and $\gamma$-phases. The introduction of CFO increased the β-phase content on the surface, while reducing overall crystallinity, unlike the membranes without MNP. NIPS is an adequate technique for incorporating cobalt ferrite oxide into the polymer matrix with an MNP loss of

only 10% in the manufacturing process. These membranes were aminolyzed by an alkali approach. Heparin and collagen were deposited on the membranes surface using a layer-by-layer technique, which proved to be as effective as standard fibronectin adsorption for hMSCs cell culture and proliferation. LbL was also necessary for hMSCs proliferation in PVDF-CFO membranes.

## 2.5. Acknowledgements

This work has been funded by the Spanish State Research Agency (AEI) and the European Regional Development Fund (ERFD) through the PID2019-106099RB-C41/AEI/ 10.13039/501100011033 and PID2019-106099RB-C43 / AEI / 10.13039/501100011033 projects and the Associate Laboratory for Green Chemistry-LAQV financed by national funds from FCT/MCTES (UIDB/50006/2020). Maria Guillot-Ferriols acknowledges the government funding of her Doctoral Thesis through a BES-2017-080398 FPI Grant. The CIBER-BBN initiative is funded by the VI National R&D&I Plan 2008-2011, Iniciativa Ingenio 2010, Consolider Program. CIBER actions are financed by the *Instituto de Salud Carlos III* with assistance from the European Regional Development Fund. D.M.C is also grateful to the *FCT-Fundação para a Ciência e Tecnologia* for grant SFRH/BPD/121526/2016. Finally, the authors acknowledge funding from the Basque Government Industry and Education Department under the ELKARTEK, HAZITEK and PIBA (PIBA-2018-06) programs, respectively, also Dr. Carlos Sá (CEMUP) for assistance with the XPS analyses.

## 2.6. References

Abzan, N., M. Kharaziha, and S. Labbaf. 2019. “Development of Three-Dimensional Piezoelectric Polyvinylidene Fluoride-Graphene Oxide Scaffold by Non-Solvent Induced Phase Separation Method for Nerve Tissue Engineering.” *Materials and Design* 167: 107636. https://doi.org/10.1016/j.matdes.2019.107636.

Ahn, A.C., and A. J. Grodzinsky. 2009. “Relevance of Collagen Piezoelectricity to ‘Wolff’s Law’: A Critical Review.” *Medical Engineering and Physics* 31 (7): 733–41. https://doi.org/10.1016/j.medengphy.2009.02.006.

Algieri, C., L. Donato, and L. Giorno. 2017. “Tyrosinase Immobilized on a Hydrophobic Membrane.” *Biotechnology and Applied Biochemistry* 64 (1): 92–99. https://doi.org/10.1002/bab.1462.

Billings, P. C., and M. Pacifici. 2015. “Interactions of Signaling Proteins, Growth Factors and Other Proteins with Heparan Sulfate: Mechanisms and Mysteries.” *Connective Tissue Research* 56 (4): 272–80. https://doi.org/10.3109/03008207.2015.1045066.

Boccaccio, T., A. Bottino, G. Capannelli, and P. Piaggio. 2002. “Characterization of PVDF Membranes by Vibrational Spectroscopy.” *Journal of Membrane Science* 210 (2): 315–29. https://doi.org/10.1016/S0376-7388(02)00407-6.

Buonomenna, M. G., P. Macchi, M. Davoli, and E. Drioli. 2007. “Poly(Vinylidene Fluoride) Membranes by Phase Inversion: The Role the Casting and Coagulation Conditions Play in

Their Morphology, Crystalline Structure and Properties." *European Polymer Journal* 43 (4): 1557–72. https://doi.org/10.1016/j.eurpolymj.2006.12.033.
Cai, X., T. Lei, D. Sun, and L. Lin. 2017. "A Critical Analysis of the α, β and γ Phases in Poly(Vinylidene Fluoride) Using FTIR." *RSC Advances* 7 (25): 15382–89. https://doi.org/10.1039/c7ra01267e.

Camacho, N. P., P. West, P. A. Torzilli, and R. Mendelsohn. 2001. "FTIR Microscopic Imaging of Collagen and Proteoglycan in Bovine Cartilage." *Biopolymers - Biospectroscopy Section* 62 (1): 1–8. https://doi.org/10.1002/1097-0282(2001)62:1<1::AID-BIP10>3.0.CO;2-O.

Castilla-Casadiego, D. A., J. R. García, A. J. García, and J. Almodovar. 2019. "Heparin/Collagen Coatings Improve Human Mesenchymal Stromal Cell Response to Interferon Gamma." *ACS Biomaterials Science and Engineering* 5 (6): 2793–2803. https://doi.org/10.1021/acsbiomaterials.9b00008.

Castilla-Casadiego, D. A., L. Pinzon-Herrera, M. Perez-Perez, B. A. Quiñones-Colón, D. Suleiman, and J. Almodovar. 2018. "Simultaneous Characterization of Physical, Chemical, and Thermal Properties of Polymeric Multilayers Using Infrared Spectroscopic Ellipsometry." *Colloids and Surfaces A: Physicochemical and Engineering Aspects* 553 (May): 155–68. https://doi.org/10.1016/j.colsurfa.2018.05.052.

Chen, J., N. H., Q. Li, C. H. Chu, L. Jun, and M. F. Maitz. 2016. "The Effect of Electrostatic Heparin/Collagen Layer-by-Layer Coating Degradation on the Biocompatibility." *Applied Surface Science* 362: 281–89. https://doi.org/10.1016/j.apsusc.2015.11.227.

Cheng, L. P. 1999. "Effect of Temperature on the Formation of Microporous PVDF Membranes by Precipitation from 1-Octanol/DMF/PVDF and Water/ DMF/PVDF Systems." *Macromolecules* 32 (20): 6668–74. https://doi.org/10.1021/ma990418l.

Cherng, W. J., Y. H. Pan, T. C. Wu, C. C. Chou, C. H. Yeh, and J. J. Ho. 2019. "Hemocompatibility and Adhesion of Heparin/Dopamine and Heparin/Collagen Self-Assembly Multilayers Coated on a Titanium Substrate." *Applied Surface Science* 463: 732–40. https://doi.org/10.1016/j.apsusc.2018.08.217.

Correia, D. M., C. Ribeiro, V. Sencadas, G. Botelho, S. A.C. Carabineiro, J. L.Gomes Ribelles, and Senentxu Lanceros-Méndez. 2015. "Influence of Oxygen Plasma Treatment Parameters on Poly(Vinylidene Fluoride) Electrospun Fiber Mats Wettability." *Progress in Organic Coatings* 85: 151–58. https://doi.org/10.1016/j.porgcoat.2015.03.019.

Costa, R. R., and J. F. Mano. 2014. "Polyelectrolyte Multilayered Assemblies in Biomedical Technologies." *Chemical Society Reviews* 43 (10): 3453–79. https://doi.org/10.1039/c3cs60393h.

Duca, M. D., C. L. Plosceanu, and T. Pop. 1998. “Effect of X-Rays on Poly(Vinylidene Fluoride) in X-Ray Photoelectron Spectroscopy.” *Journal of Applied Polymer Science* 67 (13): 2125–29.

Fernandes, M. M., D. M. Correia, C. Ribeiro, N. Castro, V. Correia, and S. Lanceros-Mendez. 2019. “Bioinspired Three-Dimensional Magnetoactive Scaffolds for Bone Tissue Engineering.” *ACS Applied Materials and Interfaces* 11 (48): 45265–75. https://doi.org/10.1021/acsami.9b14001.

Ferreira, A. M., P. Gentile, S. Toumpaniari, G. Ciardelli, and M. A. Birch. 2016. “Impact of Collagen/Heparin Multilayers for Regulating Bone Cellular Functions.” *ACS Applied Materials and Interfaces* 8 (44): 29923–32. https://doi.org/10.1021/acsami.6b09241.

Fukada, E., and I. Yasuda. 1957. “On the Piezoelectric Effect of Bone.” *Journal of the Physical Society of Japan* 12 (10): 1158–62. https://doi.org/10.1143/JPSJ.12.1158.

Gamboa-Martínez, T. C., V. Luque-Guillén, C. González-García, J. L. Gómez Ribelles, and G. Gallego-Ferrer. 2015. “Crosslinked Fibrin Gels for Tissue Engineering: Two Approaches to Improve Their Properties.” *Journal of Biomedical Materials Research - Part A* 103 (2): 614–21. https://doi.org/10.1002/jbm.a.35210.

Gonçalves, R., P. Martins, D. M. Correia, V. Sencadas, J. L. Vilas, L. M. León, G. Botelho, and S. Lanceros-Méndez. 2015. “Development of Magnetoelectric CoFe2O4/Poly(Vinylidene Fluoride) Microspheres.” *RSC Adv.* 5 (45): 35852–57. https://doi.org/10.1039/C5RA04409J.

Gonçalves, R., P. Martins, X. Moya, M. Ghidini, V. Sencadas, G. Botelho, N. D. Mathur, and S. Lanceros-Mendez. 2015. “Magnetoelectric $CoFe_2O_4$ /Polyvinylidene Fluoride Electrospun Nanofibres.” *Nanoscale* 7 (17): 8058–61. https://doi.org/10.1039/C5NR00453E.

Gregorio, R. 2006. “Determination of the Alpha, Beta, and Gamma Crystalline Phases of Poly(Vinylidene Fluoride) Films Prepared at Different Conditions.” *Journal of Applied Polymer Science* 100 (4): 3272–79. https://doi.org/10.1002/app.23137.

Gregorio, R., and D. S. Borges. 2008. “Effect of Crystallization Rate on the Formation of the Polymorphs of Solution Cast Poly(Vinylidene Fluoride).” *Polymer* 49 (18): 4009–16. https://doi.org/10.1016/j.polymer.2008.07.010.

Gregorio, R., and M. Cestari. 1994. “Effect of Crystallization Temperature on the Crystalline Phase Content and Morphology of Poly(Vinylidene Fluoride).” *Journal of Polymer Science Part B: Polymer Physics* 32 (5): 859–70. https://doi.org/10.1002/polb.1994.090320509.

Hermenegildo, B., C. Ribeiro, L. Pérez-Álvarez, J. L. Vilas, D. A. Learmonth, R. A. Sousa, P. Martins, and S. Lanceros-Méndez. 2019. “Hydrogel-Based Magnetoelectric

Microenvironments for Tissue Stimulation." *Colloids and Surfaces B: Biointerfaces* 181 (May): 1041–47. https://doi.org/10.1016/j.colsurfb.2019.06.023.

Jacob, J., N. More, K. Kalia, and G. Kapusetti. 2018. "Piezoelectric Smart Biomaterials for Bone and Cartilage Tissue Engineering." *Inflammation and Regeneration* 38 (1): 1–11. https://doi.org/10.1186/s41232-018-0059-8.

Jin, K., B. Li, L. Lou, Y. Xu, X. Ye, K. Yao, J. Ye, and C. Gao. 2016. "In Vivo Vascularization of MSC-Loaded Porous Hydroxyapatite Constructs Coated with VEGF-Functionalized Collagen/Heparin Multilayers." *Scientific Reports* 6 (December 2015): 1–13. https://doi.org/10.1038/srep19871.

Kehrer, M., J. Duchoslav, A. Hinterreiter, M. Cobet, A. Mehic, T. Stehrer, and D. Stifter. 2019. "XPS Investigation on the Reactivity of Surface Imine Groups with TFAA." *Plasma Processes and Polymers* 16 (4): 1–8. https://doi.org/10.1002/ppap.201800160.

Kim, B. W. 2017. Clinical Regenerative Medicine in Urology. Clinical Regenerative Medicine in Urology. https://doi.org/10.1007/978-981-10-2723-9.

Kim, H. D., S. Amirthalingam, S. L. Kim, S. S. Lee, J. Rangasamy, and N. S. Hwang. 2017. "Biomimetic Materials and Fabrication Approaches for Bone Tissue Engineering." *Advanced Healthcare Materials* 6 (23): 1–18. https://doi.org/10.1002/adhm.201700612.

Lim, I., S. Yoo, I. Park, and Y. Lee. 2004. "Influence of Oxyfluorination on Properties of Polyacrylonitrile (PAN)- Based Carbon Fibers." *Carbon Letters* 5 (1): 12–17.

Lin, D. J., K. Beltsios, T. H. Young, Y. S. Jeng, and L. P. Cheng. 2006. "Strong Effect of Precursor Preparation on the Morphology of Semicrystalline Phase Inversion Poly(Vinylidene Fluoride) Membranes." *Journal of Membrane Science* 274 (1–2): 64–72. https://doi.org/10.1016/j.memsci.2005.07.043.

Liu, F., N. A. Hashim, Y. Liu, M. R. M. Abed, and K. Li. 2011. "Progress in the Production and Modification of PVDF Membranes." *Journal of Membrane Science* 375 (1–2): 1–27. https://doi.org/10.1016/j.memsci.2011.03.014.

Liu, J., X. Lu, and C. Wu. 2013. "Effect of Preparation Methods on Crystallization Behavior and Tensile Strength of Poly(Vinylidene Fluoride) Membranes." *Membranes* 3 (4): 389–405. https://doi.org/10.3390/membranes3040389.

Marie, PJ. 1992. "Physiology of Bone Tissue." *Immuno-Analyse et Biologie Specialisee* 7 (6): 17–24. https://doi.org/10.1016/S0923-2532(05)80182-6.

Martins, P., C. M. Costa, and S. Lanceros-Mendez. 2011. "Nucleation of Electroactive β-Phase Poly(Vinilidene Fluoride) with CoFe2O4 and NiFe2O4 Nanofillers: A New Method for the Preparation of Multiferroic Nanocomposites." *Applied Physics A: Materials Science and Processing* 103 (1): 233–37. https://doi.org/10.1007/s00339-010-6003-7.

Martins, P., R. Gonçalves, S. Lanceros-Mendez, A. Lasheras, J. Gutiérrez, and J. M. Barandiarán. 2014. "Effect of Filler Dispersion and Dispersion Method on the Piezoelectric and Magnetoelectric Response of CoFe 2 O 4 /P(VDF-TrFE) Nanocomposites." *Applied Surface Science* 313: 215–19. https://doi.org/10.1016/j.apsusc.2014.05.187.

Martins, P., A. C. Lopes, and S. Lanceros-Mendez. 2014. "Electroactive Phases of Poly(Vinylidene Fluoride): Determination, Processing and Applications." *Progress in Polymer Science* 39 (4): 683–706. https://doi.org/10.1016/j.progpolymsci.2013.07.006.

McGovern, J. A., M. Griffin, and D. W. Hutmacher. 2018. "Animal Models for Bone Tissue Engineering and Modelling Disease." *DMM Disease Models and Mechanisms* 11 (4). https://doi.org/10.1242/dmm.033084.

Mhanna, R. F., J. Vörös, and M. Zenobi-Wong. 2011. "Layer-by-Layer Films Made from Extracellular Matrix Macromolecules on Silicone Substrates." *Biomacromolecules* 12 (3): 609–16. https://doi.org/10.1021/bm1012772.

Moise, S., E. Céspedes, D. Soukup, J. M. Byrne, A. J. El Haj, and N. D. Telling. 2017. "The Cellular Magnetic Response and Biocompatibility of Biogenic Zinc- and Cobalt-Doped Magnetite Nanoparticles." *Scientific Reports* 7 (November 2016): 1–11. https://doi.org/10.1038/srep39922.

Morales-Román, R. M., M. Guillot-Ferriols, L. Roig-Pérez, S. Lanceros-Mendez, G. Gallego-Ferrer, and J. L. Gómez Ribelles. 2019. "Freeze-Extraction Microporous Electroactive Supports for Cell Culture." *European Polymer Journal* 119 (June): 531–40. https://doi.org/10.1016/j.eurpolymj.2019.07.011.

Qi, L., E. K. Knapton, X. Zhang, T. Zhang, C. Gu, and Y. Zhao. 2017. "Pre-Culture Sudan Black B Treatment Suppresses Autofluorescence Signals Emitted from Polymer Tissue Scaffolds." *Scientific Reports* 7: 8361. https://doi.org/10.1038/s41598-017-08723-2.

Ribeiro, C., C. M. Costa, D. M. Correia, J. Nunes-Pereira, J. Oliveira, P. Martins, R. Gonçalves, V. F. Cardoso, and S. Lanceros-Méndez. 2018. "Electroactive Poly(Vinylidene Fluoride)-Based Structures for Advanced Applications." *Nature Protocols* 13 (4): 681–704. https://doi.org/10.1038/nprot.2017.157.

Ribeiro, C., J. A. Panadero, V. Sencadas, S. Lanceros-Mendez, M. N. Tamaño, D. Moratal, M. Salmeron-Sanchez, and J. L. Gomez Ribelles. 2012. "Fibronectin Adsorption and Cell Response on Electroactive Poly(Vinylidene Fluoride) Films." *Biomedical Materials* 7 (3). https://doi.org/10.1088/1748-6041/7/3/035004.

Ribeiro, C., J. Pärssinen, V. Sencadas, V. Correia, S. Miettinen, V. P. Hytönen, and S. Lanceros-Méndez. 2015. "Dynamic Piezoelectric Stimulation Enhances Osteogenic Differentiation of Human Adipose Stem Cells." *Journal of Biomedical Materials Research - Part A* 103 (6): 2172–75. https://doi.org/10.1002/jbm.a.35368.

Sencadas, V., R. Gregorio Filho, and S. Lanceros-Mendez. 2006. “Processing and Characterization of a Novel Nonporous Poly(Vinilidene Fluoride) Films in the β Phase.” *Journal of Non-Crystalline Solids* 352 (21–22): 2226–29. https://doi.org/10.1016/j.jnoncrysol.2006.02.052.

Sencadas, V., R. Gregorio, and S. Lanceros-Méndez. 2009. “α to β Phase Transformation and Microestructural Changes of PVDF Films Induced by Uniaxial Stretch.” *Journal of Macromolecular Science, Part B: Physics* 48 (3): 514–25. https://doi.org/10.1080/00222340902837527.

Silva, J., R. R. Costa, and J. F. Mano. 2016. “Biomimetic Extracellular Environment Based on Natural Origin Polyelectrolyte Multilayers.” *Small* 12 (32): 4301–4439.

Sobreiro-Almeida, R., M. Tamaño-Machiavello, E. Carvalho, L. Cordón, S. Doria, L. Senent, D. Correia, et al. 2017. “Human Mesenchymal Stem Cells Growth and Osteogenic Differentiation on Piezoelectric Poly(Vinylidene Fluoride) Microsphere Substrates.” *International Journal of Molecular Sciences* 18 (11): 2391. https://doi.org/10.3390/ijms18112391.

Supriya, S., L. Kumar, and M. Kar. 2019. “Optimization of Dielectric Properties of PVDF–CFO Nanocomposites.” *Polymer Composites* 40 (3): 1239–50. https://doi.org/10.1002/pc.24840.

Woolf, A. D., and B. Pfleger. 2003. “Burden of Major Musculoskeletal Conditions.” *Bulletin of the World Health Organization* 81 (9): 646–56.

Xiao, L., D. M. Davenport, L. Ormsbee, and D. Bhattacharyya. 2015. “Polymerization and Functionalization of Membrane Pores for Water Related Applications.” *Industrial and Engineering Chemistry Research* 54 (16): 4174–82. https://doi.org/10.1021/ie504149t.

Young, T. H., H. H. Chang, D. J. Lin, and L. P. Cheng. 2010. “Surface Modification of Microporous PVDF Membranes for Neuron Culture.” *Journal of Membrane Science* 350 (1–2): 32–41. https://doi.org/10.1016/j.memsci.2009.12.009.

Young, T. H., L. P. Cheng, D. J. Lin, L. Fane, and W. Y. Chuang. 1999. “Mechanisms of PVDF Membrane Formation by Immersion-Precipitation in Soft (1-Octanol) and Harsh (Water) Nonsolvents.” *Polymer* 40 (19): 5315–23. https://doi.org/10.1016/S0032-3861(98)00747-2.

Zhang, K., J. Y. Chen, W. Qin, J. A. Li, F. X. Guan, and N. Huang. 2016. “Constructing Bio-Layer of Heparin and Type IV Collagen on Titanium Surface for Improving Its Endothelialization and Blood Compatibility.” *Journal of Materials Science: Materials in Medicine* 27 (4). https://doi.org/10.1007/s10856-016-5693-6.

Zhang, K., D. Huang, Z. Yan, and C. Wang. 2017. “Heparin/Collagen Encapsulating Nerve Growth Factor Multilayers Coated Aligned PLLA Nanofibrous Scaffolds for Nerve Tissue

Engineering." *Journal of Biomedical Materials Research - Part A* 105 (7): 1900–1910. https://doi.org/10.1002/jbm.a.36053.

Zhang, M., A. Q. Zhang, B. K. Zhu, C.H. Du, and Y. Y. Xu. 2008. "Polymorphism in Porous Poly(Vinylidene Fluoride) Membranes Formed via Immersion Precipitation Process." *Journal of Membrane Science* 319 (1–2): 169–75. https://doi.org/10.1016/j.memsci.2008.03.029.

# Chapter 3. Piezoelectric stimulation induces a cytoskeleton response in mesenchymal stem cells cultured on electroactive 2D substrates

*Unpublished*

Guillot-Ferriols M., Costa C.M., Correia D.M., Rodríguez-Hernández J.C., Tsimbouri P. M., Lanceros-Méndez S., Dalby M. J., Gallego Ferrer G., Gómez Ribelles J.L. Piezoelectric Stimulation Induces a Cytoskeleton Response in Mesenchymal Stem Cells Cultured on Electroactive 2D Substrates.

**Personal contribution**
Film production and polarization were carried out by C.M. Costa and D.M. Correia. Film characterization, except from microscopy images (J.C. Rodríguez-Hernández) and cell culture experiments were performed by M.Guillot-Ferriols.
M. Guillot-Ferriols designed the experiments, analysed the data, prepared the figures and wrote the first version of the manuscript. P.M. Tsimbouri helped with cell culture experiment design. M.J. Dalby, S. Lanceros-Méndez, J.L. Gómez Ribelles and G. Gallego Ferrer helped with experimental design, reviewed the manuscript and provided financial support.

Part of this work was performed during a research placement at the Centre for the Cellular Microenvironment, Institute of Molecular, Cell and Systems Biology at the University of Glasgow. It was supervised by Prof. Matthew J. Dalby.

## 3. Piezoelectric stimulation induces a cytoskeleton response in mesenchymal stem cells cultured on electroactive 2D substrates

Guillot-Ferriols M.[1,2], Costa C.M. [3,4], Correia D.M.[4,5], Rodríguez-Hernández J.C.[1], Tsimbouri P.M.[6], Lanceros-Méndez S.[3,7,8], Dalby M.J.[6], Gallego Ferrer G.[1,2], Gómez Ribelles J.L.[1,2]

*[1] Centre for Biomaterials and Tissue Engineering (CBIT), Universitat Politècnica de València, 46022 Valencia, Spain*
*[2] Biomedical Research Networking Centre on Bioengineering, Biomaterials and Nanomedicine (CIBER-BBN), Valencia, Spain*
*[3] Centre/Department of Physics, Universidade do Minho, 4710-057 Braga, Portugal*
*[4] Centre of Chemistry, Universidade Do Minho, 4710-058 Braga, Portugal*
*[5] Centre of Chemistry, Universidade do Trás-os-Montes e Alto Douro, Vila Real 5000-801, Portugal*
*[6] Centre for the Cellular Microenvironment, Institute of Molecular, Cell and Systems Biology, College of Medical, Veterinary and Life Sciences, University of Glasgow, Glasgow, G12 8QQ, United Kingdom.*
*[7] BCMaterials, Basque Center for Materials, Applications and Nanostructures, UPV/EHU Science Park, 48940 Leioa, Spain*
*[8] IKERBASQUE, Basque Foundation for Science, 48013 Bilbao, Spain*

### Abstract

Physical cues have demonstrated to be effective approaches to induce osteogenic differentiation of mesenchymal stem cells (MSCs) for advanced regeneration therapies. Precisely, piezoelectric stimulation has been proposed due to the electroactive properties of bone's extracellular matrix. Piezoelectric polymers, when combined with a magnetostrictive component can be used for MSCs stimulation by applying an external magnetic field. The deformation of the magnetostrictive component will produce a deformation in the polymer matrix, generating a change in the surface charge due to the piezoelectric effect that induce an electric field that can be transmitted to the cells. Cell adhesion and cytoskeleton changes are the first evidence of MSCs osteoblastogenesis and can be used to study initial MSCs response to this kind of stimulation. In the current study, poly(vinylidene) fluoride (PVDF) piezoelectric films with and without cobalt ferrite oxide (CFO) crystallized from the melt in the presence of the ionic liquid 1-Butyl-3-methyl-imidazolium-chloride ([Bmim][Cl]) were produced. The presence of [Bmim][Cl] allowed the obtainment of the β-phase, the most electroactive one, even in the absence of CFO. After ionic liquid removal, PVDF and PVDF-CFO films presented high percentages of β-phase, 95.4 ± 3.4 % and 98.6 ± 0.6 %, respectively, and a crystalline content of 62 ± 0.7 % for PVDF and 63.9 ± 3.3 % for PVDF-CFO. The incorporation of CFO nanoparticles was effective, which allowed to electromechanically stimulate MSCs by applying a magnetic field with a bioreactor. Prior to stimulation, initial response of MSCs was characterized in static conditions, showing that the produced films were biocompatible and non-cytotoxic, allowing MSCs adhesion and proliferation at short term (1 to 7 days). Selection of the appropriate cell culture media was also optimized in static conditions for further combination with stimulation. Focal adhesion analysis revealed that a combination 1:1 of osteogenic and adipogenic media enhanced cell spreading area, focal adhesion number and length. Subsequent stimulation experiments were performed and revealed that MSCs electromechanically stimulated for 3 days in PVDF-CFO supports showed longer focal

adhesions and a decrease in vimentin density. These results prove that MSCs are able to respond to this kind of stimulation at cytoskeleton level, leading the way to further studies on MSCs fate determination using piezoelectric cell culture supports.

**Keywords**
Ionic liquid; poly(vinylidene) fluoride; magnetoelectric effect; mesenchymal stem cells; focal adhesions; cytoskeleton

## 3.1. Introduction

Mesenchymal stem cells (MSCs) are multipotent cells with the ability to differentiate into osteoblasts, adipocytes or chondrocytes (Dominici et al. 2006). As an autologous stem cell source, they are potential candidates for advanced regeneration therapies, especially for treating bone defects. MSCs are actively implicated in *in vivo* bone repair. They migrate to the injured site and differentiate to osteoblasts in response to biochemical and biophysical stimuli present in bone's microenvironment (Einhorn and Gerstenfeld 2015).

Many of the proposed therapies using MSCs rely on their potential to differentiate once injected in the injured site. Nevertheless, the altered homeostasis of the stem cell niche at the bone defect, related with some pathologies, may not provide the right cues to initiate the osteogenic differentiation cascade in MSCs (Gómez-Barrena et al. 2015). For that reason, pre-differentiation approaches are usually preferred, since the induction of an osteoblastic phenotype prior to transplantation has shown enhanced healing capacity (Yoshikawa, Ohgushi, and Tamai 1996; Castano-Izquierdo et al. 2006; Peters et al. 2009; Ye et al. 2012). Physical cues have been proposed as an alternative to biochemical induction due to their specific potential (Hodgkinson et al. 2021), avoiding undesired side effects that may be observed when using media formulations containing dexamethasone (Ghali et al. 2015). More precisely, piezoelectric stimulation is being researched since MSCs find themselves subjected to an electroactive environment due to the presence of the collagen fibers that conform bone's extracellular matrix (Minary-Jolandan and Yu 2009).

Poly(vinylidene) fluoride (PVDF) has been explored as a suitable piezoelectric polymer to design cell culture supports for the stimulation of osteogenic progenitors (C. Ribeiro, Moreira, et al. 2012; Fernandes et al. 2019; Pärssinen et al. 2015; Damaraju et al. 2017; Zhou et al. 2016). Its combination with a magnetostrictive phase, generating a magnetoelectric material, allows piezoelectric stimulation by applying a magnetic field, a minimally invasive wireless approach. When the magnetic field is applied to the composite a deformation is induced in the magnetostrictive component. This is transmitted to the piezoelectric matrix, which undergoes a change in electrical polarization (Martins and Lanceros-Méndez 2013).

This approach inevitably links electrical and mechanical stimulation, which can trigger a mechanostransduction response able to activate intracellular signalling cascades in MSCs influencing proliferation, migration and differentiation (Jacob et al. 2018). Focal adhesions (FA), multiprotein complexes under the cell membrane, are responsible for mechanosensing, perceiving and transferring the mechanical cues present on the extracellular milieu to the cellular cytoskeleton. They serve as an interface between the

integrins, directly contacting the extracellular environment, and the actin cytoskeleton (Martino et al. 2018). Changes in focal adhesion number and length and cytoskeleton tension are directly related with osteogenesis. Mature adhesions leading to high intracellular tension morphology produce tensile forces in the nucleus affecting gene expression, especially through mitogen-activated protein kinases (MAPK) pathway. MAPK downstream effector ERK1 is known to be increased due to the formation of super-mature adhesions leading to the phosphorylation of runt-related transcription factor 2 (RUNX2), the master transcription factor of the osteogenic differentiation pathway (Dalby et al. 2007; Biggs et al. 2009).

Biomedical application of PVDF relies on its crystallization in β-phase, the one showing the highest piezoelectric response. This phase is usually obtained through the stretching of α-phase films obtained from the melt, by techniques such as solvent casting at temperatures lower than 70 °C or through the induction of specific fillers such as clays, magnetostrictive nanoparticles or ionic liquids (IL) (Martins, Lopes, and Lanceros-Mendez 2014).

Ionic liquids are liquid electrolytes exclusively composed by ions and with a melting point below 100 °C. Their astonishing physical characteristics such as negligible vapor pressure, high ionic conductivity and excellent solubility and miscibility with many compounds have motivated their use as a replacement of organic solvents (Correia, Fernandes, et al. 2020). These last two properties, nevertheless, could also be of great interest for their use as PVDF nucleating agents, a less explored application. The β-phase polymorph can be induced by the presence of ionic liquids (Correia, Costa, et al. 2020; Meira et al. 2019), which after crystallization are easily removed, obtaining a PVDF cell culture support in its most electroactive phase. Specifically, IL removal allows to obtain PVDF structures without magnetostrictive nanoparticles with the same structure, electroactive and crystalline composition as the ones containing them, that can be used as controls for stimulation experiments.

Taking all of this into account, we developed PVDF films crystallized in the presence of the ionic liquid 1-Butyl-3-methyl-imidazolium-chloride ([Bmim][Cl]), containing or not magnetostrictive nanoparticles, to characterize MSCs response to electromechanical stimulation. Films were physically characterized before and after IL removal and their absence of cytotoxicity for MSCs was also evaluated. MSCs response to electromechanical stimulation regarding focal adhesion formation and cytoskeleton reorganization was studied applying a magnetic field using a bioreactor. As far as the authors know, this is the first time that PVDF films crystallized in the presence of the ionic liquid [Bmim][Cl] have been used to stimulate MSCs electromechanically.

## 3.2. Materials and methods

### 3.2.1. Electroactive film production

PVDF (Solef 6010, Mw ~ 300 kg·mol$^{-1}$) and PVDF films containing 20 % (w/w) cobalt ferrite oxide spherical nanoparticles ($CoFe_2O_4$, CFO, 35-55 nm size range, Nanostructured & Amorphous Materials) were produced. Both types of films contained a 20 % (w/w) content [Bmim][Cl] (Inc and Iolitec). The adequate amounts of [Bmim][Cl] and CFO, when

applicable, were mixed in 6 mL of N,N-dimethylformamide (DMF, anhydrous, 99.8%, Merck) and ultrasonicated for 3 h in an ultrasound bath. Afterwards, the dispersed filler solutions were mixed with 1 g of PVDF powder and mechanically stirred for 3 h to obtain a homogeneous solution. After complete mixing and dissolution of the PVDF polymer, the films were prepared by doctor blade technique onto a glass substrate and placed in an oven (P-Selecta) at 210 °C for 10 min for solvent evaporation (C. Ribeiro et al. 2018).

#### 3.2.2. Ionic liquid removal and film poling process

Films were placed in ultrapure water during 5 days for IL removal where every day the water was replaced, and the sample weight measured. After IL removal, the membranes were polled by the contact method. The polarization process was performed applying an electric field of ~10 kV at a constant current of 10 μA during 1 h at a temperature of 120 °C.

#### 3.2.3. Film characterization

##### 3.2.3.1. Field emission scanning electron microscopy

PVDF and PVDF-CFO film surfaces before and after ionic liquid removal were characterized by means of field emission scanning electron microscopy (FESEM) (AURIGA compact, Zeiss). Films before washing were imaged with an accelerated voltage of 1 kV and washed films with 2 kV. Samples were coated with platinum following a standard sputtering protocol for 90 s (JFC 1100, JEOL).

##### 3.2.3.2. Fourier transform infrared spectroscopy

Fourier transform infrared spectroscopy (FTIR) spectra were recorded using an ALPHA FTIR spectrometer (Bruker) in attenuated total reflection (ATR) mode from 4000 to 400 $cm^{-1}$ at a wavelength resolution of 4 $cm^{-1}$. FTIR spectra were performed after 64 scans for each sample. PVDF and PVDF-CFO samples before and after washing were assayed.

##### 3.2.3.3. Differential scanning calorimetry

Differential scanning calorimetry (DSC) was carried out with a DSC 8000 (PerkinElmer) for scans in the melting region under a flowing nitrogen atmosphere. A samples mass of 2-4 mg was encapsulated in aluminium pans and thermograms were recorded between 0 and 200 °C at a heating rate of 20 °C/min. PVDF and PVDF-CFO films after washing were used for the measurements.

##### 3.2.3.4. Vibrating sample magnetometer

Films containing magnetostrictive nanoparticles were magnetically characterized, after IL removal, using a Microsense 2 Tesla vibrating sample magnetometer (VSM). Magnetization loops M(H) were evaluated up to 18 kOe and the real content of CFO was calculated by comparing the pure CFO saturation magnetization value (60 emu/g) to the one obtained in the composite samples, by means of Eq. (1) (Gonçalves et al. 2015):

$$CFO\ wt\ \% = \frac{Saturation\ magnetization\ microspheres}{Saturation\ magnetization\ pure\ CFO}\ x\ 100 \qquad \text{Eq. 1}$$

### 3.2.4. Cell response

Human bone marrow mesenchymal stem cells (PromoCell) were used for cell culture assays. MSCs were expanded in basal medium containing Dulbecco's Modified Eagle Medium (DMEM) high glucose (4.5 g/L) (Gibco) supplemented with 10 % (v/v) foetal bovine serum (FBS, Gibco), 4 mM L-glutamine (Lonza), 1X non-essential aminoacids (NEAA, Gibco), 1 mM sodium pyruvate (Gibco), 70 U/mL penicillin, 70 µg/mL streptomycin (P/S, Life technologies) and 0.25 µg/mL fungizone (Life technologies), at 37 °C in a humidified atmosphere with 5 % $CO_2$. All experiments were performed at passages not superior to 5. Films were sterilized by performing three washes with ethanol 70 % (v/v) under shaking for 10 min each. After, samples were washed again three times with Dulbecco's phosphate buffer saline (DPBS, Sigma-Aldrich) and left to dry. 8 mm diameter disks were obtained and UV was applied for 30 min on each side. 8 mm glass slides were used as non-charged controls in all experiments and were sterilized by UV light for 30 min on each side. Finally, samples were placed in a 48-well plate and silicon rings were used to prevent them from floating. Due to PVDF hydrophobicity, all samples were coated with fibronectin from human plasma (Sigma-Aldrich), on the negative charged side, prior to cell seeding (C. Ribeiro, Panadero, et al. 2012). Samples were incubated in a 20 µg/mL fibronectin solution in DPBS for 1 hour at room temperature. Afterwards, samples were washed twice in DPBS to remove non adsorbed fibronectin and kept in DPBS until cell seeding.

#### 3.2.4.1. Initial mesenchymal stem cells response at static mode

##### 3.2.4.1.1. Cytotoxicity/leachable test

Cytotoxicity of CFO nanoparticles and any remaining traces of IL after washing was ruled out by performing a leachable test based on the ISO 10993-5 standard test. PVDF and PVDF-CFO films previously sterilized and placed on a 48 well plated were incubated with 300 µL of basal medium per well for 24 h at 37 °C in a humidified atmosphere with 5 % $CO_2$. As positive control latex disks of 8 mm were employed while as negative control the basal medium was used. The leachable solution was analysed for toxicity by means of the tetrazolium salt MTS (3-(4,5-dimethylthiazol-2-yl)-5-(3-carboxymethoxyphenyl)-2-(4-sulfophenyl)-2H-tetrazolium) assay. This method allows indirect measurement of cell viability by determining mitochondrial activity of cells. MSCs were seeded at a density of $10^4$ cells/cm$^2$ in a 48-tissue culture plate and kept in culture for 24 h. After, the culture medium was replaced for the extraction medium, which was in contact with the materials. Cell were incubated for 24 h. Subsequently, medium was replaced for DMEM without phenol red (Sigma-Aldrich) containing the MTS reagent (Biovision) at a working dilution of 1:10. Cells were incubated for 2 h at 37 °C. Thereafter, the supernatant was transferred to a new plate and the optical density at 490 nm was measured on a Victor3 microplate reader (PerkinElmer). Cell viability was determined applying Eq. (2) (Fernandes et al. 2019):

$$cell\ viability\ (\%) = \frac{Abs\ Sample_{\ 490\ nm}}{Abs\ Negative\ Control_{\ 490\ nm}}\ x\ 100 \qquad \text{Eq. 2}$$

##### 3.2.4.1.2. Cell spreading

Cell spreading and distribution was assessed by staining F-actin and nuclei. MSCs were seeded on PVDF, PVDF-CFO and glass slide surfaces, previously sterilized and coated with fibronectin, at a density of 5 x $10^3$ cells/cm$^2$. Cells were seeded in basal medium without

FBS to promote cell adhesion to the fibronectin present on the surfaces. A 100 μL drop containing the desired number of cells was deposited inside the silicon ring. After 3 h the required volume of basal medium and FBS for a final concentration of 10 % (v/v) were added to each well. This seeding method was used in all the subsequent cell culture experiments.
After 24 h cells were fixed in 4 % (v/v) paraformaldehyde solution (Panreac) for 20 min. Samples were washed three times in DPBS and permeabilized with permeabilization buffer (Sucrose 300 mM, NaCl 50 mM, $MgCl_2$ hexahydrate 3 mM, HEPES 20 mM, Triton X-100 0.5 % (v/v), pH 7.2) for 5 min at 4 °C. Subsequently, they were blocked in 1 % (w/v) bovine serum albumin (BSA, Sigma-Aldrich) solution in DPBS/0.1 % (v/v) Tween-20 (Sigma-Aldrich) for 1 h at room temperature and incubated with Actin Red 555 ReadyProbes reagent (Fisher Scientific) following manufacturer's instructions. Then, samples were washed 3 times with DPBS/0.1 % (v/v) Tween-20 and mounted with fluoroshield mounting medium with DAPI (Abcam). Images were taken with a fluorescence microscope (Nikon Eclipse 80i) and cell spreading was analysed using CellProfiler image analysis software (Broad Institute, USA). Briefly, masks of images were obtained from previous segmentation and cell areas were measured for the scaled images.

#### 3.2.4.1.3. Proliferation

MSCs proliferation was determined after 1, 3 and 7 days in culture. 12 h before cell seeding cells were starved in basal media containing 1 % (v/v) FBS to synchronize cell cycle. PVDF, PVDF-CFO and glass slides were seeded at a density of 5 x $10^3$ cells/$cm^2$ in basal medium without FBS following the protocol descried in section 2.4.1.2. Cell proliferation was assessed by MTS assay (protocol in section 3.2.4.1.1). Cell number was calculated by means of a calibration curve.

### 3.2.4.2. Media selection for piezoelectric stimulation

To choose the appropriate medium for subsequent differentiation experiments an analysis of focal adhesions was performed using diverse media formulations in static conditions (no stimulation applied).

MSCs were seeded on PVDF, PVDF-CFO and glass slides at a density of 2 x $10^3$ cells/$cm^2$ in basal medium without FBS. After 3 h, media was replaced for complete basal medium (containing FBS), osteogenic medium (dexamethasone 100 nM, Ascorbate-2-phosphate 200 μM and b-glycerophosphate disodium salt hydrate 10 mM) or balanced medium, a mixture 1:1 (v/v) of osteogenic and adipogenic media (dexamethasone 1 μM, 3-isobutyl-1-methylxanthine 500 μM, insulin 1,72 μM and indomethacin 100 μM) (Kilian et al. 2010).
After 3 days cells were fixed, permeabilized and blocked following the protocol described in 3.2.4.1.2. After, samples were incubated with mouse monoclonal anti-vinculin antibody (1:400, Sigma Aldrich, V9264) in conjunction with ActinGreen 488 ReadyProbes reagent (AlexaFluor 488 Phalloidin, Fisher Scientific) in blocking buffer overnight at 4 °C. After washing three times for 5 min with DPBS/Tween-20 0.1 % (v/v), cells were incubated with a biotinylated anti-mouse secondary antibody (1:50, Vector Laboratories, BA-2000) for 1 h at 37 °C. After washing, Texas Red conjugated streptavidin (1:50, Vector Laboratories, SA-

5006) was added to the samples and incubated 30 min at 4 °C followed by washing and mounting using fluoroshield mounting medium with DAPI (Abcam).

Samples were imaged using a confocal microscope (Zeiss LSM 880 Confocal Microsystem). Individual cells were analysed using CellProfiler. Briefly, an image processing pipeline was generated to load the DNA (DAPI), F-actin (phalloidin) and vinculin (antibody conjugate Texas Red) for each image set. This was followed by automated detection of cell nuclei, cell morphology and detection of focal adhesions. Focal adhesion number per cell, mean length of focal adhesion per cell and focal adhesion length distribution were quantified. An example of the identification of focal adhesions performed using CellProfiler is shown in Figure 3.1.

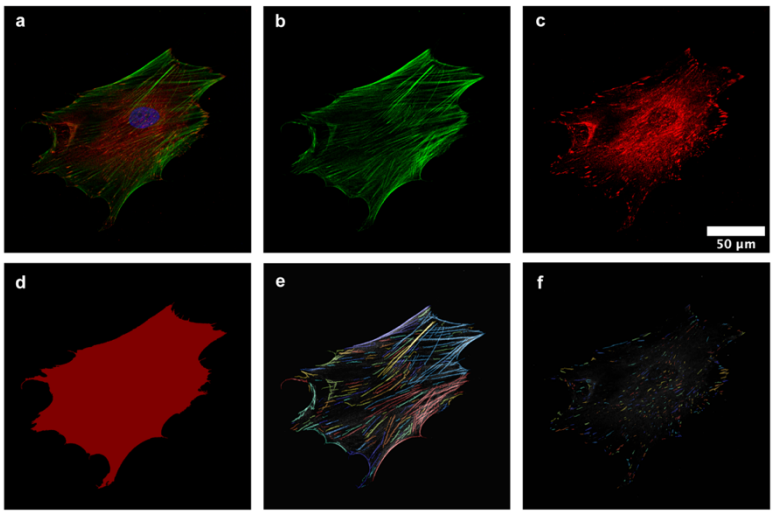


**Figure 3.1. Identification and quantification of focal adhesions, stress fibres and cell spreading using CellProfiler software. a) Merged immunofluorescence image of vinculin (red), F-actin (green) and nucleus (blue). b) F-actin cytoskeleton. c) Vinculin immunofluorescence. d) Masked cell area obtained after processing F-actin images. e) Image overlay of identified stress fibres and F-actin. f) Image overlay of identified focal adhesions and vinculin immunofluorescence. Scale bar 50 μm.**

#### 3.2.4.3. Mesenchymal stem cells response at dynamic mode

To electromechanically stimulate MSCs, samples were stimulated using a home-made magnetic bioreactor able to generate an alternating magnetic field (0-230 Oe) due to the movement of neodymium magnets below the 48-well tissue culture plate (Castro et al. 2020). A frequency of 0.3 Hz and a 10 mm displacement were applied together with a stimulation program divided into an active stimulation period of 16 h, based on 5 min of magnetic stimulation and 25 min of resting time, followed by a non-active period of 8 h, when no magnetic stimulation was applied (Fernandes et al. 2019; S. Ribeiro et al. 2020). Stimulated (S) glass slides and PVDF samples were used as controls for the effect of the magnetic field itself and the surface charge generated by polarization, respectively. Non-stimulated (NS) surfaces were compared to their stimulated counterparts.

#### 3.2.4.3.1. Vinculin and vimentin immunofluorescence

MSCs were seeded at a density of 2 x $10^3$ cells/$cm^2$ in basal medium without FBS. After 3 h, medium was replaced for balanced medium, chosen from previous experiments, and 1 h later stimulated samples were placed in the bioreactor. After 3 days in culture, cells were fixed and immunostained following the protocol previously described. Focal adhesions were stained through the detection of vinculin using a mouse monoclonal anti-vinculin antibody (1:400, Sigma Aldrich, V9264) and vimentin, a cytoskeleton intermediate filament, was detected using a goat polyclonal anti-vimentin antibody (1:100, Sigma-Aldrich, V4630).
Vinculin was imaged and analysed as described in the previous section. Also, the number of stress fibres per cell was analysed using F-actin images. CellProfiler was used to generate a pipeline for their identification and quantification, an example is shown in Figure 3.1. Vimentin images from representative areas of each well were acquired using an inverted fluorescence microscope EVOS M7000 (Fisher Scientific) and analysed using CellProfiler. Again, an image processing pipeline was generated to load the DNA (DAPI), F-actin (phalloidin) and vimentin (antibody conjugate Texas Red) for each image set. This was followed by automated detection of cell nuclei, cell morphology and marker staining intensity.

### 3.2.5. Data and statistical analysis

Material characterization was performed by analysing samples produced in three different batches. Cell culture experiments were performed, at least, in triplicates. For MTS analysis a minimum of two technical replicates were used. Focal adhesions, for media selection and piezoelectric stimulation, and stress fibres were analysed from a minimum of 25 individual cells per condition, from three different replicates. Cell spreading at static mode and vimentin intensity were quantified using 4 different representative zones per well, using three wells per condition.
All results are expressed as mean ± standard deviation. Statistical analysis was performed on GraphPad Prism 9 (USA). Samples following a normal distribution, determined by Shapiro-Wilk test, were analysed using a two-tailed t-test or one-way ANOVA for multiple comparisons. The rest of the samples were analysed by the non-parametric tests two-tailed Mann-Whitney or Kruskall-Wallis (with Dunn's multiple comparison test). 95 % confidence interval was set to accept significant inter-group differences ($p$-value < 0.05).

## 3.3. Results and discussion

### 3.3.1. Film characterization

PVDF and PVDF-CFO films were produced by doctor blade technique and crystallized in the presence of the ionic liquid [Bmim][Cl]. After crystallization from the melt, IL was removed by performing several washes with water. As can be seen in Figure 3.2a, before [Bmim][Cl] was washed, its presence could be detected on the film surface, in the form of dark stains covering PVDF spherulites. This indicates that part of the IL is moved to the surface of the sample by the growth of PVDF crystals. After IL removal (Figure 3.2a) the dark areas disappear due to the soluble character of [Bmim][Cl] in water. The elimination of the IL allowed to visualize PVDF characteristic spherulitic structure when crystallized from the melt. The spherulites show a slightly smaller size in PVDF-CFO films compared to PVDF due to the role of CFO nanoparticles as nucleating agents. The dispersion of these

nanoparticles in the initial solution provides a higher number of crystallization nuclei where polymer spherulites start to grow until they contact a neighbour one due to the limited space (Martins, Costa, and Lanceros-Mendez 2011).

IL removal was also confirmed by infrared spectroscopy. PVDF and PVDF-CFO film spectra before and after [Bmim][Cl] elimination are shown in Figure 3.2b. The characteristic absorption bands of the IL are observed before the removal. A clear peak appears at 3385 $cm^{-1}$ corresponding to the quaternary amine of the [Bmim] cation and another one at 1635 $cm^{-1}$ from the C=C stretching can also be detected (Dharaskar et al. 2016). After washing the peaks can no longer be seen, indicating the correct removal of the IL and confirming the results already visualized by electron microscopy.

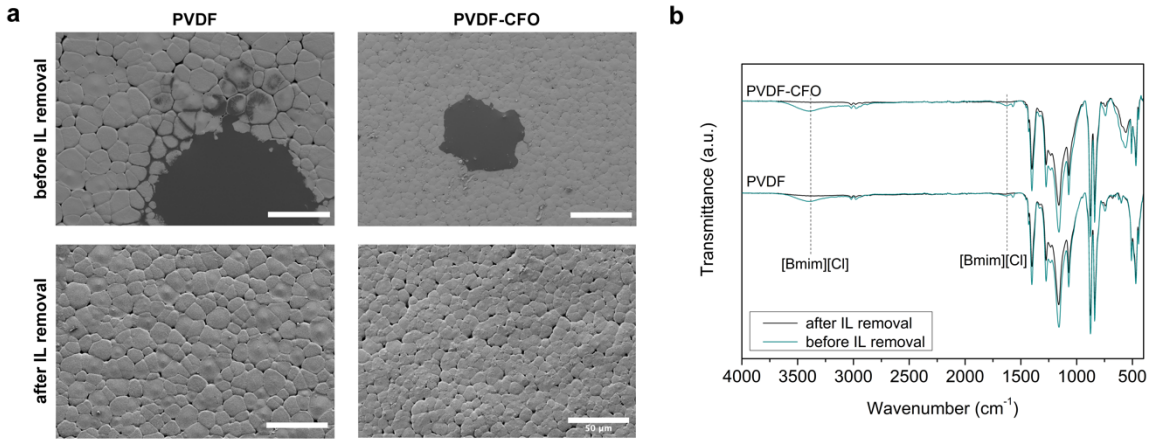


**Figure 3.2. Characterization of PVDF and PVDF-CFO films before and after ionic liquid (IL) removal. a) Field emission scanning electron microscopy images of PVDF and PVDF-CFO surfaces before (upper line) and after (lower line) IL was removed by washing. Scale bar 50 µm. b) Infrared spectra of PVDF and PVDF-CFO films before (green line) and after (black line) IL removal. Characteristic peaks of [Bmim][Cl] disappeared after performing several washes with water.**

Once the removal of the IL was confirmed, washed films were physically characterized. PVDF can present five polymorphs ($\alpha$, $\beta$, $\gamma$, $\delta$ and $\varepsilon$), but not all of them are electroactive. $\alpha$, $\beta$, $\gamma$ are the most commonly obtained phases by the standard manufacturing techniques and $\beta$ is the preferred one due to its highest piezoelectric coefficient (Martins, Lopes, and Lanceros-Mendez 2014). The vibrational spectra of PVDF polymorphs via FTIR has been validated for phase identification. This approach consists of the identification of characteristic absorption bands that are unequivocally present in the spectra of one of the phases (Cai et al. 2017). $\alpha$-phase is the easiest one to identify due to the high number of representative peaks (410, 489, 532, 614, 762, 795, 854, 975, 1149, 1209, 1383 and 1423 $cm^{-1}$), being 762 $cm^{-1}$ the one typically used to recognize it. Regarding $\beta$-phase, 840 $cm^{-1}$ has usually been considered as the most characteristic peak, nevertheless, it has recently been accepted that this band can also have a contribution from the $\gamma$-phase, although the component due to the latter tends to appear as a shoulder of the 833 $cm^{-1}$ band. This controversy can be solved by identifying the absorption peak at 1279 $cm^{-1}$, which

unequivocally distinguishes β from γ-phase (Cai et al. 2017; Martins, Lopes, and Lanceros-Mendez 2014).

To ensure the obtainment of the most electroactive polymorph, β-phase, PVDF and PVDF-CFO film FTIR-ATR spectra were analysed. As can be seen in Figure 3.3a, α-phase identification band at 762 $cm^{-1}$ appears as a shoulder in both spectra, revealing the scarce participation of this phase to the total amount of crystalline content. PVDF and PVDF-CFO films present the typical β-phase absorption band 1279 $cm^{-1}$, which corroborates the presence of this polymorph. Moreover, a strong peak at 840 $cm^{-1}$ can be seen, which was used to quantify β-phase percentage in the samples by applying Eq. (3) (Gregorio and Cestari 1994):

$$F(\beta) = \frac{A_\beta}{\left(\frac{K_\beta}{K_\alpha}\right)A_\alpha + A_\beta} \qquad \text{Eq. 3}$$

where $A_\alpha$ and $A_\beta$ are the absorbances at 762 and 840 $cm^{-1}$, corresponding to the α and β phase, respectively, and $K_\alpha$ (6.1 × $10^4$ $cm^2/mol$) and $K_\beta$ (7.7 × $10^4$ $cm^2/mol$) are the corresponding absorption coefficients of pristine α or β-phase samples (Gregorio and Cestari 1994). Quantification revealed that the percentages of β-phase in the PVDF and PVDF-CFO films after IL removal were 95.4 ± 3.4 % and 98.6 ± 0.6 %, respectively.

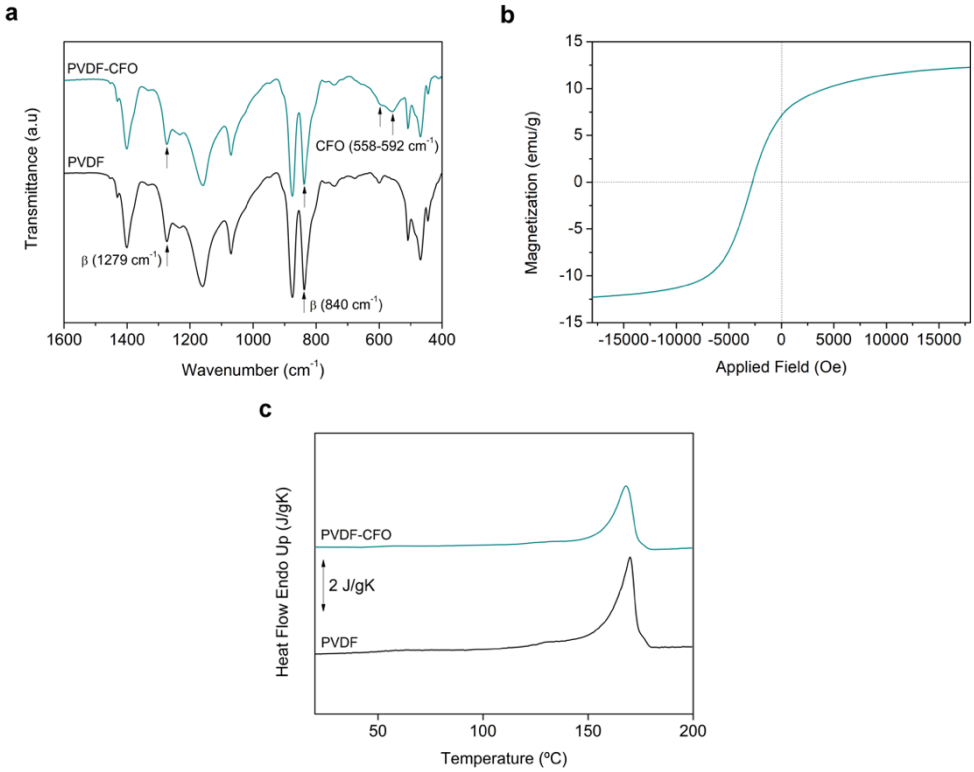


**Figure 3.3. Physical characterization of PVDF and PVDF-CFO films after ionic liquid removal. a) Fourier transform infrared spectra of PVDF and PVDF-CFO films where β-phase and CFO characteristic peaks are highlighted. b) Room-temperature hysteresis loop of PVDF-CFO films. c) DSC heating thermograms of PVDF and PVDF-CFO films.**

Films obtained using a temperature below 70 °C, without the presence of a nucleating filler, usually lead to the production of β-phase highly porous, fragile, opaque and difficult to polarize films. Nevertheless, when the films are produced using higher temperatures (>70 °C) or produced from the melt (T ~ 210 °C) to ensure complete solvent evaporation, as is the case, they are crystallized mainly in the non-electroactive α-phase (Martins, Lopes, and Lanceros-Mendez 2014). When using the same protocol, but incorporating magnetostrictive nanoparticles, electrically active films can be obtained. CFO nanoparticles are negatively charged which promotes the interaction with the positive $CH_2$ charge density of the PVDF chains. This allows the alignment of the chains on the surface of the nanoparticle in the extended all-trans (TTT) conformation, which is characteristic of the electroactive β-phase (Martins, Costa, Benelmekki, et al. 2012).

β-phase can be induced in neat PVDF films after mechanical stretching of the α-phase material, although the microscopic structure of the films is altered. The characteristic spherulite structure, is replaced by a microfibrillar one (Sencadas, Gregorio, and Lanceros-Méndez 2009). Cell culture assays involving electromechanical stimulation require the use of neat PVDF as a control, where no magnetoelectric effect is observed regardless the presence of a magnetic field. Microstructural variations due to stretching difficult result interpretation, since MSCs can sense diverse nanotopographical cues, which may affect cell behaviour (Nikukar et al. 2013). The introduction of [Bmim][Cl] allows crystallization of neat PVDF in β-phase, following the same protocol as PVDF-CFO films, without the need of further uniaxial stretching which alters PVDF microstructure. IL acts in a similar way than CFO nanoparticles. The interaction between [Bmim][Cl] and the polymer chain between the cation and the $CF_2$ groups in PVDF structure and the anion with $CH_2$ leads to the induction of the all-trans planar zigzag β-phase conformation. In fact, these results correlate with the ones obtained by Meira et al. (Meira et al. 2019) where PVDF films were manufactured using the same technique and crystallized in the presence of [Bmim][Cl] showed a high content of β-phase, indicating that IL can act as nucleating agents for this polymorph. Other ionic liquids have been reported as inductors of β-phase crystallization in PVDF substrates as is the case of 2-hydroxyethyl-trimethylammonium dihydrogen phosphate ([Ch][DHP]) or 1-ethyl-3-methylimidazolium chloride ([Emim][Cl]) (Correia, Costa, et al. 2020; Meira et al. 2019).

It is also worthy to note the appearance of characteristic CFO absorption bands at 558 $cm^{-1}$ (Co-O stretching) (He, Dai, and Zhou 2017) and 591 $cm^{-1}$ (Fe-O bond) (Aboelazm, Gomaa, and Chong 2018) in PVDF-CFO films, which confirms the incorporation of the nanoparticles. Their presence was also assessed using a vibrating sample magnetometer that allowed to calculate the nanoparticle content applying Eq. (1). The typical hysteresis loop for PVDF-CFO nanocomposites is presented in Figure 3.3b. Quantification showed that the CFO final concentration was 20.4 ± 0.5 % (w/w) which, as expected for this manufacturing technique, corresponds to the initial concentration in solution, revealing no CFO loss.

Lastly, thermal properties of the produced films, after IL removal, were investigated by means of differential scanning calorimetry to determine the melting temperature ($T_m$) and

the degree of crystallinity ($X_c$). As can be seen in Figure 3.3c, a single endothermic peak at around 170 °C for both types of films, indicative of the polymer melting, is observed. $T_m$ corresponding to PVDF and PVDF-CFO films show no significant differences, being 169.7 and 169.3 °C respectively. Regarding $X_c$, it was calculated applying Eq. (4):

$$Xc = \frac{\Delta H_m}{w_{PVDF}\ (x\Delta H_\alpha + y\Delta H_\beta)} \qquad \text{Eq. 4}$$

where $\Delta H_m$ is the melting enthalpy of PVDF and PVDF-CFO films measured by DSC and $\Delta H_\alpha$ and $\Delta H_\beta$ are the melting enthalpies of a 100 % crystalline sample in the α and β phases, whose values are 93.07 J/g and 103.4 J/g, respectively (Lovinger 1981). $w_{PVDF}$ is the mass fraction of PVDF within the films (provided by their magnetic properties), and x and y are the percentage of $\alpha$ and $\beta$ phases present in the sample, obtained by FTIR measurements.

Again, the quantification showed no significant differences in the crystalline content of both types of samples, which were 62 ± 0.7 % for PVDF and 63.9 ± 3.3 % for PVDF-CFO. In this case, the incorporation of CFO does not reduce the degree of crystallinity of the composites by inducing defects during polymer crystallization as has been reported for other types of substrates combining PVDF and CFO (Martins, Costa, Ferreira, et al. 2012; Sencadas et al. 2011).

### 3.3.2. Mesenchymal stem cells response to electroactive films at static mode

MSCs initial behaviour at static mode without electromechanical stimulation was tested. The first step was to prove the absence of cytotoxicity of possible IL traces or CFO nanoparticles non correctly incorporated into the polymer matrix. Biocompatibility of the films was studied by means of an indirect cytotoxicity assay or leachable test, where PVDF and PVDF-CFO films were placed in contact with basal medium for 24 h. MSCs viability after 48 h in contact with the conditioned medium was analysed (Figure 3.4a), revealing no toxicity due to any type of leaching. There is no release of either IL (confirming the results obtained by FTIR), or if so it does not affect MSCs viability, nor CFO nanoparticles, which are well incorporated into the polymer matrix.

The correct incorporation of the nanoparticles into the polymer matrix does not rule out the fact that the presence of CFO exposed on the film surface may affect MSCs initial adhesion and proliferation. FTIR-ATR spectra revealed the existence of magnetostrictive nanoparticles on the film surface, as demonstrated by the presence of their characteristic absorption bands in the composite spectra (Figure 3.3a). As can be seen in Figure 3.4b after 24 h there is a significant difference between the number of cells on glass and PVDF substrates compared to PVDF-CFO, where the cell count is lower than the initial seeding density (dashed line). The presence of exposed CFO nanoparticles may be hindering initial MSCs adhesion. Nevertheless, after 3 days, cell count on PVDF-CFO substrates shows no significant differences with the other conditions, a trend that is also maintained after 7 days, MSCs continue to proliferate without further difficulties. In fact, cell increase in PVDF-CFO substrates between day 1 and 3 should be faster than in the rest of the conditions to make up for the lower number of cells attached at the beginning of the culture. Even though cell

count was significantly lower after 24 h in PVDF-CFO substrates, cell spreading analysis revealed that attached cells display similar cell area, compared to glass slide control (Figure 3.4c). Cell spreading shows no significant differences between conditions, which indicates that even if the cell count is lower in PVDF-CFO substrates after 24 h, MSCs are properly attached.

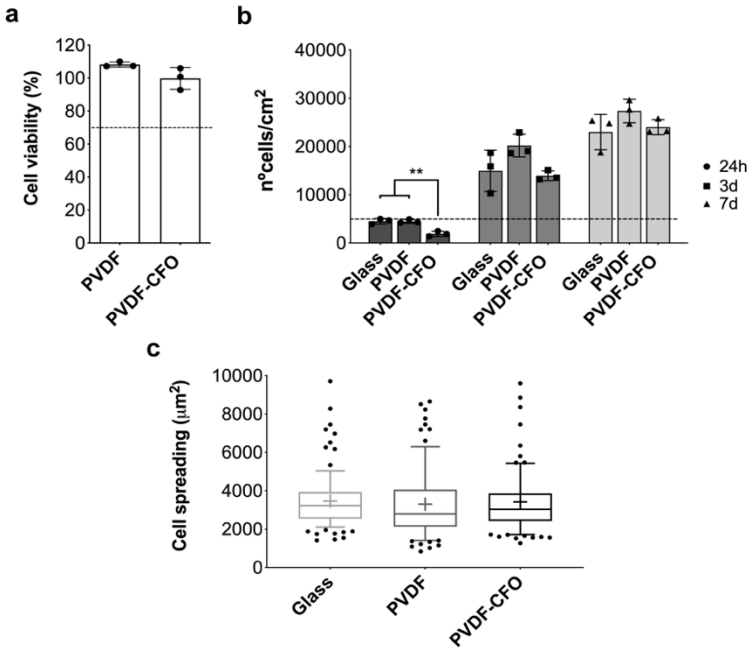


**Figure 3.4. Characterization of initial MSCs response on glass, PVDF and PVDF-CFO films after ionic liquid removal. a) Leachable test to determine CFO or possible traces of ionic liquid cytotoxicity. Dashed line corresponds to 70 % cell viability, fixed limit by ISO 10993-5 to consider a biomaterial as cytotoxic. No significant differences are observed (n=3, two-tailed t-test). b) Cell number per cm$^2$ after 1, 3 and 7 days based on MTS test. Dashed line indicates initial seeding density (5 x 10$^3$ cells/cm$^2$) p-value < 0.01 (**) (n=3, One-way ANOVA with Holm-Sídák multiple comparison test). c) Box plot (10-90 percentile) of MSCs cell area measured after 24 h on different cell culture substrates. No significant differences are observed determined by Kruskall-Wallis with Dunn's multiple comparison test. 85 cells per condition, at least, from three different replicates were used for the analysis.**

### 3.3.3. Media selection for piezoelectric stimulation

Cell culture medium plays a fundamental role in the differentiation process when combined with electromechanical stimulation. Lack of consensus on this matter favours the appearance of different combinations of biochemical and physical stimuli in literature, comprising the use of basal and osteogenic media (Guillot-Ferriols et al. 2022). Selecting the appropriate cell culture medium is essential to enhance the stimulation effect on MSCs osteogenic differentiation. Therefore, different media were tested in static conditions to study their effect on cell area and the formation of focal adhesions, which are crucial during MSCs osteogenic differentiation process.

Cell spreading area in different substrates and different media formulations (basal, osteogenic and balanced) was analysed after 3 days in culture, as can be seen in Figure 3.5a. Balanced medium was also included because the mixture 1:1 between osteogenic

and adipogenic media allows MSCs to choose the desired differentiation pathway influenced by other cues, as is the case of piezoelectric stimulation (Kilian et al. 2010). Contrary to what was expected, balanced medium showed a higher cell spreading area in all the substrates used, including the glass slide control, although differences are only significant in PVDF films. Despite not all the studied conditions showing statistically significant differences in terms of cell area, there is a maintained trend. Larger cell spreading areas are beneficial for osteogenic differentiation of MSCs and maintenance of their differentiated phenotype (McBeath et al. 2004; Yang et al. 2019).

This trend was also followed by the focal adhesion analysis. Using different cell media formulations cells showed an increase in FA number and FA mean length per cell when cultured on balanced media. Regarding FA count per cell, differences were only significant, again, in PVDF surfaces (Figure 3.5b). Nevertheless, the trend was observed on the other surfaces. When analysing FA mean length per cell, differences are significant for glass, PVDF and PVDF-CFO when comparing cells cultured with balanced and basal media. Balanced medium favours the formation of longer FA, as can be seen in Figure 3.5c.

Finally, measured FA were binned and represented as focal adhesion distribution according to their length on different substrates and cell media following the classification stablished by Biggs et al. (Biggs et al. 2007). Structures measuring less than 2 μm were assigned as focal complexes, those from 2 to 5 μm were designated as focal adhesions, while those over 5 μm long were accordingly classified as super mature adhesions. Focal complexes start to appear as dot-like structures around 1 μm long, which evolve into focal adhesions due to the intracellular and extracellular tension when integrin packing density can increase by a factor of three-fold. Matured FAs are typically dashed shaped, 2-5 μm, and contain vinculin, paxillin and talin. As demonstrated by Biggs et al., osteoblasts require the formation of longer focal adhesions, which leads to an increase in intracellular tension, linked to osteogenesis (Biggs et al. 2007).

As can be seen in Figure 3.5d, MSCs cultured on glass, PVDF and PVDF-CFO using basal medium demonstrate an increase in frequency of focal complexes in the range of 0 to 2 μm compared to balanced and osteogenic media. Nevertheless, when cells were cultured in balanced and osteogenic media, they possessed greater numbers of focal adhesions measuring between 2 and 5 μm. Although the number of super mature adhesions (>5 μm) was not superior to 10 %, the trend observed for focal adhesions is maintained, with an increase in balanced and osteogenic media.

Taking all these results together, balanced medium was selected for subsequent differentiation experiments. Balanced medium provides favourable cues for MSCs osteogenic differentiation, as demonstrated by the increased cell area and number and length of FA. Moreover, the exposure to adipogenesis and osteogenesis-promoting soluble cues does not condition MSCs to choose a differentiation pathway, but provides the right stimuli to guide them in combination with electromechanical stimulation.

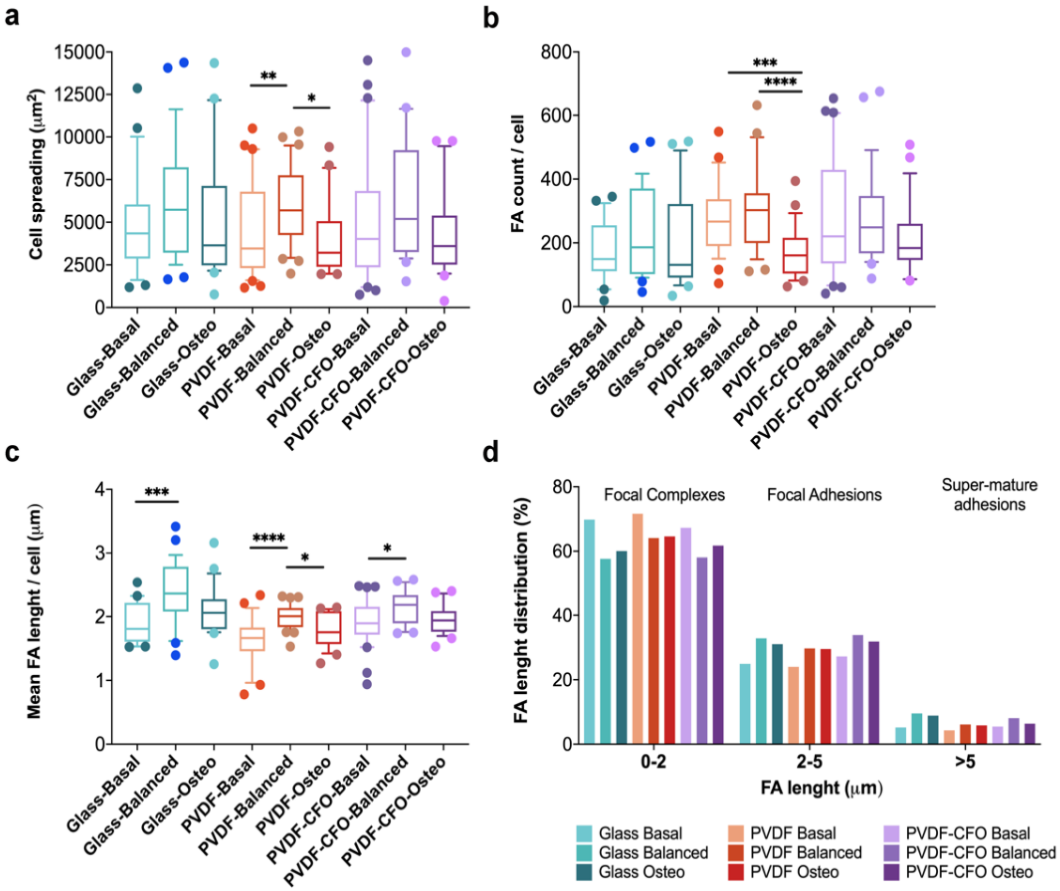


**Figure 3.5. Focal adhesion (FA) and cell area analysis of MSCs after 3 days, cultured in different media formulations and cell culture supports. Box plot (10-90 percentile) of MSCs a) cell area b) number of FA per cell and c) mean FA length per cell. d) Histogram of FA length distribution (%) classified according to FA length in focal complexes (0-2 μm), focal adhesions (2-5 μm) or super mature focal adhesions (>5 μm). Statistical differences between cells cultured in the same support with different media formulations were determined by non-parametric Kruskall-Wallis and Dunn's multiple comparison test. p-value legend: p < 0.05 (*), p < 0.01 (**), p < 0.001 (***), p < 0.0001 (****). 20 individual cells per condition, at least, from three different replicates were used for all the analysis**

### 3.3.4. Mesenchymal stem cells response to piezoelectric stimulation at cytoskeleton level

After selecting the appropriate medium, MSCs were seeded on different cell culture supports and stimulated using a magnetic bioreactor applying a stimulation program based on reproducing daily human activity. Cells were cultured for 3 days and focal adhesions, actin stress fibres and intermediate filaments were studied to try to elucidate how electromechanical stimulation affects cytoskeleton dynamics.

Figure 3.6a shows representative fluorescence images of F-actin cytoskeleton and vinculin immunostaining of non-stimulated (NS) and stimulated (S) MSCs. Cells show a well-

developed cytoskeleton and a spindle-shaped morphology in every condition, characteristic of this pluripotent cells. Those images were used to study MSCs response to piezoelectric stimulation. Cell spreading was again quantified, and the results presented in Figure 3.6b show no significant differences between the studied conditions, regardless the cell culture substrate or the presence of a magnetic field applied by the bioreactor. In the case of PVDF-CFO supports, the magnetic field induces an electromechanical stimulation, which is transmitted to the MSCs cultured on the surface, nevertheless, this cue did not affect cell spreading area.

Focal adhesions were also quantified and FA count and mean FA length per cell were compared between non-stimulated and stimulated cell culture supports. As can be seen in Figure 3.6d and 3.6e there are significant differences between PVDF-CFO NS and S. These differences cannot be seen in PVDF and glass slides, where the application of a magnetic field generates no piezoelectric stimulation due to the absence of the CFO nanoparticles. The electromechanical cue provided by the combination of a piezoelectric matrix and a magnetostrictive component enhances the appearance of FAs and their mean length. These results can clearly be seen when FA length is classified in focal complexes (0-2 μm), focal adhesions (2-5 μm) and super-mature focal adhesions (>5 μm) (Figure 3.6f and 3.6g). Non-stimulated PVDF-CFO samples present an increase in frequency of focal complexes. On the other hand, stimulated PVDF-CFO samples present a higher number of focal adhesions ranging from 2 to 5 μm and super-mature adhesions, compared to PVDF-CFO the NS. The lengthen of focal adhesion is a requisite for MSCs osteogenesis to occur (Biggs et al. 2009). Longer FA support more contractile morphologies and show higher levels of intracellular tension (McBeath et al. 2004; Kilian et al. 2010). In fact, in the stem cell niche, MSCs display small and transient adhesions, which allow them more dynamic interactions with the extracellular matrix, fundamental for MSCs self-renewal (Scadden 2006). This concept was demonstrated by Tsimbouri et al. using specific nanotopographies. MSCs cultured on nanotopographies that promote the formation of smaller FA retained multipotency, whereas nanoconfigurations promoting the formation of larger FA induced osteogenesis (Tsimbouri et al. 2012, 2014).

Changes in cytoskeleton tension and reorganization, correlated with the increase in length of focal adhesions, are observed when MSCs are subjected to physical cues (Dalby, Gadegaard, and Oreffo 2014). Trying to elucidate cytoskeleton response to MSCs electromechanical stimulation, the number of stress fibres per cell was evaluated. Figure 3.6c shows that this kind of stimulation does not produce significant changes in the stress fibre count per cell. On the contrary, a clear effect can be seen on the intermediate filament vimentin upon piezoelectric stimulation. Figure 3.7a displays characteristic images of vimentin immunostaining in MSCs after 3 days in culture under the influence or not of a magnetic field applied by the bioreactor. Quantification (Figure 3.7b) reveals that there is a significant decrease in vimentin intensity in PVDF-CFO stimulated samples compared to non-stimulated PVDF-CFO. A decrease in vimentin expression could be correlated with the MSCs osteogenic differentiation, as reported by Lian et al. (Lian et al. 2009). Their findings confirmed that vimentin down-regulation during osteoblasts differentiation is a required mechanism to relieve its inhibition of ATF4 transcriptional factor producing the expression of the downstream effector osteocalcin.

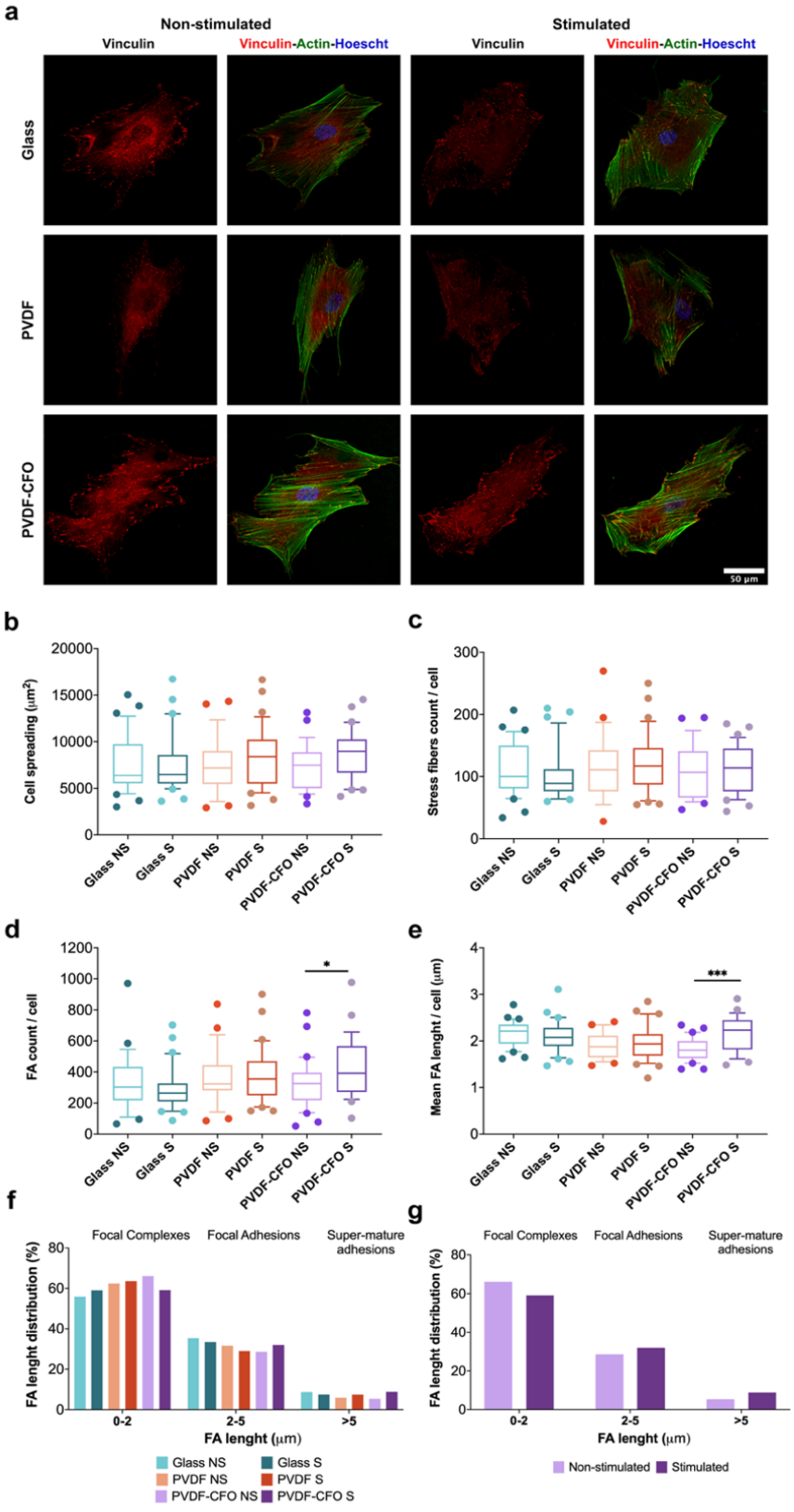


**Figure 3.6. Focal adhesion (FA), cell area and stress fiber analysis of MSCs after 3 days cultured on glass, PVDF and PVDF-CFO in static (non-stimulated (NS)) or dynamic (stimulated**

**(S)) conditions. a) Representative fluorescence images of vinculin (red), F-actin (green) and nuclei (Hoescht-blue). Scale bar: 50 μm. Box and whiskers (10-90 percentile) of b) cell area, c) number of stress fibres per cell, d) number of FA per cell and e) mean FA length per cell. f) Histogram of FA length distribution (%) of stimulated and non-stimulated MSCs cultured on glass, PVDF and PVDF-CFO classified according to FA length in focal complexes (0-2 μm), focal adhesions (2-5 μm) or super mature focal adhesions (>5 μm). g) Histogram of FA length distribution (%) of stimulated and non-stimulated MSCs cultured on PVDF-CFO films following the same classification. Statistical differences between cells cultured on the same support (Glass, PVDF or PVDF-CFO) in static and dynamic conditions were determined by two-tailed t-test when following a normal distribution (Shapiro-Wilk test). If not two-tailed Mann-Whitney test was used. p-value legend: $p < 0.05$ (*), $p < 0.01$ (**), $p < 0.001$ (***). 25 individual cells per condition, at least, from three different replicates were used for all the analysis.**

These reduction in vimentin expression followed a similar pattern in MC3T3-E1 primary osteoblasts as well as in bone marrow stromal progenitors, where vimentin mRNA decreased over the differentiation process. Fan et al (Fan et al. 2021) explored the changes in the spatial distribution of vimentin and actin stress fibers during MSCs osteogenic differentiation. During MSCs osteogenesis a reduction in vimentin intensity was correlated with vimentin losing part of its cytoplasmatic space and being replaced by actin stress fibres. Vimentin was restrained to the top of the cells, away from the nucleus and ventral side and its network became smaller. Vimentin alterations due to MSCs response to physical cues has also been reported by Tsimbouri et al. (Tsimbouri et al. 2014), where MSCs cultured on nanopatterned surfaces showed significantly lower density of vimentin which was correlated with alternations in packing of chromosome territories and changes in transcription factor activity.

Altogether, the evidence here presented indicates that MSCs are able to respond to electromechanical stimulation on 2D substrates by means of focal adhesions. The lengthen of adhesions leads to a cytoskeleton response, where vimentin density is decreased. Moreover, as far as the authors know selection of cell culture media using piezoelectric cell culture supports has been presented for the first time, favouring the stimulation effect.

Further experiments need to be performed to test osteogenic differentiation because of FA lengthen and cytoskeleton response. Nevertheless, these results lead the way to the use of piezoelectric cell culture supports combined with magnetostrictive nanoparticles for MSCs piezoelectric stimulation to study and control stem cell fate.

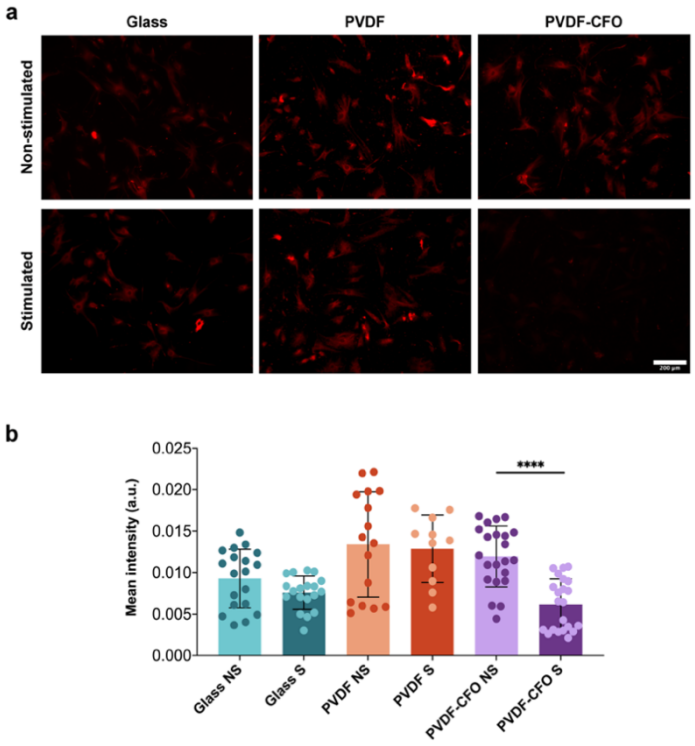


**Figure 3.7. Vimentin analysis of MSCs after 3 days cultured on glass, PVDF and PVDF-CFO in static (non-stimulated (NS)) or dynamic (stimulated (S)) conditions. a) Representative fluorescence images of vimentin immunofluorescence. Scale bar: 200 μm. b) Quantification of vimentin mean intensity on different cell culture supports. 4 representative zones per well were analyzed from at least 3 replicates. Statistical differences were determined by Kruskal-Wallis with Dunn's multiple comparison test. p-value < 0.0001 (****).**

## 3.4. Conclusions

PVDF and PVDF-CFO electroactive films were produced by doctor blade technique in β-phase. Crystallization of PVDF in the presence of [Bmim][Cl] allowed the induction of its most electroactive phase even in neat PVDF films, without the need of further uniaxial stretching. After crystallization, the ionic liquid was successfully removed by several washes with water. Films proved to be biocompatible, allowed MSCs adhesion and proliferation at short term compared to glass slide controls. The incorporation of magnetostrictive nanoparticles allowed the electromechanical stimulation of MSCs to try to elucidate their response in terms of cytoskeleton dynamics. To do so, the selection of the appropriate cell culture media was optimized in static conditions for further combination with stimulation. Focal adhesion analysis revealed that a combination 1:1 of osteogenic and adipogenic media enhanced cell spreading area, focal adhesion number and length. Balanced medium was combined the with electromechanical stimulation revealing that stimulated PVDF-CFO surfaces enhanced focal adhesion length compared to PVDF-CFO non-stimulated supports, also vimentin density was decreased in the presence of piezoelectric stimulation. These results prove that MSCs respond to this kind of stimulation by means of focal adhesions and cytoskeleton reorganization, opening the way for further studies on MSCs fate determination using piezoelectric cell culture supports.

### 3.5. Acknowledgements

This work was supported by the Spanish State Research Agency (AEI) through Projects PID2019-106099RB-C41 and –C43 / AEI / 10.13039/501100011033. The CIBER-BBN initiative is funded by the VI National R&D&I Plan 2008-2011, Iniciativa Ingenio 2010, Consolider Program. CIBER actions are financed by the Instituto de Salud Carlos III with assistance from the European Regional Development Fund. Maria Guillot Ferriols received government funding for her Doctoral Thesis [Grant Number BES-2017-080398FPI]. The authors thank FCT (Fundação para a Ciência e a Tecnologia) for financial support under the framework of Strategic Funding grant UID/FIS/04650/2021, projects PTDC/FIS-MAC/28157/2017 and POCI-01-0145-FEDER-007688) and contract under the Stimulus of Scientific Employment, Individual Support 2020.04028 CEECIND (CMC).

### 3.6. References

Aboelazm, E. A. A., A. M. A. K Gomaa, and K. F. Chong. 2018. “Cobalt Oxide Supercapacitor Electrode Recovered from Spent Lithium-Ion Battery.” *Chemistry of Advanced Materials* 3 (4): 67–74.

Biggs, M. J. P., R. G. Richards, N. Gadegaard, C. D. W. Wilkinson, and M. J. Dalby. 2007. “Regulation of Implant Surface Cell Adhesion: Characterization and Quantification of S-Phase Primary Osteoblast Adhesions on Biomimetic Nanoscale Substrates.” *Journal of Orthopaedic Research* 25: 273–82. https://doi.org/10.1002/jor.

Biggs, M. J. P., R. G. Richards, N. Gadegaard, C. D. W. Wilkinson, R. O. C. Oreffo, and M. J. Dalby. 2009. “The Use of Nanoscale Topography to Modulate the Dynamics of Adhesion Formation in Primary Osteoblasts and ERK/MAPK Signalling in STRO-1+ Enriched Skeletal Stem Cells.” *Biomaterials* 30 (28): 5094–5103. https://doi.org/10.1016/j.biomaterials.2009.05.049.

Cai, X., T. Lei, D. Sun, and L. Lin. 2017. “A Critical Analysis of the α, β and γ Phases in Poly(Vinylidene Fluoride) Using FTIR.” *RSC Advances* 7 (25): 15382–89. https://doi.org/10.1039/c7ra01267e.

Castano-Izquierdo, H., J. Álvarez-Barreto, J. van den Dolder, J. A. Jansen, A. G. Mikos, and V. I. Sikavitsas. 2006. “Pre-Culture Period of Mesenchymal Stem Cells in Osteogenic Media Influences Their in Vivo Bone Forming Potential.” *Journal of Biomedical Materials Research Part A* 79 (4): 129–38. https://doi.org/10.1002/jbm.a.31082.

Castro, N., M. M. Fernandes, C. Ribeiro, V. Correia, R. Minguez, and S. Lanceros-Mendez. 2020. “Magnetic Bioreactor for Magneto-, Mechano- and Electroactive Tissue Engineering Strategies.” *Sensors* 20 (12): 1–13. https://doi.org/10.3390/s20123340.

Correia, D. M., C. M. Costa, J. C. Rodríguez-Hernández, I. Tort Ausina, L. Teruel Biosca, C. Torregrosa Cabanilles, J. M. Meseguer-Duenãs, S. Lanceros-Méndez, and J. L. Gomez Ribelles. 2020. “Effect of Ionic Liquid Content on the Crystallization Kinetics and Morphology of Semicrystalline Poly(Vinylidene Fluoride)/Ionic Liquid Blends.” *Crystal Growth and Design* 20 (8): 4967–79. https://doi.org/10.1021/acs.cgd.0c00042.

Correia, D. M., L. C. Fernandes, P. M. Martins, C. García-Astrain, C. M. Costa, J. Reguera, and S. Lanceros-Méndez. 2020. "Ionic Liquid–Polymer Composites: A New Platform for Multifunctional Applications." *Advanced Functional Materials* 30 (24): 1–43. https://doi.org/10.1002/adfm.201909736.

Dalby, M. J., M. J. P. Biggs, N. Gadegaard, G. Kalna, C. D. W. Wilkinson, and A. S. G. Curtis. 2007. "Nanotopographical Stimulation of Mechanotransduction and Changes in Interphase Centromere Positioning." *Journal of Cellular Biochemistry* 100 (2): 326–38. https://doi.org/10.1002/jcb.21058.

Dalby, M. J., N. Gadegaard, and R. O .C. Oreffo. 2014. "Harnessing Nanotopography and Integrin-Matrix Interactions to Influence Stem Cell Fate." *Nature Materials* 13 (6): 558–69. https://doi.org/10.1038/nmat3980.

Damaraju, S. M., Y. Shen, E. Elele, B. Khusid, A. Eshghinejad, J. Li, M. Jaffe, and T. L. Arinzeh. 2017. "Three-Dimensional Piezoelectric Fibrous Scaffolds Selectively Promote Mesenchymal Stem Cell Differentiation." *Biomaterials* 149: 51–62. https://doi.org/10.1016/j.biomaterials.2017.09.024.

Dharaskar, S. A., K. L. Wasewar, M. N. Varma, D. Z. Shende, and C. K. Yoo. 2016. "Synthesis, Characterization and Application of 1-Butyl-3-Methylimidazolium Tetrafluoroborate for Extractive Desulfurization of Liquid Fuel." *Arabian Journal of Chemistry* 9 (4): 578–87. https://doi.org/10.1016/j.arabjc.2013.09.034.

Dominici, M., K. Le Blanc, I. Mueller, I. Slaper-Cortenbach, F. C. Marini, D. S. Krause, R. J. Deans, A. Keating, D. J. Prockop, and E. M. Horwitz. 2006. "Minimal Criteria for Defining Multipotent Mesenchymal Stromal Cells. The International Society for Cellular Therapy Position Statement." *Cytotherapy* 8 (4): 315–17. https://doi.org/10.1080/14653240600855905.

Einhorn, T. A., and L. C. Gerstenfeld. 2015. "Fracture Healing: Mechanisms and Interventions." *Nature Reviews Rheumatology* 11 (1): 45–54. https://doi.org/10.1038/nrrheum.2014.164.

Fan, T., R. Qu, X. Jiang, Y. Yang, B. Sun, X. Huang, Z. Zhou, J. Ouyang, S. Zhong, and J. Dai. 2021. "Spatial Organization and Crosstalk of Vimentin and Actin Stress Fibers Regulate the Osteogenic Differentiation of Human Adipose-Derived Stem Cells." *FASEB Journal* 35 (2): 1–16. https://doi.org/10.1096/fj.202000378RR.

Fernandes, M. M., D. M. Correia, C. Ribeiro, N. Castro, V. Correia, and S. Lanceros-Mendez. 2019. "Bioinspired Three-Dimensional Magnetoactive Scaffolds for Bone Tissue Engineering." *ACS Applied Materials and Interfaces* 11 (48): 45265–75. https://doi.org/10.1021/acsami.9b14001.

Ghali, O., O. Broux, G. Falgayrac, N. Haren, J. P.T.M. Van Leeuwen, G. Penel, P. Hardouin, and C. Chauveau. 2015. "Dexamethasone in Osteogenic Medium Strongly Induces

Adipocyte Differentiation of Mouse Bone Marrow Stromal Cells and Increases Osteoblast Differentiation." *BMC Cell Biology* 16 (1): 1–15. https://doi.org/10.1186/s12860-015-0056-6.

Gómez-Barrena, E., P. Rosset, D. Lozano, J. Stanovici, C. Ermthaller, and F. Gerbhard. 2015. "Bone Fracture Healing: Cell Therapy in Delayed Unions and Nonunions." *Bone* 70: 93–101. https://doi.org/10.1016/j.bone.2014.07.033.

Gonçalves, R., P. Martins, D. M. Correia, V. Sencadas, J. L. Vilas, L. M. León, G. Botelho, and S. Lanceros-Méndez. 2015. "Development of Magnetoelectric CoFe2O4/Poly(Vinylidene Fluoride) Microspheres." *RSC Adv.* 5 (45): 35852–57. https://doi.org/10.1039/C5RA04409J.

Gregorio, R., and M. Cestari. 1994. "Effect of Crystallization Temperature on the Crystalline Phase Content and Morphology of Poly(Vinylidene Fluoride)." *Journal of Polymer Science Part B: Polymer Physics* 32 (5): 859–70. https://doi.org/10.1002/polb.1994.090320509.

Guillot-Ferriols, M., S. Lanceros-Méndez, J. L. Gómez Ribelles, and G. Gallego-Ferrer. 2022. "Electrical Stimulation: Effective Cue to Direct Osteogenic Differentiation of Mesenchymal Stem Cells?" *Biomaterials Advances* 138 (May): 1–18. https://doi.org/10.1016/j.bioadv.2022.212918.

He, Y., C. Dai, and X. Zhou. 2017. "Magnetic Cobalt Ferrite Composite as an Efficient Catalyst for Photocatalytic Oxidation of Carbamazepine." *Environmental Science and Pollution Research* 24 (2): 2065–74. https://doi.org/10.1007/s11356-016-7978-1.

Hodgkinson, T., P. M. Tsimbouri, V. Llopis-Hernandez, P. Campsie, D. Scurr, P. G. Childs, D. Phillips, et al. 2021. "The Use of Nanovibration to Discover Specific and Potent Bioactive Metabolites That Stimulate Osteogenic Differentiation in Mesenchymal Stem Cells." *Science Advances* 7 (9): 1–16. https://doi.org/10.1126/sciadv.abb7921.

Jacob, J., N. More, K. Kalia, and G. Kapusetti. 2018. "Piezoelectric Smart Biomaterials for Bone and Cartilage Tissue Engineering." *Inflammation and Regeneration* 38 (1): 1–11. https://doi.org/10.1186/s41232-018-0059-8.

Kilian, K. A., B. Bugarija, B. T. Lahn, and M. Mrksich. 2010. "Geometric Cues for Directing the Differentiation of Mesenchymal Stem Cells." *Proceedings of the National Academy of Sciences of the United States of America* 107 (11): 4872–77. https://doi.org/10.1073/pnas.0903269107.

Lian, N., W. Wang, L. Li, F. Elefteriou, and X. Yang. 2009. "Vimentin Inhibits ATF4-Mediated Osteocalcin Transcription and Osteoblast Differentiation." *Journal of Biological Chemistry* 284 (44): 30518–25. https://doi.org/10.1074/jbc.M109.052373.

Lovinger, A.J. 1981. “Poly(Vinylidene Fluoride).” In *Developments in Crystalline Polymers - 1*, edited by D.C Basset, 195–273. Springer Dordrecht. https://doi.org/doi.org/10.1007/978-94-009-7343-5.

Martino, F., A. R. Perestrelo, V. Vinarský, S. Pagliari, and G. Forte. 2018. “Cellular Mechanotransduction: From Tension to Function.” *Frontiers in Physiology* 9: 1–21. https://doi.org/10.3389/fphys.2018.00824.

Martins, P., C. M. Costa, M. Benelmekki, G. Botelho, and S. Lanceros-Mendez. 2012. “On the Origin of the Electroactive Poly(Vinylidene Fluoride) β-Phase Nucleation by Ferrite Nanoparticles via Surface Electrostatic Interactions.” *CrystEngComm* 14 (8): 2807–11. https://doi.org/10.1039/c2ce06654h.

Martins, P., C. M. Costa, J. C.C. Ferreira, and S. Lanceros-Mendez. 2012. “Correlation between Crystallization Kinetics and Electroactive Polymer Phase Nucleation in Ferrite/Poly(Vinylidene Fluoride) Magnetoelectric Nanocomposites.” *Journal of Physical Chemistry B* 116 (2): 794–801. https://doi.org/10.1021/jp210493t.

Martins, P., C. M. Costa, and S. Lanceros-Mendez. 2011. “Nucleation of Electroactive β-Phase Poly(Vinilidene Fluoride) with CoFe2O4 and NiFe2O4 Nanofillers: A New Method for the Preparation of Multiferroic Nanocomposites.” *Applied Physics A: Materials Science and Processing* 103 (1): 233–37. https://doi.org/10.1007/s00339-010-6003-7.

Martins, P., and S. Lanceros-Méndez. 2013. “Polymer-Based Magnetoelectric Materials.” *Advanced Functional Materials* 23 (27): 3371–85. https://doi.org/10.1002/adfm.201202780.

Martins, P., A. C. Lopes, and S. Lanceros-Mendez. 2014. “Electroactive Phases of Poly(Vinylidene Fluoride): Determination, Processing and Applications.” *Progress in Polymer Science* 39 (4): 683–706. https://doi.org/10.1016/j.progpolymsci.2013.07.006.

McBeath, R., D. M. Pirone, C. M. Nelson, K. Bhadriraju, and C. S. Chen. 2004. “Cell Shape, Cytoskeletal Tension, and RhoA Regulate Stem Cell Lineage Commitment.” *Developmental Cell* 6 (4): 483–95. https://doi.org/10.1016/S1534-5807(04)00075-9.

Meira, R. M., D. M. Correia, S. Ribeiro, P. Costa, A. C. Gomes, F. M. Gama, S. Lanceros-Méndez, and C. Ribeiro. 2019. “Ionic-Liquid-Based Electroactive Polymer Composites for Muscle Tissue Engineering.” *ACS Applied Polymer Materials* 1 (10): 2649–58. https://doi.org/10.1021/acsapm.9b00566.

Minary-Jolandan, M., and M. F. Yu. 2009. “Uncovering Nanoscale Electromechanical Heterogeneity in the Subfibrillar Structure of Collagen Fibrils Responsible for the Piezoelectricity of Bone.” *ACS Nano* 3 (7): 1859–63. https://doi.org/10.1021/nn900472n.

Nikukar, H., S. Reid, P. M. Tsimbouri, M. O. Riehle, A. S.G. Curtis, and M. J. Dalby. 2013. “Osteogenesis of Mesenchymal Stem Cells by Nanoscale Mechanotransduction.” *ACS Nano* 7 (3): 2758–67. https://doi.org/10.1021/nn400202j.

Pärssinen, J., H. Hammarén, R. Rahikainen, V. Sencadas, C. Ribeiro, S. Vanhatupa, S. Miettinen, S. Lanceros-Méndez, and V. P. Hytönen. 2015. "Enhancement of Adhesion and Promotion of Osteogenic Differentiation of Human Adipose Stem Cells by Poled Electroactive Poly(Vinylidene Fluoride)." *Journal of Biomedical Materials Research - Part A* 103 (3): 919–28. https://doi.org/10.1002/jbm.a.35234.

Peters, A., D. Toben, J. Lienau, H. Schell, H. J. Bail, G. Matziolis, G. N. Duda, and K. Kaspar. 2009. "Locally Applied Osteogenic Predifferentiated Progenitor Cells Are More Effective than Undifferentiated Mesenchymal Stem Cells in the Treatment of Delayed Bone Healing." *Tissue Engineering - Part A* 15 (10): 2947–54. https://doi.org/10.1089/ten.tea.2009.0058.

Ribeiro, C., S. Moreira, V. Correia, V. Sencadas, J. G. Rocha, F. M. Gama, J. L. Gómez Ribelles, and S. Lanceros-Méndez. 2012. "Enhanced Proliferation of Pre-Osteoblastic Cells by Dynamic Piezoelectric Stimulation." *RSC Advances* 2 (30): 11504–9. https://doi.org/10.1039/c2ra21841k.

Ribeiro, C., J. A. Panadero, V. Sencadas, S. Lanceros-Mendez, M. N. Tamaño, D. Moratal, M. Salmeron-Sanchez, and J. L. Gomez Ribelles. 2012. "Fibronectin Adsorption and Cell Response on Electroactive Poly(Vinylidene Fluoride) Films." *Biomedical Materials* 7 (3). https://doi.org/10.1088/1748-6041/7/3/035004.

Ribeiro, S., C. Ribeiro, E. O. Carvalho, C. R. Tubio, N. Castro, N. Pereira, V. Correia, A. C. Gomes, and S. Lanceros-Méndez. 2020. "Magnetically Activated Electroactive Microenvironments for Skeletal Muscle Tissue Regeneration." *ACS Applied Bio Materials* 3 (7): 4239–52. https://doi.org/10.1021/acsabm.0c00315.

Scadden, D. T. 2006. "The Stem-Cell Niche as an Entity of Action." *Nature* 441: 1075–79. https://doi.org/doi.org/10.1038/nature04957.

Sencadas, V., R. Gregorio, and S. Lanceros-Méndez. 2009. "α to β Phase Transformation and Microestructural Changes of PVDF Films Induced by Uniaxial Stretch." *Journal of Macromolecular Science, Part B: Physics* 48 (3): 514–25. https://doi.org/10.1080/00222340902837527.

Sencadas, V., P. Martins, A. Pitães, M. Benelmekki, J. L. Gómez Ribelles, and S. Lanceros-Mendez. 2011. "Influence of Ferrite Nanoparticle Type and Content on the Crystallization Kinetics and Electroactive Phase Nucleation of Poly(Vinylidene Fluoride)." *Langmuir* 27 (11): 7241–49. https://doi.org/10.1021/la2008864.

Tsimbouri, P. M., N. Gadegaard, K. Burgess, K. White, P. Reynolds, P. Herzyk, R. Oreffo, and M. J. Dalby. 2014. "Nanotopographical Effects on Mesenchymal Stem Cell Morphology and Phenotype." *Journal of Cellular Biochemistry* 115: 380–90. https://doi.org/10.1002/jcb.24673.

Tsimbouri, P. M., R. J. McMurray, K. V. Burgess, E. V. Alakpa, P. M. Reynolds, K. Murawski, E. Kingham, R. O. C. Oreffo, N. Gadegaard, and M. J. Dalby. 2012. “Using Nanotopography and Metabolomics to Identify Biochemical Effectors of Multipotency.” *ACS Nano* 6 (11): 10239–49. https://doi.org/10.1021/nn304046m.

Yang, Y., X. Wang, Y. Wang, X. Hu, N. Kawazoe, Y. Yang, and G. Chen. 2019. “Influence of Cell Spreading Area on the Osteogenic Commitment and Phenotype Maintenance of Mesenchymal Stem Cells.” *Scientific Reports* 9 (1): 1–11. https://doi.org/10.1038/s41598-019-43362-9.

Ye, X., X. Yin, D. Yang, J. Tan, and G. Liu. 2012. “Ectopic Bone Regeneration by Human Bone Marrow Mononucleated Cells, Undifferentiated and Osteogenically Differentiated Bone Marrow Mesenchymal Stem Cells in Beta-Tricalcium Phosphate Scaffolds.” *Tissue Engineering - Part C: Methods* 18 (7): 545–56. https://doi.org/10.1089/ten.tec.2011.0470.

Yoshikawa, T., H. Ohgushi, and S. Tamai. 1996. “Immediate Bone Forming Capability of Prefabricated Osteogenic Hydroxyapatite.” *Journal of Biomedical Materials Research* 32 (3): 481–92. https://doi.org/10.1002/(SICI)1097-4636(199611)32:3<481::AID-JBM23>3.0.CO;2-I.

Zhou, Z., W. Li, T. He, L. Qian, G. Tan, and C. Ning. 2016. “Polarization of an Electroactive Functional Film on Titanium for Inducing Osteogenic Differentiation.” *Scientific Reports* 6: 1–8. https://doi.org/10.1038/srep35512

# Chapter 4. Piezoelectric 3D platform based on poly(vinylidene) fluoride microspheres for mesenchymal stem cells osteogenic differentiation

This chapter was adapted from the research paper published in *Gels*

Guillot-Ferriols, M.; García-Briega, M.I.; Tolosa, L.; Costa, C.M.; Lanceros-Méndez, S.; Gómez Ribelles, J.L.; Gallego Ferrer, G. Magnetically Activated Piezoelectric 3D Platform Based on Poly (Vinylidene) Fluoride Microspheres for Osteogenic Differentiation of Mesenchymal Stem Cells. *Gels* 2022, 8, 680.

DOI: 10.3390/gels8100680.

**Personal contribution**

Microsphere production, microsphere characterization and encapsulation in gelatin hydrogels were performed by M. Guillot-Ferriols, as well as cell culture tests to determine MSCs viability, proliferation and osteogenic differentiation. I. García-Briega helped with microsphere production and characterization, C.M. Costa polarized the microspheres and L. Tolosa provided help and advice with gene expression analysis.

M. Guillot-Ferriols designed the experiments, analysed the data, prepared the figures and wrote the first version of the manuscript. L. Tolosa, S. Lanceros-Méndez, J.L. Gómez Ribelles and G. Gallego Ferrer helped with experimental design, reviewed the manuscript and provided financial support.

## 4. Piezoelectric 3D platform based on poly(vinylidene) fluoride microspheres for mesenchymal stem cell osteogenic differentiation

Guillot-Ferriols, M.[1,2], García-Briega, M. I.[1,2], Tolosa, L. [2,3], Costa, C. M. [4,5,6], Lanceros-Méndez, S. [4,5,7,8], Gómez Ribelles, J.L. [1,2], Gallego Ferrer, G. [1,2]

*[1]Centre for Biomaterials and Tissue Engineering (CBIT) Universitat Politècnica de València, 46022 Valencia, Spain*
*[2]Biomedical Research Networking Center on Bioengineering, Biomaterials and Nanomedicine (CIBER-BBN), Valencia, Spain*
*[3]Experimental Hepatology Unit, Health Research Institute La Fe (IIS La Fe), Valencia, Spain*
*[4]Physics Centre of Minho and Porto Universities (CF-UM-UP), University of Minho, 4710-057 Braga, Portugal*
*[5]Laboratory of Physics for Materials and Emergent Technologies, LapMET, University of Minho, 4710-057 Braga, Portugal*
*[6]Institute of Science and Innovation for Bio-Sustainability (IB-S), University of Minho, 4710-057 Braga, Portugal*
*[7]BCMaterials, Basque Center for Materials, Applications and Nanostructures, UPV/EHU Science Park, 48940 Leioa, Spain*
*[8]IKERBASQUE, Basque Foundation for Science, 48009 Bilbao, Spain.*

### Abstract
Mesenchymal stem cells (MSCs) osteogenic commitment before injection enhances bone regeneration therapy results. Piezoelectric stimulation may be an effective cue to promote MSCs pre-differentiation, and poly(vinylidene) fluoride (PVDF) cell culture supports, when combined with $CoFe_2O_4$ (CFO), offer a wireless *in vitro* stimulation strategy. Under an external magnetic field, CFO shift and magnetostriction deform the polymer matrix varying the polymer surface charge due to the piezoelectric effect. To test the effect of piezoelectric stimulation on MSCs, our approach is based on a gelatin hydrogel with embedded MSCs and PVDF-CFO electroactive microspheres. Microspheres were produced by electrospray technique, favouring CFO incorporation, crystallisation in β-phase (85 %) and a crystallinity degree of around 55 %. The absence of cytotoxicity of the 3D construct was confirmed 24 h after cell encapsulation. Cells were viable, evenly distributed in the hydrogel matrix and surrounded by microspheres, allowing local stimulation. Hydrogels were stimulated using a magnetic bioreactor, and no significant changes were observed in MSCs proliferation in the short or long term. Nevertheless, piezoelectric stimulation upregulated RUNX2 expression after 7 days, indicating the activation of the osteogenic differentiation pathway. These results open the door for optimising a stimulation protocol allowing the application of the magnetically activated 3D electroactive cell culture support for MSCs pre-differentiation before transplantation. optimization of a stimulation protocol allowing the application of this magnetically activated 3D electroactive cell culture support for advanced tissue engineering strategies

### Keywords
Mesenchymal stem cells; osteoblastogenesis; piezoelectricity; poly(vinylidene) fluoride; magnetoelectric effect; hydrogel.

## 4.1. Introduction

Mesenchymal stem cells (MSCs) are multipotent stem cells that can be found in a large set of connective tissues, usually isolated from the bone marrow for osteogenic applications. MSCs are characterized by their ability to proliferate *in vitro* as plastic-adherent cells and form colonies, their fibroblastic morphology and their differentiation capacity into bone, cartilage and fat cells (Dominici et al. 2006).

This cell type has held great promise for bone tissue engineering (TE) approaches since it was first described by Friedenstein in 1974 (Friedenstein 1976) and designated as stem cells by Caplan later on (Caplan 1991). TE takes advantage of MSCs poor immunogenicity and their ability to differentiate into osteoblasts to promote the functional repair of injured bone tissue using an autologous, or even allogeneic, cell source.

It has been proven that MSCs osteogenic pre-differentiation prior to transplantation results in an enhancement of mineral deposition and better integration in the damaged site compared to undifferentiated MSCs injection (Peters et al. 2009; Castano-Izquierdo et al. 2006; Ye et al. 2012). MSCs osteogenic differentiation *in vitro* is typically based on the use of osteoinductive cell culture media containing dexamethasone, β-glycerophosphate and ascorbic acid in a tissue culture plate. This approach lacks specificity and can produce mixed populations containing fat cells due to the off-target effects of some medium components, such as dexamethasone (Ghali et al. 2015). Biochemical pre-treatment or priming does not preserve the osteogenic phenotype once the stimulus is removed unless cells are deployed with an extracellular matrix (ECM) resembling environment (Hoch et al. 2016).

Physical cues have emerged as suitable candidates for MSCs differentiation control (Chen et al. 2018; Hwang et al. 2015; Khaw et al. 2021; Tsimbouri et al. 2014; Nikukar et al. 2013). Biophysical stimulation has demonstrated to be more specific, solving the off-target problem of dexamethasone supplementation (Hodgkinson et al. 2021). On the other hand, these cues can be applied using three-dimension (3D) cell culture supports that resemble the native extracellular matrix and recapitulate aspects of the *in vivo* niche, solving two of the main drawbacks of current MSCs osteogenic priming procedure.

MSCs are the main effectors of bone tissue regeneration, migrating to the injured site in response to inflammatory cytokines. MSCs *in vivo* differentiation process takes place in an electrically active environment due to the presence of collagen type I fibers that conform 90 % of bone's organic ECM (Minary-Jolandan and Yu 2009). -NH- and -CO- groups participating in amino acid amide bonds generate a permanent polarization in the fibers, producing a change in the surface charge when a mechanical stress is applied, thus, a piezoelectric effect (Rajabi, Jaffe, and Arinzeh 2015). This bioelectricity produced under mechanical stimulation at the macro and nanoscale has been associated with bone's ability to grow and remodel (Marino and Becker 1970; A. C. Basset and Pawluk 1964). And so, it has been proposed as a key factor to induce MSCs differentiation towards the osteogenic lineage.

Piezoelectric biomaterials have emerged as candidates to induce MSCs osteoblastogenesis reproducing bone's inherent piezoelectricity. Among the existent piezoelectric polymers, poly(vinylidene) fluoride (PVDF) has been widely used for TE approaches due to its high piezoelectric coefficient, when crystallized in β-phase, offering an electroactive environment for MSCs growth and differentiation (Pärssinen et al. 2015; Sobreiro-Almeida et al. 2017; Damaraju et al. 2017; Fernandes et al. 2019; Zhou et al. 2016, 2019). Even so, PVDF absence of functional groups hinders its functionalization, requiring the application of complex protocols to generate biomimetic environments for cell culture (Guillot-Ferriols et al. 2020, 2021).

Transferring piezoelectric stimulation to MSCs at cell culture level has been achieved using different bioreactors, comprising ultrasound activation (Cafarelli et al. 2021; Yang et al. 2020; Fan et al. 2020), mechanical deformation (C. Ribeiro et al. 2015, 2012) or dynamic compression (Zhou et al. 2019; Damaraju et al. 2017; Huang et al. 2004). Magnetic bioreactors can be used when the piezoelectric polymer is combined with magnetostrictive nanoparticles in the form of composite materials. The magnetic bioreactor induces an alternating magnetic field producing a mechanical deformation in the magnetostrictive phase, resulting in a dielectric polarization variation ascribable to the piezoelectric properties of the polymer, known as magnetoelectric effect (Baji et al. 2014; Maceiras et al. 2015). Coupling of piezoelectric PVDF and magnetostrictive CFO has proven to be effective to provide electrical stimulation under the influence of a magnetic field (Gonçalves, Martins, Correia, et al. 2015; Gonçalves, Martins, Moya, et al. 2015; Fernandes et al. 2019), which is a suitable approach also for translational applications, based on the wireless nature of the magnetic field, allowing minimally invasive stimulation strategies.

We hypothesise that piezoelectric stimulation may induce specific MSCs osteogenic commitment for pre-differentiation approaches by using an electroactive and biomimetic cell culture platform. To prove our hypothesis, we have designed a 3D platform based on a gelatin hydrogel containing PVDF-CFO electroactive microspheres together with MSCs, stimulable using a magnetic bioreactor. To do so, PVDF microspheres with and without CFO have been produced, characterised, and encapsulated in the hydrogel. Effects of piezoelectric stimulation on MSCs proliferation and osteogenic differentiation have been tested by metabolic activity, gene expression and alkaline phosphatase production. The study of gene expression and an early osteogenic marker, such as alkaline phosphatase, at 7 and 14 days allows a quick evaluation of cell commitment. They provide a starting point to adjust several variables that may affect the stimulation outcome (cell culture media, stimulation parameters and times).

As far as the authors know, this is the first time that this kind of platform has been described to study the effect of piezoelectric stimulation on MSCs' osteogenic pre-differentiation in vitro before cell transplantation. We have generated an electroactive and biomimetic environment that recapitulates several aspects of the bone niche. Gelatin hydrogels are easily processable for cell recovery after stimulation, obtaining a population of committed MSCs for regeneration therapies alone or in combination with a biodegradable scaffold.

## 4.2. Materials and methods

### 4.2.1. Microsphere production by electrospray technique

PVDF microspheres with and without magnetostrictive nanoparticles were obtained by electrospray technique, adapting the protocol from references (Correia et al. 2014; Gonçalves, Martins, Correia, et al. 2015). A 9 % (w/v) PVDF (Solef® 6010 PVDF Homopolymer, Solvay) solution was prepared by dissolving the polymer in a mixture 85/15 (v/v) of N,N-dimethyl formamide ((DMF) synthesis grade, Scharlab) and tetrahydrofuran ((THF) synthesis grade, Scharlab) at room temperature for 2 hours. The composite solution was prepared by dispersing Cobalt Ferrite Oxide (CFO) nanoparticles (Nanoamor, 35-55 nm diameter) at a concentration of 20 % (w/w) in DMF solvent containing 1 % (v/v) Triton X-100 (Sigma-Aldrich) to prevent particle agglomeration. A high-performance dispersing machine (ULTRA-TURRAX ®, IKA) at 6500 rpm was used to disperse the CFO for 30 minutes and thereafter PVDF (4 % w/v) and THF solvent were added. PVDF concentration was reduced for PVDF-CFO microsphere manufacturing due to the presence of the MNPs in the solution, which produced an increase in viscosity and in the dielectric constant. The mixture was stirred for another hour, until complete dissolution of the polymer.

The solutions were placed in a commercial plastic syringe fitted with a steel needle of 1.7 mm inner diameter. Electrospray was conducted by applying a voltage of 20 kV with a high voltage power supply (Glassman High Voltage, Inc.). A syringe pump (SyringePump) was used to drive the fluid trough the tip at a rate of 2 mL/h. Microspheres were collected in a grounded conductive aluminum collector immersed in a bath of liquid nitrogen (McCann, Marquez, and Xia 2006) placed at 20 cm from the needle tip. For the composite solution, the content of the syringe was replaced every 20 minutes, to avoid nanoparticle precipitation. Microspheres were rinsed with ethanol, sonicated in an ultrasound bath and sieved with a 40 μm strainer to eliminate polymer aggregates.

### 4.2.2. Microsphere characterization

#### 4.2.2.1. Field Emission Electron Microscopy

Microspheres were morphologically characterized by means of field emission scanning electron microscopy (FESEM) (AURIGA compact, Zeiss) with an accelerating voltage of 2 kV. Samples were coated with platinum following a standard sputtering protocol for 90 s (JFC 1100, JEOL).

For observation of nanoparticle distribution, PVDF-CFO microspheres were cross-sectioned using a focused ion beam (FIB) device coupled to FESEM, and images were taken after sectioning.

Microsphere diameter was assessed from FESEM images. At least 700 microspheres from three independent batches were measured using ImageJ software (National Institutes of Health, USA).

#### 4.2.2.2. Vibrating sample magnetometer

Magnetic properties and nanoparticle content in the PVDF-CFO microspheres were determined using a Microsense 2 Tesla vibrating sample magnetometer (VSM). Magnetization loops M(H) were evaluated up to ± 18 kOe, and pure CFO saturation magnetization value (60 emu/g) was compared to the one obtained in the composite

samples, to obtain the effective filler content in the microspheres, by means of Eq. (1) (Gonçalves, Martins, Correia, et al. 2015):

$$CFO\ wt\ \% = \frac{Saturation\ magnetization\ microspheres}{Saturation\ magnetization\ pure\ CFO}\ x\ 100 \qquad \text{Eq. 1}$$

Measurements were taken from samples produced in three different batches.

#### 4.2.2.3. Fourier Transform Infrared Spectroscopy

Fourier transform infrared spectroscopy (FTIR) has proven to be an effective technique to determine the electroactive phase content of PVDF. Gregorio and Cestari (Gregorio and Cestari 1994) described a method based on the identification of representative absorption bands at 840 $cm^{-1}$ and 762 $cm^{-1}$, which correspond to the β and α phase, respectively, and their quantification applying Eq. (2):

$$F(\beta) = \frac{A_\beta}{\left(K_\beta / K_\alpha\right)A_\alpha + A_\beta} \qquad \text{Eq. 2}$$

Assuming Lambert-Beer's law $K_\alpha$ and $K_\beta$ are the characteristic absorption coefficients at the characteristic wavenumbers of the α and β-phases (762 and 840 $cm^{-1}$, respectively). These data were obtained from reference (Gregorio and Cestari 1994) where pristine α or β-phase samples were analysed, obtaining values of $6.1 \times 10^4$ and $7.7 \times 10^4$ $cm^2/mol$, respectively. $A_\alpha$ and $A_\beta$ are the obtained absorbances at 762 and 840 $cm^{-1}$, respectively, measured with an ALPHA FTIR spectrometer (Bruker) in ATR mode from 4000 to 400 $cm^{-1}$ at a wavelength resolution of 4 $cm^{-1}$.
Measurements were taken from samples produced in three different batches.

#### 4.2.2.4. Differential Scanning Calorimetry

PVDF semicrystalline nature requires its thermal characterization to determine the crystallinity degree ($X_c$). Produced samples were evaluated by differential scanning calorimetry (DSC) in a DSC 8000 (PerkinElmer). A mass of 2-4 mg of microspheres was encapsulated in aluminium pans and heated from 0 °C to 200 °C at a heating rate of 20 °C $min^{-1}$ in a dry nitrogen atmosphere.
Degree of crystallinity was calculated with the obtained data applying Eq. (3) (Martins, Costa, and Lanceros-Mendez 2011):

$$Xc = \frac{\Delta H_m}{w_{PVDF}\ (x\Delta H_\alpha + y\Delta H_\beta)} \qquad \text{Eq. 3}$$

where $\Delta H_m$ is the melting enthalpy of PVDF and PVDF-CFO microspheres measured by DSC and $\Delta H_\alpha$ and $\Delta H_\beta$ are the melting enthalpies of a 100 % crystalline sample in the α and β phases, whose values are 93.07 J/g and 103.4 J/g, respectively (Lovinger, 1981) $w_{PVDF}$ is the mass fraction of PVDF within the microspheres (provided by their magnetic properties), and x and y are the percentage of α and β phases present in the sample, obtained by FTIR measurements.

### 4.2.3. Microsphere polarization

In order to maximize their macroscopic piezoelectric response, microspheres were polarized by corona poling method in a home-made poling chamber. Samples were poled for 60 minutes at 100 °C and ~ 10 kV.

### 4.2.4. Cell response

#### 4.2.4.1. Microsphere and mesenchymal stem cells encapsulation in 3D gelatin injectable hydrogels

Human bone marrow mesenchymal stem cells (PromoCell) together with PVDF (Gel-PVDF) or PVDF-CFO (Gel-PVDF-CFO) microspheres were encapsulated in gelatin hydrogels to generate a 3D cell culture platform.

Gelatin (from porcine skin, gel strength 300, type A, Sigma-Aldrich) was conjugated with tyramine (Sigma-Aldrich) following the protocol described in reference (Moulisová et al. 2017), based on N-hydroxysuccinimide (NHS) (Sigma-Aldrich) and 1-ethyl-3-(3 dimethylaminopropyl) carbodiimide hydrochloride (EDC) (Iris Biotech GmbH) chemistry. Tyramine conjugation allows gelatin enzymatic *in situ* cross-linking as described in reference (Poveda-Reyes et al. 2016).

To obtain the hydrogels, tyramine conjugated gelatin was dissolved at 2 % (w/v) in Calcium-free Krebs Ringer buffer (CF-KRB; 115 mM sodium chloride, 5 mM potassium chloride, 1 mM potassium dihydrogen phosphate, and 25 mM 4-(2-hydroxyethyl)piperazine-1-ethanesulphonic acid)) for 30 minutes at 37 °C. Hydrogels were prepared with 80 % (v/v) of the gelatin solution, 10 % (v/v) horseradish peroxidase ((HRP) Sigma-Aldrich) at 12.5 U/mL (1.25 U/mL in the final volume), and 10 % (v/v) $H_2O_2$ (Sigma-Aldrich) 20 mM (2 mM in the final volume). All solutions were sterile filtered after complete dissolution. 50 μL hydrogels were used for cell culture assays. For hydrogels containing microspheres, those were added at 0.6 % (w/v) concentration. Microspheres were weighted, resuspended in ethanol and placed in an ultrasound bath to avoid agglomeration. Microspheres were sterilized by performing three washes with ethanol 70 % under shaking for 5 minutes each. After sterilization, due to PVDF hydrophobicity, ethanol was gradually replaced by sterile deionized water and microspheres were incubated in a 20 % v/v FBS aqueous solution overnight. Then, microspheres were washed three times with deionized water and were finally resuspended in a solution of HRP/Gel at a volume ratio of 10/80 (mL of HRP/mL of Gel).

MSCs were expanded in basal medium containing Dulbecco's Modified Eagle Medium (DMEM) high glucose (4.5 g/L) (Gibco) supplemented with 10 % (v/v) fetal bovine serum ((FBS) Gibco), 4 mM L-glutamine (Lonza), 1X non-essential aminoacids ((NEAA) Gibco), 1 mM sodium pyruvate (Gibco), 70 U/mL penicillin, 70 μg/mL streptomycin (P/S; Life technologies) and 0.25 μg/mL fungizone (Life technologies), at 37 °C in a humidified atmosphere with 5 % $CO_2$. All experiments were performed at passages not superior to 4. Cells were resuspended at a concentration of 1 x $10^6$ cells/mL in the HRP/Gel solution containing the microspheres, when applicable. 45 μL of cell suspension were cross-linked by adding 5 μL of $H_2O_2$ on each well of a 48 well plate and left in an incubator for 15 min to

ensure hydrogel cross-linking. Once crosslinked, cell culture medium was added. An illustration of the 3D cell culture platform and its components is presented in Scheme 4.1.

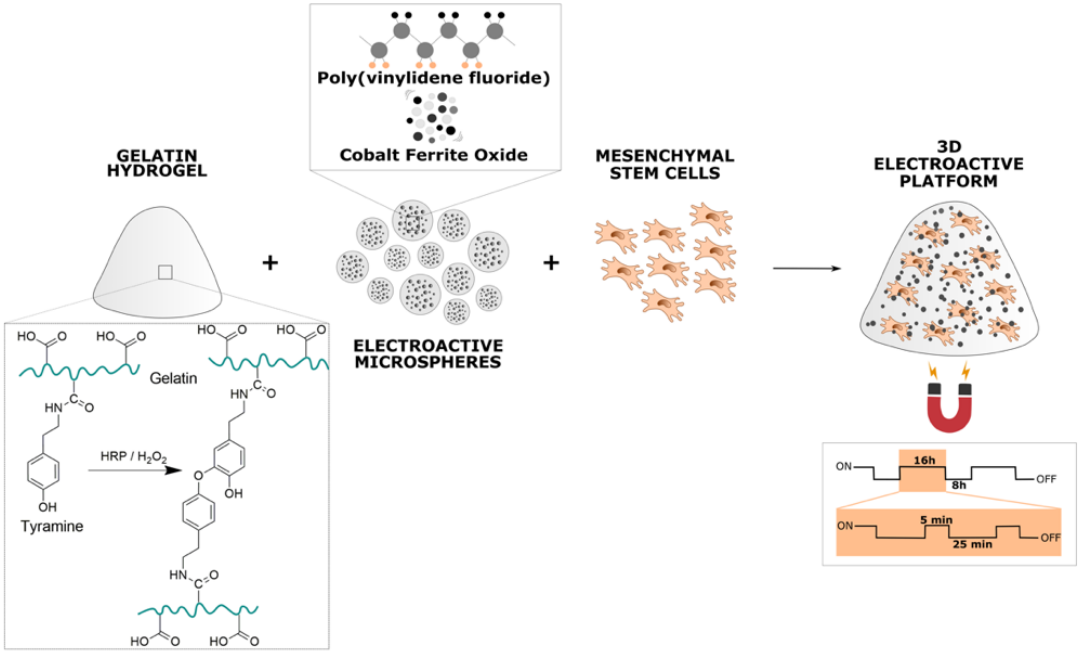


**Scheme 4.1. Illustration of the 3D cell culture platform based on the combination of an injectable gelatin hydrogel and electroactive microspheres of poly(vinylidene) fluoride containing cobalt ferrite oxide. Figure not in scale.**

#### 4.2.4.2. Cell viability assessment

After 24 hours, viability of MSCs encapsulated with PVDF and PVDF-CFO microspheres was evaluated. Hoechst 3342 (1.5 μg/mL, Thermo Fisher) and propidium iodide (1.5 μg/mL, Sigma-Aldrich) were added to the cell culture medium and incubated for 20 minutes at 37 °C. After incubation with fluorescent probes, cells were imaged using the INCELL 6000 Analyzer system (GE Healthcare). Four randomized visual fields per well were analysed and viability was determined using ImageJ software and applying Eq. (4):

$$Viability\ (\%) = \frac{blue\ counts - red\ counts}{blue\ counts}\ x\ 100 \qquad \text{Eq. 4}$$

Gelatin hydrogels without microspheres (Gel) were used as viability controls

#### 4.2.4.3. Cell spreading and microsphere distribution

Cell spreading and microsphere distribution within the gelatin matrix were evaluated after 1 and 14 days of culture. Hydrogels were fixed in paraformaldehyde 4 % (v/v) for 15 min at room temperature. Subsequently, samples were submerged in sucrose (Sigma-Aldrich) solution 30 % (w/v) overnight, immersed in OCT (Tissue Tek) and stored at -80 °C. Hydrogel sections of 30 μm were obtained using a cryostat (Leica CM 1860 UV) and placed on SuperFrost slides (Thermo Scientific).

Samples were washed twice with Dulbecco's Phosphate Buffer Saline ((DPBS) Gibco) and permeabilized using Triton X-100 (Sigma-Aldrich) 0.1 % (v/v) in DPBS for 10 minutes. Permeabilization solution was removed and samples were washed again twice with DPBS. Slides were incubated with Rhodamine Phalloidin (ActinRed 555 ReadyProbes Reagent, Invitrogen), following manufacturer's instructions, and Hoechst 3342 (1:250) for 1 hour. Slides were finally washed with DPBS and mounting medium was added. Representative images were taken using a fluorescence microscope (Nikon Eclipse 80i). Gelatin hydrogels without microspheres (Gel) were used as controls.

Non-cryosectioned hydrogels were also observed in a confocal microscope (Leica DMI8), following the same staining protocol, and image processing for 3D reconstructions was performed using ImageJ software.

#### 4.2.4.4. Piezoelectric stimulation influence on mesenchymal stem cells proliferation

Influence of piezoelectric stimulation on MSCs proliferation was assessed by analysing cell metabolic activity at day 2, 7, 14 and 21 under static (no applied stimuli) and dynamic (cell culture under magnetic stimulation) conditions. An alternating magnetic field (0-230 Oe) was provided by means of a magnetic home-made bioreactor placed inside the incubator, applying a 0.3 Hz frequency and a 10 mm magnet displacement under the 48 well plate (Castro et al. 2020). The stimulation program was divided into an active period of 16 h based on 5 minutes of magnetic stimulation and 25 minutes of resting time, followed by a non-active period of 8 h, when no magnetic stimulation was applied (Fernandes et al. 2019; S. Ribeiro et al. 2020). A diagram of the magnetic stimulation program can be found in Scheme 4.1.

At the different time points, hydrogels were transferred to a new culture plate and basal medium was replaced for DMEM without phenol red (Sigma-Aldrich) containing the tetrazolium salt MTS (3-(4,5-dimethylthiazol-2-yl)-5-(3-carboxymethoxyphenyl)-2-(4-sulfophenyl)-2H-tetrazolium) (Biovision) at a working dilution of 1:10. Hydrogels were incubated for 1 hour at 37 °C. Thereafter, the supernatant was transferred to a new plate and absorbance at 490 nm was read with a Victor3 microplate reader (PerkinElmer). Gelatin hydrogels without microspheres, stimulated (S) and non-stimulated (NS) were used as controls.

#### 4.2.4.5. Influence of piezoelectric stimulation on mesenchymal stem cells osteogenic differentiation

##### 4.2.4.5.1. Gene expression analysis

To determine the influence of piezoelectric stimulation on MSCs osteogenic differentiation, gene expression of characteristic osteogenic markers was analysed.

Gel-PVDF and Gel-PVDF-CFO hydrogels were seeded and after 24 h of culture in basal medium it was replaced by commercial osteogenic differentiation medium (PromoCell) and stimulated samples were placed in the bioreactor. After 7 and 14 days of culture, hydrogels were digested with collagenase 993 U/mL (Collagenase from Clostridium Histolyticum, Sigma-Aldrich) in DPBS for 30 minutes at 37 °C. Qiazol lysis reagent (Qiagen) and

chloroform (Scharlab) were then added with ratio 5:1 to purify nucleic acids. RNA was purified using an RNA extraction kit (RNeasy Micro Kit, Qiagen) and the obtained concentration was measured by spectrophotometer (Nanodrop ONE, Thermo Scientific). 300 ng of total RNA were reverse transcribed using the Superscript III reverse transcriptase (Invitrogen) and oligo dT primers (Invitrogen), following manufacturer's instructions. Real time qPCR was performed using LightCycler 480 SYBR Green I Master (Roche) in a LightCycler 480 Instrument (Roche) and amplifications were performed for 40 cycles. Primers used for amplification were designed from sequences found in the GeneBank database and are listed in Table S4.1. For normalization glyceraldehyde-3-phosphate dehydrogenase (GAPDH) was used.

Primer sequences were validated by dissociation curve/melt curve analysis. The relative changes in gene expression were calculated by E-method, applying Eq. (5) (Pfaffl 2004):

$$\text{Fold difference} = (E_{target})^{Ct(target)\ calibrator - Ct(target)\ sample} / (E_{normalizer})^{Ct(normalizer)\ calibrator - Ct(normalizer)\ sample} \quad \text{Eq. 5}$$

Where E is the efficiency of the target gene or the normalizer housekeeping gene GAPDH. Non-stimulated Gel-PVDF-CFO hydrogels were used as calibrators. The raw data were transferred using the LC480 conversion software (version 2014) and then PCR efficiency for each pair of primers was calculated by LineReg PCR (version 2021.1) (Ruijter et al. 2009).

#### 4.2.4.5.2. Alkaline phosphatase activity determination

Following the same cell culture protocol as described in section 2.4.5.1, hydrogels were kept in culture for 7 and 14 days and alkaline phosphatase (ALP) activity was assessed using SensoLyte ® pNPP Alkaline Phosphatase Assay Kit (Anaspec). Briefly, hydrogels were digested by adding 200 μL of collagenase 993 U/mL in 1X Assay Buffer for 30 minutes at 37 °C. After digestion, 50 μL of Triton X-100 (Sigma-Aldrich) 1.2 % (v/v) in 1X Assay Buffer were added and samples were incubated 10 minutes at 4 °C in an orbital shaker. Thereafter, samples were centrifuged at 4275 rpm for 10 minutes at 4 °C and the supernatant was used to determine ALP activity following kit's manufacturer instructions. Acellular hydrogels were used as blanks.
ALP activity was normalized against cell metabolic activity determined by MTS assay, following the protocol described in section 4.2.4.4. Non-stimulated Gel-PVDF-CFO hydrogels were used as controls.

### 4.2.5. Statistical analysis

Cell culture experiments were performed, at least, in triplicates and a minimum of two replicates were used per technique. All results were expressed as mean ± standard deviation. Statistical analysis was performed on GraphPad Prism 9 (USA). Non-parametric Kruskall-Wallis and Dunn's multiple comparison test were applied, and a 95 % confidence interval was set to accept significant inter-group differences ($p$-value < 0.05).

## 4.3. Results and discussion

### 4.3.1. Microsphere characterization

PVDF and PVDF-CFO microspheres were produced by electrospray. Electrospray is a one-step technique allowing to produce narrow size distributions of microspheres, overcoming the limitations of emulsion-based approaches. As presented in Figure 4.1a, the produced microspheres show a diameter distribution comprised between 0.5 to 6 μm in the case of PVDF and 0.5 to 4 μm for PVDF-CFO, with mean diameters of 2.46 ± 1.08 and 1.64 ± 0.6 μm, respectively. Differences in size distribution and mean diameters are originated on the different PVDF concentration in the initial solution. The addition of CFO nanoparticles to the PVDF solution increased its electrical properties and viscosity, hindering the droplet formation, so a lower concentrated solution had to be used (Bock et al. 2011). PVDF concentrations from 4 to 10 % (w/v) lead to microsphere production, with increasing diameters, whereas higher concentrations favour fibre formation, as described by Correia et al. (Correia et al. 2014). This concentration range allows a semi-dilute moderate entanglement of the polymer chains, giving rise to round dense microspheres, as the ones presented in Figure 4.1a.

CFO incorporation was assessed cross-sectioning the microspheres by means of FIB. Figure 4.1b shows a representative cross-section image of PVDF-CFO microspheres where CFO nanoparticles are observed, as pointed by white arrows. CFO aggregates are in direct contact with the polymer matrix, allowing the coupling of the magnetostrictive and the piezoelectric phases, favouring the magnetoelectric effect once a magnetic field is applied, as already described by Gonçalves et al. for the same type of microspheres (Gonçalves, Martins, Correia, et al. 2015). The amount of incorporated CFO nanoparticles was determined by vibrating sample magnetometer (VSM) and so, the nanoparticle loss during the manufacturing process is also assessed. The typical hysteresis loop for PVDF-CFO nanocomposites is presented in Figure 4.1c. Comparing saturation magnetization of the analysed sample with pure CFO powder by applying Eq. (2) revealed that CFO final concentration was 7.8 ± 1.8 % (w/w). Composite solution concentration corresponded to a 20 % (w/w), which indicates a MNPs loss of more than 50 % during microsphere production. These results are in agreement with the ones obtained by Gonçalves et al. (Gonçalves, Martins, Correia, et al. 2015) where different concentrations of CFO in the composite solution were compared to the final concentration present in the electrosprayed spheres, revealing that the content in the multiferroic spheres is always lower than in solution, due to the higher density of the CFO, compared to the polymer matrix, which causes the settling of the nanoparticles on the bottom of the syringe, reducing their content in the microspheres and reaching a plateau maximum concentration.

Characterization of PVDF cell culture supports implies the analysis of their different crystalline phases since PVDF can present five polymorphs (α, β, γ, δ and ε), but not all of them are electroactive. α, β, γ are the most commonly obtained phases by the standard manufacturing techniques. Piezoelectric stimulation of different cell types requires the presence of an electrically active phase, thus β-phase crystallization is usually preferred due to its high piezoelectric coefficient. The vibrational spectra of PVDF polymorphic polymers via FTIR has been validated for phase identification (Cai et al. 2017).

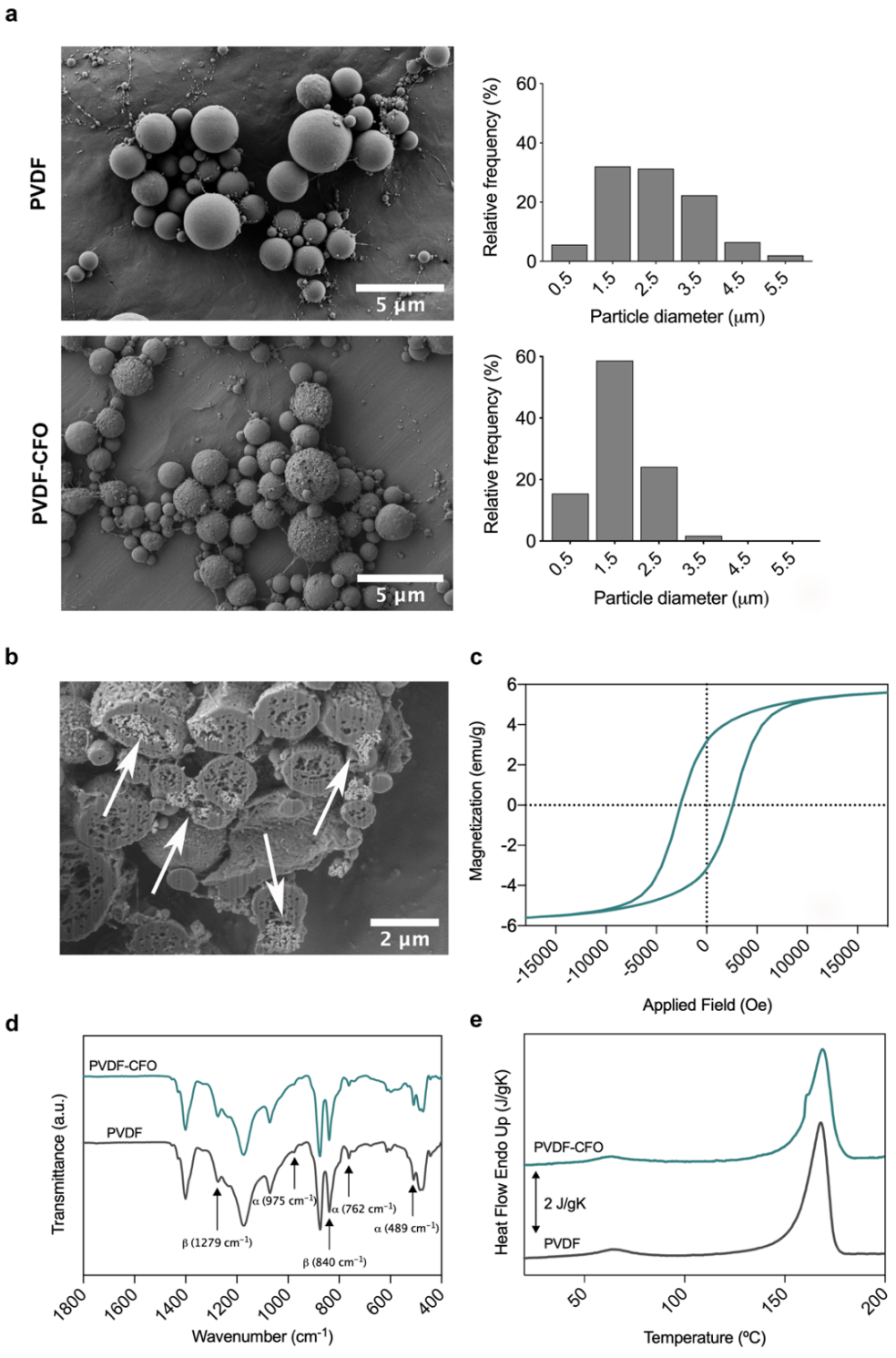


**Figure 4.1. Physical characterization of PVDF and PVDF-CFO electrosprayed microspheres. a) FESEM images of PVDF and PVDF-CFO microspheres and their corresponding diameter frequency distribution. Scale bar 5 µm b) Cross-section image of PVDF-CFO microspheres showing the presence of CFO nanoparticles embedded in the polymer matrix. Scale bar 2 µm c) Room temperature hysteresis loop of PVDF-CFO microspheres. d) FTIR-ATR spectra of**

**PVDF and PVDF-CFO microspheres. e) DSC heating thermograms of PVDF and PVDF-CFO microspheres.**

The method is based on the identification of absorption peaks that exclusively appear in one of the phases. In the case of the α-phase, the non-electroactive one, its characteristic peaks are around 410, 489, 532, 614, 762, 795, 854, 975, 1149, 1209, 1383 and 1423 $cm^{-1}$, being 762 $cm^{-1}$ the one used to unequivocally identify it (Cai et al. 2017; Martins, Lopes, and Lanceros-Mendez 2014).

In the case of the electrically active phases β and γ, their identification by means of FTIR has been a matter of debate in the recent years. Traditionally, the peak around 840 $cm^{-1}$, present in the studied samples (Figure 4.1d), has been considered a characteristic β-phase peak. Nevertheless, it has been recently accepted that this band is common to both polymorphs, but it is just a strong band for the β-phase. For the γ-phase, it appears as a shoulder of the 833 $cm^{-1}$ band (Boccaccio et al. 2002; Imamura, Silva, and Gregorio 2008). To clearly distinguish between these two polymorphs, the bands at 1279 and 1234 $cm^{-1}$, which are exclusive of β and γ phases, respectively, can be consistently used (Cai et al. 2017).

The representative FTIR-ATR spectra of both types of microspheres are displayed in Figure 4.1d, showing α-phase characteristic bands at 489, 762 and 975 $cm^{-1}$, as highlighted in the graph. The existence of the β-phase in the microspheres can be corroborated by the presence of the band at 1279 $cm^{-1}$, exclusive of this polymorph, and of course, the strong band at 840 $cm^{-1}$, used to quantify the percentage of the crystalline phase in the samples applying Eq. (2). Quantification revealed that the percentages of β-phase in PVDF and PVDF-CFO microspheres were 84.8 ± 2.9 % and 84.6 ± 3.3 %. The crystallization of β-phase during electrospray process is due to the processing at temperatures below 70 °C which favours polymer crystallization in this electroactive phase (Gregorio and Cestari 1994; Sencadas, Gregorio Filho, and Lanceros-Mendez 2006). The high voltage applied to the initial solution and high stretching ratio of the jet (Davis et al. 1978) and the incorporation of fillers in the PVDF matrix (Martins, Costa, and Lanceros-Mendez 2011) can also contribute to improve β-phase content, but in the present case, those effects are negligible when compared to the effect of the solvent evaporation temperature (C. Ribeiro et al. 2018). Finally, thermal properties of the electrosprayed microspheres were investigated by means of differential scanning calorimetry (DSC). Since PVDF is a semi-crystalline polymer, its crystalline regions are immersed in an amorphous polymer matrix and the degree of crystallinity ($X_c$) can be calculated from the obtained melting enthalpies applying Eq. (3). Figure 4.1e shows the presence of endothermic peaks around 170 °C. Melting temperatures ($T_m$) corresponding to PVDF and PVDF-CFO microspheres were similar, being 167.9 and 168.8 °C, respectively. The main difference between both thermograms was the presence of a double endothermic peak in the samples containing magnetostrictive nanoparticles. This double peak can be attributed to crystalline imperfection, since the presence of CFO can generate crystal defects in the sample. These data correlate with the $X_c$, being higher in PVDF microspheres (58 %) compared to PVDF-CFO (54 %). As described by Martins et al. (Martins, Costa, and Lanceros-Mendez 2011) composite

materials tend to have a lower degree of crystallinity compared to pristine PVDF due to the presence of CFO.

### 4.3.2. Human mesenchymal stem cells viability and distribution within the 3D construct

PVDF or PVDF-CFO microspheres and MSCs were encapsulated in gelatin hydrogels to generate an injectable electroactive 3D cell culture platform. MSCs viability was evaluated after 24 h of encapsulation, since CFO has proven to be cytotoxic for this cell type (Moise et al. 2017). Figure 4.2a shows representative images of hydrogels, where MSCs nuclei were stained with Hoechst and dead cells nuclei with propidium iodide. Gel-PVDF and Gel-PVDF-CFO hydrogels images show the presence of the microspheres, which appear as black dots in the case of the ones containing ferrite. After quantification (Figure 4.2b) no significant differences were observed compared to the gelatin hydrogels without microspheres, used as viability control (Vaca-González et al. 2020). These results revealed, on the one hand, that the magnetostrictive nanoparticles were enclosed inside the polymer matrix, reducing their cytotoxicity, and not affecting MSCs viability. On the other hand, the inclusion of electroactive microspheres inside the gelatin hydrogel was successful, resulting in a viable 3D cell culture platform that could be used to stimulate MSCs.

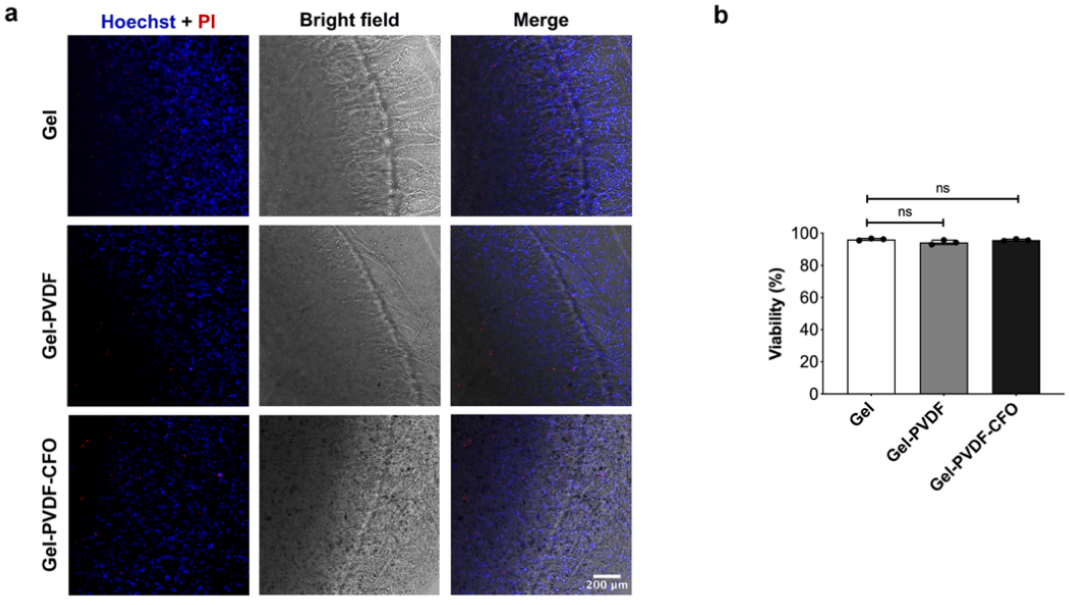


**Figure 4.2. Viability assessment of MSCs encapsulated in gelatin hydrogels (Gel), gelatin hydrogels containing PVDF (Gel-PVDF) or PVDF-CFO (Gel-PVDF-CFO) microspheres after 24 h in culture. a) Representative fluorescence microscope images of cell nuclei (Hoechst - blue) and dead cell nuclei (propidium iodide-red) merged with hydrogel brightfield images. Scale bar 200 μm. b) Quantification of cell viability (n=3). Statistical differences were determined by non-parametric Kruskal-Wallis and Dunn's multiple comparison test.**

This is not the first time that a hydrogel-based magnetoelectric microenvironment has been described for cell stimulation. Hermenegildo et al. (Hermenegildo et al. 2019) used methacrylated Gellan Gum to encapsulate PVDF-CFO microspheres, nevertheless, cells

were not embedded in the hydrogels, but were seeded on the surface reducing the effect of the local piezoelectric stimulation. In a similar way, Carvalho et al (Carvalho et al. 2020) used the same type of hydrogel but combined with poly-L-lactic acid (PLLA)-CFO microspheres. In these case cells were both seeded on the surface and also injected inside the hydrogels to generate a 3D environment.

After assessing MSCs viability, a closer look into cell spreading and distribution within the hydrogel was taken by cryo-sectioning the samples after 1 and 14 days of culture. Figure 4.3 shows an evenly cell distribution along the gelatin matrix in every type of sample. In the case of the hydrogels containing microspheres, these appear also uniformly distributed, surrounding the cells and assuring a local electromechanical stimulation. Regarding cell spreading, after 24 h cells show a rounded morphology with a scarcely developed cytoskeleton. Nevertheless, after 14 days in culture MSCs present a fibroblastic morphology with a spindled-shape, characteristic of this cell type in adherent substrates.
Gelatin is a molecular derivative of type I collagen, although less organized, it is biocompatible, cheaper and preserves the linear tripeptide Arginine-Glycine-Aspartate (RGD) recognition sequence that binds to several integrin proteins promoting cell attachment, migration, and survival (Bello et al. 2020), as demonstrated by the images taken after 14 days. MSCs encapsulation in a gelatin hydrogel provides the biological active cues lacking in PVDF chemical structure, avoiding PVDF surface modification, in a 3D environment allowing ECM-cell and cell-cell interaction.

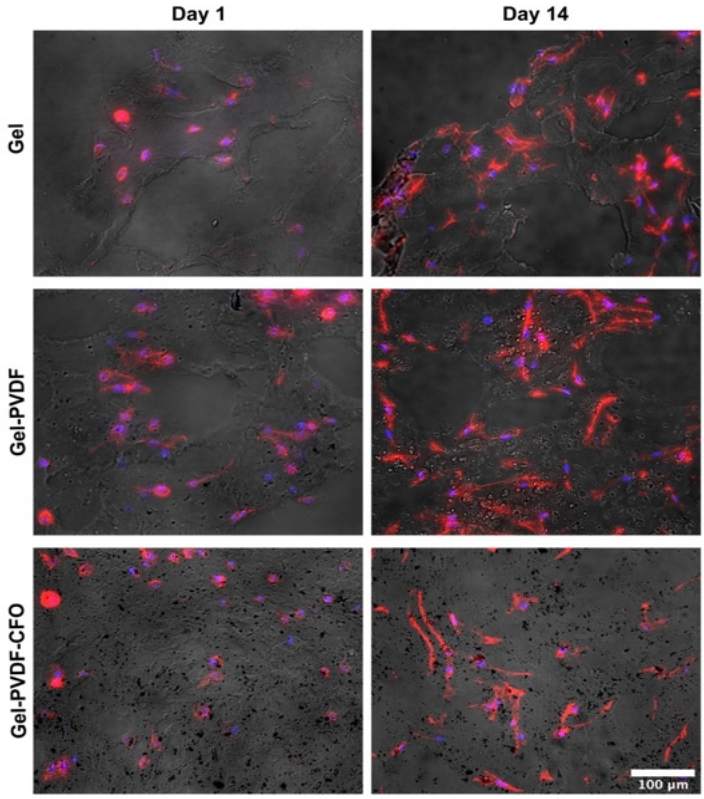


**Figure 4.3. Representative fluorescence images of Gel, Gel-PVDF and Gel-PVDF-CFO cryo-sectioned hydrogels merged with hydrogel brightfield images after 1 and 14 days of static culture. Actin cytoskeleton appears in red and cell nuclei in blue. Scale bar 100 µm.**

These results are supported by Figure S4.1, where a 3D reconstruction of a non-cryo-sectioned Gel-PVDF hydrogel is shown (see Z projections in supporting information). In their interior, MSCs are completely elongated and forming a 3D interconnected network.

### 4.3.3. Effect of piezoelectric stimulation on mesenchymal stem cells proliferation and osteogenic differentiation

Proliferation of MSCs was determined after 2, 7, 14 and 21 days in static (non-stimulated) and dynamic (stimulated) conditions. Gelatin hydrogels without microspheres were used as controls to evaluate the effect of the magnetic field itself, generated by the bioreactor. Each condition tested, Gel, Gel-PVDF and Gel-PVDF-CFO was compared with its stimulated counterpart and the rest of the conditions at every time point. Gel-PVDF-CFO stimulated condition is the only one able to provide piezoelectric stimulation, due to the presence of the magnetostrictive nanoparticles and the magnetic field.

As presented in Figure 4.4a, no significant differences in proliferation are observed after, 2, 7 and 14 days. A significant change in proliferation can be noted after 21 days between Gel NS and Gel-PVDF-CFO S. Nevertheless, no rise nor decrease in proliferation is observed when comparing Gel-PVDF-CFO stimulated and non-stimulated condition at any of the studied times. Since there is no difference between Gel NS and S hydrogels it can be assumed that the magnetic field generated by the bioreactor has no influence on MSCs proliferation. In the same way, the lack of significant difference in Gel-PVDF-CFO NS and S demonstrates that piezoelectric stimulation has no influence, either positive or negative, in MSCs proliferation using this 3D cell culture support and with the applied stimulation parameters.

These results are different to the ones obtained by Fernandes et al. (Fernandes et al. 2019) where an increase in cell proliferation was observed after 4 days when comparing static and dynamic conditions. Although they used a 3D scaffold and stimulation parameters applied were the same, the study was performed using MC3T3-E1 pre-osteoblast cells, a different cell type that might respond in a different way to piezoelectric stimulation. Carvalho et al (Carvalho et al. 2020) also described an increase in proliferation after 3 days when using a combination of a gelatin hydrogel with embedded PLLA-CFO microspheres stimulated with similar parameters, compared with non-stimulated samples. Even though the cell culture platform is similar to the one here described, they also used MC3T3-E1 cell line, which, as already mentioned, can respond different to this kind of stimulation.

Differences between time points, thus the increase or decrease in proliferation between 2, 7, 14 and 21 days within the same hydrogel composition, were also assayed but no significant changes were found, meaning that there is no proliferation observed over time in any type of hydrogel. This phenomenon was also observed by Moulisová et al. (Moulisová et al. 2017), not showing MSCs proliferation in gelatin hydrogels when using basal medium after a period of 14 days. In our case, the presence of microspheres alone or its combination with a magnetic field inducing electromechanical stimulation in the 3D support does not alter MSCs proliferation behaviour in the gelatin matrix.

The effect of electromechanical stimulation on MSCs osteogenic differentiation was tested after 7 and 14 days in culture by analysing gene expression of characteristic osteogenic markers and ALP activity. For differentiation assays, electromechanical stimulation was combined with commercial osteogenic medium.

Figure 4.4b shows the relative expression of ALP, COL I and RUNX2 at 7 days of culture, and ALP, COL I and OCN at 14 days. As can be seen in the graph, there are significant differences in the expression of the early osteogenic marker RUNX2 at day 7 when comparing Gel-PVDF-CFO stimulated and non-stimulated samples. Nevertheless, no expression differences are observed in mid-stage markers ALP and COL I. After 14 days it is surprising to find that not only there is no increase in the expression in the Gel-PVDF-CFO S condition, but there is a rise in the expression of COL I in Gel-PVDF S, which is under the influence of the magnetic field, but where no electromechanical stimulation is experienced since it does not contain magnetostrictive nanoparticles. These expression results are in agreement with the ones obtained for the ALP activity at a protein level (Figure 4.4c). At 7 days of culture no differences in ALP activity are observed between the studied conditions, as is the case for the ALP gene expression at the same time point.

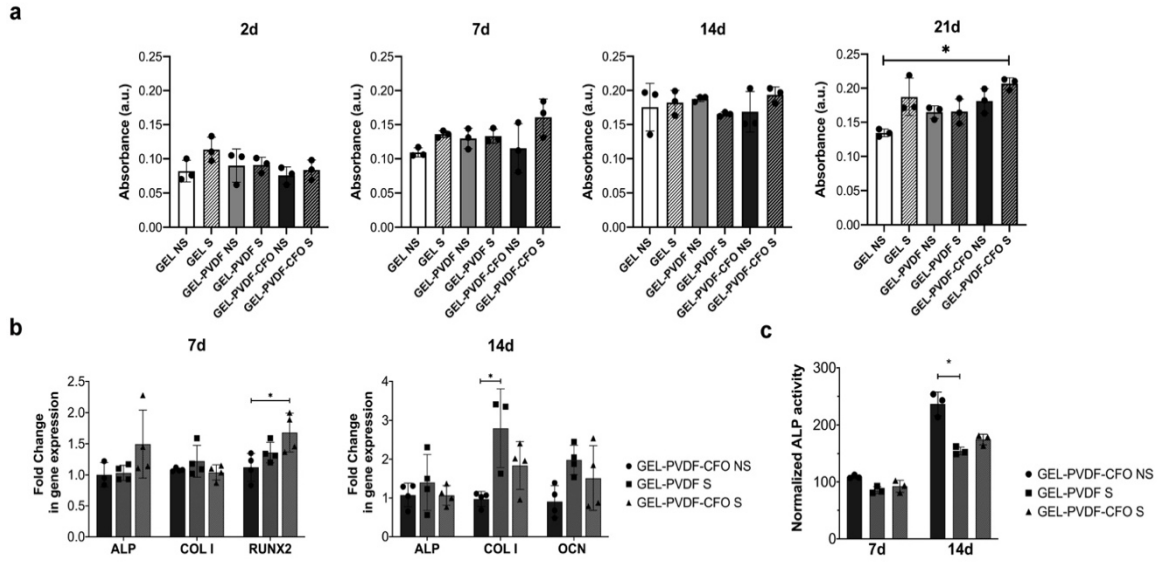


**Figure 4.4. Effect of electromechanical stimulation on MSCs proliferation and differentiation in non-stimulated (NS) and stimulated (S) conditions. a) MTS assay at short and long term (2, 7, 14 and 21 days). Graphs show significant differences for each time point between different hydrogel compositions (n=3). Differences between time points for the same hydrogel composition were also assayed but no significant changes were found. b) Relative gene expression of characteristic osteogenic markers (Alkaline phosphatase (ALP), collagen type I (COL I), Runt-related transcription factor 2 (RUNX2) and osteocalcin (OCN)) after 7 and 14 days of culture (n=4). Glyceraldehyde-3-phosphate dehydrogenase (GAPDH) was used to normalise gene expression c) ALP activity determination after 7 and 14 days of culture (n = 3). Circles correspond to data collected for Gel-PVDF-CFO NS, squares for Gel-PVDF S and triangles represent Gel-PVDF-CFO S samples, for both b) and c) graphs. All statistical**

**differences were determined by non-parametric Kruskal-Wallis and Dunn's multiple comparison test. * indicates p-value < 0.05.**

However, after 14 days, there is an increase in ALP activity in the non-stimulated condition compared to Gel-PVDF S and Gel-PVDF-CFO S, which does not match the results obtained for gene expression levels at this time point, where no differences are observed. It is possible that the analysis of gene expression at only two time points may have missed ALP expression peak, which is usually reported after 10 days of culture and after that, the differences are only shown in ALP activity at protein level after 14 days.

RUNX2 is a key transcriptional regulator of osteoblast differentiation and bone formation. Its activation by phosphorylation in MSCs leads to osteogenic commitment and the subsequent expression of downstream genes involved in the differentiation process such as alkaline phosphatase, collagen type I, osteopontin and osteocalcin (Rahman et al. 2015). Piezoelectric stimulation in the proposed 3D cell culture platform is able to activate the osteogenic differentiation pathway with an increased expression of the master regulator RUNX2, nevertheless this effect is not sustained in time. The following expression of mid-stage markers such as ALP and COL I is not enhanced, and neither is the ALP activity.

Several factors may influence the effect of piezoelectric stimulation on MSCs differentiation towards the osteogenic lineage (Guillot-Ferriols et al. 2022). Selection of cell culture media, stimulation parameters and treatment times are non-trivial choices when designing stimulation experiments. The lack of a standardized stimulation protocol for MSCs makes the comparison difficult between published results.

Regarding stimulation parameters, the use of different bioreactors for the activation of piezoelectric substrates comprises the use of different stimulation parameters in literature. Treatment times are also a matter of debate when stimulating MSCs for differentiation. In this work, a stimulation program divided into an active period of 16 h based on 5 minutes of magnetic stimulation and 25 minutes of resting time, followed by a nonactive period of 8 h, was selected to simulate human daily activity. Stimulation was applied for the total duration of the culture. Again, despite the influence that treatment time may have in a highly orchestrated and time-dependent process such as osteoblastogenesis no studies have been published on its optimization when using piezoelectric cell culture supports. Other types of electrical stimulation, the one using conductive cell culture supports and an external power generator, have explored the effectiveness of diverse factors regarding treatment time. First, stimulation time per day, thus, the number of hours that cells are subjected to stimulation each culture day, second, the number of days those cells receive the stimulation along the duration of the culture and last, the moment where the stimulation is introduced (early, mid or late stages).

Wechsler et al. (Wechsler, Hermann, and Bizios 2016) demonstrated that for MSCs cultured in indium tin oxide-coated glass the optimal stimulation time per day was 6 hours rather than shorter (1-3 hours) and longer (24 hours). On another note, Zhu et al. (Zhu et al. 2017) artificially divided the 21-day culture time into 7-day periods and applied ES for 1.5 hours a day for the selected period. Day 1 to 7 stimulation resulted in an improved expression of

MSCs bone related markers rather than application from day 8 to 14 and 15 to 21. This corroborates the results obtained by Hu at al. (Hu et al. 2019) where stimulation was applied for 4 h on a selected day (day 0, 2, 4, 6, 8, 10 and 12) demonstrating that day 8 was the optimal one since MSCs showed a higher level of mineral deposition after 14 days, supported by the upregulation of osteogenic genes.

These data reveal that stimulation application for osteogenic differentiation induction is a time-dependent process and if optimized it should only be applied at specific time-points. In this case, application along the culture may have a detrimental effect in the differentiation process, as shown by the results in gene expression and ALP activity after 14 days, where no improvement is seen in electromechanical stimulated conditions.

Finally, media selection in combination with electromechanical stimulation may influence the result. In this work, commercial osteogenic medium was used, nevertheless MSCs osteogenic fate determination has been widely reported as a result of using piezoelectric biomaterials as cell culture supports in the presence of growth medium (X. Zhang et al. 2016; C. Zhang et al. 2018; Zhou et al. 2016, 2019; Yu et al. 2017; Yang et al. 2020; Li et al. 2017). The strong effect of biochemical inducers present in the osteogenic medium may have covered the effect of piezoelectric stimulation. Even so, this physical cue combined with osteogenic medium is able to trigger RUNX2 expression in a greater extent than osteogenic induced non-stimulated samples.
These results leave room for improvement and open the door for future optimization of the stimulation protocol, regarding treatment times and parameters. The study of different cell culture media may also be beneficial for the use of this biomimetic and biocompatible 3D piezoelectric cell culture platform in bone tissue engineering approaches.

## 4.4. Conclusions

PVDF and PVDF-CFO microspheres were produced by electrospray, a reliable technique that allows PVDF crystallization in β-phase, its most electroactive polymorph. The produced PVDF-CFO microspheres incorporated CFO nanoparticles in their interior, without compromising their crystallinity degree, which was similar to the one obtained in the ones non-containing magnetostrictive nanoparticles. Microspheres, together with MSCs, were successfully encapsulated in a tyraminated gelatin hydrogel, generating a 3D cell culture platform. This platform resulted non cytotoxic for MSCs, meaning that the CFO was well enclosed in the microsphere polymer matrix. MSCs and microspheres were evenly distributed in the gelatin matrix after 1 day of culture allowing local stimulation. After 14 days MSCs showed a well-developed cytoskeleton with fibroblastic-like shape, forming an interconnected 3D network when cultured in expansion medium and no stimulation. Magnetically induced piezoelectric stimulation had no influence, either positive or negative, on MSCs proliferation in the proposed 3D cell culture platform. Regarding MSCs osteogenic differentiation, combination with osteogenic medium revealed an increase of RUNX2 expression after 7 days compared to non-stimulated samples, indicating a stronger activation of the osteogenic differentiation pathway.

## 4.5. Acknowledgements

This work was supported by the Spanish State Research Agency (AEI): GGF acknowledges support of the PID2019-106000RB-C21 / AEI / 10.13039/501100011033 project; JLGR and SLM acknowledge support of the PID2019-106099RB-C41 and –C43 / AEI / 10.13039/501100011033 projects. The CIBER-BBN initiative is funded by the VI National R&D&I Plan 2008-2011, Iniciativa Ingenio 2010, Consolider Program. CIBER actions are financed by the Instituto de Salud Carlos III with assistance from the European Regional Development Fund. MGF received government funding for her Doctoral Thesis [Grant Number BES-2017-080398FPI]. The authors thank FCT (Fundação para a Ciência e a Tecnologia) for financial support under the framework of Strategic Funding grant UID/FIS/04650/2021, projects PTDC/FIS-MAC/28157/2017 and POCI-01-0145-FEDER-007688) and contract under the Stimulus of Scientific Employment, Individual Support 2020.04028 CEECIND (CMC).

## 4.6. References

Baji, A., Y. W. Mai, R. Yimnirun, and S. Unruan. 2014. “Electrospun Barium Titanate/Cobalt Ferrite Composite Fibers with Improved Magnetoelectric Performance.” *RSC Advances* 4 (98): 55217–23. https://doi.org/10.1039/c4ra09449b.

Basset, A. C., and R. J. Pawluk. 1964. “Effets of Electric Currents on Bone in Vivo.” *Nature* 204: 652–54. https://doi.org/10.1038/204652a0.

Bello, A. B., D. Kim, D. Kim, H. Park, and S. H. Lee. 2020. “Engineering and Functionalization of Gelatin Biomaterials: From Cell Culture to Medical Applications.” *Tissue Engineering - Part B: Reviews* 26 (2): 164–80. https://doi.org/10.1089/ten.teb.2019.0256.

Boccaccio, T., A. Bottino, G. Capannelli, and P. Piaggio. 2002. “Characterization of PVDF Membranes by Vibrational Spectroscopy.” *Journal of Membrane Science* 210 (2): 315–29. https://doi.org/10.1016/S0376-7388(02)00407-6.

Bock, N., M. A. Woodruff, D. W. Hutmacher, and T.R. Dargaville. 2011. “Electrospraying, a Reproducible Method for Production of Polymeric Microspheres for Biomedical Applications.” *Polymers* 3 (1): 131–49. https://doi.org/10.3390/polym3010131.

Cafarelli, A., A. Marino, L. Vannozzi, J. Puigmartí-Luis, S. Pané, G. Ciofani, and L. Ricotti. 2021. “Piezoelectric Nanomaterials Activated by Ultrasound: The Pathway from Discovery to Future Clinical Adoption.” *ACS Nano* 15 (7): 11066–86. https://doi.org/10.1021/acsnano.1c03087.

Cai, X., T. Lei, D. Sun, and L. Lin. 2017. “A Critical Analysis of the α, β and γ Phases in Poly(Vinylidene Fluoride) Using FTIR.” *RSC Advances* 7 (25): 15382–89. https://doi.org/10.1039/c7ra01267e.

Caplan, A. I. 1991. “Mesenchymal Stem Cells.” *Journal of Orthopaedic Research* 9 (5): 641–50. https://doi.org/10.1002/jor.1100090504.

Carvalho, E. O., C. Ribeiro, D. M. Correia, G. Botelho, and S. Lanceros-Mendez. 2020. "Biodegradable Hydrogels Loaded with Magnetically Responsive Microspheres as 2D and 3D Scaffolds." *Nanomaterials* 10 (12): 1–12. https://doi.org/10.3390/nano10122421.

Castano-Izquierdo, H., J. Álvarez-Barreto, J. van den Dolder, J. A. Jansen, A. G. Mikos, and V. I. Sikavitsas. 2006. "Pre-Culture Period of Mesenchymal Stem Cells in Osteogenic Media Influences Their in Vivo Bone Forming Potential." *Journal of Biomedical Materials Research Part A* 79 (4): 129–38. https://doi.org/10.1002/jbm.a.31082.

Castro, N., M. M. Fernandes, C. Ribeiro, V. Correia, R. Minguez, and S. Lanceros-Mendez. 2020. "Magnetic Bioreactor for Magneto-, Mechano- and Electroactive Tissue Engineering Strategies." *Sensors* 20 (12): 1–13. https://doi.org/10.3390/s20123340.

Chen, X., J. Yan, F. He, D. Zhong, H. Yang, M. Pei, and Z.-P. Luo. 2018. "Mechanical Stretch Induces Antioxidant Responses and Osteogenic Differentiation in Human Mesenchymal Stem Cells Through." *Free Radical Biology and Medicine* 126: 187–201. https://doi.org/doi:10.1016/j.freeradbiomed.2018.08.001.

Correia, D. M., R. Gonçalves, C. Ribeiro, V. Sencadas, G. Botelho, J. L. Gomez Ribelles, and S. Lanceros-Méndez. 2014. "Electrosprayed Poly(Vinylidene Fluoride) Microparticles for Tissue Engineering Applications." *RSC Adv.* 4 (62): 33013–21. https://doi.org/10.1039/C4RA04581E.

Damaraju, S. M., Y. Shen, E. Elele, B. Khusid, A. Eshghinejad, J. Li, M. Jaffe, and T. L. Arinzeh. 2017. "Three-Dimensional Piezoelectric Fibrous Scaffolds Selectively Promote Mesenchymal Stem Cell Differentiation." *Biomaterials* 149: 51–62. https://doi.org/10.1016/j.biomaterials.2017.09.024.

Davis, G. T., J. E. McKinney, M. G. Broadhurst, and S. C. Roth. 1978. "Electric-Field-Induced Phase Changes in Poly(Vinylidene Fluoride)." *Journal of Applied Physics* 49 (10): 4998–5002. https://doi.org/10.1063/1.324446.

Dominici, M., K. Le Blanc, I. Mueller, I. Slaper-Cortenbach, F. C. Marini, D. S. Krause, R. J. Deans, A. Keating, D. J. Prockop, and E. M. Horwitz. 2006. "Minimal Criteria for Defining Multipotent Mesenchymal Stromal Cells. The International Society for Cellular Therapy Position Statement." *Cytotherapy* 8 (4): 315–17. https://doi.org/10.1080/14653240600855905.

Fan, B., Z. Guo, X. Li, S. Li, P. Gao, X. Xiao, J. Wu, C. Shen, Y. Jiao, and W. Hou. 2020. "Electroactive Barium Titanate Coated Titanium Scaffold Improves Osteogenesis and Osseointegration with Low-Intensity Pulsed Ultrasound for Large Segmental Bone Defects." *Bioactive Materials* 5 (4): 1087–1101. https://doi.org/10.1016/j.bioactmat.2020.07.001.

Fernandes, M. M., D. M. Correia, C. Ribeiro, N. Castro, V. Correia, and S. Lanceros-Mendez. 2019. "Bioinspired Three-Dimensional Magnetoactive Scaffolds for Bone Tissue

Engineering." *ACS Applied Materials and Interfaces* 11 (48): 45265–75. https://doi.org/10.1021/acsami.9b14001.

Friedenstein, A. J. 1976. "Precursor Cells of Mechanocytes." *International Review of Cytology* 47 (C): 327–59. https://doi.org/10.1016/S0074-7696(08)60092-3.

Ghali, O., O. Broux, G. Falgayrac, N. Haren, J. P.T.M. Van Leeuwen, G. Penel, P. Hardouin, and C. Chauveau. 2015. "Dexamethasone in Osteogenic Medium Strongly Induces Adipocyte Differentiation of Mouse Bone Marrow Stromal Cells and Increases Osteoblast Differentiation." *BMC Cell Biology* 16 (1): 1–15. https://doi.org/10.1186/s12860-015-0056-6.

Gonçalves, R., P. Martins, D. M. Correia, V. Sencadas, J. L. Vilas, L. M. León, G. Botelho, and S. Lanceros-Méndez. 2015. "Development of Magnetoelectric CoFe2O4/Poly(Vinylidene Fluoride) Microspheres." *RSC Adv.* 5 (45): 35852–57. https://doi.org/10.1039/C5RA04409J.

Gonçalves, R., P. Martins, X. Moya, M. Ghidini, V. Sencadas, G. Botelho, N. D. Mathur, and S. Lanceros-Mendez. 2015. "Magnetoelectric $CoFe_2O_4$ /Polyvinylidene Fluoride Electrospun Nanofibres." *Nanoscale* 7 (17): 8058–61. https://doi.org/10.1039/C5NR00453E.

Gregorio, R., and M. Cestari. 1994. "Effect of Crystallization Temperature on the Crystalline Phase Content and Morphology of Poly(Vinylidene Fluoride)." *Journal of Polymer Science Part B: Polymer Physics* 32 (5): 859–70. https://doi.org/10.1002/polb.1994.090320509.

Guillot-Ferriols, M., A. del Barrio, C. M. Costa, S. Lanceros Méndez, J. C. Rodríguez-Cabello, J. L. Gómez Ribelles, M. Santos, and G. Gallego Ferrer. 2021. "Effective Elastin-like Recombinamers Coating on Poly(Vinylidene) Fluoride Membranes for Mesenchymal Stem Cell Culture." *European Polymer Journal* 146 (January): 1–10. https://doi.org/10.1016/j.eurpolymj.2021.110269.

Guillot-Ferriols, M., S. Lanceros-Méndez, J. L. Gómez Ribelles, and G. Gallego-Ferrer. 2022. "Electrical Stimulation : Effective Cue to Direct Osteogenic Differentiation of Mesenchymal Stem Cells ?" *Biomaterials Advances* 138 (May): 1–18. https://doi.org/10.1016/j.bioadv.2022.212918.

Guillot-Ferriols, M., J. C. Rodríguez-Hernández, D. M. Correia, S. A. C. Carabineiro, S. Lanceros-Méndez, J. L. Gómez Ribelles, and G. Gallego Ferrer. 2020. "Poly(Vinylidene) Fluoride Membranes Coated by Heparin / Collagen Layer-by-Layer, Smart Biomimetic Approaches for Mesenchymal Stem Cell Culture." *Materials Science & Engineering C* 117: 1–12. https://doi.org/10.1016/j.msec.2020.111281.

Hermenegildo, B., C. Ribeiro, L. Pérez-Álvarez, J. L. Vilas, D. A. Learmonth, R. A. Sousa, P. Martins, and S. Lanceros-Méndez. 2019. "Hydrogel-Based Magnetoelectric

Microenvironments for Tissue Stimulation." *Colloids and Surfaces B: Biointerfaces* 181 (May): 1041–47. https://doi.org/10.1016/j.colsurfb.2019.06.023.

Hoch, A. I., V. Mittal, D. Mitra, N. Vollmer, C. A. Zikry, and J. K. Leach. 2016. "Cell-Secreted Matrices Perpetuate the Bone-Forming Phenotype of Differentiated Mesenchymal Stem Cells." *Biomaterials* 74: 178–87. https://doi.org/10.1016/j.biomaterials.2015.10.003.

Hodgkinson, T., P. M. Tsimbouri, V. Llopis-Hernandez, P. Campsie, D. Scurr, P. G. Childs, D. Phillips, et al. 2021. "The Use of Nanovibration to Discover Specific and Potent Bioactive Metabolites That Stimulate Osteogenic Differentiation in Mesenchymal Stem Cells." *Science Advances* 7 (9): 1–16. https://doi.org/10.1126/sciadv.abb7921.

Hu, W. W., T. C. Chen, C. W. Tsao, and Y. C. Cheng. 2019. "The Effects of Substrate-Mediated Electrical Stimulation on the Promotion of Osteogenic Differentiation and Its Optimization." *Journal of Biomedical Materials Research - Part B Applied Biomaterials* 107 (5): 1607–19. https://doi.org/10.1002/jbm.b.34253.

Huang, C. C-Y, K. L. Hagar, L. E. Frost, Y. Sun, and H. S. Cheung. 2004. "Effects of Cyclic Compressive Loading on Chondrogenesis of Rabbit Bone-Marrow Derived Mesenchymal Stem Cells." *Stem Cells* 22 (3): 313–23. https://doi.org/10.1634/stemcells.22-3-313.

Hwang, J. H., M. R. Byun, A. R. Kim, K. M. Kim, H. J. Cho, Y. H. Lee, J. Kim, M. G. Jeong, E. S. Hwang, and J. H. Hong. 2015. "Extracellular Matrix Stiffness Regulates Osteogenic Differentiation through MAPK Activation." *PLoS ONE* 10 (8): 1–16. https://doi.org/10.1371/journal.pone.0135519.

Imamura, R, A.B. Silva, and Jr Gregorio. 2008. "Gamma to Beta Phase Transformation Induced in Poly(Vinylidene Fluoride) by Stretching." *Journal of Applied Polymer Science* 110: 3242–46. https://doi.org/10.1002/app.

Khaw, J. S., R. Xue, N. J. Cassidy, and S. H. Cartmell. 2021. "Electrical Stimulation of Titanium to Promote Stem Cell Orientation, Elongation and Osteogenesis." *Acta Biomaterialia* 139: 204–17. https://doi.org/10.1016/j.actbio.2021.08.010.

Li, Y., X. Dai, Y. Bai, Y. Liu, Y. Wang, O. Liu, F. Yan, Z. Tang, X. Zhang, and X. Deng. 2017. "Electroactive BaTiO3 Nanoparticle-Functionalized Fibrous Scaffolds Enhance Osteogenic Differentiation of Mesenchymal Stem Cells." *International Journal of Nanomedicine* 12: 4007–18. https://doi.org/10.2147/IJN.S135605.

Lovinger, A.J. n.d. "Poly(Vinylidene Fluoride)." In *Developments in Crystalline Polymers - 1*, edited by D.C Basset, 195–273. Springer Dordrecht. https://doi.org/doi.org/10.1007/978-94-009-7343-5.

Maceiras, A., P. Martins, R. Gonçalves, G. Botelho, E. Venkata Ramana, S. K. Mendiratta, M. San Sebastián, J. L. Vilas, S. Lanceros-Mendez, and L. M. León. 2015. "High-

Temperature Polymer Based Magnetoelectric Nanocomposites." *European Polymer Journal* 64: 224–28. https://doi.org/10.1016/j.eurpolymj.2015.01.020.

Marino, A., and R. O. Becker. 1970. "Piezoelectric Effect and Growth Control in Bone." *Nature* 228: 473–74. https://doi.org/10.1038/228473a0.

Martins, P., C. M. Costa, and S. Lanceros-Mendez. 2011. "Nucleation of Electroactive β-Phase Poly(Vinilidene Fluoride) with CoFe2O4 and NiFe2O4 Nanofillers: A New Method for the Preparation of Multiferroic Nanocomposites." *Applied Physics A: Materials Science and Processing* 103 (1): 233–37. https://doi.org/10.1007/s00339-010-6003-7.

Martins, P., A. C. Lopes, and S. Lanceros-Mendez. 2014. "Electroactive Phases of Poly(Vinylidene Fluoride): Determination, Processing and Applications." *Progress in Polymer Science* 39 (4): 683–706. https://doi.org/10.1016/j.progpolymsci.2013.07.006.

McCann, J. T., M. Marquez, and Y. Xia. 2006. "Highly Porous Fibers by Electrospinning into a Cryogenic Liquid." *Journal of the American Chemical Society* 128 (5): 1436–37. https://doi.org/10.1021/ja056810y.

Minary-Jolandan, M., and M. F. Yu. 2009. "Uncovering Nanoscale Electromechanical Heterogeneity in the Subfibrillar Structure of Collagen Fibrils Responsible for the Piezoelectricity of Bone." *ACS Nano* 3 (7): 1859–63. https://doi.org/10.1021/nn900472n.

Moise, S., E. Céspedes, D. Soukup, J. M. Byrne, A. J. El Haj, and N. D. Telling. 2017. "The Cellular Magnetic Response and Biocompatibility of Biogenic Zinc- and Cobalt-Doped Magnetite Nanoparticles." *Scientific Reports* 7 (November 2016): 1–11. https://doi.org/10.1038/srep39922.

Moulisová, V., S. Poveda-Reyes, E. Sanmartín-Masiá, L. Quintanilla-Sierra, M. Salmerón-Sánchez, and G. Gallego Ferrer. 2017. "Hybrid Protein-Glycosaminoglycan Hydrogels Promote Chondrogenic Stem Cell Differentiation." *ACS Omega* 2 (11): 7609–20. https://doi.org/10.1021/acsomega.7b01303.

Nikukar, H., S. Reid, P. M. Tsimbouri, M. O. Riehle, A. S.G. Curtis, and M. J. Dalby. 2013. "Osteogenesis of Mesenchymal Stem Cells by Nanoscale Mechanotransduction." *ACS Nano* 7 (3): 2758–67. https://doi.org/10.1021/nn400202j.

Pärssinen, J., H. Hammarén, R. Rahikainen, V. Sencadas, C. Ribeiro, S. Vanhatupa, S. Miettinen, S. Lanceros-Méndez, and V. P. Hytönen. 2015. "Enhancement of Adhesion and Promotion of Osteogenic Differentiation of Human Adipose Stem Cells by Poled Electroactive Poly(Vinylidene Fluoride)." *Journal of Biomedical Materials Research - Part A* 103 (3): 919–28. https://doi.org/10.1002/jbm.a.35234.

Peters, A., D. Toben, J. Lienau, H. Schell, H. J. Bail, G. Matziolis, G. N. Duda, and K. Kaspar. 2009. "Locally Applied Osteogenic Predifferentiated Progenitor Cells Are More Effective than Undifferentiated Mesenchymal Stem Cells in the Treatment of Delayed Bone

Healing." *Tissue Engineering - Part A* 15 (10): 2947–54. https://doi.org/10.1089/ten.tea.2009.0058.

Pfaffl, M. W. 2004. "Quantification Strategies in Real-Time PCR." In *A-Z of Quantitative PCR*, edited by S.A. Bustin, 87–112. La Jolla, CA, USA. https://doi.org/10.1029/JA089iA05p02945.

Poveda-Reyes, S., V. Moulisova, E. Sanmartín-Masiá, L. Quintanilla-Sierra, M. Salmerón-Sánchez, and G. Gallego Ferrer. 2016. "Gelatin—Hyaluronic Acid Hydrogels with Tuned Stiffness to Counterbalance Cellular Forces and Promote Cell Differentiation." *Macromolecular Bioscience*, 1311–24. https://doi.org/10.1002/mabi.201500469.

Rahman, M. S., N. Akhtar, H. M. Jamil, R. S. Banik, and S. M. Asaduzzaman. 2015. "TGF-β/BMP Signaling and Other Molecular Events: Regulation of Osteoblastogenesis and Bone Formation." *Bone Research* 3 (November 2014). https://doi.org/10.1038/boneres.2015.5.

Rajabi, A. H., M. Jaffe, and T. L. Arinzeh. 2015. "Piezoelectric Materials for Tissue Regeneration: A Review." *Acta Biomaterialia* 24: 12–23. https://doi.org/10.1016/j.actbio.2015.07.010.

Ribeiro, C., C. M. Costa, D. M. Correia, J. Nunes-Pereira, J. Oliveira, P. Martins, R. Gonçalves, V. F. Cardoso, and S. Lanceros-Méndez. 2018. "Electroactive Poly(Vinylidene Fluoride)-Based Structures for Advanced Applications." *Nature Protocols* 13 (4): 681–704. https://doi.org/10.1038/nprot.2017.157.

Ribeiro, C., S. Moreira, V. Correia, V. Sencadas, J.G. Rocha, F. M. Gama, J. L. Gómez Ribelles, and S. Lanceros-Méndez. 2012. "Enhanced Proliferation of Pre-Osteoblastic Cells by Dynamic Piezoelectric Stimulation." *RSC Advances* 2 (30): 11504. https://doi.org/10.1039/c2ra21841k.

Ribeiro, C., J. Pärssinen, V. Sencadas, V. Correia, S. Miettinen, V. P. Hytönen, and S. Lanceros-Méndez. 2015. "Dynamic Piezoelectric Stimulation Enhances Osteogenic Differentiation of Human Adipose Stem Cells." *Journal of Biomedical Materials Research - Part A* 103 (6): 2172–75. https://doi.org/10.1002/jbm.a.35368.

Ribeiro, S., C. Ribeiro, E. O. Carvalho, C. R. Tubio, N. Castro, N. Pereira, V. Correia, A. C. Gomes, and S. Lanceros-Méndez. 2020. "Magnetically Activated Electroactive Microenvironments for Skeletal Muscle Tissue Regeneration." *ACS Applied Bio Materials* 3 (7): 4239–52. https://doi.org/10.1021/acsabm.0c00315.

Ruijter, J. M., C. Ramakers, W. M.H. Hoogaars, Y. Karlen, O. Bakker, M. J.B. van den hoff, and A. F.M. Moorman. 2009. "Amplification Efficiency: Linking Baseline and Bias in the Analysis of Quantitative PCR Data." *Nucleic Acids Research* 37 (6). https://doi.org/10.1093/nar/gkp045.

Sencadas, V., R. Gregorio Filho, and S. Lanceros-Mendez. 2006. “Processing and Characterization of a Novel Nonporous Poly(Vinilidene Fluoride) Films in the β Phase.” *Journal of Non-Crystalline Solids* 352 (21–22): 2226–29. https://doi.org/10.1016/j.jnoncrysol.2006.02.052.

Sobreiro-Almeida, R., M. Tamaño-Machiavello, E. Carvalho, L. Cordón, S. Doria, L. Senent, D. Correia, et al. 2017. “Human Mesenchymal Stem Cells Growth and Osteogenic Differentiation on Piezoelectric Poly(Vinylidene Fluoride) Microsphere Substrates.” *International Journal of Molecular Sciences* 18 (11): 1–17. https://doi.org/10.3390/ijms18112391.

Tsimbouri, P. M., N. Gadegaard, K. Burgess, K. White, P. Reynolds, P. Herzyk, R. Oreffo, and M. J. Dalby. 2014. “Nanotopographical Effects on Mesenchymal Stem Cell Morphology and Phenotype.” *Journal of Cellular Biochemistry* 115: 380–90. https://doi.org/10.1002/jcb.24673.

Vaca-González, J. J., S. Clara-Trujillo, M. Guillot-Ferriols, J. Ródenas-Rochina, M. J. Sanchis, J- L. Gómez Ribelles, D. A. Garzón-Alvarado, and G. Gallego Ferrer. 2020. “Effect of Electrical Stimulation on Chondrogenic Differentiation of Mesenchymal Stem Cells Cultured in Hyaluronic Acid – Gelatin Injectable Hydrogels.” *Bioelectrochemistry* 134: 1–11. https://doi.org/10.1016/j.bioelechem.2020.107536.

Wechsler, M. E., B. P. Hermann, and R. Bizios. 2016. “Adult Human Mesenchymal Stem Cell Differentiation at the Cell Population and Single-Cell Levels Under Alternating Electric Current.” *Tissue Engineering Part C: Methods* 22 (2): 155–64. https://doi.org/10.1089/ten.tec.2015.0324.

Yang, Y., S. Peng, F. Qi, J. Zan, G. Liu, Z. Zhao, and C. Shuai. 2020. “Graphene-Assisted Barium Titanate Improves Piezoelectric Performance of Biopolymer Scaffold.” *Materials Science and Engineering C* 116 (April): 111195. https://doi.org/10.1016/j.msec.2020.111195.

Ye, X., X. Yin, D. Yang, J. Tan, and G. Liu. 2012. “Ectopic Bone Regeneration by Human Bone Marrow Mononucleated Cells, Undifferentiated and Osteogenically Differentiated Bone Marrow Mesenchymal Stem Cells in Beta-Tricalcium Phosphate Scaffolds.” *Tissue Engineering - Part C: Methods* 18 (7): 545–56. https://doi.org/10.1089/ten.tec.2011.0470.

Yu, P., C. Ning, Y. Zhang, G. Tan, Z. Lin, S. Liu, X. Wang, et al. 2017. “Bone-Inspired Spatially Specific Piezoelectricity Induces Bone Regeneration.” *Theranostics* 7 (13): 3387–97. https://doi.org/10.7150/THNO.19748.

Zhang, C., W. Liu, C. Cao, F. Zhang, Q. Tang, S. Ma, J. J. Zhao, L. Hu, Y. Shen, and L. Chen. 2018. “Modulating Surface Potential by Controlling the β Phase Content in Poly(Vinylidene Fluoridetrifluoroethylene) Membranes Enhances Bone Regeneation.” *Advanced Healthcare Materials* 7 (11): 1–12. https://doi.org/10.1002/adhm.201701466.

Zhang, X., C. Zhang, Y. Lin, P. Hu, Y. Shen, K. Wang, S. Meng, et al. 2016. “Nanocomposite Membranes Enhance Bone Regeneration Through Restoring Physiological Electric Microenvironment.” *ACS Nano* 10 (8): 7279–86. https://doi.org/10.1021/acsnano.6b02247.

Zhou, Z., W. Li, T. He, L. Qian, G. Tan, and C. Ning. 2016. “Polarization of an Electroactive Functional Film on Titanium for Inducing Osteogenic Differentiation.” *Scientific Reports* 6: 1–8. https://doi.org/10.1038/srep35512.

Zhou, Z., P. Yu, L. Zhou, L. Tu, L. Fan, F. Zhang, C. Dai, et al. 2019. “Polypyrrole Nanocones and Dynamic Piezoelectric Stimulation-Induced Stem Cell Osteogenic Differentiation.” *ACS Biomaterials Science and Engineering* 5 (9): 4386–92. https://doi.org/10.1021/acsbiomaterials.9b00812.

Zhu, S., W. Jing, X. Hu, Z. Huang, Q. Cai, Y. Ao, and X. Yang. 2017. “Time-Dependent Effect of Electrical Stimulation on Osteogenic Differentiation of Bone Mesenchymal Stromal Cells Cultured on Conductive Nanofibers.” *Journal of Biomedical Materials Research - Part A* 105 (12): 3369–83. https://doi.org/10.1002/jbm.a.36181.

## 4.7. Supplementary material

Supplementary data associated with this article can be found in supplementary material: Real time qPCR primer sequences and Z projection of non-cryosectioned Gel, Gel-PVDF and Gel-PVDF-CFO hydrogels after 14 days in culture.

**Table S4.1. Primer sequences used for real time qPCR.**

| *Gene* | *Forward Primer (5’-3’)* | *Reverse Primer (5’-3’)* | *Annealing Temperature (°C)* |
|---|---|---|---|
| *ALP* | ATGAAGGAAAAGCCAAGCAG | CCACCAAATGTGAAGACGTG | 55.2 |
| *COL I* | GCCAAGACGAAGACATCCCA | GGCAGTTCTTGGTCTCGTCA | 59.5 |
| *RUNX2* | TCACAAATCCTCCCCAAGTA | GGCGGTCAGAGAACAAACTA | 55.7 |
| *OCN* | GTGCAGAGTCCAGCAAAGGT | TCAGCCAACTCGTCACAGTC | 59.2 |
| *GAPDH* | GTCTCCTCTGACTTCAACAGCG | ACCACCCTGTTGCTGTAGCCAA | 62.4 |

**Figure S4.1. Representative Z projection of non-cryosectioned Gel, Gel-PVDF and Gel-PVDF-CFO hydrogels after 14 days in culture in static conditions. Actin cytoskeleton appears in red and cell nuclei in blue. Scale bar 100 μm.**

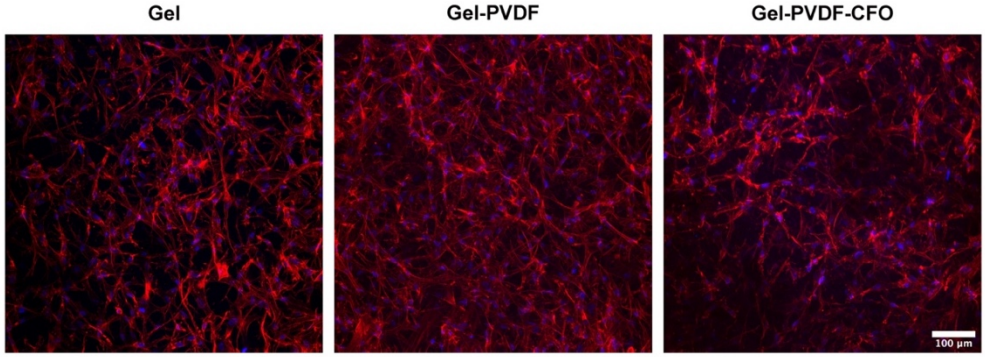

# Discussion

Mesenchymal stem cells meet the requirements for their use in advanced osteogenic regeneration therapies. Besides their immunomodulatory properties and easy obtainment from an autologous source, their differentiation capacity to osteoblasts is their most valuable asset for bone reconstruction purposes. Directing stem cell fate towards a specific lineage is a challenging process, which requires to have a complete view from the embryonic developmental process to the adult stem cell niche and the signals that govern it. Specifically, MSCs osteogenic priming induced by electromechanical or piezoelectric stimulation tries to reproduce the electroactive microenvironment of the stem cell niche.

To do so, different poly(vinylidene) fluoride cell culture supports for MSCs culture in two-dimensions (2D) (Chapters 1, 2 and 3) and three-dimensions (3D) (Chapter 4) have been developed. Different manufacturing techniques have been presented allowing to tailor cell culture support structure and crystallization in the electroactive phases $\beta$ or $\gamma$. All of them were also compatible with the introduction of magnestostrictive CFO nanoparticles to create magnetoelectric composites stimulable with a magnetic bioreactor.

PVDF membrane structure and crystalline polymorphs can be tuned by using different non-solvents when non-solvent induced phase separation (NIPS) is used as processing technique. In this work, ethanol (Chapter 1) and water (Chapter 2) were used as examples of soft and harsh non-solvents, respectively. The use of ethanol reduces the solvent-nonsolvent exchange, allowing crystallization, a slower process, before liquid-liquid demixing takes place, giving rise to completely homogeneous porous membranes. Nevertheless, the presence of water in the coagulation bath leads to rapid liquid-liquid

demixing before crystallization and asymmetric membranes containing a flat surface are obtained (Young et al. 1999). Crystalline phases present on the membranes also depend on the use of the different solvents and therefore, the events governing crystallization. In the case of ethanol membranes presented a high percentage of γ-phase, probably related with the use of polar solvents that favour crystallization in trans phases due to their interaction with the polymer, rotating the C-F bond around the C-C bonds of the chain backbone (Salimi and Yousefi 2004). In the case of water, the asymmetry present in the structure is also associated with the presence of different polymorphs. The membranes are mostly β-phase in the finger-like structure, with a contribution of γ-phase to the porous part. The smooth surface, some microns thick, is composed of α and β crystals. This difference between the electroactive phases present in the membranes is obviously related with the crystallization process affected by the type of non-solvent used, although the underlying mechanism associated with the crystallization of every polymorph is still far from being understood.

Mesenchymal stem cell deficient initial response to highly porous surfaces, as is the case of the membranes developed in Chapter 1, has gradually moved the research focus on obtaining flatter and thinner surfaces. Membranes produced in Chapter 2 presented a smooth surface where MSCs were cultured, nevertheless, the high contribution to the overall structure of the porous part difficulted polarization of the samples because high porosities induce electrical breakdown during the polarization process. Usually, films obtained using a temperature below 70 °C, without the presence of a nucleating filler, lead to the production of β-phase highly porous, fragile, opaque and difficult to polarize films. Nevertheless, when the films are produced using higher temperatures (>70 °C) or produced from the melt (T ~ 210 °C) to ensure complete solvent evaporation they show smoother surfaces, but are crystallized mainly in the non-electroactive α-phase (C. Ribeiro et al. 2018). In the case of the films produced in Chapter 3, the introduction of the ionic liquid [Bmim][Cl] favoured the interaction of PVDF chains with the ionic species present, promoting the nucleation in the most electroactive polymorph even if the films were produced by crystallization from the melt (Meira et al. 2019). They were thinner, presented flatter spherulites and a high percentage, superior to 80 %, of β-phase, solving the aforementioned drawbacks and making them perfect candidates for stimulation experiments.

PVDF is a highly hydrophobic polymer, with contact angles values reaching 130 º on porous surfaces, not allowing efficient cell attachment and interaction with cellular populations. Many have been the attempts to modify PVDF's surface to enhance initial cell response. Simple techniques such as plasma treatment (Kitsara et al. 2019; Mirzaei et al. 2019), pre-incubation in culture media to favour serum protein adsorption (S. Wu et al. 2018; Guo et al. 2012) or adsorption of specific proteins such as poly-L-lysine or fibronectin have been described (Hoop et al. 2017; Sobreiro-Almeida et al. 2017; C. Ribeiro, Panadero, et al. 2012). Protein grafting has also been reported in PVDF substrates, which may enhance protein functionality by exposing in a more efficient way functional sequences (Young et al. 2009, 2010; Park et al. 2020; Klee et al. 2003). Although these approaches may result suitable to enhance cell adhesion, a new generation of smart materials which aspire to go

beyond basic attachment and proliferation functionalities is being developed. In this Doctoral Thesis, PVDF membranes have been coated with different proteins and polysaccharides by means of the layer-by-layer technique. LbL is a versatile approach that allows the deposition of different polyelectrolytes with other charged or uncharged macromolecules. This versatility allows to coat almost every surface with an endless number of molecules. It can help to create a biomimetic microenvironment resembling the extracellular matrix, which can include features that enhance cell adhesion, promote osteogenic differentiation or present growth factors efficiently (Petrila et al. 2021).

As far as we know, this is the first time that LbL technique has been described to coat electroactive PVDF substrates for cell culture. Elastin-like recombinamers containing RGD sequences (Chapter 1) and collagen type I/heparin (Chapter 2) have been deposited on PVDF membranes, to enhance their initial adhesion properties. Besides, the presence of the adhesion sequence RGD in both types of coatings promotes integrin mediated binding of cells being the foundation for cell growth and differentiation (Alberts et al. 2002). The importance of the presented work relies on the versatility of the techniques used, that can be adapted to meet the needs for different tissue engineering applications. The absence of functional groups on PVDF structure requires its pre-treatment to introduce active chemical species that can react with the first layer. Two methods to modify PVDF surface have been described. In Chapter 1 membranes were first treated with plasma to activate the surface while in Chapter 2 membranes were aminolized by means of an alkali treatment, introducing amine groups in the surface. These groups can be used either to covalently bond molecules of interest or, as is the case, to deposit the first LbL layer. After surface modification, LbL was carried out and surfaces were coated by the electrostatic interaction of heparin and collagen type I molecules or strong covalent bonds mediated by click chemistry between the ELR peptides (González De Torre et al. 2014). These techniques here described can be tailored to meet the needs for different approaches. In our case, membrane coating resulted fundamental to enhance MSCs initial adhesion and proliferation, especially due to the porous character and hydrophobicity of ethanol-based NIPS membranes.

These surface modifications were carried out using 2D substrates, which provide an easier platform to develop and characterize coating techniques, as well as to study MSCs behaviour. Nevertheless, 2D cell culture supports offer a reductionist approach to understand cell phenomena and do not reflect the physiological behaviour of cells *in vivo.* 3D culture elicits a more physiological state and allows more realistic cell-to-cell and cell-to-matrix interactions that are important for differentiation, proliferation and cellular functions (Baker and Chen 2012). 3D cell culture platforms were produced and characterized (Chapter 4) to test MSCs osteogenic differentiation under electromechanical stimulation. Encapsulation of MSCs together with electroactive PVDF microspheres containing magnetostrictive nanoparticles in an injectable gelatin hydrogel allowed to create an electroactive biomimetic 3D environment. The presence of the gelatin matrix generates a biomimetic platform and avoids the need of PVDF functionalization while the presence of the PVDF-CFO microspheres allows MSCs stimulation using a wireless approach based on a magnetic bioreactor.

The use of piezoelectric stimulation for MSCs priming implies necessarily to culture these cells *in vitro*, adding into the equation several factors that need to be considered and that can modify its outcomes. Stimulation parameters, combination with biochemical cues using an osteoinductive cell culture medium or treatment times are not independent and their combined effects tend to overlap revealing that their boundaries are not tight.

Mesenchymal stem cell osteogenic commitment is the first step in the osteoblast differentiation pathway. These cells become preosteoblasts, characterized by the expression of RUNX2 followed by the activation of OSX which subsequently activates ALP and COL I expression (Nakashima et al. 2002). Further on, these preosteoblasts acquire the characteristic cuboidal osteoblastic phenotype, expressing mature markers such as osteocalcin and osteopontin (Gavazzo et al. 2021). Conceiving differentiation as an organized cascade of expression events involves the fact that electrical stimulation can be applied at different time points. Three parameters may be carefully adjusted to determine the most suitable stimulation program to induce MSCs osteogenic differentiation regarding treatment time. On the one hand, stimulation time per day, thus, the number of hours that cells are under stimulation each day. On the other hand, stimulation period along the duration of the culture should be considered, ergo, the number of days cells are subjected to ES. Finally, the moment in which stimulation is introduced, at earlier, middle or later stages of the osteogenic differentiation process.

Authors that use bioreactors to produce electromechanical stimulation by means of piezoelectric samples usually apply it for the total duration of the culture. Short periods a few times a day or continued stimulation may be chosen although there is no consensus. Damaraju et al. (Damaraju et al. 2017) applied dynamic compression three times a day for 1 hour on and 1 hour off. In the case of Zhou et al. (Z. Zhou et al. 2019) a 5 N constant dynamic cyclic force was applied. Liu et al. (W. Liu et al. 2020) used a pressurized culture and stimulated the cells for 1 hour a day for the whole duration of the culture. In the case of piezoelectric scaffolds activated by ultrasounds, stimulation was applied three times a day for 20 seconds each time by Yang et al. (Yang et al. 2020) and 10 minutes daily for 4, 7 and 14 days in the case of Fan et al. (Fan et al. 2020). In this work, a stimulation program defined by Lanceros-Méndez group was applied to stimulate 2D and 3D cell culture platforms to test the response on MSCs in chapters 3 and 4, respectively. The program was based on reproducing human daily activity, which means 16 hours of stimulation, where a short cycle of 5 minutes of stimulation and 25 minutes of rest is repeated, and 8 hours of rest (Fernandes et al. 2019; S. Ribeiro et al. 2020). Stimulation was able to induce changes in MSCs cytoskeleton after 3 days of culture in the 2D platform, although long term effects were not studied. For the 3D cell culture support, application of constant stimulation resulted detrimental for MSCs expression of osteogenic related genes, such as ALP, and was also confirmed by enzyme activity analysis at the same time point, 14 days. This result confirms the importance of treatment time optimization, as has already been demonstrated by different authors using conductive substrate mediated ES. Application of stimulation only at earlier stages of the osteogenic differentiation process (day 1 to 7) favours the expression of bone-related markers compared to its use after this time point (8-14 and 14-21 days) (Zhu et al. 2017). In fact, stimulation period may be reduced to one day if it is properly introduced, as demonstrated by Hu et al., where cells stimulated only at day 8 showed a

higher level of mineralization after 14 days, which was supported by the upregulation of osteogenic genes, especially RUNX2 immediately after the ES treatment (W. W. Hu et al. 2019).

As far as we know, just few authors have considered treatment time as a determining parameter when studying the effects of ES on MSCs osteogenic differentiation, thus the number of studies covering this aspect is reduced. It is even more reduced, nearly inexistent, when using piezoelectric cell culture supports. This could be a new path to explore, since osteoblastogenesis is a time-dependent process and applying stimulation at early stages of the differentiation process may be enough to determine MSCs fate.

Nevertheless, it is worth to mention that treatment time cannot be considered as an isolated parameter that may affect ES outcome. It influences MSCs osteogenic differentiation together with other factors such as cell culture medium. The presence of a biochemical osteogenic inductor may be essential to trigger the effect of stimulation, especially in the case of ES using general stimulation or substrate mediated by means of conductive supports (Leppik et al. 2018; Mobini et al. 2017; Srirussamee et al. 2021; Hronik-Tupaj et al. 2011; W. W. Hu et al. 2014; J. Zhang, Neoh, and Kang 2018; W. W. Hu et al. 2019; Jing et al. 2019). Nevertheless, MSCs osteogenic fate determination has been reported as a result of using piezoelectric biomaterials as cell culture supports in the presence of growth and osteogenic media (X. Zhang et al. 2016; C. Zhang et al. 2018; Z. Zhou et al. 2016, 2019; Yu et al. 2017; Yang et al. 2020; Y. Li et al. 2017; Damaraju et al. 2017; Jia et al. 2019; J. Li et al. 2015; Fan et al. 2020) demonstrating less reliance on the need of an osteogenic triggering. Optimization of the appropriate cell culture medium, again, has been scarcely reported in combination with electromechanical stimulation. The importance of media selection was demonstrated by Damaraju et al. where the combination of piezoelectric stimulation with either chondrogenic or osteogenic media favoured MSCs osteogenesis or chondrogenesis depending on media formulation and scaffold piezoresponse (Damaraju et al. 2017). As cell culture medium may actuate in synergy to exploit the effect of stimulation, we have tested the role of different cell culture media on MSCs initial adhesion in 2D piezoelectric supports through the study of focal adhesion complexes (Chapter 3). The use of combined osteogenic and adipogenic media resulted in longer focal adhesions and larger cells, a required step for MSCs osteogenic differentiation (Biggs et al. 2009). Moreover, the presence of osteogenic and adipogenic cues does not condition MSCs to choose a differentiation pathway but provides the right stimuli to guide them in combination with electromechanical stimulation. This is the first time that cell culture medium formulation was optimized prior to electromechanical stimulation experiments for MSCs osteogenic differentiation. In the case of the 3D cell culture platform (Chapter 4) osteogenic medium was directly used. Although the stimulated samples in combination with biochemical induction showed a stronger expression of RUNX2 after 7 days compared to non-stimulated ones, this effect faded after 14 days. As already mentioned, constant stimulation and the powerful effect of commercial osteogenic media may mask the effect of electromechanical stimulation. It is important to note that many parameters need to be adjusted giving rise to endless combinations, which are difficult to test *in vitro*. This forces to randomly set some of them to facilitate the experimental design and the handling of the obtained data.

Treatment times, cell culture media or cell source may vary along the different research papers. At the same time, outcome comparison between published studies results difficult due to the amount of different conductive and piezoelectric cell culture supports, with 2D and 3D configurations, and the applied parameters (waveforms, electric fields, frequencies, bioreactors…) (Guillot-Ferriols et al. 2022). This reflects the need of performing systematic studies that may lead to a standardized stimulation protocol for clinical translation. Nevertheless, protocol standardization is the first step in a devious and long road until these approaches could be used in clinic. Ensuring a stable and non-reversible MSCs osteogenic phenotype may be the next goal for the scientific community working in the field. To the date the main application with future translation into clinics is the use of piezoelectric cell culture supports *in vivo* to treat critical size bone defects. Positive results when compared with non-poled piezoelectric materials or non-piezoelectric ones have been obtained (X. Zhang et al. 2016; Yu et al. 2017; H. B. Lopes et al. 2014; Fan et al. 2020; C. Zhang et al. 2018; Y. Liu et al. 2017; F. Zhao et al. 2020). The scaffolds are implanted in the defect without previous seeding of MSCs. When placed in the injured site cells from the surrounding healthy tissue invade the scaffold, recruited by the biomaterial electrical cues (X. Zhang et al. 2016). Among the different cell types, MSCs are present and can be induced to differentiate into osteoblasts in response to the electrical stimulus, initiating the process of bone regeneration. Their biggest advantage relies on the piezoelectric effect itself. The absence of an external power supply is overcome by the mechanical deformation of the scaffold, produced by the movements of the human body, which generates an electrical output. Moreover, the presence of an associated surface charge provides an electric microenvironment enhancing protein adsorption in an active conformation favoring cell adhesion (Jia et al. 2019).This approach presents some drawbacks, as can be the non-degradability of the piezoelectric scaffolds, which in most cases are ceramics or non-biodegradable polymers that will reside in the body unless surgically removed. Moreover, bone microenvironment at the injured site can be compromised due to immune-mediated, inflammatory, and degenerative diseases hindering MSCs homing and thus the regeneration process. This problem may be solved by using piezoelectric biodegradable materials or piezoelectric cell culture supports as priming platforms for MSCs pre-differentiation. In the latest, once a stable phenotype is achieved, cells can be harvested and seeded onto biodegradable and already FDA approved scaffolds.

During the development of this Doctoral Thesis, the manufacturing process and functionalization of 2D and 3D biomimetic cell culture supports for mesenchymal stem cell electromechanical stimulation has been described. Results show that MSCs are able to respond to this physical cue in terms of adhesion and cytoskeleton reorganization in 2D cell culture supports. Also, 3D stimulation is able to enhance RUNX2 expression, master regulator of the osteogenic differentiation pathway. These promising results lead the way for future uses of these biomaterials as priming platforms after systematic optimization of the involved parameters.

# Conclusions

After the experimental evidence shown along this work concerning the development of electroactive PVDF cell culture supports and the influence of electromechanical stimulation on MSCs, the following conclusions can be highlighted:

***Chapter 1***

1. Non-solvent induced phase separation using ethanol as non-solvent gives rise to highly porous symmetrical and electroactive PVDF membranes mostly in $\gamma$-phase.
2. Argon plasma treatment allows PVDF membrane activation reducing hydrophobicity and facilitating the deposition of the first LbL layer.
3. Layer-by-layer is a suitable and versatile technique for PVDF membrane coating, allowing the deposition of elastin like recombinamers.
4. Deposition of ELRs containing RGD sequences is needed to enhance MSCs initial adhesion and proliferation due to PVDF hydrophobicity but also due to the spherulite porous surface. Fibronectin absorption is not enough to promote MSCs initial adhesion.

***Chapter 2***

5. Non-solvent induced phase separation using water as non-solvent produces asymmetric membranes with a thin smooth surface and a highly porous structure underneath.
6. The smooth surface presents a mixture of $\alpha$ and $\beta$ phase, while the membrane bulk crystallizes mostly in $\beta$-phase, the most electroactive one, with a contribution of the electroactive $\gamma$-phase.

7. Incorporation of CFO magnetostrictive nanoparticles is effective using NIPS and does not change the overall structure but increases spherulite diameter. Presence of the different polymorphs and crystalline content are slightly modified due to CFO presence.
8. Alkali treatment allows the incorporation of amine groups onto the membrane surface, facilitating the deposition of the first heparin layer.
9. Layer-by-layer enables to create a biomimetic environment for MSCs culture combining collagen type I and heparin bilayers.
10. PVDF-CFO membranes are non-cytotoxic for MSCs culture, regardless the type of coating. Although initial MSCs adhesion is similar both with traditional fibronectin or LbL coating, the presence of the LbL coating favours MSCs proliferation in PVDF-CFO membranes compared to fibronectin.

***Chapter 3***

11. The ionic liquid [Bmim][Cl] induces PVDF crystallization in β-phase when manufacturing films by doctor blade technique. PVDF and PVDF-CFO films with the same microstructure and physical properties can be produced in the presence of [Bmim][Cl].
12. [Bmim][Cl] is efficiently removed after several washes with water.
13. PVDF and PVDF-CFO films, once the IL is removed, are non-cytotoxic and support MSCs initial adhesion and proliferation after 7 days.
14. Balanced medium, a mixture 1:1 of osteogenic and adipogenic media, promotes larger cell areas and longer FA adhesions when MSCs are cultured in static conditions, regardless the cell culture support.
15. Electromechanical stimulation in the presence of balanced medium promotes the formation of longer focal adhesions and a decrease in vimentin intensity, which may be an earlier sign of osteogenic differentiation.

***Chapter 4***

16. Electrospray enables PVDF crystallization in β-phase, obtaining magnetostrictive microspheres with incorporated CFO into the polymer matrix.
17. Gelatin hydrogels provide a continuous matrix for mesenchymal stem cell encapsulation together with electroactive microspheres for MSCs piezoelectric stimulation.
18. The 3D electroactive cell culture platform is not cytotoxic for mesenchymal stem cells, regardless the presence of microspheres containing CFO.
19. Electromechanical stimulation does not affect MSCs proliferation, either positively or negatively.
20. Piezoelectric stimulation enhances the expression of early osteogenic marker RUNX2 but does not affect the expression of later markers such as ALP, COL I or OCN.

# Future perspectives

In this Doctoral Thesis different cell culture platforms for mesenchymal stem cell piezoelectric stimulation have been successfully produced and functionalized to present a biomimetic environment. The potential of electromechanical stimulation as an inductive cue for MSCs osteogenic differentiation has been studied.

The implication of several factors (stimulation parameters, treatment time, cell culture medium) in the differentiation process implies the need for optimization to obtain the best results. Cell stimulation platforms have already been produced and characterized, therefore, next steps of the project entail to design systematic studies combining interesting variables that may affect differentiation outcomes. Optimized parameters, already described in this Doctoral Thesis, may be used as a starting point. Optimization should lead to a standardized priming stimulation protocol that may be tested for clinical translation. Once a standard protocol for MSCs pre-differentiation is achieved, these platforms must accomplish the criteria of quality cell therapy standards following good manufacturing practices (GMP), maintaining and ensuring a long-lasting osteogenic phenotype but at the same time resulting convenient for their commercialization.

Usually, therapies based on the use of MSCs require the injection of a large number of cells. The platforms here described are suitable for *in vitro* MSCs stimulation from a research point of view, but its use as real priming platforms for clinical application imply their scale up. Electrospray, as demonstrated, is a good candidate for electroactive microsphere production, but it is a time-consuming technique which presents some difficulties for scaling up. Moreover, environmental parameters play a crucial role in microsphere obtainment.

Alternative methods for microsphere production are currently under investigation in our research group. Microfluidics has been postulated as an option for automatized microsphere production which allows to obtain a higher number of microspheres per unit of time with a higher range of diameters. Additionally, this technique facilitates environmental conditions control giving rise to a more reproducible protocol for microsphere production. PVDF and PVDF-CFO microspheres have already been produced by this method and their electroactive properties have been characterized, so the next steps will involve testing their use as cell culture supports for MSCs piezoelectric stimulation.

On the other hand, the proposed 3D system for MSCs culture requires hydrogel break-up to recover pre-differentiated MSCs. Optimization of the recovering protocol may be another interesting objective. At the moment, cells are being obtained for their characterization by means of a collagenase treatment, although cell integrity has not been assured. Further studies are required to stablish a protocol that allow to obtain undamaged MSCs after stimulation. Moreover, other 3D approaches combining electroactive microspheres are being studied. The use of MSCs spheroids has been widely described and it is possible to combine spheroids together with electroactive microspheres, which are incorporated when the spheroid is formed due to cell-cell interaction. This gives rise to a 3D cell culture environment which can be stimulated using a magnetic bioreactor, and the process for cell recovery becomes easier, since no hydrogel needs to be processed. Our research group is currently working towards the use of layer-by-layer functionalized microspheres incorporated into MSCs spheroids for piezoelectric stimulation.

The proposed models and the obtained results here described lay the groundwork for future research projects. Although there is still room for improvement, this fact motivates us to keep researching with the aim to achieve the use of piezoelectric stimulation as a real applicable tool for mesenchymal stem cell differentiation.

# Contributions

This Thesis has produced a significant number of results that have been diffused through several publications in scientific journals and national and international conferences.

## 1. Publications in scientific journals

Publications as first author:

1. Poly(Vinylidene) Fluoride Membranes Coated by Heparin / Collagen Layer-by-Layer, Smart Biomimetic Approaches for Mesenchymal Stem Cell Culture. **Maria Guillot-Ferriols**, José Carlos Rodríguez-Hernández, Daniela M. Correia, Sonia A.C. Carabineiro, Senentxu Lanceros-Méndez, José Luis Gómez Ribelles, Gloria Gallego Ferrer. *Materials Science and Engineering C*. **2020**. 117, 1–12. https://doi.org/10.1016/j.msec.2020.111281.

2. Effective Elastin-like Recombinamers Coating on Poly(Vinylidene) Fluoride Membranes for Mesenchymal Stem Cell Culture. **Maria Guillot-Ferriols**, Ana del Barrio, Carlos M. Costa, Senentxu Lanceros-Méndez, José Carlos Rodríguez-Cabello, José Luis Gómez Ribelles, Mercedes Santos, Gloria Gallego Ferrer. *European Polymer Journal*. **2021**. 146 (January), 1–10. https://doi.org/10.1016/j.eurpolymj.2021.110269.

3. Electrical Stimulation: Effective Cue to Direct Osteogenic Differentiation of Mesenchymal Stem Cells? **Maria Guillot-Ferriols**, Senentxu Lanceros-Méndez, José Luis Gómez Ribelles, Gloria Gallego Ferrer. *Biomaterials Advances*. **2022**. 138 (May), 1–18. https://doi.org/10.1016/j.bioadv.2022.212918.

4. Magnetically Activated Piezoelectric 3D Platform Based on Poly(Vinylidene) Fluoride Microspheres for Osteogenic Differentiation of Mesenchymal Stem Cells. **Maria Guillot-Ferriols**, Inmaculada M. García-Briega, Laia Tolosa, Carlos M. Costa, Senentxu Lanceros-Méndez, José Luis Gómez Ribelles, Gloria Gallego Ferrer. *Gels* **2022**, 8, 680. https://doi.org/10.3390/gels8100680.

Other contributions:

1. Freeze-Extraction Microporous Electroactive Supports for Cell Culture. Rosa M. Morales-Román, **Maria Guillot-Ferriols,** Laura Roig-Pérez, Senentxu Lanceros-Méndez, Gloria Gallego Ferrer, José Luis Gómez Ribelles. *European Polymer Journal*. **2019**. 119 (June), 531–540. https://doi.org/10.1016/j.eurpolymj.2019.07.011.

2. Effect of Electrical Stimulation on Chondrogenic Differentiation of Mesenchymal Stem Cells Cultured in Hyaluronic Acid – Gelatin Injectable Hydrogels. Juan J. Vaca-González, Sandra Clara-Trujillo, **Maria Guillot-Ferriols**, Joaquín Ródenas-Rochina, Maria J. Sanchis, José Luis Gómez Ribelles, Diego A. Garzón-Alvarado, Gloria Gallego Ferrer. *Bioelectrochemistry*. **2020**. 134, 1–11. https://doi.org/10.1016/j.bioelechem.2020.107536.

## 2. International conferences

1. Microporous electroactive supports for cell culture
   Conference: European Society for Artificial Organs (ESAO). Winter School 2019
   City, Country / Year: Baden, Austria / 2019
   Format: Poster
   Authors: Rosa M. Morales-Román, **Maria Guillot-Ferriols**, Laura Roig-Pérez, Senentxu Lanceros-Méndez, Gloria Gallego Ferrer, José Luis Gómez Ribelles
   2nd Prize Young Researchers Poster Session

2. Stem cell chondrogenesis in electrically stimulated 3D injectable hydrogels
   Conference: 6th International Symposium Interface Biology of Implants (IBI 2019)
   City, Country / Year: Rostock, Germany / 2019
   Format: Poster
   Authors: Juan J. Vaca-González, Sandra Clara-Trujillo, **Maria Guillot-Ferriols**, Joaquín Ródenas-Rochina, María J. Sanchis, José Luis Gómez Ribelles, Diego A. Garzón-Alvarado, Gloria Gallego Ferrer

3. Electrical stimulation to mesenchymal stem cells cultured in hyaluronic acid gelatin hydrogel.
   Conference: 8th Meeting of the International Federation for Artificial Organs (IFAO 2019). 57th Annual Meeting of the Japanese Society for Artificial Organs (JSAO 2019)
   City, Country / Year: Osaka, Japan / 2019
   Format: Poster

Authors: Juan J. Vaca-González, Sandra Clara-Trujillo, **Maria Guillot-Ferriols**, Joaquín Ródenas-Rochina, María J. Sanchis, José Luis Gómez Ribelles, Diego A. Garzón-Alvarado, Gloria Gallego Ferrer

4. Elastin-like recombinamers coated poly(vinylidene) fluoride membranes, new approach for mesenchymal stem cell culture and differentiation
   Conference: EMBL-IBEC Winter Conference
   City, Country / Year: Barcelona, Spain / 2020
   Format: Poster
   Authors: **Maria Guillot-Ferriols**, Ana del Barrio, Senentxu Lanceros-Méndez, José Carlos Rodríguez-Cabello, José Luis Gómez Ribelles, Mercedes Santos, Gloria Gallego Ferrer

5. Hydrogel-poly(vinylidene) fluoride microspheres platform for mesenchymal stem cell differentiation
   Conference: European Society for Artificial Organs (ESAO). Winter School 2020
   City, Country / Year: Lutherstadt Wittenberg, Germany / 2020
   Format: Poster
   Authors: **Maria Guillot-Ferriols**, Inmaculada M. García-Briega, Senentxu Lanceros-Méndez, José Luis Gómez Ribelles, Gloria Gallego Ferrer

6. Synthesis and characterization of an electromagnetic system for mesenchymal stem cell culture and predifferentiation
   Conference: Cloud Young European Society for Artificial Organs (Cloud-yESAO 2020)
   City, Country / Year: Online, 2020
   Format: Poster
   Authors: **Maria Guillot-Ferriols**, Inmaculada M. García-Briega, Senentxu Lanceros-Méndez, José Luis Gómez Ribelles, Gloria Gallego Ferrer

7. Layer-by-layer engineered biomimetic poly(vinylidene) fluoride membranes, piezoelectric approaches for bone regeneration
   Conference: European Society for Artificial Organs (ESAO). Winter School 2021
   City, Country / Year: Jaca, Spain / 2021 (Online)
   Format: Poster
   Authors: **Maria Guillot-Ferriols**, Jose Carlos Rodríguez-Hernández, Daniela M. Correia, Sonia A. C. Carabineiro, Senentxu Lanceros-Méndez, Gloria Gallego Ferrer, José Luis Gómez Ribelles

8. Piezoelectric 3D platform based on hydrogel-poly(vinylidene) fluoride microspheres for mesenchymal stem cell osteogenic differentiation
   Conference: 6$^{th}$ World Congress of the Tissue Engineering and Regenerative Medicine International Society (TERMIS 2021)
   City, Country / Year: Maastrich, The Netherlands / 2021 (Online)
   Format: Oral communication

Authors: **Maria Guillot-Ferriols**, Inmaculada M. García-Briega, Laia Tolosa, Senentxu Lanceros-Méndez, José Luis Gómez Ribelles, Gloria Gallego Ferrer

## 3. National conferences

1. Piezoelectric membranes coated with elastin-like recombinamers for mesenchymal stem cell culture and differentiation
   Conference: CIBER-BBN Annual Congress 2019
   City, Country / Year: Tarragona, Spain / 2019
   Format: Poster
   Authors: **Maria Guillot-Ferriols**, Ana del Barrio, Senentxu Lanceros-Méndez, José Carlos Rodríguez-Cabello, José Luis Gómez Ribelles, Mercedes Santos, Gloria Gallego Ferrer

2. Biomimetic smart materials for bone tissue engineering
   Conference: CIBER-BBN Annual Congress 2021
   City, Country / Year: Online / 2021
   Format: Oral communication
   Authors: **Maria Guillot-Ferriols**, Senentxu Lanceros-Méndez, Gloria Gallego Ferrer, José Luis Gómez Ribelles

## 4. Educational related publications

During this Doctoral Thesis it has been possible to participate in the project entitled “Critical thinking as a step forward in VET education: VET students immersed in high technology teams”. This European project enjoyed the participation of partners from Spain, Portugal, Czech Republic and Greece. It was cofounded by the Erasmus+ Program of the European Commission.

The main objective was to provide VET centers and high technology companies with tools that encourage and train the implementation of critical thinking skills in VET students. Different intellectual outputs were generated as a result of this project:

1. El pensamiento crítico como un paso adelante en la Formación Profesional. Estudiantes de Formación Profesional inmersos en centros de alta tecnología
   Conference: V Congreso Nacional de Innovación Educativa y Docencia en Red (IN-RED 2019)
   City, Country / Year: Valencia, Spain / 2019
   Format: Oral communication
   Authors: Concepción Solano Martínez, Sandra Clara-Trujillo, **Maria Guillot-Ferriols**, José Luis Gómez Estrada, José Luis Gómez Ribelles

2. Methodological guide for high tech centers to host VET student internships
   Authors: José Luis Gómez Estrada, Concepción Solano Martínez, **Maria Guillot-Ferriols**, Sandra Clara-Trujillo, Jivago Nunes, Senentxu Lanceros-Méndez, Pedro Martins, Panagiotis Chatzipapas, Panagiotis Karampelas, Dimitrios Flygjos, Ioannis Kaliakatsos, Konstantinos Petridis, Ivan Krakovski.

# References


Ahn, A.C., and A. J. Grodzinsky. 2009. “Relevance of Collagen Piezoelectricity to ‘Wolff’s Law’: A Critical Review.” *Medical Engineering and Physics* 31 (7): 733–41. https://doi.org/10.1016/j.medengphy.2009.02.006.

Alberts, B, A Johnson, J Lewis, M Raff, K Roberts, and P Walter. 2002. *Molecular Biology of the Cell. 4th Edition*. New Yor: Garland Science. https://www.ncbi.nlm.nih.gov/books/NBK26867/.

Allendorph, G. P., W. W. Vale, and S. Choe. 2006. “Structure of the Ternary Signaling Complex of a TGF-β Superfamily Member.” *Proceedings of the National Academy of Sciences of the United States of America* 103 (20): 7643–48. https://doi.org/10.1073/pnas.0602558103.

Bagheri, L., A. Pellati, P. Rizzo, G. Aquila, L. Massari, M. De Mattei, and A. Ongaro. 2017. “Notch Pathway Is Active during Osteogenic Differentiation of Human Bone Marrow Mesenchymal Stem Cells Induced by Pulsed Electromagnetic Fields.” *Journal of Tissue Engineering and Regenerative Medicine* 12 (2): 304–15. https://doi.org/10.1002/term.2455.

Baker, B. M., and C. S. Chen. 2012. “Deconstructing the Third Dimension-How 3D Culture Microenvironments Alter Cellular Cues.” *Journal of Cell Science* 125 (13): 3015–24. https://doi.org/10.1242/jcs.079509.

Balikov, D. A., B. Fang, Y. W. Chun, S. W. Crowder, D. Prasai, J. B. Lee, K. I. Bolotin, and H. J. Sung. 2016. “Directing Lineage Specification of Human Mesenchymal Stem Cells by Decoupling Electrical Stimulation and Physical Patterning on Unmodified Graphene.” *Nanoscale* 8 (28): 13730–39. https://doi.org/10.1039/c6nr04400j.

Balint, R., N. J. Cassidy, and S. H. Cartmell. 2013. “Electrical Stimulation: A Novel Tool for Tissue Engineering.” *Tissue Engineering - Part B: Reviews* 19 (1): 48–57. https://doi.org/10.1089/ten.teb.2012.0183.

Balint, R., N. J. Cassidy, L. A. Hidalgo-Bastida, and S. Cartmell. 2013. “Electrical

Stimulation Enhanced Mesenchymal Stem Cell Gene Expression for Orthopaedic Tissue Repair." *Journal of Biomaterials and Tissue Engineering* 3 (2): 212–21. https://doi.org/10.1166/jbt.2013.1081.

Bar-Cohen, Y., and Q. Zhang. 2008. "Electroactive Polymer Actuators and Sensors" 33 (March): 173–81. https://doi.org/10.1557/mrs2008.42.

Basset, A. C., R. J. Pawluk, and A. A. Pilla. 1974. "Augmentation of Bone Repair by Inductively Coupled Electromagnetic Fields." *Science* 184 (4136): 575–77. https://doi.org/10.1126/science.184.4136.575.

Berridge, M. J., P. Lipp, and M. D. Bootman. 2000. "The Versatility and Universality of Calcium Signalling." *Nature Reviews Molecular Cell Biology* 1 (1): 11–21. https://doi.org/10.1038/35036035.

Bianco, P., M. Riminucci, S. Gronthos, and P. Gehron Robey. 2001. "Bone Marrow Stromal Stem Cells: Nature, Biology, and Potential Applications." *Stem Cells* 19 (3): 180–92. https://doi.org/10.1634/stemcells.19-3-180.

Biggs, M. J. P., R. G. Richards, N. Gadegaard, C. D. W. Wilkinson, R. O. C. Oreffo, and M. J. Dalby. 2009. "The Use of Nanoscale Topography to Modulate the Dynamics of Adhesion Formation in Primary Osteoblasts and ERK/MAPK Signalling in STRO-1+ Enriched Skeletal Stem Cells." *Biomaterials* 30 (28): 5094–5103. https://doi.org/10.1016/j.biomaterials.2009.05.049.

Bock, N., T. R. Dargaville, and M. A. Woodruff. 2012. "Electrospraying of Polymers with Therapeutic Molecules: State of the Art." *Progress in Polymer Science* 37 (11): 1510–51. https://doi.org/10.1016/j.progpolymsci.2012.03.002.

Boyette, L. B., O. A. Creasey, L. Guzik, T. Lozito, and R. S. Tuan. 2014. "Human Bone Marrow-Derived Mesenchymal Stem Cells Display Enhanced Clonogenicity but Impaired Differentiation With Hypoxic Preconditioning." *Stem Cells Translational Medicine* 3 (2): 241–54. https://doi.org/10.5966/sctm.2013-0079.

Boyle, W. J., W. S. Simonet, and D. L. Lacey. 2003. "Osteoclast Differentiation and Activation." *Nature* 423 (May): 337–42. https://doi.org/10.1038/nature01658.

Cafarelli, A., A. Marino, L. Vannozzi, J. Puigmartí-Luis, S. Pané, G. Ciofani, and L. Ricotti. 2021. "Piezoelectric Nanomaterials Activated by Ultrasound: The Pathway from Discovery to Future Clinical Adoption." *ACS Nano* 15 (7): 11066–86. https://doi.org/10.1021/acsnano.1c03087.

Castano-Izquierdo, H., J. Álvarez-Barreto, J. van den Dolder, J. A. Jansen, A. G. Mikos, and V. I. Sikavitsas. 2006. "Pre-Culture Period of Mesenchymal Stem Cells in Osteogenic Media Influences Their in Vivo Bone Forming Potential." *Journal of Biomedical Materials Research Part A* 79 (4): 129–38. https://doi.org/10.1002/jbm.a.31082.

Castro, N., M. M. Fernandes, C. Ribeiro, V. Correia, R. Minguez, and S. Lanceros-Mendez. 2020. "Magnetic Bioreactor for Magneto-, Mechano- and Electroactive Tissue Engineering Strategies." *Sensors* 20 (12): 1–13. https://doi.org/10.3390/s20123340.

Cebrián, J. L., G. L. Milano, A. Francés, Y. Lopiz, F. Marco, and L. López-Durán. 2014. "Role of Electromagnetic Stimulation in the Treatment of Osteonecrosis of the Femoral Head in Early Stages." *Journal of Biomedical Science and Engineering* 07 (05): 252–57. https://doi.org/10.4236/jbise.2014.75028.

Chang, J., F. Liu, M. Lee, B. Wu, K. Ting, J. N. Zara, C. Soo, et al. 2013. "NF-KB Inhibits Osteogenic Differentiation of Mesenchymal Stem Cells by Promoting β-Catenin Degradation." *Proceedings of the National Academy of Sciences of the United States of America* 110 (23): 9469–74. https://doi.org/10.1073/pnas.1300532110.

Chen, C., X. Bai, Y. Ding, and I. S. Lee. 2019. "Electrical Stimulation as a Novel Tool for Regulating Cell Behavior in Tissue Engineering." *Biomaterials Research* 23 (1): 1–12. https://doi.org/10.1186/s40824-019-0176-8.

Chen, J. H., C. Liu, L. You, and C. A. Simmons. 2010. "Boning up on Wolff's Law: Mechanical Regulation of the Cells That Make and Maintain Bone." *Journal of*

*Biomechanics* 43 (1): 108–18. https://doi.org/10.1016/j.jbiomech.2009.09.016.
Choi, Y. H., J. H. Choi, J. W. Oh, and K. Y. Lee. 2013. "Calmodulin-Dependent Kinase II Regulates Osteoblast Differentiation through Regulation of Osterix." *Biochemical and Biophysical Research Communications* 432 (2): 248–55. https://doi.org/10.1016/j.bbrc.2013.02.005.
Chorsi, M. T., E. J. Curry, H. T. Chorsi, R. Das, J. Baroody, P. K. Purohit, H. Ilies, and T. D. Nguyen. 2019. "Piezoelectric Biomaterials for Sensors and Actuators." *Advanced Materials* 31 (1): 1–15. https://doi.org/10.1002/adma.201802084.
Clark, C. C., W. Wang, and C. T. Brighton. 2014. "Up-Regulation of Expression of Selected Genes in Human Bone Cells with Specific Capacitively Coupled Electric Fields." *Journal of Orthopaedic Research* 32 (7): 894–903. https://doi.org/10.1002/jor.22595.
Cohen, M. M. Jr. 2006. "The New Bone Biology: Pathologic, Molecular, and Clinical Correlates." *American Journal of Medical Genetics Part A* 140 (23): 2646–2706. https://doi.org/10.1002/ajmg.a.31368.
Correia, D. M., R. Gonçalves, C. Ribeiro, V. Sencadas, G. Botelho, J. L. Gomez Ribelles, and S. Lanceros-Méndez. 2014. "Electrosprayed Poly(Vinylidene Fluoride) Microparticles for Tissue Engineering Applications." *RSC Adv.* 4 (62): 33013–21. https://doi.org/10.1039/C4RA04581E.
Correia, H. M. G., and M. M. D. Ramos. 2005. "Quantum Modelling of Poly(Vinylidene Fluoride)." *Computational Materials Science* 33 (1–3): 224–29. https://doi.org/10.1016/j.commatsci.2004.12.040.
Creecy, C. M., C. F. O'Neill, B. P. Arulanandam, V. L. Sylvia, C. S. Navara, and R. Bizios. 2013. "Mesenchymal Stem Cell Osteodifferentiation in Response to Alternating Electric Current." *Tissue Engineering - Part A* 19 (3–4): 467–74. https://doi.org/10.1089/ten.tea.2012.0091.
Dalby, M. J., N. Gadegaard, R. Tare, A. Andar, M. Riehle, P. Herzyk, C. D. W. Wilkinson, and R. O. C. Oreffo. 2007. "The Control of Human Mesenchymal Cell Differentiation Using Nanoscale Symmetry and Disorder." *Nature Materials* 6 (12): 997–1003. https://doi.org/10.1038/nmat2013.
Damaraju, S. M., Y. Shen, E. Elele, B. Khusid, A. Eshghinejad, J. Li, M. Jaffe, and T. L. Arinzeh. 2017. "Three-Dimensional Piezoelectric Fibrous Scaffolds Selectively Promote Mesenchymal Stem Cell Differentiation." *Biomaterials* 149: 51–62. https://doi.org/10.1016/j.biomaterials.2017.09.024.
Damaraju, S. M., S. Wu, M. Jaffe, and T. L. Arinzeh. 2013. "Structural Changes in PVDF Fibers Due to Electrospinning and Its Effect on Biological Function." *Biomedical Materials* 8 (4): 045007. https://doi.org/10.1088/1748-6041/8/4/045007.
Davis, G. T., J. E. McKinney, M. G. Broadhurst, and S. C. Roth. 1978. "Electric-Field-Induced Phase Changes in Poly(Vinylidene Fluoride)." *Journal of Applied Physics* 49 (10): 4998–5002. https://doi.org/10.1063/1.324446.
Day, T. F., X. Guo, L. Garrett-Beal, and Y. Yang. 2005. "Wnt/β-Catenin Signaling in Mesenchymal Progenitors Controls Osteoblast and Chondrocyte Differentiation during Vertebrate Skeletogenesis." *Developmental Cell* 8 (5): 739–50. https://doi.org/10.1016/j.devcel.2005.03.016.
Deregowski, V., E. Gazzerro, L. Priest, S. Rydziel, and E. Canalis. 2006. "Notch 1 Overexpression Inhibits Osteoblastogenesis by Suppressing Wnt/β-Catenin but Not Bone Morphogenetic Protein Signaling." *Journal of Biological Chemistry* 281 (10): 6203–10. https://doi.org/10.1074/jbc.M508370200.
Dominici, M., K. Le Blanc, I. Mueller, I. Slaper-Cortenbach, F. C. Marini, D. S. Krause, R. J. Deans, A. Keating, D. J. Prockop, and E. M. Horwitz. 2006. "Minimal Criteria for Defining Multipotent Mesenchymal Stromal Cells. The International Society for Cellular Therapy Position Statement." *Cytotherapy* 8 (4): 315–17. https://doi.org/10.1080/14653240600855905.
Einhorn, T. A., and L. C. Gerstenfeld. 2015. "Fracture Healing: Mechanisms and

Interventions." *Nature Reviews Rheumatology* 11 (1): 45–54. https://doi.org/10.1038/nrrheum.2014.164.

Engler, A. J., S. Sen, H. L. Sweeney, and D. E. Discher. 2006. "Matrix Elasticity Directs Stem Cell Lineage Specification." *Cell* 126 (4): 677–89. https://doi.org/10.1016/j.cell.2006.06.044.

Fan, B., Z. Guo, X. Li, S. Li, P. Gao, X. Xiao, J. Wu, C. Shen, Y. Jiao, and W. Hou. 2020. "Electroactive Barium Titanate Coated Titanium Scaffold Improves Osteogenesis and Osseointegration with Low-Intensity Pulsed Ultrasound for Large Segmental Bone Defects." *Bioactive Materials* 5 (4): 1087–1101. https://doi.org/10.1016/j.bioactmat.2020.07.001.

Fehrer, C., R. Brunauer, G. Laschober, H. Unterluggauer, S. Reitinger, F. Kloss, C. Gülly, R. Gaßner, and G. Lepperdinger. 2007. "Reduced Oxygen Tension Attenuates Differentiation Capacity of Human Mesenchymal Stem Cells and Prolongs Their Lifespan." *Aging Cell* 6 (6): 745–57. https://doi.org/10.1111/j.1474-9726.2007.00336.x.

Fernandes, M. M., D. M. Correia, C. Ribeiro, N. Castro, V. Correia, and S. Lanceros-Mendez. 2019. "Bioinspired Three-Dimensional Magnetoactive Scaffolds for Bone Tissue Engineering." *ACS Applied Materials and Interfaces* 11 (48): 45265–75. https://doi.org/10.1021/acsami.9b14001.

Ferroni, L., C. Gardin, O. Dolkart, M. Salai, S. Barak, A. Piattelli, H. Amir-Barak, and B. Zavan. 2018. "Pulsed Electromagnetic Fields Increase Osteogenetic Commitment of MSCs via the MTOR Pathway in TNF-α Mediated Inflammatory Conditions: An in-Vitro Study." *Scientific Reports* 8 (1): 1–13. https://doi.org/10.1038/s41598-018-23499-9.

Forciniti, L., J. Ybarra, M. H. Zaman, and C. E. Schmidt. 2014. "Schwann Cell Response on Polypyrrole Substrates upon Electrical Stimulation." *Acta Biomaterialia* 10 (6): 2423–33. https://doi.org/10.1016/j.actbio.2014.01.030.

Franz-Odendaal, T. A., B. K. Hall, and P. E. Witten. 2006. "Buried Alive: How Osteoblasts Become Osteocytes." *Developmental Dynamics* 235 (1): 176–90. https://doi.org/10.1002/dvdy.20603.

Friedenstein, A. J. 1976. "Precursor Cells of Mechanocytes." *International Review of Cytology* 47 (C): 327–59. https://doi.org/10.1016/S0074-7696(08)60092-3.

Fu, Y. C., C. C. Lin, J. K. Chang, C. H. Chen, I. C. Tai, G. J. Wang, and M. L. Ho. 2014. "A Novel Single Pulsed Electromagnetic Field Stimulates Osteogenesis of Bone Marrow Mesenchymal Stem Cells and Bone Repair." *PLoS ONE* 9 (3). https://doi.org/10.1371/journal.pone.0091581.

Fukada, E., and I. Yasuda. 1957. "On the Piezoelectric Effect of Bone." *Journal of the Physical Society of Japan* 12 (10): 1158–62. https://doi.org/10.1143/JPSJ.12.1158.

Gavazzo, P., F. Viti, H. Donnelly, M. Azevedo Gonzalez Oliva, M. Salmeron-Sanchez, M. J. Dalby, and M. Vassalli. 2021. "Biophysical Phenotyping of Mesenchymal Stem Cells along the Osteogenic Differentiation Pathway." *Cell Biology and Toxicology* 37 (6): 915–33. https://doi.org/10.1007/s10565-020-09569-7.

Ghali, O., O. Broux, G. Falgayrac, N. Haren, J. P.T.M. Van Leeuwen, G. Penel, P. Hardouin, and C. Chauveau. 2015. "Dexamethasone in Osteogenic Medium Strongly Induces Adipocyte Differentiation of Mouse Bone Marrow Stromal Cells and Increases Osteoblast Differentiation." *BMC Cell Biology* 16 (1): 1–15. https://doi.org/10.1186/s12860-015-0056-6.

Giannetti, E. 2001. "Semi-Crystalline Fluorinated Polymers." *Polymer International* 50 (1): 10–26. https://doi.org/10.1002/1097-0126(200101)50:1<10::AID-PI614>3.0.CO;2-W.

Gomes, J., J. Serrado Nunes, V. Sencadas, and S. Lanceros-Mendez. 2010. "Influence of the β-Phase Content and Degree of Crystallinity on the Piezo-and Ferroelectric Properties of Poly(Vinylidene Fluoride)." *Smart Materials and Structures* 19 (6). https://doi.org/10.1088/0964-1726/19/6/065010.

Gómez-Barrena, Enrique, Philippe Rosset, Daniel Lozano, Julien Stanovici, Christian Ermthaller, and Florian Gerbhard. 2015. "Bone Fracture Healing: Cell Therapy in

Delayed Unions and Nonunions." *Bone* 70: 93–101. https://doi.org/10.1016/j.bone.2014.07.033.

Gonçalves, R., P. Martins, D. M. Correia, V. Sencadas, J. L. Vilas, L. M. León, G. Botelho, and S. Lanceros-Méndez. 2015. "Development of Magnetoelectric CoFe2O4/Poly(Vinylidene Fluoride) Microspheres." *RSC Adv.* 5 (45): 35852–57. https://doi.org/10.1039/C5RA04409J.

Gonçalves, R., P. Martins, X. Moya, M. Ghidini, V. Sencadas, G. Botelho, N. D. Mathur, and S. Lanceros-Mendez. 2015. "Magnetoelectric CoFe $_2$ O $_4$ /Polyvinylidene Fluoride Electrospun Nanofibres." *Nanoscale* 7 (17): 8058–61. https://doi.org/10.1039/C5NR00453E.

González De Torre, I., M. Santos, L. Quintanilla, A. Testera, M. Alonso, and J. C. Rodríguez Cabello. 2014. "Elastin-like Recombinamer Catalyst-Free Click Gels: Characterization of Poroelastic and Intrinsic Viscoelastic Properties." *Acta Biomaterialia* 10 (6): 2495–2505. https://doi.org/10.1016/j.actbio.2014.02.006.

Gopalakrishnan-Prema, V., A. Mohanan, S. B. Shivaram, P. Madhusudanan, G. Raju, D. Menon, and S. A. Shankarappa. 2020. "Electrical Stimulation of Co-Woven Nerve Conduit for Peripheral Neurite Differentiation." *Biomedical Materials (Bristol)* 15 (6). https://doi.org/10.1088/1748-605X/abaf06.

Grayson, W. L., F. Zhao, R. Izadpanah, B. Bunnell, and M. Teng. 2006. "Effects of Hypoxia on Human Mesenchymal Stem Cell Expansion." *Journal of Cellular Physiology* 207 (10.1002/jcp.20571): 331–39. https://doi.org/10.1002/JCP.

Gregorio, R., and M. Cestari. 1994. "Effect of Crystallization Temperature on the Crystalline Phase Content and Morphology of Poly(Vinylidene Fluoride)." *Journal of Polymer Science Part B: Polymer Physics* 32 (5): 859–70. https://doi.org/10.1002/polb.1994.090320509.

Griffin, M., S. A. Iqbal, A. Sebastian, J. Colthurst, and A. Bayat. 2011. "Degenerate Wave and Capacitive Coupling Increase Human MSC Invasion and Proliferation While Reducing Cytotoxicity in an in Vitro Wound Healing Model." *PLoS ONE* 6 (8). https://doi.org/10.1371/journal.pone.0023404.

Guan, J. L. 1997. "Focal Adhesion Kinase in Integrin Signaling." *Matrix Biology* 16 (4): 195–200. https://doi.org/10.1016/S0945-053X(97)90008-1.

Guillot-Ferriols, M., S. Lanceros-Méndez, J. L. Gómez Ribelles, and G. Gallego-Ferrer. 2022. "Electrical Stimulation: Effective Cue to Direct Osteogenic Differentiation of Mesenchymal Stem Cells?" *Biomaterials Advances* 138 (May): 1–18. https://doi.org/10.1016/j.bioadv.2022.212918.

Guillot-Ferriols, M., J. C. Rodríguez-Hernández, D. M. Correia, S. A. C. Carabineiro, S. Lanceros-Méndez, J. L. Gómez Ribelles, and G. Gallego Ferrer. 2020. "Poly(Vinylidene) Fluoride Membranes Coated by Heparin / Collagen Layer-by-Layer, Smart Biomimetic Approaches for Mesenchymal Stem Cell Culture." *Materials Science & Engineering C* 117: 1–12. https://doi.org/10.1016/j.msec.2020.111281.

Guo, H. F., Z. S. Li, S. W. Dong, W. J. Chen, L. Deng, Y. F. Wang, and D. J. Ying. 2012. "Piezoelectric PU/PVDF Electrospun Scaffolds for Wound Healing Applications." *Colloids and Surfaces B: Biointerfaces* 96: 29–36. https://doi.org/10.1016/j.colsurfb.2012.03.014.

Gupta, A. K., K. P. Srivastava, and S. Avasthi. 2009. "Pulsed Electromagnetic Stimulation in Nonunion of Tibial Diaphyseal Fractures." *Indian Journal of Orthopaedics* 43 (2): 156–60. https://doi.org/10.4103/0019-5413.50850.

Halim, A., A. D. Ariyanti, Q. Luo, and G. Song. 2020. "Recent Progress in Engineering Mesenchymal Stem Cell Differentiation." *Stem Cell Reviews and Reports* 16 (4): 661–74. https://doi.org/10.1007/s12015-020-09979-4.

Hammerick, K. E., A. W. James, Z. Huang, F. B. Prinz, and M. T. Longaker. 2010. "Pulsed Direct Current Electric Fields Enhance Osteogenesis in Adipose-Derived Stromal Cells." *Tissue Engineering - Part A* 16 (3): 917–31.

https://doi.org/10.1089/ten.tea.2009.0267.
Hardy, J. G., M. K. Villancio-Wolter, R. C. Sukhavasi, D. J. Mouser, D. Aguilar Jr., S. A. Geissler, D. L. Kaplan, and C. E. Schmidt. 2015. “Electrical Stimulation of Human Mesenchymal Stem Cells on Conductive Nanofibers Enhances Their Differentiation toward Osteogenic Outcomes.” *Macromolecular Rapid Communications* 36: 1884–90. https://doi.org/DOI: 10.1002/marc.201500233.
Harrison, J.S., and Z. Ounaies. 2001. “Piezoelectric Polymers; ICASE Report No: 2001-43; Langley Research Center: Hampton, Virginia.”
Hartig, M., U. Joos, and H. P. Wiesmann. 2000. “Capacitively Coupled Electric Fields Accelerate Proliferation of Osteoblast-like Primary Cells and Increase Bone Extracellular Matrix Formation in Vitro.” *European Biophysics Journal* 29 (7): 499–506. https://doi.org/10.1007/s002490000100.
Hernigou, P., G. Mathieu, A. Poignard, O. Manicom, F. Beaujean, and H. Rouard. 2006. “Percutaneous Autologous Bone-Marrow Grafting for Nonunions. Surgical Technique.” *The Journal of Bone and Joint Surgery* 88 Suppl 1: 322–27. https://doi.org/10.2106/JBJS.F.00203.
Hess, R., A. Jaeschke, H. Neubert, V. Hintze, S. Moeller, M. Schnabelrauch, H. P. Wiesmann, D. A. Hart, and D. Scharnweber. 2012. “Synergistic Effect of Defined Artificial Extracellular Matrices and Pulsed Electric Fields on Osteogenic Differentiation of Human MSCs.” *Biomaterials* 33 (35): 8975–85. https://doi.org/10.1016/j.biomaterials.2012.08.056.
Hess, R, H Neubert, A Seifert, S Bierbaum, D A Hart, and D Scharnweber. 2012. “A Novel Approach for In Vitro Studies Applying Electrical Fields to Cell Cultures by Transformer-Like Coupling.” *Cell Biochemistry and Biophysics* 64: 223–32. https://doi.org/10.1007/s12013-012-9388-4.
Hoch, A. I., V. Mittal, D. Mitra, N. Vollmer, C. A. Zikry, and J. K. Leach. 2016. “Cell-Secreted Matrices Perpetuate the Bone-Forming Phenotype of Differentiated Mesenchymal Stem Cells.” *Biomaterials* 74: 178–87. https://doi.org/10.1016/j.biomaterials.2015.10.003.
Hodgkinson, T., P. M. Tsimbouri, V. Llopis-Hernandez, P. Campsie, D. Scurr, P. G. Childs, D. Phillips, et al. 2021. “The Use of Nanovibration to Discover Specific and Potent Bioactive Metabolites That Stimulate Osteogenic Differentiation in Mesenchymal Stem Cells.” *Science Advances* 7 (9): 1–16. https://doi.org/10.1126/sciadv.abb7921.
Holzwarth, C., M. Vaegler, F. Gieseke, S. M. Pfister, R. Handgretinger, G. Kerst, and I. Müller. 2010. “Low Physiologic Oxygen Tensions Reduce Proliferation and Differentiation of Human Multipotent Mesenchymal Stromal Cells.” *BMC Cell Biology* 11. https://doi.org/10.1186/1471-2121-11-11.
Hoop, M., X. Z. Chen, A. Ferrari, F. Mushtaq, G. Ghazaryan, T. Tervoort, D. Poulikakos, B. Nelson, and S. Pané. 2017. “Ultrasound-Mediated Piezoelectric Differentiation of Neuron-like PC12 Cells on PVDF Membranes.” *Scientific Reports* 7 (1): 1–8. https://doi.org/10.1038/s41598-017-03992-3.
Hronik-Tupaj, M., W. L. Rice, M. Cronin-Golomb, D. L. Kaplan, and I. Georgakoudi. 2011. “Osteoblastic Differentiation and Stress Response of Human Mesenchymal Stem Cells Exposed to Alternating Current Electric Fields.” *BioMedical Engineering Online* 10 (1): 9. https://doi.org/10.1186/1475-925X-10-9.
Hu, W. W., T. C. Chen, C. W. Tsao, and Y. C. Cheng. 2019. “The Effects of Substrate-Mediated Electrical Stimulation on the Promotion of Osteogenic Differentiation and Its Optimization.” *Journal of Biomedical Materials Research - Part B Applied Biomaterials* 107 (5): 1607–19. https://doi.org/10.1002/jbm.b.34253.
Hu, W. W., Y. T. Hsu, Y. C. Cheng, C. Li, R. C. Ruaan, C. C. Chien, C. A. Chung, and C. W. Tsao. 2014. “Electrical Stimulation to Promote Osteogenesis Using Conductive Polypyrrole Films.” *Materials Science and Engineering C* 37 (1): 28–36. https://doi.org/10.1016/j.msec.2013.12.019.

Hu, Y., B. Lou, X. Wu, R. Wu, H. Wang, L. Gao, J. Pi, and Y. Xu. 2018. “Comparative Study on in Vitro Culture of Mouse Bone Marrow Mesenchymal Stem Cells.” *Stem Cells International* 2018. https://doi.org/10.1155/2018/6704583.

Huang, C. C-Y, K. L. Hagar, L. E. Frost, Y. Sun, and H. S. Cheung. 2004. “Effects of Cyclic Compressive Loading on Chondrogenesis of Rabbit Bone-Marrow Derived Mesenchymal Stem Cells.” *Stem Cells* 22 (3): 313–23. https://doi.org/10.1634/stemcells.22-3-313.

Huang, J., X. Hu, L. Lu, Z. Ye, Q. Zhang, and Z. Luo. 2010. “Electrical Regulation of Schwann Cells Using Conductive Polypyrrole/Chitosan Polymers.” *Journal of Biomedical Materials Research - Part A* 93 (1): 164–74. https://doi.org/10.1002/jbm.a.32511.

Huang, Y., H. Deng, Y. Fan, L. Zheng, J. Che, X. Li, and K. E. Aifantis. 2019. “Conductive Nanostructured Si Biomaterials Enhance Osteogeneration through Electrical Stimulation.” *Materials Science and Engineering C* 103 (April): 109748. https://doi.org/10.1016/j.msec.2019.109748.

Jaiswal, R. K., N. Jaiswal, S. P. Bruder, G. Mbalaviele, D. R. Marshak, and M. F. Pittenger. 2000. “Adult Human Mesenchymal Stem Cell Differentiation to the Osteogenic or Adipogenic Lineage Is Regulated by Mitogen-Activated Protein Kinase.” *Journal of Biological Chemistry* 275 (13): 9645–52. https://doi.org/10.1074/jbc.275.13.9645.

Jamal, D., and R. C. De Guzman. 2017. “Silicone Substrate with Collagen and Carbon Nanotubes Exposed to Pulsed Current for MSC Osteodifferentiation.” *International Journal of Biomaterials* 2017. https://doi.org/10.1155/2017/3684812.

Jamjoom, A., and R. E. Cohen. 2015. “Grafts for Ridge Preservation.” *Journal of Functional Biomaterials* 6: 833–48. https://doi.org/10.3390/jfb6030833.

Jansen, J. H. W., O. P. Van Der Jagt, B. J. Punt, J. A. N. Verhaar, J. P.T.M. Van Leeuwen, H. Weinans, and H. Jahr. 2010. “Stimulation of Osteogenic Differentiation in Human Osteoprogenitor Cells by Pulsed Electromagnetic Fields: An in Vitro Study.” *BMC Musculoskeletal Disorders* 11: 1–11. https://doi.org/10.1186/1471-2474-11-188.

Jia, F., S. Lin, X. He, J. Zhang, S. Shen, Z. Wang, B. Tang, et al. 2019. “Comprehensive Evaluation of Surface Potential Characteristics on Mesenchymal Stem Cells Osteogenic Differentiation.” *ACS Applied Materials and Interfaces*. https://doi.org/10.1021/acsami.9b07161.

Jing, W., Y. Huang, P. Wei, Q. Cai, X. Yang, and W. Zhong. 2019. “Roles of Electrical Stimulation in Promoting Osteogenic Differentiation of BMSCs on Conductive Fibers.” *Journal of Biomedical Materials Research - Part A*, 1443–54. https://doi.org/10.1002/jbm.a.36659.

Kitsara, M., A. Blanquer, G. Murillo, V. Humblot, S. De Bragança Vieira, C. Nogués, E. Ibáñez, J. Esteve, and L. Barrios. 2019. “Permanently Hydrophilic, Piezoelectric PVDF Nanofibrous Scaffolds Promoting Unaided Electromechanical Stimulation on Osteoblasts.” *Nanoscale* 11 (18): 8906–17. https://doi.org/10.1039/c8nr10384d.

Klee, D., Z. Ademovic, A. Bosserhoff, H. Hoecker, G. Maziolis, and H. J. Erli. 2003. “Surface Modification of Poly(Vinylidenefluoride) to Improve the Osteoblast Adhesion.” *Biomaterials* 24 (21): 3663–70. https://doi.org/10.1016/S0142-9612(03)00235-7.

Laurencin, C., Y. Khan, and S. F. El-Amin. 2006. “Bone Graft Substitutes.” *Expert Review of Medical Devices* 3 (1): 49–57. https://doi.org/10.1586/17434440.3.1.49.

Lennon, Donald P., John M. Edmison, and Arnold I. Caplan. 2001. “Cultivation of Rat Marrow-Derived Mesenchymal Stem Cells in Reduced Oxygen Tension: Effects on in Vitro and in Vivo Osteochondrogenesis.” *Journal of Cellular Physiology* 187 (3): 345–55. https://doi.org/10.1002/jcp.1081.

Leppik, L., H. Zhihua, S. Mobini, V. Thottakkattumana Parameswaran, M. Eischen-Loges, A. Slavici, J. Helbing, et al. 2018. “Combining Electrical Stimulation and Tissue Engineering to Treat Large Bone Defects in a Rat Model.” *Scientific Reports* 8 (1): 1–14. https://doi.org/10.1038/s41598-018-24892-0.

Li, J., X. Liu, J. M. Crook, and G. G. Wallace. 2020. “Electrical Stimulation-Induced Osteogenesis of Human Adipose Derived Stem Cells Using a Conductive Graphene-Cellulose Scaffold.” *Materials Science and Engineering C* 107 (October 2019): 110312. https://doi.org/10.1016/j.msec.2019.110312.

Li, J., X. Mou, J. Qiu, S. Wang, D. Wang, D. Sun, W. Guo, et al. 2015. “Surface Charge Regulation of Osteogenic Differentiation of Mesenchymal Stem Cell on Polarized Ferroelectric Crystal Substrate.” *Advanced Healthcare Materials* 4 (7): 998–1003. https://doi.org/10.1002/adhm.201500032.

Li, Y., X. Dai, Y. Bai, Y. Liu, Y. Wang, O. Liu, F. Yan, Z. Tang, X. Zhang, and X. Deng. 2017. “Electroactive BaTiO3 Nanoparticle-Functionalized Fibrous Scaffolds Enhance Osteogenic Differentiation of Mesenchymal Stem Cells.” *International Journal of Nanomedicine* 12: 4007–18. https://doi.org/10.2147/IJN.S135605.

Lim, K., J. Hexiu, J. Kim, H. Seonwoo, W. J. Cho, P-H. Choung, and J. H. Chung. 2013. “Effects of Electromagnetic Fields on Osteogenesis of Human Alveolar Bone-Derived Mesenchymal Stem Cells.” *BioMed Research International* 2013: 296019. https://doi.org/https://doi.org/10.1155/2013/296019.

Liu, H. F., L. Yang, H. C. He, J. Zhou, Y. Liu, C. Y. Wang, Y. C. Wu, and C. Q. He. 2013. “Pulsed Electromagnetic Fields on Postmenopausal Osteoporosis in Southwest China: A Randomized, Active-Controlled Clinical Trial.” *Bioelectromagnetics* 34 (4): 323–32. https://doi.org/10.1002/bem.21770.

Liu, J., H. Hao, H. Huang, C. Tong, D. Ti, L. Dong, D. Chen, et al. 2015. “Hypoxia Regulates the Therapeutic Potential of Mesenchymal Stem Cells through Enhanced Autophagy.” *International Journal of Lower Extremity Wounds* 14 (1): 63–72. https://doi.org/10.1177/1534734615573660.

Liu, Wenwen, Xiaokang Li, Yilai Jiao, Cong Wu, Shuo Guo, Xin Xiao, Xinghui Wei, et al. 2020. “Biological Effects of a Three-Dimensionally Printed Ti6Al4V Scaffold Coated with Piezoelectric BaTiO3Nanoparticles on Bone Formation.” *ACS Applied Materials and Interfaces* 12 (46): 51885–903. https://doi.org/10.1021/acsami.0c10957.

Liu, Yun, Xuehui Zhang, Cen Cao, Yuelin Zhang, Jinqi Wei, Yong jun Li, Weiwei Liang, et al. 2017. “Built-In Electric Fields Dramatically Induce Enhancement of Osseointegration.” *Advanced Functional Materials* 27 (47): 1–9. https://doi.org/10.1002/adfm.201703771.

Lopes, D., C. Martins-Cruz, M. B. Oliveira, and J. F. Mano. 2018. “Bone Physiology as Inspiration for Tissue Regenerative Therapies.” *Biomaterials* 185 (April): 240–75. https://doi.org/10.1016/j.biomaterials.2018.09.028.

Lopes, H. B., T. S. Santos, F. S. De Oliveira, G. P. Freitas, A. L. De Almeida, R. Gimenes, A. L. Rosa, and M. M. Beloti. 2014. “Poly(Vinylidene-Trifluoroethylene)/Barium Titanate Composite for in Vivo Support of Bone Formation.” *Journal of Biomaterials Applications* 29 (1): 104–12. https://doi.org/10.1177/0885328213515735.

Lund, A., and B. Hagström. 2010. “Melt Spinning of B-Phase Poly(Vinylidene Fluoride) Yarns with and without a Conductive Core.” *Journal of Applied Polymer Science* 116: 1080–89. https://doi.org/10.1002/app.33239.

Luo, Z., X. Shang, H. Zhang, G. Wang, P. A. Massey, S. R. Barton, C. G. Kevil, and Y. Dong. 2019. “Notch Signaling in Osteogenesis, Osteoclastogenesis, and Angiogenesis.” *American Journal of Pathology* 189 (8): 1495–1500. https://doi.org/10.1016/j.ajpath.2019.05.005.

Maharjan, B., V. K. Kaliannagounder, S. R. Jang, G. P. Awasthi, D. P. Bhattarai, G. Choukrani, C. H. Park, and C. S. Kim. 2020. “In-Situ Polymerized Polypyrrole Nanoparticles Immobilized Poly(ε-Caprolactone) Electrospun Conductive Scaffolds for Bone Tissue Engineering.” *Materials Science and Engineering C* 114 (April): 111056. https://doi.org/10.1016/j.msec.2020.111056.

Malladi, P., Y. Xu, M. Chiou, A. J. Giaccia, and M. T. Longaker. 2006. “Effect of Reduced Oxygen Tension on Chondrogenesis and Osteogenesis in Adipose-Derived

Mesenchymal Cells." *American Journal of Physiology - Cell Physiology* 290 (4): 1139–45. https://doi.org/10.1152/ajpcell.00415.2005.

Mandal, D., K. Kim, and J. S. Lee. 2012. "Simple Synthesis of Palladium Nanoparticles, β-Phase Formation, and the Control of Chain and Dipole Orientations in Palladium-Doped Poly(Vinylidene Fluoride) Thin Films." *Langmuir* 28 (28): 10310–17. https://doi.org/10.1021/la300983x.

Mao, J., and Z. Zhang. 2018. "Polypyrrole as Electrically Conductive Biomaterials: Synthesis, Biofunctionalization, Potential Applications and Challenges." *Advances in Experimental Medicine and Biology*, 347–70. https://doi.org/10.1007/978-981-13-0950-2_18.

Martini, F., A. Pellati, E. Mazzoni, S. Salati, G. Caruso, D. Contartese, and M. De Mattei. 2020. "Bone Morphogenetic Protein-2 Signaling in the Osteogenic Differentiation of Human Bone Marrow Mesenchymal Stem Cells Induced by Pulsed Electromagnetic Fields." *International Journal of Molecular Sciences* 21 (6). https://doi.org/10.3390/ijms21062104.

Martins, P., C. M. Costa, M. Benelmekki, G. Botelho, and S. Lanceros-Mendez. 2012. "On the Origin of the Electroactive Poly(Vinylidene Fluoride) β-Phase Nucleation by Ferrite Nanoparticles via Surface Electrostatic Interactions." *CrystEngComm* 14 (8): 2807–11. https://doi.org/10.1039/c2ce06654h.

Martins, P., C. M. Costa, J. C.C. Ferreira, and S. Lanceros-Mendez. 2012. "Correlation between Crystallization Kinetics and Electroactive Polymer Phase Nucleation in Ferrite/Poly(Vinylidene Fluoride) Magnetoelectric Nanocomposites." *Journal of Physical Chemistry B* 116 (2): 794–801. https://doi.org/10.1021/jp210493t.

Martins, P., C. M. Costa, and S. Lanceros-Mendez. 2011. "Nucleation of Electroactive β-Phase Poly(Vinilidene Fluoride) with CoFe2O4 and NiFe2O4 Nanofillers: A New Method for the Preparation of Multiferroic Nanocomposites." *Applied Physics A: Materials Science and Processing* 103 (1): 233–37. https://doi.org/10.1007/s00339-010-6003-7.

Martins, P., and S. Lanceros-Méndez. 2013. "Polymer-Based Magnetoelectric Materials." *Advanced Functional Materials* 23 (27): 3371–85. https://doi.org/10.1002/adfm.201202780.

Martins, P., A. C. Lopes, and S. Lanceros-Mendez. 2014. "Electroactive Phases of Poly(Vinylidene Fluoride): Determination, Processing and Applications." *Progress in Polymer Science* 39 (4): 683–706. https://doi.org/10.1016/j.progpolymsci.2013.07.006.

Massari, L., M. Fini, R. Cadossi, S. Setti, and G. C. Traina. 2006. "Biophysical Stimulation with Pulsed Electromagnetic Fields in Osteonecrosis of the Femoral Head." *Journal of Bone and Joint Surgery - Series A* 88 (SUPPL. 3): 56–60. https://doi.org/10.2106/00004623-200611001-00009.

Meira, R. M., D. M. Correia, S. Ribeiro, P. Costa, A. C. Gomes, F. M. Gama, S. Lanceros-Méndez, and C. Ribeiro. 2019. "Ionic-Liquid-Based Electroactive Polymer Composites for Muscle Tissue Engineering." *ACS Applied Polymer Materials* 1 (10): 2649–58. https://doi.org/10.1021/acsapm.9b00566.

Minary-Jolandan, M., and M. F. Yu. 2009. "Uncovering Nanoscale Electromechanical Heterogeneity in the Subfibrillar Structure of Collagen Fibrils Responsible for the Piezoelectricity of Bone." *ACS Nano* 3 (7): 1859–63. https://doi.org/10.1021/nn900472n.

Mirzaei, A., A. S. Moghadam, M. F. Abazari, F. Nejati, S. Torabinejad, M. Kaabi, S. E. Enderami, et al. 2019. "Comparison of Osteogenic Differentiation Potential of Induced Pluripotent Stem Cells on 2D and 3D Polyvinylidene Fluoride Scaffolds." *Journal of Cellular Physiology* 234: 17854–62. https://doi.org/10.1002/jcp.28415.

Mobini, S., L. Leppik, and J. H. Barker. 2016. "Direct Current Electrical Stimulation Chamber for Treating Cells in Vitro." *BioTechniques* 60 (2): 95–98.

https://doi.org/10.2144/000114382.
Mobini, S., L. Leppik, V. T. Parameswaran, and J. H. Barker. 2017. “In Vitro Effect of Direct Current Electrical Stimulation on Rat Mesenchymal Stem Cells.” *PeerJ* 2017 (1): 1–15. https://doi.org/10.7717/peerj.2821.
Mojsilović, S., A. Krstić, V. Ilić, I. Okić-Dordević, J. Kocić, D. Trivanović, J. F. Santibañez, G. Jovčić, and D. Bugarski. 2011. “IL-17 and FGF Signaling Involved in Mouse Mesenchymal Stem Cell Proliferation.” *Cell and Tissue Research* 346 (3): 305–16. https://doi.org/10.1007/s00441-011-1284-5.
Morales-Román, R. M., M. Guillot-Ferriols, L. Roig-Pérez, S. Lanceros-Mendez, G. Gallego-Ferrer, and J. L. Gómez Ribelles. 2019. “Freeze-Extraction Microporous Electroactive Supports for Cell Culture.” *European Polymer Journal* 119 (June): 531–40. https://doi.org/10.1016/j.eurpolymj.2019.07.011.
Nair, A. K., A. Gautieri, S. W. Chang, and M. J. Buehler. 2013. “Molecular Mechanics of Mineralized Collagen Fibrils in Bone.” *Nature Communications* 4: 1–9. https://doi.org/10.1038/ncomms2720.
Nakashima, K., X. Zhou, G. Kunkel, Z. Zhang, J. M. Deng, and B. de Crombrugghe. 2002. “The Novel Zinc Finger-Containing Transcription Factor Osterix Is Required for Osteoblast Differentiation and Bone Formation.” *Cell* 108: 17–29.
Nauth, A., M. D. McKee, T. A. Einhorn, J. T. Watson, R. Li, and E. H. Schemitsch. 2011. “Managing Bone Defects.” *Journal of Orthopaedic Trauma* 25 (8): 462–66. https://doi.org/10.1097/BOT.0b013e318224caf0.
Nolte, P. A., J. Klein-Nulend, G. H.R. Albers, R. K. Marti, C. M. Semeins, S. W. Goei, and E. H. Burger. 2001. “Low-Intensity Ultrasound Stimulates Endochondral Ossification in Vitro.” *Journal of Orthopaedic Research* 19 (2): 301–7. https://doi.org/10.1016/S0736-0266(00)00027-9.
Noronha, N. C., A. Mizukami, C. Caliári-Oliveira, J. G. Cominal, J. L. M. Rocha, D. T. Covas, K. Swiech, and K. C. R. Malmegrim. 2019. “Priming Approaches to Improve the Efficacy of Mesenchymal Stromal Cell-Based Therapies.” *Stem Cell Research and Therapy* 10 (1): 1–21. https://doi.org/10.1186/s13287-019-1259-0.
Oryan, A., S. Alidadi, A. Moshiri, and N. Maffulli. 2014. “Bone Regenerative Medicine: Classic Options, Novel Strategies, and Future Directions.” *Journal of Orthopaedic Surgery and Research* 9 (1): 1–27. https://doi.org/10.1186/1749-799X-9-18.
Pall, M. L. 2013. “Electromagnetic Fields Act via Activation of Voltage-Gated Calcium Channels to Produce Beneficial or Adverse Effects.” *Journal of Cellular and Molecular Medicine* 17 (8): 958–65. https://doi.org/10.1111/jcmm.12088.
Park, S. E., G-B. Yeon, H-G. Goo, D. S. Seo, A. A. Dayem, K. E. Lee, H-M. Park, S-G. Cho, and D-S. Kim. 2020. “Maintenance and Differentiation of Human ES Cells on Polyvinylidene Fluoride Scaffolds Immobilized with a Vitronectin-Derived Peptide.” *Journal of Cellular Physiology* 236: 3510–20. https://doi.org/10.1002/jcp.30095.
Pärssinen, J., H. Hammarén, R. Rahikainen, V. Sencadas, C. Ribeiro, S. Vanhatupa, S. Miettinen, S. Lanceros-Méndez, and V. P. Hytönen. 2015. “Enhancement of Adhesion and Promotion of Osteogenic Differentiation of Human Adipose Stem Cells by Poled Electroactive Poly(Vinylidene Fluoride).” *Journal of Biomedical Materials Research - Part A* 103 (3): 919–28. https://doi.org/10.1002/jbm.a.35234.
Pelto, J., M. Björninen, A. Pälli, E. Talvitie, J. Hyttinen, B. Mannerström, R. Suuronen Seppanen, M. Kellomäki, S. Miettinen, and S. Haimi. 2013. “Novel Polypyrrole-Coated Polylactide Scaffolds Enhance Adipose Stem Cell Proliferation and Early Osteogenic Differentiation.” *Tissue Engineering - Part A* 19 (7–8): 882–92. https://doi.org/10.1089/ten.tea.2012.0111.
Perez, J. R., D. Kouroupis, D. J. Li, T. M. Best, L. Kaplan, and D. Correa. 2018. “Tissue Engineering and Cell-Based Therapies for Fractures and Bone Defects.” *Frontiers in Bioengineering and Biotechnology* 6 (July): 1–23. https://doi.org/10.3389/fbioe.2018.00105.

Petecchia, L., F. Sbrana, R. Utzeri, M. Vercellino, C. Usai, L. Visai, M. Vassalli, and P. Gavazzo. 2015. “Electro-Magnetic Field Promotes Osteogenic Differentiation of BM-HMSCs through a Selective Action on Ca2+ -Related Mechanisms.” *Scientific Reports* 5 (September): 1–13. https://doi.org/10.1038/srep13856.

Peters, A., D. Toben, J. Lienau, H. Schell, H. J. Bail, G. Matziolis, G. N. Duda, and K. Kaspar. 2009. “Locally Applied Osteogenic Predifferentiated Progenitor Cells Are More Effective than Undifferentiated Mesenchymal Stem Cells in the Treatment of Delayed Bone Healing.” *Tissue Engineering - Part A* 15 (10): 2947–54. https://doi.org/10.1089/ten.tea.2009.0058.

Petrila, L. M., F. Bucatariu, M. Mihai, and C. Teodosiu. 2021. “Polyelectrolyte Multilayers: An Overview on Fabrication, Properties, and Biomedical and Environmental Applications.” *Materials* 14 (15): 1–29. https://doi.org/10.3390/ma14154152.

Pickering, S. A.W., and B. E. Scammell. 2002. “Electromagnetic Fields for Bone Healing.” *The International Journal of Lower Extremity Wounds* 1 (3): 152–60. https://doi.org/10.1177/153473460200100302.

Potier, E., E. Ferreira, R. Andriamanalijaona, J. P. Pujol, K. Oudina, D. Logeart-Avramoglou, and H. Petite. 2007. “Hypoxia Affects Mesenchymal Stromal Cell Osteogenic Differentiation and Angiogenic Factor Expression.” *Bone* 40 (4): 1078–87. https://doi.org/10.1016/j.bone.2006.11.024.

Qi, F., Y. Wang, T. Ma, S. Zhu, W. Zeng, X. Hu, Z. Liu, J. Huang, and Z. Luo. 2013. “Electrical Regulation of Olfactory Ensheathing Cells Using Conductive Polypyrrole/Chitosan Polymers.” *Biomaterials* 34 (7): 1799–1809. https://doi.org/10.1016/j.biomaterials.2012.11.042.

Rahman, M. S., N. Akhtar, H. M. Jamil, R. S. Banik, and S. M. Asaduzzaman. 2015. “TGF-β/BMP Signaling and Other Molecular Events: Regulation of Osteoblastogenesis and Bone Formation.” *Bone Research* 3 (November 2014). https://doi.org/10.1038/boneres.2015.5.

Rajabi, Amir Hossein, Michael Jaffe, and Treena Livingston Arinzeh. 2015. “Piezoelectric Materials for Tissue Regeneration: A Review.” *Acta Biomaterialia* 24: 12–23. https://doi.org/10.1016/j.actbio.2015.07.010.

Ramadan, K. S., D. Sameoto, and S. Evoy. 2014. “A Review of Piezoelectric Polymers as Functional Materials for Electromechanical Transducers.” *Smart Materials and Structures* 23 (3). https://doi.org/10.1088/0964-1726/23/3/033001.

Ravikumar, K., Sunil Kumar Boda, and Bikramjit Basu. 2017. “Synergy of Substrate Conductivity and Intermittent Electrical Stimulation towards Osteogenic Differentiation of Human Mesenchymal Stem Cells.” *Bioelectrochemistry* 116: 52–64. https://doi.org/10.1016/j.bioelechem.2017.03.004.

Ribeiro, C., D. M. Correia, S. Ribeiro, V. Sencadas, G. Botelho, and S. Lanceros-Méndez. 2015. “Piezoelectric Poly(Vinylidene Fluoride) Microstructure and Poling State in Active Tissue Engineering.” *Engineering in Life Sciences* 15 (4): 351–56. https://doi.org/10.1002/elsc.201400144.

Ribeiro, C., C. M. Costa, D. M. Correia, J. Nunes-Pereira, J. Oliveira, P. Martins, R. Gonçalves, V. F. Cardoso, and S. Lanceros-Méndez. 2018. “Electroactive Poly(Vinylidene Fluoride)-Based Structures for Advanced Applications.” *Nature Protocols* 13 (4): 681–704. https://doi.org/10.1038/nprot.2017.157.

Ribeiro, C., S. Moreira, V. Correia, V. Sencadas, J.G. Rocha, F. M. Gama, J. L. Gómez Ribelles, and S. Lanceros-Méndez. 2012. “Enhanced Proliferation of Pre-Osteoblastic Cells by Dynamic Piezoelectric Stimulation.” *RSC Advances* 2 (30): 11504. https://doi.org/10.1039/c2ra21841k.

Ribeiro, C., J. A. Panadero, V. Sencadas, S. Lanceros-Mendez, M. N. Tamaño, D. Moratal, M. Salmeron-Sanchez, and J. L. Gomez Ribelles. 2012. “Fibronectin Adsorption and Cell Response on Electroactive Poly(Vinylidene Fluoride) Films.” *Biomedical Materials* 7 (3). https://doi.org/10.1088/1748-6041/7/3/035004.

Ribeiro, C., J. Pärssinen, V. Sencadas, V. Correia, S. Miettinen, V. P. Hytönen, and S. Lanceros-Méndez. 2015. “Dynamic Piezoelectric Stimulation Enhances Osteogenic Differentiation of Human Adipose Stem Cells.” *Journal of Biomedical Materials Research - Part A* 103 (6): 2172–75. https://doi.org/10.1002/jbm.a.35368.

Ribeiro, C., V. Sencadas, J. L. Gómez Ribelles, and S. Lanceros-Méndez. 2010. “Influence of Processing Conditions on Polymorphism and Nanofiber Morphology of Electroactive Poly(Vinylidene Fluoride) Electrospun Membranes.” *Soft Materials* 8 (3): 274–87. https://doi.org/10.1080/1539445X.2010.495630.

Ribeiro, S., C. Ribeiro, E. O. Carvalho, C. R. Tubio, N. Castro, N. Pereira, V. Correia, A. C. Gomes, and S. Lanceros-Méndez. 2020. “Magnetically Activated Electroactive Microenvironments for Skeletal Muscle Tissue Regeneration.” *ACS Applied Bio Materials* 3 (7): 4239–52. https://doi.org/10.1021/acsabm.0c00315.

Roddy, E., M. R. DeBaun, A. Daoud-Gray, Y. P. Yang, and M. J. Gardner. 2018. “Treatment of Critical-Sized Bone Defects: Clinical and Tissue Engineering Perspectives.” *European Journal of Orthopaedic Surgery and Traumatology* 28 (3): 351–62. https://doi.org/10.1007/s00590-017-2063-0.

Sayyar, S., M. Bjorninen, S. Haimi, S. Miettinen, K. Gilmore, D. Grijpma, and G. Wallace. 2016. “UV Cross-Linkable Graphene/Poly(Trimethylene Carbonate) Composites for 3D Printing of Electrically Conductive Scaffolds.” *ACS Applied Materials and Interfaces* 8 (46): 31916–25. https://doi.org/10.1021/acsami.6b09962.

Schindeler, A., M. M. McDonald, P. Bokko, and D. G. Little. 2008. “Bone Remodeling during Fracture Repair: The Cellular Picture.” *Seminars in Cell and Developmental Biology* 19 (5): 459–66. https://doi.org/10.1016/j.semcdb.2008.07.004.

Schwartz, Z., B. J. Simon, M. A. Duran, G. Barabino, R. Chaudhri, and B. D. Boyan. 2008. “Pulsed Electromagnetic Fields Enhance BMP-2 Dependent Osteoblastic Differentiation of Human Mesenchymal Stem Cells.” *Journal of Orthopaedic Research* 26 (9): 1250–55. https://doi.org/10.1002/jor.20591.

Sencadas, V., R. Gregorio Filho, and S. Lanceros-Mendez. 2006. “Processing and Characterization of a Novel Nonporous Poly(Vinilidene Fluoride) Films in the β Phase.” *Journal of Non-Crystalline Solids* 352 (21–22): 2226–29. https://doi.org/10.1016/j.jnoncrysol.2006.02.052.

Sencadas, V., R. Gregorio, and S. Lanceros-Méndez. 2009. “α to β Phase Transformation and Microestructural Changes of PVDF Films Induced by Uniaxial Stretch.” *Journal of Macromolecular Science, Part B: Physics* 48 (3): 514–25. https://doi.org/10.1080/00222340902837527.

Shapiro, F. 2008. “Bone Development and Its Relation to Fracture Repair. The Role of Mesenchymal Osteoblasts and Surface Osteoblasts.” *European Cells and Materials* 15: 53–76. https://doi.org/10.22203/eCM.v015a05.

Shin, J. H., D. W. Shin, and M. Noh. 2009. “Interleukin-17A Inhibits Adipocyte Differentiation in Human Mesenchymal Stem Cells and Regulates pro-Inflammatory Responses in Adipocytes.” *Biochemical Pharmacology* 77 (12): 1835–44. https://doi.org/10.1016/j.bcp.2009.03.008.

Simonis, R. B., E. J. Parnell, P. S. Ray, and J. L. Peacock. 2003. “Electrical Treatment of Tibial Non-Union: A Prospective, Randomised, Double-Blind Trial.” *Injury* 34 (5): 357–62. https://doi.org/10.1016/S0020-1383(02)00209-7.

Sobreiro-Almeida, R., M. Tamaño-Machiavello, E. Carvalho, L. Cordón, S. Doria, L. Senent, D. Correia, et al. 2017. “Human Mesenchymal Stem Cells Growth and Osteogenic Differentiation on Piezoelectric Poly(Vinylidene Fluoride) Microsphere Substrates.” *International Journal of Molecular Sciences* 18 (11): 1–17. https://doi.org/10.3390/ijms18112391.

Srirussamee, K., R. Xue, S. Mobini, N. J. Cassidy, and S. H. Cartmell. 2021. “Changes in the Extracellular Microenvironment and Osteogenic Responses of Mesenchymal Stem/Stromal Cells Induced by in Vitro Direct Electrical Stimulation.” *Journal of Tissue*

*Engineering* 12. https://doi.org/10.1177/2041731420974147.
Stephan, M., J. Zimmermann, A. Klinder, F. Sahm, U. van Rienen, P. W. Kämmerer, R. Bader, and A. Jonitz-Heincke. 2020. "Establishment and Evaluation of an In Vitro System for Biophysical Stimulation of Human Osteoblasts." *Cells* 9 (9): 1–19. https://doi.org/10.3390/cells9091995.
Strandring, S. 2008. *Gray's Anatomy: The Anatomical Basis of Clinical Practice*. 40th ed. Elsevier Health Sciences.
Sun, L. Y., D. K. Hsieh, P. C. Lin, H. T. Chiu, and T. W. Chiou. 2010. "Pulsed Electromagnetic Fields Accelerate Proliferation and Osteogenic Gene Expression in Human Bone Marrow Mesenchymal Stem Cells during Osteogenic Differentiation." *Bioelectromagnetics* 31 (3): 209–19. https://doi.org/10.1002/bem.20550.
Sun, S., Y. Liu, S. Lipsky, and M. Cho. 2007. "Physical Manipulation of Calcium Oscillations Facilitates Osteodifferentiation of Human Mesenchymal Stem Cells." *The FASEB Journal* 21 (7): 1472–80. https://doi.org/10.1096/fj.06-7153com.
Supriya, S., L. Kumar, and M. Kar. 2019. "Optimization of Dielectric Properties of PVDF–CFO Nanocomposites." *Polymer Composites* 40 (3): 1239–50. https://doi.org/10.1002/pc.24840.
Tabrah, F., M. Hoffmeier, F. Gilbert, S. Batkin, and C. A. L. Bassett. 1990. "Bone Density Changes in Osteoporosis-prone Women Exposed to Pulsed Electromagnetic Fields (PEMFs)." *Journal of Bone and Mineral Research* 5 (5): 437–42. https://doi.org/10.1002/jbmr.5650050504.
Tandon, N., B. Goh, A. Marsano, P. H. G. Chao, C. Montouri-Sorrentino, J. Gimble, and G. Vunjak-Novakovic. 2009. "Alignment and Elongation of Human Adipose-Derived Stem Cells in Response to Direct-Current Electrical Stimulation." *Proceedings of the 31st Annual International Conference of the IEEE Engineering in Medicine and Biology Society: Engineering the Future of Biomedicine, EMBC 2009*, 6517–21. https://doi.org/10.1109/IEMBS.2009.5333142.
Tang, D., R. S. Tare, L. Y. Yang, D. F. Williams, K. L. Ou, and R. O. C. Oreffo. 2016. "Biofabrication of Bone Tissue: Approaches, Challenges and Translation for Bone Regeneration." *Biomaterials* 83: 363–82. https://doi.org/10.1016/j.biomaterials.2016.01.024.
Thrivikraman, G., S. K. Boda, and B. Basu. 2018. "Unraveling the Mechanistic Effects of Electric Field Stimulation towards Directing Stem Cell Fate and Function: A Tissue Engineering Perspective." *Biomaterials* 150: 60–86. https://doi.org/10.1016/j.biomaterials.2017.10.003.
Tomaskovic-Crook, E., Q. Gu, S. N. A. Rahim, G. G. Wallace, and J. M. Crook. 2020. "Conducting Polymer Mediated Electrical Stimulation Induces Multilineage Differentiation with Robust Neuronal Fate Determination of Human Induced Pluripotent Stem Cells." *Cells* 9 (3): 1–14. https://doi.org/10.3390/cells9030658.
Traina, G.C, G. Fontanesi, P. Costa, G.I. Mammi, F. Pisano, F. Giancecchi, and P. Adravanti. 1991. "Effect of Electromagnetic Stimulation on Patients Suffering from Non-Union. A Retrospective Study with a Control Group." *Journal of Bioelectricity* 10: 101–17. https://doi.org/10.3109/15368379109031402.
Tsai, M. T., W. J. Li, R. S. Tuan, and W. H. Chang. 2009. "Modulation of Osteogenesis in Human Mesenchymal Stem Cells by Specific Pulsed Electromagnetic Field Stimulation." *Journal of Orthopaedic Research* 27 (9): 1169–74. https://doi.org/10.1002/jor.20862.
Tzelepi, V., A. C. Tsamandas, V. Zolota, and C. D. Scopa. 2014. "Bone Anatomy, Physiology and Function." In *Cancer Metastasis - Biology and Treatment*, 21:3–30. https://doi.org/10.1007/978-94-007-7569-5.
Uccelli, A., L. Moretta, and V. Pistoia. 2008. "Mesenchymal Stem Cells in Health and Disease." *Nature Reviews Immunology* 8 (9): 726–36. https://doi.org/10.1038/nri2395.
Vijayavenkataraman, S., N. Vialli, J. Y. H. Fuh, and W. F. Lu. 2019. "Conductive

Collagen/Polypyrrole-b-Polycaprolactone Hydrogel for Bioprinting of Neural Tissue Constructs." *International Journal of Bioprinting* 5 (2.1 Special Issue): 31–43. https://doi.org/10.18063/ijb.v5i2.1.229.

Volkmer, E., B. C. Kallukalam, J. Maertz, S. Otto, I. Drosse, H. Polzer, W. Bocker, et al. 2010. "Hypoxic Preconditioning of Human Mesenchymal Stem Cells Overcomes Hypoxia-Induced Inhibition of Osteogenic Differentiation." *Tissue Engineering - Part A* 16 (1): 153–64. https://doi.org/10.1089/ten.tea.2009.0021.

Wang, W., S. Zhang, L. O. Srisombat, T. R. Lee, and R. C. Advincula. 2011. "Gold-Nanoparticle- and Gold-Nanoshell-Induced Polymorphism in Poly(Vinylidene Fluoride)." *Macromolecular Materials and Engineering* 296 (2): 178–84. https://doi.org/10.1002/mame.201000271.

Wang, Z. L. 2007. "Nanopiezotronics." *Advanced Materials* 19 (6): 889–92. https://doi.org/10.1002/adma.200602918.

Wortzel, I., and R. Seger. 2011. "The ERK Cascade: Distinct Functions within Various Subcellular Organelles." *Genes and Cancer* 2 (3): 195–209. https://doi.org/10.1177/1947601911407328.

Wu, S., M. S. Chen, P. Maurel, Y. S. Lee, M. B. Bunge, and T. L. Arinzeh. 2018. "Aligned Fibrous PVDF-TrFE Scaffolds with Schwann Cells Support Neurite Extension and Myelination in Vitro." *Journal of Neural Engineering* 15 (5). https://doi.org/10.1088/1741-2552/aac77f.

Wu, Y., S. L. Hsu, C. Honeker, D. J. Bravet, and D. S. Williams. 2012. "The Role of Surface Charge of Nucleation Agents on the Crystallization Behavior of Poly(Vinylidene Fluoride)." *Journal of Physical Chemistry B* 116 (24): 7379–88. https://doi.org/10.1021/jp3043494.

Xu, Y., Z. Huang, X. Pu, G. Yin, and J. Zhang. 2019. "Fabrication of Chitosan/Polypyrrole-Coated Poly(L-Lactic Acid)/Polycaprolactone Aligned Fibre Films for Enhancement of Neural Cell Compatibility and Neurite Growth." *Cell Proliferation* 52 (3): 1–11. https://doi.org/10.1111/cpr.12588.

Yang, Y., S. Peng, F. Qi, J. Zan, G. Liu, Z. Zhao, and C. Shuai. 2020. "Graphene-Assisted Barium Titanate Improves Piezoelectric Performance of Biopolymer Scaffold." *Materials Science and Engineering C* 116 (April): 111195. https://doi.org/10.1016/j.msec.2020.111195.

Yasuda, I. 1953. "The Classic: Fundamental Aspects of Fracture Treatment." *J. Kyoto Med. Soc.* 4: 395–406.

Ye, H-J., W-Z. Shao, and L. Zhen. 2013. "Crystallization Kinetics and Phase Transformation of Poly(Vinylidene Fluoride) Films Incorporated with Functionalized BaTiO3 Nanoparticles." *Journal of Applied Polymer Science*, 2940–49. https://doi.org/10.1002/app.38949.

Ye, X., X. Yin, D. Yang, J. Tan, and G. Liu. 2012. "Ectopic Bone Regeneration by Human Bone Marrow Mononucleated Cells, Undifferentiated and Osteogenically Differentiated Bone Marrow Mesenchymal Stem Cells in Beta-Tricalcium Phosphate Scaffolds." *Tissue Engineering - Part C: Methods* 18 (7): 545–56. https://doi.org/10.1089/ten.tec.2011.0470.

Yong, Y., Z. D. Ming, L. Feng, Z. W. Chun, and W. Hua. 2014. "Electromagnetic Fields Promote Osteogenesis of Rat Mesenchymal Stem Cells through the PKA and ERK1/2 Pathways." *Journal of Tissue Engineering and Regenerative Medicine*. https://doi.org/10.1002/term.1864.

Yoshikawa, T., H. Ohgushi, and S. Tamai. 1996. "Immediate Bone Forming Capability of Prefabricated Osteogenic Hydroxyapatite." *Journal of Biomedical Materials Research* 32 (3): 481–92. https://doi.org/10.1002/(SICI)1097-4636(199611)32:3<481::AID-JBM23>3.0.CO;2-I.

Young, T. H., H. H. Chang, D. J. Lin, and L. P. Cheng. 2010. "Surface Modification of Microporous PVDF Membranes for Neuron Culture." *Journal of Membrane Science*

350 (1–2): 32–41. https://doi.org/10.1016/j.memsci.2009.12.009.

Young, T. H., L. P. Cheng, D. J. Lin, L. Fane, and W. Y. Chuang. 1999. "Mechanisms of PVDF Membrane Formation by Immersion-Precipitation in Soft (1-Octanol) and Harsh (Water) Nonsolvents." *Polymer* 40 (19): 5315–23. https://doi.org/10.1016/S0032-3861(98)00747-2.

Young, T. H., U. H. Lin, D. J. Lin, Hsu Hsien Chang, and Liao Ping Cheng. 2009. "Immobilization of L-Lysine on Microporous PVDF Membranes for Neuron Culture." *Journal of Biomaterials Science, Polymer Edition* 20 (5–6): 703–20. https://doi.org/10.1163/156856209X426574.

Younger, E. M., and M. W. Chapman. 1989. "Morbidity at Bone Graft Donor Sites." *Journal of Orthopaedic Trauma* 3 (3): 192–95. https://doi.org/10.1097/00005131-198909000-00002.

Yu, P., C. Ning, Y. Zhang, G. Tan, Z. Lin, S. Liu, X. Wang, et al. 2017. "Bone-Inspired Spatially Specific Piezoelectricity Induces Bone Regeneration." *Theranostics* 7 (13): 3387–97. https://doi.org/10.7150/THNO.19748.

Zhang, C., W. Liu, C. Cao, F. Zhang, Q. Tang, S. Ma, J. J. Zhao, L. Hu, Y. Shen, and L. Chen. 2018. "Modulating Surface Potential by Controlling the β Phase Content in Poly(Vinylidene Fluoridetrifluoroethylene) Membranes Enhances Bone Regeneration." *Advanced Healthcare Materials* 7 (11): 1–12. https://doi.org/10.1002/adhm.201701466.

Zhang, J., M. Li, E. T. Kang, and K. G. Neoh. 2016. "Electrical Stimulation of Adipose-Derived Mesenchymal Stem Cells in Conductive Scaffolds and the Roles of Voltage-Gated Ion Channels." *Acta Biomaterialia* 32: 46–56. https://doi.org/10.1016/j.actbio.2015.12.024.

Zhang, J., K. G. Neoh, X. Hu, E. T. Kang, and W. Wang. 2013. "Combined Effects of Direct Current Stimulation and Immobilized BMP-2 for Enhancement of Osteogenesis." *Biotechnology and Bioengineering* 110 (5): 1466–75. https://doi.org/10.1002/bit.24796.

Zhang, J., K. G. Neoh, and E. T. Kang. 2018. "Electrical Stimulation of Adipose-Derived Mesenchymal Stem Cells and Endothelial Cells Co-Cultured in a Conductive Scaffold for Potential Orthopaedic Applications." *Journal of Tissue Engineering and Regenerative Medicine* 12 (4): 878–89. https://doi.org/10.1002/term.2441.

Zhang, Jiamin, Xuzhao He, Xiaoyi Chen, Yongjun Wu, Lingqing Dong, Kui Cheng, Jun Lin, Huiming Wang, and Wenjian Weng. 2020. "Enhancing Osteogenic Differentiation of BMSCs on High Magnetoelectric Response Films." *Materials Science and Engineering C* 113 (February). https://doi.org/10.1016/j.msec.2020.110970.

Zhang, P., N. Ha, Q. Dai, S. Zhou, C. Yu, and L. Jiang. 2017. "Hypoxia Suppresses Osteogenesis of Bone Mesenchymal Stem Cells via the Extracellular Signal-Regulated 1/2 and P38-Mitogen Activated Protein Kinase Signaling Pathways." *Molecular Medicine Reports* 16 (4): 5515–22. https://doi.org/10.3892/mmr.2017.7276.

Zhang, X., C. Zhang, Y. Lin, P. Hu, Y. Shen, K. Wang, S. Meng, et al. 2016. "Nanocomposite Membranes Enhance Bone Regeneration Through Restoring Physiological Electric Microenvironment." *ACS Nano* 10 (8): 7279–86. https://doi.org/10.1021/acsnano.6b02247.

Zhang, Z., L. H. Klausen, M. Chen, and M. Dong. 2018. "Electroactive Scaffolds for Neurogenesis and Myogenesis: Graphene-Based Nanomaterials." *Small* 14 (1801983): 1–22. https://doi.org/10.1002/smll.201801983.

Zhao, F., C. Zhang, J. Liu, L. Liu, X. Cao, X. Chen, B. Lei, and L. Shao. 2020. "Periosteum Structure/Function-Mimicking Bioactive Scaffolds with Piezoelectric/Chem/Nano Signals for Critical-Sized Bone Regeneration." *Chemical Engineering Journal* 402 (July): 126203. https://doi.org/10.1016/j.cej.2020.126203.

Zhao, Y., Y. Liang, S. Ding, K. Zhang, H. Q. Mao, and Y. Yang. 2020. "Application of Conductive PPy/SF Composite Scaffold and Electrical Stimulation for Neural Tissue

Engineering." *Biomaterials* 255 (June): 120164. https://doi.org/10.1016/j.biomaterials.2020.120164.

Zhao, Z., C. Watt, A. Karystinou, A. J. Roelofs, C. D. McCaig, I. R. Gibson, and C. De Bari. 2011. "Directed Migration of Human Bone Marrow Mesenchymal Stem Cells in a Physiological Direct Current Electric Field." *European Cells and Materials* 22 (0): 344–58. https://doi.org/10.22203/eCM.v022a26.

Zheng, J., A. He, J. Li, and C. C. Han. 2007. "Polymorphism Control of Poly(Vinylidene Fluoride) through Electrospinning." *Macromolecular Rapid Communications* 28 (22): 2159–62. https://doi.org/10.1002/marc.200700544.

Zheng, T., Y. Huang, X. Zhang, Q. Cai, X. Deng, and X. Yang. 2020. "Mimicking the Electrophysiological Microenvironment of Bone Tissue Using Electroactive Materials to Promote Its Regeneration." *Journal of Materials Chemistry B* 8 (45): 10221–56. https://doi.org/10.1039/d0tb01601b.

Zhong, G., L. Zhang, R. Su, K. Wang, H. Fong, and L. Zhu. 2011. "Understanding Polymorphism Formation in Electrospun Fibers of Immiscible Poly(Vinylidene Fluoride) Blends." *Polymer* 52 (10): 2228–37. https://doi.org/10.1016/j.polymer.2011.03.024.

Zhou, Y., T. L. Tsai, and W. J. Li. 2017. "Strategies to Retain Properties of Bone Marrow-Derived Mesenchymal Stem Cells Ex Vivo." *Annals of the New York Academy of Sciences* 1409 (1): 3–17. https://doi.org/10.1111/nyas.13451.

Zhou, Z., W. Li, T. He, L. Qian, G. Tan, and C. Ning. 2016. "Polarization of an Electroactive Functional Film on Titanium for Inducing Osteogenic Differentiation." *Scientific Reports* 6: 1–8. https://doi.org/10.1038/srep35512.

Zhou, Z., P. Yu, L. Zhou, L. Tu, L. Fan, F. Zhang, C. Dai, et al. 2019. "Polypyrrole Nanocones and Dynamic Piezoelectric Stimulation-Induced Stem Cell Osteogenic Differentiation." *ACS Biomaterials Science and Engineering* 5 (9): 4386–92. https://doi.org/10.1021/acsbiomaterials.9b00812.

Zhu, S., W. Jing, X. Hu, Z. Huang, Q. Cai, Y. Ao, and X. Yang. 2017. "Time-Dependent Effect of Electrical Stimulation on Osteogenic Differentiation of Bone Mesenchymal Stromal Cells Cultured on Conductive Nanofibers." *Journal of Biomedical Materials Research - Part A* 105 (12): 3369–83. https://doi.org/10.1002/jbm.a.36181.

Zou, Y., J. Qin, Z. Huang, G. Yin, X. Pu, and D. He. 2016. "Fabrication of Aligned Conducting PPy-PLLA Fiber Films and Their Electrically Controlled Guidance and Orientation for Neurites." *ACS Applied Materials and Interfaces* 8 (20): 12576–82. https://doi.org/10.1021/acsami.6b00957.